



3 4456 0382752 6

CENTRAL RESEARCH LIBRARY
DOCUMENT COLLECTION

184

ORNL-4433
UC-34 - Physics

**NEUTRON PHYSICS DIVISION
ANNUAL PROGRESS REPORT
FOR PERIOD ENDING MAY 31, 1969**

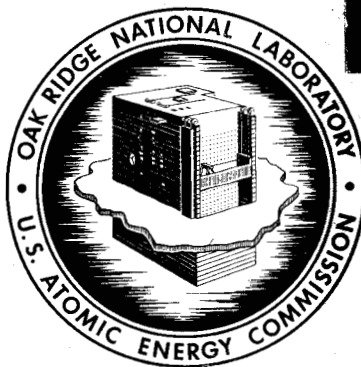
OAK RIDGE NATIONAL LABORATORY
CENTRAL RESEARCH LIBRARY
DOCUMENT COLLECTION

LIBRARY LOAN COPY

DO NOT TRANSFER TO ANOTHER PERSON

If you wish someone else to see this
document, send in name with document
and the library will arrange a loan.

UCN-7969
13 3-67



OAK RIDGE NATIONAL LABORATORY

operated by

UNION CARBIDE CORPORATION

for the

U.S. ATOMIC ENERGY COMMISSION

Printed in the United States of America. Available from Clearinghouse for Federal
Scientific and Technical Information, National Bureau of Standards,
U.S. Department of Commerce, Springfield, Virginia 22151
Price: Printed Copy \$3.00; Microfiche \$0.65

— LEGAL NOTICE —

This report was prepared as an account of Government sponsored work. Neither the United States, nor the Commission, nor any person acting on behalf of the Commission:

- A. Makes any warranty or representation, expressed or implied, with respect to the accuracy, completeness, or usefulness of the information contained in this report, or that the use of any information, apparatus, method, or process disclosed in this report may not infringe privately owned rights; or
- B. Assumes any liabilities with respect to the use of, or for damages resulting from the use of any information, apparatus, method, or process disclosed in this report.

As used in the above, "person acting on behalf of the Commission" includes any employee or contractor of the Commission, or employee of such contractor, to the extent that such employee or contractor of the Commission, or employee of such contractor prepares, disseminates, or provides access to, any information pursuant to his employment or contract with the Commission, or his employment with such contractor.

Contract No. W-7405-eng-26

**NEUTRON PHYSICS DIVISION
ANNUAL PROGRESS REPORT
For Period Ending May 31, 1969**

F. C. Maienschein, Director
R. G. Alsmiller, Associate Director
C. E. Clifford, Associate Director
R. W. Peelle, Associate Director

SEPTEMBER 1969

OAK RIDGE NATIONAL LABORATORY
Oak Ridge, Tennessee
operated by
UNION CARBIDE CORPORATION
for the
U.S. ATOMIC ENERGY COMMISSION



3 4456 0382752 6

Reports previously issued in this series are as follows:

ORNL-2081	Period Ending September 10, 1956
ORNL-2389	Period Ending September 1, 1957
ORNL-2609	Period Ending September 1, 1958
ORNL-2842	Period Ending September 1, 1959
ORNL-3016	Period Ending September 1, 1960
ORNL-3193	Period Ending September 1, 1961
ORNL-3360	Period Ending September 1, 1962
ORNL-3499, Vols. I and II	Period Ending August 1, 1963
ORNL-3714, Vols. I and II	Period Ending August 1, 1964
ORNL-3858, Vols. I and II	Period Ending August 1, 1965
ORNL-3973, Vols. I and II	Period Ending May 31, 1966
ORNL-4134	Period Ending May 31, 1967
ORNL-4280	Period Ending May 31, 1968

Contents

ABSTRACT	xi
1. NUCLEAR AND REACTOR PHYSICS	1
1.0 Introduction.....	1
1.1 Measurement of the Neutron Fission and Absorption Cross Sections of ^{239}Pu over the Energy Region 0.02 eV to 30 keV – R. Gwin, L. W. Weston, G. de Saussure, R. W. Ingle, J. H. Todd, F. E. Gillespie, R. W. Hockenbury, and R. C. Block.....	1
1.2 Neutron Fission and Capture Cross-Section Measurements for ^{233}U in the Energy Region 0.02 to 1 eV – L. W. Weston, R. Gwin, G. de Saussure, R. W. Ingle, J. H. Todd, C. W. Craven, R. W. Hockenbury, and R. C. Block.....	3
1.3 Statistical Tests for the Detection of Intermediate Structures in the Fission Cross Sections of ^{235}U and ^{239}Pu – R. B. Perez, G. de Saussure, and M. N. Moore.....	3
1.4 POLLA, A Fortran Program to Convert R-Matrix-Type Multilevel Resonance Parameters for Fissile Nuclei into Equivalent Kapur-Peierls-Type Parameters – G. de Saussure and R. B. Perez	4
1.5 On the Structure of the Subthreshold Fission Modes – R. B. Perez and G. de Saussure.....	4
1.6 The Variation of the R Matrix – A. Mockel and R. B. Perez	6
1.7 The Spectrum of Prompt Gamma Rays from the Fission of ^{235}U by Thermal Neutrons – R. W. Peelle, W. Zobel, F. C. Maienschein, and R. O. Chester	7
1.8 Oak Ridge Electron Linear Accelerator (ORELA) – A. L. Boch, J. A. Harvey, T. A. Lewis, F. C. Maienschein, N. C. Pering, and H. A. Todd.....	9
1.9 Performance of 140-MeV High-Current Short-Pulse LINAC at ORNL – N. C. Pering and T. A. Lewis.....	10
1.10 Rapid Data Acquisition into More than 10^5 Channels at ORELA – N. A. Betz, J. W. Reynolds, and G. G. Slaughter.....	11
1.11 Assembly and Initial Operation of the ORELAST – E. G. Silver, J. H. Todd, and J. Lewin	11
1.12 Status of the Neutron Time-of-Flight Data – W. E. Kinney and F. G. Perey	15
1.13 Improvements to the Neutron Time-of-Flight Experiment – W. E. Kinney, C. O. LeRigoleur, J. W. McConnell, and F. G. Perey.....	15
1.14 Data Reduction Codes for the Neutron Time-of-Flight Experiment – F. G. Perey and W. E. Kinney.....	16
1.15 The Correction of Neutron Scattering Cross Sections for Finite-Sample Effects – W. E. Kinney.....	16

1.16	The $^{14}\text{N}(n,xy)$ Reaction for $5.8 \leq E_n \leq 8.6$ MeV – J. K. Dickens and F. G. Perey.....	17
1.17	The $^{14}\text{N}(n,xy)$ Reaction for $8.6 \leq E_n \leq 11$ MeV – J. K. Dickens and F. G. Perey.....	17
1.18	The $^{16}\text{O}(n,xy)$ Reaction for $6.7 \leq E_n \leq 11$ MeV – J. K. Dickens and F. G. Perey.....	18
1.19	(n,xy) Studies on Samples of Aluminum, Silicon, and Iron for $5.5 \leq E_n \leq 11$ MeV – J. K. Dickens and F. G. Perey	21
1.20	(n,xy) Studies on Samples of Sodium, Chromium, and Nickel for $E_n = 7.5$ MeV – J. K. Dickens and F. G. Perey	21
1.21	11-MeV Proton Optical-Model Analysis – C. M. Perey, J. K. Dickens, F. G. Perey, and R. J. Silva.....	22
1.22	The $^{64,66,68}\text{Zn}(d,n)^{65,67,69}\text{Ga}$ Reactions – R. G. Couch, F. G. Perey, J. A. Biggerstaff, and S. Raman	22
1.23	Measurements of (d,n) Reactions of ^{58}Ni , ^{60}Ni , ^{62}Ni , and ^{64}Ni at 5 and 10 MeV – A. L. Marusak.....	23
1.24	^{120}Sn Optical-Model Analysis – F. G. Perey, F. E. Bertrand, T. A. Love, N. Baron, and J. K. Dickens	23
1.25	^{60}Ni Optical-Model Analysis – C. M. Perey and F. G. Perey	25
1.26	Measurements of the Lifetimes of Isomers of ^{92}Nb and ^{94}Nb – R. Kuebbing, E. Eichler, and J. K. Dickens.....	26
1.27	The Experimental Aspects of Neutron Wave and Pulse Propagation – R. B. Perez.....	27
2.	REACTOR AND WEAPONS RADIATION SHIELDING.....	28
2.0	Introduction – C. E. Clifford.....	28
2.1	Reactor and Weapons Radiation Shielding Program at the Tower Shielding Facility – F. J. Muckenthaler, J. L. Hull, J. J. Manning, K. M. Henry, L. B. Holland, L. W. Gilley, and J. W. Paul.....	29
2.2	Intensities of Gamma Rays from the Radiative Capture in Natural Tungsten of Neutrons from 0.02 eV to 100 keV – V. Orphan and J. John	30
2.3	Measurements of the Absolute Power and Fission Distribution in the TSF-SNAP Reactor and Comparison with Monte Carlo and Discrete-Ordinates Calculations – E. A. Straker.....	30
2.4	Comparisons of Monte Carlo Calculations with Measurements of Neutron Leakage from the TSF-SNAP Reactor – V. R. Cain.....	31
2.5	Modifications to the Monte Carlo Codes Used to Calculate Power Distribution and Neutron Leakage from the TSF-SNAP Reactor – K. D. Franz and V. R. Cain.....	31
2.6	Fast-Neutron Collimator Studies and the Design of the TSF-SNAP Core Mapping Collimator – E. A. Straker.....	31
2.7	Comparisons of Discrete-Ordinates Calculations with Neutron and Gamma-Ray Slab Transmission Data for the TSF-SNAP Reactor – F. R. Mynatt, M. L. Gritzner, and R. J. Rogers.....	31
2.8	Comparison of Monte Carlo Calculations with Measurements of Fast-Neutron Dose Transmitted from a Beam Source Through a SNAP-2 LiH Shield – V. R. Cain and K. D. Franz.....	35
2.9	Experimental Gamma-Ray Spectra Above 1 MeV from Thermal-Neutron Absorption in ^{235}U – R. S. Booth and F. J. Muckenthaler.....	36

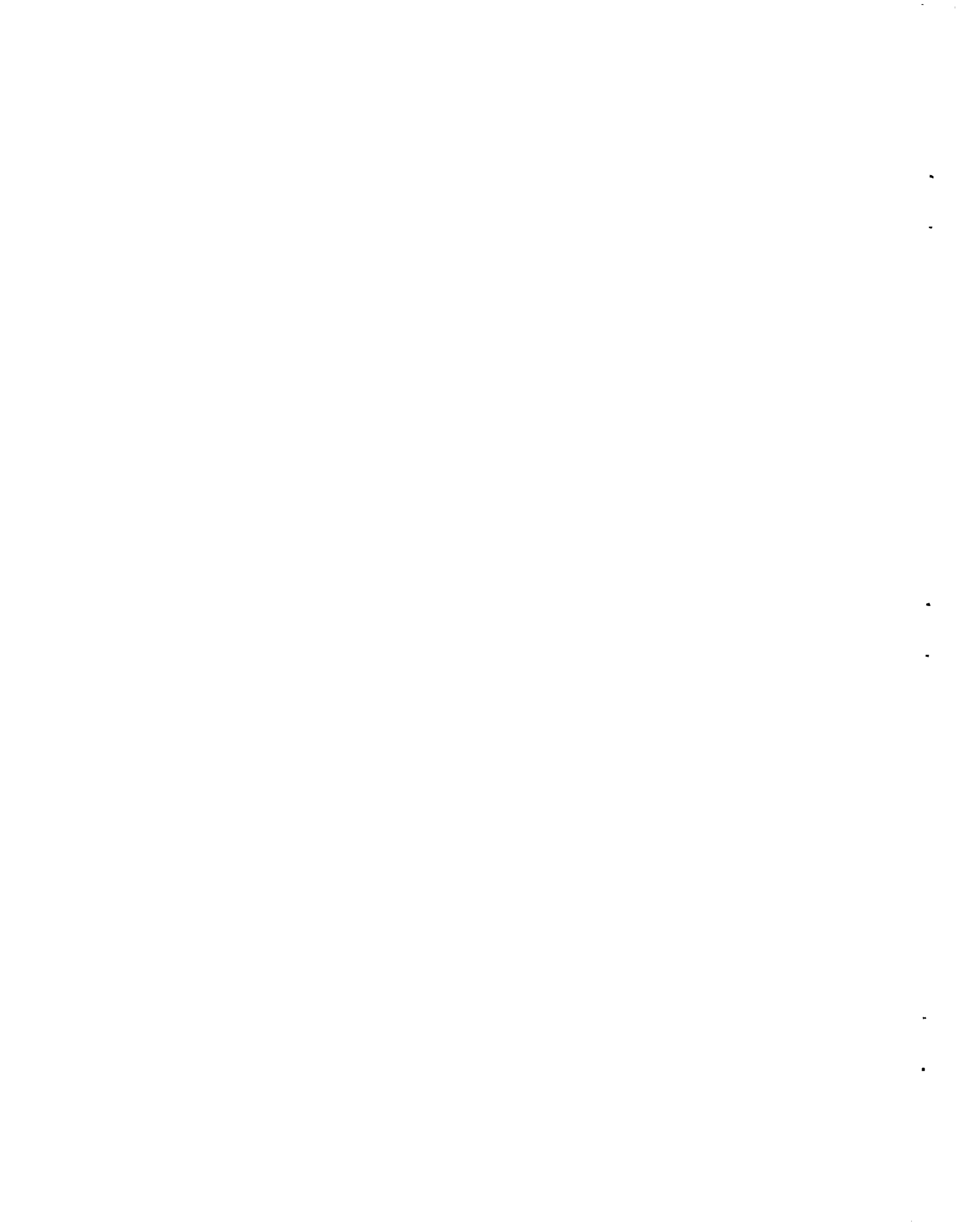
2.10	Gamma-Ray Spectra Arising from Thermal-Neutron Capture in Elements Found in Soils, Concretes, and Structural Materials – R. E. Maerker and F. J. Muckenthaler	38
2.11	Experimental Evaluation of Minima in the Total Neutron Cross Sections of Several Shielding Materials – E. A. Straker	38
2.12	An On-Line Data Acquisition, Display, and Analysis System for the Tower Shielding Facility – R. M. Freestone, Jr., and K. M. Henry.....	38
2.13	RESPMG: A Response Matrix Generation Code Package – W. R. Burrus and R. M. Freestone, Jr.	39
2.14	Gamma-Ray Response of the NE-213 Liquid Scintillation Detector – C. Y. Fu, V. R. Cain, E. A. Straker, P. N. Stevens, and F. J. Muckenthaler	39
2.15	A Unified Nuclear Model for the Generation of Nuclear Data – K. J. Yost, P. H. Pitkanen, and C. Y. Fu	39
2.16	The Application of a Gamma-Ray Cascade Model to the Calculation of Neutron-Energy-Dependent Capture Gamma-Ray Production Cross Sections – K. J. Yost and S. M. Kremer	40
2.17	A Nuclear Model for Data Generation and Analysis in Light Nuclei – K. J. Yost, P. H. Pitkanen, and C. Y. Fu	40
2.18	HELENE: A Computer Program to Calculate Nuclear Cross Sections Employing the Hauser-Feshbach Model, Porter-Thomas Width Fluctuations, and Continuum States – S. K. Penny.....	41
2.19	Calculation of Neutron Capture and Inelastic Gamma-Ray Yields Using a Modified Version of the Computer Code DUCAL – S. K. Penny, K. J. Yost, and J. White	42
2.20	Calculation of Neutron Inelastic Scattering Cross Sections for Iron and Uranium – S. K. Penny.....	44
2.21	POPOP4: A Code for Converting Gamma-Ray Spectra to Secondary Gamma-Ray Production Cross Sections – Walter E. Ford III and David H. Wallace.....	47
2.22	Discrete-Ordinates Calculation of Secondary Gamma-Ray Spectra for Comparison with Tower Shielding Facility Experiments – Walter E. Ford III and D. H. Wallace	48
2.23	The Use of Kernels in Studying Neutron Transport Problems – S. N. Cramer, V. R. Cain, R. R. Coveyou, P. N. Stevens, and E. A. Straker.....	52
2.24	Evaluation of the Total Cross Section of Iron – D. C. Irving and E. A. Straker.....	52
2.25	Nuclear Data Requirements and Acquisition for Shielding Application – K. J. Yost and J. R. Beyster.....	54
2.26	Recent Developments in Transport Solutions to Shielding Problems – C. E. Clifford, F. R. Mynatt, and E. A. Straker.....	54
2.27	The MORSE Code: A Multigroup Neutron and Gamma-Ray Monte Carlo Transport Code – E. A. Straker, P. N. Stevens, D. C. Irving, and V. R. Cain	54
2.28	O6R: An Improved Version of the O5R Monte Carlo Code – D. C. Irving, E. A. Straker, and C. L. Thompson.....	56
2.29	Applications of Adjoint Flux Calculations to Monte Carlo Biasing – F. A. R. Schmidt, E. A. Straker, and V. R. Cain	57
2.30	A General Method of Biasing the Angle of Scattering in Monte Carlo Calculations – C. E. Burgart	57
2.31	Monte Carlo Path-Length Selection Routines Based on Some Specific Forms of the Importance Function – V. R. Cain, E. A. Straker, and G. Thayer	59

2.32	An Amplification of Selected Portions of the O5R Monte Carlo Code User's Manual – D. C. Irving, V. R. Cain, and R. M. Freestone, Jr.....	59
2.33	The Development of a Time-Dependent One-Dimensional Discrete-Ordinates Code – ANISN-T1 – W. W. Engle, Jr., F. R. Mynatt, and R. S. Booth	60
2.34	Features in the DOT-II Code – F. R. Mynatt, W. W. Engle, Jr., and R. J. Rogers	61
2.35	Development of Two-Dimensional Discrete-Ordinates Transport Theory for Radiation Shielding – F. R. Mynatt, F. J. Muckenthaler, and P. N. Stevens.....	61
2.36	A User's Manual for ASOP – ANISN Shield Optimization Program – W. W. Engle, Jr.	62
2.37	AVKER: A Program for Determining Neutron Kerma Factors for Use in Energy Deposition Calculations – M. Solomito, J. J. Ritts, and H. C. Claiborne	63
2.38	SPACETRAN: A Code to Calculate Dose at Detectors at Various Distances from the Surface of a Cylinder – S. N. Cramer and M. Solomito.....	63
2.39	Shield Analysis and Design Services – H. C. Claiborne and M. Solomito	63
2.40	Some Calculated Milestone Solutions to Time-Dependent Radiation Transport Problems – E. A. Straker, W. W. Engle, Jr., and P. N. Stevens.....	63
2.41	Time-Dependent Neutron and Secondary Gamma-Ray Transport in an Air-over-Ground Geometry. Volume II. Tabulated Data – E. A. Straker.....	64
2.42	Neutron and Secondary Gamma-Ray Transport in Infinite Homogeneous Air – E. A. Straker and M. L. Gritzner.....	64
2.43	Shield Design Study for a Space Station Concept – F. R. Mynatt, W. W. Engle, Jr., and L. R. Williams.....	64
2.44	Analysis of Void Streaming Effects in a Missile Silo Cover Shield – F. R. Mynatt and L. R. Williams.....	66
2.45	Sensitivity of Neutron Transport in Oxygen to Various Cross-Section Sets – E. A. Straker.....	68
2.46	Ground Heating Due to a Point Source of 12.2- to 15-MeV Neutrons at an Altitude of 50 ft – E. A. Straker, M. B. Emmett, and C. L. Thompson.....	68
2.47	Heat Transfer Study of a Lithium Hydride Space Shield – J. Lewin, J. D. White, R. D. Sabin, and K. Yamada	68
2.48	Dose Rates in a Slab Phantom from Monoenergetic Gamma Rays – H. C. Claiborne and D. K. Trubey.....	71
2.49	A Simple Method for Determining a Lead-Steel Shield for Shipping Casks That Is Equivalent to a Lead Shield – E. Solomito and H. C. Claiborne.....	71
2.50	OGRE-CDE: A Monte Carlo Code for Calculating Response Functions of a Compton Diode Detector to Gamma Rays – C. Y. Fu, R. W. Roussin, and V. R. Cain.....	71
2.51	The Shielding Effectiveness of Single-Compartment Above-Ground Concrete Structures Against the Initial Radiation from Nuclear Weapons – L. G. Mooney.....	71
2.52	Analysis of Initial Radiation Protection Aboard Ship – R. L. French and J. M. Newell	73
2.53	A Review of Current Technology for Predicting the Initial Nuclear Radiation Environments Produced by Nuclear Weapons – R. L. French	73
2.54	Shielding Analysis of Military Structures – R. L. French.....	73

2.55	Calculations of the Radiation Leakage into Missile Silos Exposed to Nuclear Weapons Initial Radiation – M. B. Wells and J. D. Marshall	74
2.56	Calculations of Neutron and Secondary Gamma-Ray Doubly Differential Albedo Data for Steel-Covered Concrete Slabs – M. B. Wells and J. D. Marshall	75
2.57	Weapons Radiation Shielding Handbook: Status Report – L. S. Abbott, H. C. Claiborne, and C. E. Clifford (Editors)	75
3.	RADIATION SHIELDING INFORMATION CENTER.....	77
3.1	Recent Developments in RSIC Operations – D. K. Trubey, Betty F. Maskewitz, and R. W. Roussin.....	77
3.2	Handbook on Protection Against Radiation in Space – J. Wallace Webster.....	80
3.3	Shielding Benchmark Problems – A. E. Profio, Editor	81
3.4	Analytical Radiation Shielding Calculations for Concrete – F. A. R. Schmidt.....	82
3.5	An Examination of Several Computational Models for Use in Computing Gamma-Ray Penetration of Structures – Hisao Yamakoshi.....	83
3.6	Bibliography, Subject Index, and Author Index of the Literature Examined by the Radiation Shielding Information Center (Reactor and Weapons Radiation Shielding) – D. K. Trubey and J. Gurney.....	83
3.7	Abstracts of the Literature Examined by the Radiation Shielding Information Center (Reactor and Weapons Radiation Shielding).....	83
3.8	Programs for the Automatic Translation of Cross-Section Data Between the ENDF and UKNDL Formats – D. C. Irving and R. Q. Wright.....	84
4.	THEORETICAL STUDIES FOR MEDIUM- AND HIGH-ENERGY RADIATION SHIELDING	85
4.0	Introduction.....	85
4.1	Intranuclear-Cascade Calculation of the Secondary Nucleon Spectra from Nucleon-Nucleus Interactions in the Energy Range 340 to 2900 MeV and Comparisons with Experiment – H. W. Bertini, Arline H. Culkowski, and Miriam P. Guthrie	85
4.2	Protons from 2.7-GeV Protons on Ag and Br – D. T. King.....	86
4.3	Calculation of the Capture of Negative Pions in Light Elements and Comparison with Experiments Pertaining to Cancer Radiotherapy – M. P. Guthrie, R. G. Alsmiller, Jr., and H. W. Bertini.....	86
4.4	Absorption, Charge-Exchange, and Double-Charge-Exchange Reactions of π Mesons with Complex Nuclei: Comparisons of Theoretical Predictions with Experimental Results – H. W. Bertini	86
4.5	Phenomenological Determination of the Angular Distribution of Isobars Produced in High-Energy Nucleon-Nucleon and Pion-Nucleon Reactions – H. W. Bertini, Arline H. Culkowski, and Miriam P. Guthrie.....	90
4.6	Analytic Representation of Nucleon- and Pion-Emission Spectra from Nucleon-Nucleus Collisions in the Energy Range 750–2000 MeV – R. G. Alsmiller, Jr., and J. Barish	92
4.7	EVAP-2 and EVAP-3: Modifications of a Code to Calculate Particle Evaporation from Excited Compound Nuclei – Miriam P. Guthrie	92
4.8	Photonuclear Disintegration at High (<350 MeV) Energies – T. A. Gabriel and R. G. Alsmiller, Jr.....	93
4.9	Photonucleon and Photopion Production from High-Energy (50–400 MeV) Electrons in Thick Copper Targets – T. A. Gabriel and R. G. Alsmiller, Jr.....	93

4.10	Modification and Further Development of the Nucleon Transport Code NTC – D. C. Irving, H. S. Moran, and W. E. Kinney	94
4.11	Calculation of the Neutron and Proton Spectra from Thick Targets Bombarded by 450-MeV Protons and Comparison with Experiment – R. G. Alsmiller, Jr., J. W. Wachter, and H. S. Moran	95
4.12	Calculation of the Energy Deposited by Nucleons in a Spherical Phantom and Comparison with Experiment – D. C. Irving, R. G. Alsmiller, Jr., and H. S. Moran.....	95
4.13	Calculation of the Photon Production Spectrum from High-Energy Nucleon-Nucleus Collisions – Y. Shima and R. G. Alsmiller, Jr.....	95
4.14	High-Energy (<400 MeV) Neutron Transport Using the Method of Discrete Ordinates – R. G. Alsmiller, Jr., F. R. Mynatt, J. Barish, and W. W. Engle, Jr.	96
4.15	Shielding Against Neutrons in the Energy Range 50 to 400 MeV – R. G. Alsmiller, Jr., F. R. Mynatt, J. Barish, and W. W. Engle, Jr.....	97
4.16	The Effects of Multiple Coulomb Scattering and Range Straggling in Shielding Against Solar-Flare Protons – R. G. Alsmiller, Jr., J. Barish, and W. W. Scott.....	97
4.17	Calculation of the Radiation Hazard at Supersonic Aircraft Altitudes Produced by an Energetic Solar Flare – T. W. Armstrong, R. G. Alsmiller, Jr., and J. Barish.....	97
4.18	Monte Carlo Calculations of Residual Nuclei Production in Thick Iron Targets Bombarded by 1- and 3-GeV Protons and Comparison with Experiment – T. W. Armstrong	97
4.19	Calculation of the Residual Photon Dose Rate Induced in Iron by 200-MeV Protons – T. W. Armstrong and J. Barish	98
4.20	Calculation of the Residual Photon Dose Rate Around High-Energy Proton Accelerators – T. W. Armstrong and R. G. Alsmiller, Jr.....	99
4.21	Calculation of the Residual Photon Dose Rate Due to the Activation of Concrete by Neutrons from a 3-GeV Proton Beam in Iron – T. W. Armstrong and J. Barish.....	99
4.22	Calculation of the Energy Deposited in Thick Targets by High-Energy (1 GeV) Electron-Photon Cascades and Comparison with Experiment – R. G. Alsmiller, Jr., and H. S. Moran	100
4.23	Shielding Calculations for a 200-MeV Proton Accelerator – R. G. Alsmiller, Jr., J. Barish, R. T. Boughner, and W. W. Engle, Jr.	100
4.24	The Transport of Neutrons Produced by 3-GeV Proton-Lead Nucleus Collisions Through a Labyrinth and Comparison with Experiment – R. G. Alsmiller, Jr., and E. Solomito	101
4.25	High-Energy (<18 GeV) Muon Transport Calculations and Comparison with Experiment – R. G. Alsmiller, Jr., and J. Barish.....	101
4.26	High-Energy Muon Transport and the Muon Backstop for a 200-GeV Proton Accelerator – R. G. Alsmiller, Jr., M. Leimdorfer, and J. Barish.....	101
4.27	High-Energy Muon Transport and the Muon Backstop for a Multi-GeV Proton Accelerator – R. G. Alsmiller, Jr., and J. Barish	101
5.	MEDIUM-ENERGY NUCLEON SPECTROSCOPY STUDIES	102
5.0	Introduction.....	102
5.1	Continuum Charged-Particle Reactions Induced in Nuclei by 29-, 39-, and 61-MeV Protons – R. W. Peelle and F. E. Bertrand.....	103

5.2	Secondary Neutron Spectra from 20- to 40-MeV Protons on Various Targets – J. W. Wachter, R. T. Santoro, and T. A. Love.....	104
5.3	Measurement of Neutron Spectra in the Energy Range 2 to 40 MeV in the Upper Atmosphere – W. Zobel, T. A. Love, J. T. DeLorenzo, and C. O. McNew, Jr.....	106
5.4	Calibration of an NE-213 Detector with 40-MeV Neutrons – L. D. Cohen, T. A. Love, R. T. Santoro, J. W. Wachter, and W. Zobel.....	108
5.5	Calculation of Response Functions for a Proton-Recoil Telescope with Active Radiator – J. W. Wachter	110
5.6	Observation of the Light Output from an NE-213 Liquid Scintillator for 40-MeV Protons – R. T. Santoro, J. W. Wachter, and T. A. Love	112
5.7	Monte Carlo Calculations to Determine the Time Distribution of Scattered Neutrons in Time-of-Flight Experiments – D. I. Putzulu, R. T. Santoro, and J. W. Wachter.....	113
5.8	A Library System for the PDP-8 with DEC Type 580 Magnetic Tape System Utilizing a Redundant Rim Record Format – J. W. Wachter.....	115
5.9	SMOOTHIE: A Program for Smoothing O5S Histogram Output – R. T. Santoro, R. E. Textor, and W. Zobel	115
	PUBLICATIONS AND PAPERS PRESENTED AT SCIENTIFIC MEETINGS.....	116



Abstract

This document consists of abstracts and summaries describing the work performed in the ORNL Neutron Physics Division during the period May 31, 1968 to May 31, 1969.* The categories covered are nuclear and reactor physics, reactor and weapons radiation shielding, the Radiation Shielding Information Center, theoretical studies for medium- and high-energy radiation shielding, and medium-energy nucleon spectroscopy studies. A list of publications and papers presented by staff members at scientific meetings is also included.

*In the past this report has contained a substantial section on the research conducted at the Critical Experiments Facility which does not appear this year. As a result of changing programmatic emphasis, the work carried out at the Critical Experiments Facility was transferred to the Y-12 Plant, which is also operated by Union Carbide Corporation, Nuclear Division, on September 1, 1968. For information concerning this work, you may contact Dixon Callihan, Post Office Box Y, Oak Ridge, Tennessee 37830.



1. Nuclear and Reactor Physics

1.0 INTRODUCTION

Last year's major crisis concerning the "high" values of $\alpha(E)$ for ^{239}Pu in the energy region from 1 to 10 keV has been largely dissipated. Fortunately, the final ORNL results, which are reported here, agree very well with the preliminary results reported a year ago. The only significant difference is the substantial reduction in the error estimates.

The measurements of α for ^{233}U in the thermal energy range and the subsequent deduction of $\eta(E)$ from these data illustrate the requirements for extreme accuracy which are currently established by reactor designers. The discrepancy in η between the two best values in the 0.16-eV dip in η is less than 2%, but this is considered unacceptable and additional measurements must be made.

Our efforts in understanding the resonance region have included a search for "intermediate structure" in the fission cross sections of ^{235}U and ^{239}Pu . A straightforward application of noise-analysis techniques developed for reactor study has apparently resulted in fallacious answers as judged from a carefully constructed test case. This should serve as a warning to others inclined to apply noise-analysis methods to this problem.

Steady progress has been made in preparing the Oak Ridge Electron Linear Accelerator (ORELA) for use as an intense pulsed neutron source for time-of-flight measurements of neutron cross sections. With the exception of two as yet untested parameters, the accelerator appears to substantially meet the specifications. The installation of necessary equipment for performing experiments in four flight stations is largely completed. This equipment includes collimators for the flight paths and the very large scintillator tank (ORELAST) designed for cross-section measurements with fissile and fertile materials. The initial data-acquisition equipment has been accepted from the manufacturer.

In the neutron elastic and inelastic scattering experiments, a major breakthrough was made in the analysis of data by linking together the series of calculations required for the conversion from measured count rates to fully corrected cross sections. A major effort was made during the year in attacking the backlog of unanalyzed data so that they could be presented for publication. This effort has made a real reduction in the backlog, but the ever-ending struggle to keep up with the output of data obtained from the three ORNL Van de Graaffs continues. The measurement of gamma rays produced in inelastic scattering continues to be closely tied to the requirements for shielding design, particularly of systems exposed to nuclear weapons radiations. Measurements of the continuum portion of the inelastically scattered neutron energy distribution have shown large fluctuations which may require additional attention by reactor designers. The use of a nuclear temperature to characterize the continuum no longer appears reasonable in some cases, and efforts are under way to incorporate the experimental data into the evaluated nuclear data file (ENDF-B). Finally, the charged-particle experiments and analysis using the optical model continue as part of a program to allow the efficient and believable prediction of cross sections for reactor design.

1.1 MEASUREMENT OF THE NEUTRON FISSION AND ABSORPTION CROSS SECTIONS OF ^{239}Pu OVER THE ENERGY REGION 0.02 eV TO 30 keV¹

R. Gwin	J. H. Todd ²
L. W. Weston	F. E. Gillespie ²
G. de Saussure	R. W. Hockenbury ³
R. W. Ingle ²	R. C. Block ³

The analysis of the ^{239}Pu experiments on the neutron fission and absorption cross section re-

ported in the Neutron Physics Division Progress Report for 1968 has been extended. The main development in the analysis has been the reduction of the data to neutron cross sections.

The data obtained using the fission chamber were normalized at 0.025 eV to an absorption cross section of 1008 b and a fission cross section of 742 b. The normalization was completed by setting the value of $\alpha(\sigma_c/\sigma_f)$ in the 0.3-eV resonance to 0.66. The present normalization is consistent with that used previously.⁴

Figure 1.1.1 shows the experimentally derived values of α as a function of energy over the energy range from 0.1 to 30 keV. Also shown are α values calculated by Pitterle *et al.*⁵ The errors shown are standard deviations obtained from the experiments using the metal foils of ²³⁹Pu (10- and 20-g samples). The various experiments differed in sample thickness and/or neutron filters used to measure the background. Below 1 keV the measurements with the fission chamber may be expected to have a smaller uncertainty than that for the metal foils. No errors are shown for normalization, since

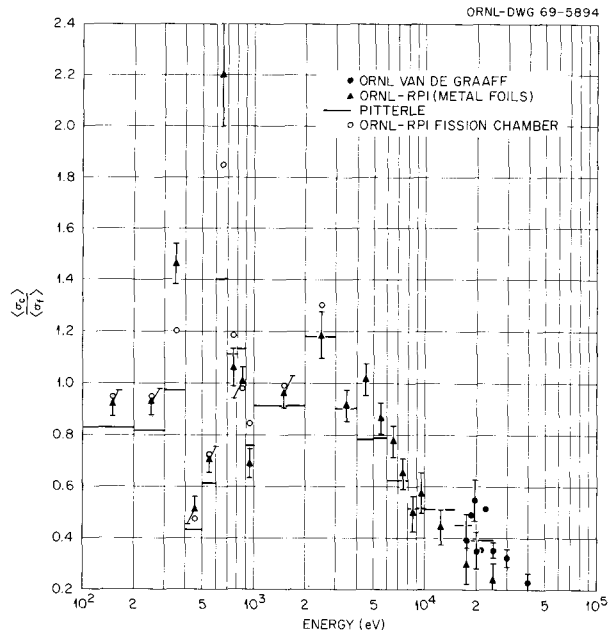


Fig. 1.1.1. Ratio of Capture to Fission vs Energy for ²³⁹Pu.

Table 1.1.1. Comparison of ORNL-RPI ²³⁹Pu Fission Cross Section with Other Measurements

Energy (keV)	Cross Section (b)					
	Fission Chamber	Metal Foils	Deduced Cross Section, James and Patrick ^a	James ^a	Shunk ^b	Patrick ^c
1.5	4.49 ± 0.04	4.53 ± 0.08	3.85 ± 0.21	4.40	3.43	3.64
2.5	3.30 ± 0.30	3.30	3.07 ± 0.20	3.46	2.64	2.83
3.5	3.20 ± 0.30	3.05 ± 0.21	2.95 ± 0.17	2.86	2.74	2.73
4.5	2.39 ± 0.03	2.42 ± 0.06	2.45 ± 0.09	2.54	2.31	2.31
5.5	2.17 ± 0.06	2.36 ± 0.18	2.50 ± 0.13	2.41	2.71	2.17
6.5	2.16 ± 0.06	2.14 ± 0.11	2.19 ± 0.13	1.97	2.20	1.96
7.5	2.13 ± 0.08	2.13 ± 0.07	2.14 ± 0.07	2.27	2.24	2.17
8.5	2.23 ± 0.10	2.26 ± 0.12	2.25 ± 0.12	2.25	2.46	2.32
9.5	1.88 ± 0.07	1.88 ± 0.06	2.06 ± 0.10	1.85	2.14	1.99
15.0	1.79 ± 0.09	1.79 ± 0.12	1.71 ± 0.04	1.76		1.67
25.0	1.66 ± 0.10	1.68 ± 0.12	1.57 ± 0.08	1.62		1.53

^aG. D. James and B. H. Patrick, *Evaluation of the ²³⁹Pu Fission Cross Section in the Energy Range 1 keV to 100 keV*, AERE-M 2065 (amended) (October 1968).

^bE. R. Shunk, W. K. Brown, and R. LaBauve, "Fission Cross Section of ²³⁹Pu, 20 eV to 2 MeV," *Conf. on Neutron Cross Section Technology, March 22-24, 1966, Washington, D.C.*, Conf. 660303, p. 979. See also LA-3586.

^cB. H. Patrick *et al.*, *Proc. of IAEA Conf. on Nuclear Data for Reactors, Paris, 1966*, vol. II, p. 117, and footnote a.

this type of uncertainty usually produces a biased result. If the uncertainty in α at 0.3 eV is 0.66 ± 0.02 , then an uncertainty in α of ± 0.05 is expected where α is unity.

Table 1.1.1 shows average values of the ^{239}Pu fission cross section for the neutron energy range from 1 to 30 keV. All of the values shown in Table 1.1.1 except the ORNL-RPI values were taken from a paper by James and Patrick⁶ and included the results of experiments by Shunk,⁷ Patrick,⁸ and James.⁶ In the evaluation of the data, James and Patrick used for the $^{10}\text{B}(n,\alpha)$ cross section the relation

$$\sigma(n,\alpha) = \left(\frac{610.3}{\sqrt{E}} - 0.28 \right) \text{ b},$$

where E is in electron volts. This relation was also used for the present work in obtaining the neutron flux from measurements made using a ^{10}B ionization chamber.

The agreement between the present results using the metal foils and the fission chamber is good. This agreement gives a measure of confidence in the α values obtained with the metal foils. The present experiments, fission chamber and metal foils, yield fission cross sections which are consistent with those of James, while the results due to Patrick and Shunk are lower on the average than the present results.

References

- ¹Abstract of ORNL-TM-2598 (in press).
- ²Instrumentation and Controls Division.
- ³Rensselaer Polytechnic Institute, Troy, N.Y.
- ⁴R. Gwin *et al.*, *Neutron Phys. Div. Ann. Progr. Rept. May 31, 1968*, ORNL-4280.
- ⁵T. A. Pitterle, E. M. Page, and M. Yamamoto, "Calculation of Fast Critical Experiments using ENDF/B Data and a Modified ENDF/B File," *Proceedings Neutron Cross Sections and Technology Conference, March 4-7, 1968, Washington, D.C.*, vol. 2.
- ⁶G. D. James and B. H. Patrick, *Evaluation of the ^{239}Pu Fission Cross Section in the Energy Range 1 keV to 100 keV*, AERE-M 2065 (amended) (October 1968).
- ⁷E. R. Shunk, W. K. Brown, and R. LaBauve, "Fission Cross Section of ^{239}Pu , 20 eV to 2 MeV," *Conf. on Neutron Cross Section Technology, March*

22-24, 1966, Washington, D.C., Conf. 660303, p. 979. See also LA-3586.

⁸B. H. Patrick *et al.*, *Proc. of IAEA Conf. on Nuclear Data for Reactors, Paris, 1966*, vol. II, p. 117, and ref. 6.

1.2 NEUTRON FISSION AND CAPTURE CROSS-SECTION MEASUREMENTS FOR ^{233}U IN THE ENERGY REGION 0.02 TO 1 eV¹

L. W. Weston	J. H. Todd ²
R. Gwin	C. W. Craven ³
G. de Saussure	R. W. Hockenbury ⁴
R. W. Ingle ²	R. C. Block ⁴

The relative neutron capture and fission cross sections in the neutron energy range 0.02 to 1.0 eV have been simultaneously measured. The data were normalized by means of the previously reported total cross section. The technique used was passing a pulsed neutron beam through a ^{233}U fission chamber placed at the center of a large liquid scintillator. The prompt neutron capture gamma rays were detected only in the liquid scintillator, whereas a fission event was characterized by coincident signals from the liquid scintillator and fission chamber. This technique provides a new method of obtaining η in this neutron energy range which is not subject to the same type of errors as a direct measurement. Comparisons with previously published data are given.

References

- ¹Abstract of ORNL-TM-2353 (Feb. 1, 1969).
- ²Instrumentation and Controls Division.
- ³Reactor Division.
- ⁴Rensselaer Polytechnic Institute, Troy, N.Y.

1.3 STATISTICAL TESTS FOR THE DETECTION OF INTERMEDIATE STRUCTURES IN THE FISSION CROSS SECTIONS OF ^{235}U AND ^{239}Pu ¹

R. B. Perez	G. de Saussure
M. N. Moore ²	

The existence of intermediate structures in the neutron-induced fission cross sections of ^{235}U and ^{239}Pu was pointed out in 1957 by Egelstaff. An interpretation recently proposed by Cao *et al.* and Bons *et al.* was based on the Strutinsky calcula-

tions of the deformation energies of the compound nucleus when shell effects are included in the liquid drop model. The theoretical interpretation in terms of current reaction theories has been given by Weigmann and Lynn.

The purpose of this paper is to develop and evaluate various statistical tests intended for the detection and interpretation of these narrow intermediate fission structures. A fission cross section was computed in the interval 0–5 keV using randomly generated parameters with distributions chosen to mock up the ^{235}U nucleus. The $J^\pi = 4^-$ state fission width was “modulated” in the manner suggested by Weigmann’s work.

Various statistical tests were done on these mockup cross sections to determine if the correct average spacing of the shape isomer levels could be obtained by such tests.

References

¹Abstract of paper to be presented at the *International Atomic Energy Agency Symposium on Physics and Chemistry of Fission*, Vienna, Austria, July 28–Aug. 1, 1969.

²San Fernando Valley State College, Northridge, Calif.

1.4 POLLA: A FORTRAN PROGRAM TO CONVERT R-MATRIX-TYPE MULTILEVEL RESONANCE PARAMETERS FOR FISSILE NUCLEI INTO EQUIVALENT KAPUR-PEIERLS-TYPE PARAMETERS¹

G. de Saussure R. B. Perez

The program POLLA converts a set of *R*-matrix resonance parameters for fissile nuclei into an equivalent set of Kapur-Peierls parameters. The program utilizes the multilevel formalism developed by Reich and Moore and avoids the diagonalization of the level matrix; hence, it is particularly useful where many levels and few fission channels are involved. Some applications of the program are given, and a FORTRAN listing is given in an appendix.

Reference

¹Abstract of ORNL-TM-2599 (in press).

1.5 ON THE STRUCTURE OF THE SUBTHRESHOLD FISSION MODES

R. B. Perez G. de Saussure

The presence of fission resonance groups in the subthreshold fission cross section of various fissile nuclei has been observed recently by various experimenters.^{1,2} Current theoretical explanations of this phenomenon are based on the existence of a second minimum in the fission barrier at high nuclear deformations.^{3–5} In order to obtain the structure of the subthreshold fission modes, we assume a physical picture in which the neutron and radiation eigenstates interact only with the first potential well. The fission modes have sources at both potential minima, which in turn interact with each other. Calling $b_\alpha(t)$ the time-dependent amplitudes of the various modes ($\alpha = n, r, f, j$, and k for the neutron, radiation, fission, and bound states of the first and second wells respectively), we have from classical time-dependent perturbation theory:

$$\frac{d}{dt} a_\alpha(t) = -\frac{i}{\hbar} \sum_j H_{\alpha j} a_j(t) e^{i(\omega_\alpha - \omega_j)t}, \quad \alpha = n, r, \quad (1)$$

$$\begin{aligned} \frac{d}{dt} a_f(t) = & -\frac{i}{\hbar} \sum_j H_{fj} a_j(t) e^{i(\omega_f - \omega_j)t} \\ & -\frac{i}{\hbar} \sum_k H_{fk} a_k(t) e^{i(\omega_f - \omega_k)t}, \quad (2) \end{aligned}$$

$$\begin{aligned} \frac{d}{dt} a_j(t) = & -\frac{i}{\hbar} \sum_\alpha H_{j\alpha} a_\alpha(t) e^{i(\omega_j - \omega_\alpha)t} \\ & -\frac{i}{\hbar} \sum_k H_{jk} a_k(t) e^{i(\omega_j - \omega_k)t}, \quad \alpha = n, r, f, \quad (3) \end{aligned}$$

and

$$\begin{aligned} \frac{d}{dt} a_k(t) = & -\frac{i}{\hbar} \sum_f H_{kf} a_f(t) e^{i(\omega_k - \omega_f)t} \\ & -\frac{i}{\hbar} \sum_j H_{kj} a_j(t) e^{i(\omega_k - \omega_j)t}, \quad (4) \end{aligned}$$

where calling H_1 the perturbation operator one has

$$\begin{aligned} H_{\alpha\beta} &= \langle \phi_\alpha | H_1 | \phi_\beta \rangle, \\ a_\alpha(t) &= b_\alpha(t) e^{i\omega_\alpha t}, \\ \hbar\omega_\alpha &= E_\alpha. \end{aligned} \quad (5)$$

Utilization of standard Laplace transform techniques allows solving for the amplitude $b_f(t)$ of the fission modes. From these magnitudes the transition probability and the corresponding cross section are obtained. For a given spin the result is, after neglecting the effect of neighboring levels:

$$\sqrt{E} \sigma(E) = \frac{c}{\hbar^2} \sum_j \left\{ \frac{\Gamma_{onj} \Gamma_{fj}}{|W_j + \delta_j|^2} + \frac{\Gamma_{onj} \Gamma_{fk} A_{kj}}{\hbar^2 |W_j|^2 |W_k|^2} \right\}, \quad (6)$$

where Γ_{onj} and Γ_{fj} are the neutron and fission widths, respectively, of the levels in the first well, Γ_{fk} the fission width for the second minimum, and

$$c = 6.59 \times 10^5 \text{ (b} \times \text{eV}^{1/2}\text{)},$$

$$A_{kj} = H_{kj} H_{jk},$$

$$W_j = \frac{1}{2\hbar} \Gamma_j + i(\omega_j - \omega_0),$$

$$W_k = \frac{1}{2\hbar} \Gamma_k + i(\omega_k - \omega_0), \quad (7)$$

$$\hbar\omega_0 = E \text{ (neutron energy)},$$

$$\delta_j = \sum_k \frac{A_{kj}}{\hbar^2 W_k},$$

$$\Gamma_k = \Gamma_{fk} + \Gamma_{ks} \quad (\Gamma_{ks} = \text{spreading width}).$$

The result, Eq. (6), shows that there are two contributions to the fission cross section. The first term within the braces corresponds to Breit-Wigner lines with effective total widths equal to $\Gamma_j + \delta_j$. An additional contribution arises from the second well by virtue of the coupling between the two potential minima. Under the assumption that the

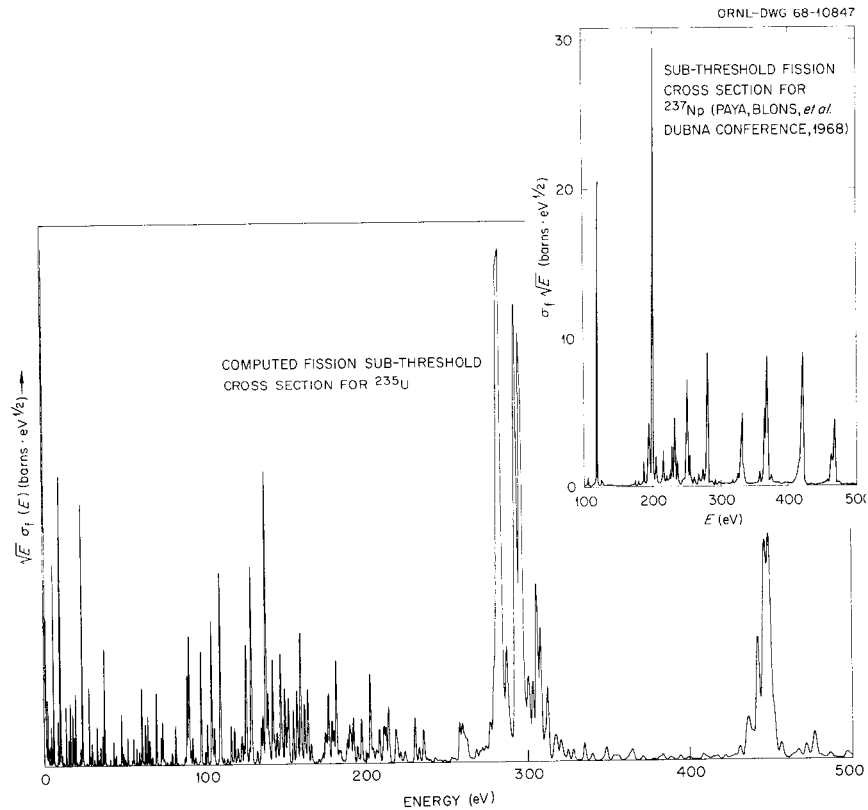


Fig. 1.5.1. Qualitative Comparison Between the Structure of the Subthreshold Fission Cross Section Obtained Theoretically and the Experimental Results of Paya et al. for ^{237}Np .

spreading width Γ_{ks} is smaller than Γ_{fk} , one obtains, neglecting fourth-order terms in the coupling matrix coefficients H_{jk} , the result:

$$\sqrt{E} \sigma(E) = c\hat{g} \sum_j \frac{\Gamma_{onj} \hat{\Gamma}_{fj}}{(E_j - E)^2 + (\hat{\Gamma}_j)^2/4}, \quad (8)$$

with

$$\hat{\Gamma}_{fj} = \Gamma_{fj} + \sum_k \frac{\Gamma_{fk} A_{kj}}{(E_k - E)^2 + \Gamma_{fk}^2/4}, \quad (9)$$

$$\hat{\Gamma}_j = \Gamma_{nj} + \Gamma_{\gamma j} + \hat{\Gamma}_{fj}. \quad (10)$$

Hence the subthreshold fission modes are given in terms of Breit-Wigner lines with resonant fission widths. Figure 1.5.1 shows a qualitative comparison between the measured subthreshold fission cross section of $^{237}\text{Np}^2$ and a mocked-up one obtained from Eq. (8). The average parameters and their statistical distribution functions correspond to those of ^{235}U . The average fission width $\langle \Gamma_{fk} \rangle$ was chosen to be 12 eV and to obey a χ^2 distribution with one degree of freedom. The average level spacing for the second well was taken to be 106 eV. The theoretical subthreshold fission cross section shows the typical fission resonances grouping observed experimentally.

References

- ¹E. Migneco and J. P. Theobald, *Nucl. Phys.* **A112**, 603 (1968).
- ²D. Paya *et al.*, "Intermediate Structure Observed in the Fission Cross Sections of ^{237}Np and Possibly of ^{239}Pu ," SMNF 624/68, Dubna Conference (1968).
- ³J. E. Lynn, *Structure in Subthreshold Fission Modes*, AERE-R-5891 (1968).
- ⁴H. Weigmann, *Z. Physik* **214**, 420 (1968).
- ⁵V. M. Strutinsky, *Nucl. Phys.* **A95**, 420 (1967).

1.6 THE VARIATION OF THE R MATRIX

A. Mockel¹ R. B. Perez

The common goal of all nuclear reaction theories is to obtain an energy parametrization of the cross

section suitable for application to the experimental results and containing a minimum amount of parameters. This is accomplished by the construction of the collision matrix U , or its closely related S matrix. A class of theories arrives at this result directly through the use of various prescriptions; classical examples are the Kapur-Peierls,² Siegert,³ Humblet and Rosenfeld,⁴ and more recently Feshbach⁵ theories. In contrast, Wigner and Eisenbud⁶ construct the R matrix first and obtain the collision matrix via matrix inversion. The relative advantages of either method have been extensively discussed by Lane and Thomas.⁷

A special feature of the Wigner-Eisenbud approach is the presence of a set of parameters, the channel radii a_c , which play a central role in the theory. At first sight it seems rather inconvenient to introduce such a set of artificial parameters in the theory, in view of the fact that the actual collision matrix cannot depend on the values chosen for the set. Our purpose is to obtain the relationship between the changes in the parameters of the theory and the subsequent variation of the R matrix.

To this end we have used invariant embedding techniques⁸⁻¹¹ to obtain the variation of the Green's function for the many-body Schrödinger equation. From the connection between this function and the R matrix a general expression for the variation of the R matrix with respect to any of the parameters of the theory has been obtained which is valid for arbitrary deformations of the nucleus. In particular, this relationship, for spherically deformed nuclei, takes the form

$$\begin{aligned} \frac{\partial}{\partial \tau} R_{cc'} &= \frac{1}{r_c} \frac{\partial r_c}{\partial \tau} \delta_{cc'} + \left(B_c - \frac{1}{2} \right) \frac{1}{r_c} \frac{\partial r_c}{\partial \tau} R_{cc'} \\ &+ R_{cc'} \left(B_{c'} - \frac{1}{2} \right) \frac{1}{r_{c'}} \frac{\partial r_{c'}}{\partial \tau} + \sum_{c''} R_{cc''} \left\{ \frac{\partial B_{c''}}{\partial \tau} \right. \\ &+ \left. \left(\frac{2M_{c''} r_{c''}}{\hbar^2} \right) (E - \hat{V}_{oc}) \frac{\partial r_{c''}}{\partial \tau} \right\} R_{c''c'} \\ &+ \sum_{\lambda, \lambda'} \frac{\gamma_{\lambda c} \gamma_{\lambda' c'}}{(E_{\lambda} - E)(E_{\lambda'} - E)} M_{\lambda \lambda'}, \quad (1) \end{aligned}$$

where τ is any of the R -matrix parameters; B_c , r_c , $\gamma_{\lambda c}$ are the boundary condition numbers, channel

radii, and reduced level widths for the c channel, respectively, with

$$\hat{V}_{oc} = V_c - (B_c^2 - B_c) \frac{\hbar^2}{2M_c r_c}, \quad (2)$$

$$V_c = \left\langle \phi(S_c) | V(S_c) r_c \frac{\partial r_c}{\partial \tau} | \phi(S_c) \right\rangle, \quad (3)$$

$$M_{\lambda\lambda'} = \frac{\partial E}{\partial \tau} \delta_{\lambda\lambda'} - \left\langle X_\lambda | \frac{\partial}{\partial \tau} V(r, \tau) | X_{\lambda'} \right\rangle. \quad (4)$$

The above matrix elements are given in terms of the channel functions $\phi(S_c)$, interior eigenfunctions X_λ , and the many-body potential $V(r, \tau)$.

The general result (1) shows that the dependence of the R matrix on the parameters introduced in the theory is always expressed as the solution of a Riccati matrix equation. In particular, identification of the parameter τ with the channel radius r_c yields (assuming the independence of the potential with respect to r_c)

$$r_c \frac{\partial}{\partial r_c} R_{cc} = 1 + (2B_c - 1)R_{cc} + \frac{2M_c r_c^2}{\hbar^2} (E - \hat{V}_c)R_{cc}^2,$$

with

$$\hat{V}_c = \hat{V}_{oc} - \frac{\hbar^2}{2M_c r_c^2} \frac{\partial B_c}{\partial r_c},$$

which is a result first obtained by Wigner and quoted by Vogt.¹² A whole class of sum rules can be obtained from Eq. (1) that generalizes Wigner's sum rules to any parameter entering in the theory and to the multichannel case.

The meaning of the result (1) becomes more significant when the variation of the parameters arises from physical processes rather than from arbitrary changes. Such is the case of the isobaric spin analogs, which can be studied by making τ equal to the charge of the nucleus. Another instance is the introduction of a set of fission saddle-point channels in the spirit of Lynn.¹³ From this viewpoint the presence of the channel radii in R -matrix theory allows the injection of physical models and intuition in the study of nuclear processes.

References

- ¹Department of Nuclear Engineering Sciences, University of Florida.
- ²P. L. Kapur and R. E. Peierls, *Proc. Roy. Soc. (London)* **A166**, 277 (1938).
- ³A. J. F. Siegert, *Phys. Rev.* **56**, 750 (1939).
- ⁴J. Humblet and L. Rosenfeld, *Nucl. Phys.* **26**, 529 (1961).
- ⁵H. Feshbach, *Ann. Phys.* **5**, 357 (1958); **19**, 10287 (1962).
- ⁶E. P. Wigner and L. Eisenbud, *Phys. Rev.* **72**, 29 (1947).
- ⁷A. M. Lane and R. G. Thomas, *Rev. Mod. Phys.* **30**, 257 (1958).
- ⁸R. Bellman, R. Kalaba, and M. Wing, *J. Math. Phys.* **1**, 280 (1960).
- ⁹J. Devooght, *J. Math. Anal. Appl.* **13**, 216 (1966).
- ¹⁰A. Mockel, *J. Math. Phys.* **8**, 2318 (1967).
- ¹¹J. Devooght, *J. Math. Phys.* **7**, 1764 (1966).
- ¹²E. Vogt, *Rev. Mod. Phys.* **34**, 723 (1962).
- ¹³J. E. Lynn, *Structure in Subthreshold Fission Modes*, AERE-R-5891 (1968).

1.7 THE SPECTRUM OF PROMPT GAMMA RAYS FROM THE FISSION OF ²³⁵U BY THERMAL NEUTRONS¹

R. W. Peelle F. C. Maienschein
W. Zobel R. O. Chester²

The energy spectrum of gamma rays from the fission of ²³⁵U must be used as input data for reactor shielding and heating calculations, along with the spectra for fission product decay and neutron capture in uranium. Analysis has now been completed of the prompt gamma-ray spectral data obtained in 1958 using pair and Compton scintillation spectrometers operated in ~ 60 nsec coincidence with a fission chamber exposed to thermal neutrons from the BSF thermal column. The spectrum obtained in a preliminary analysis of part of this data was published^{3,4} and is in general use. The portion of the fully analyzed spectrum corresponding to data obtained with the pair spectrometer was presented last year.⁵ Since that time the Compton spectrometer fission and calibration data, obtained for pulse heights corresponding to the 0.3-to-2.4-MeV energy range, have in turn been reviewed and cast in the proper form for "unscrambling" analysis using the FERD system.⁶

The pair and Compton data were analyzed simultaneously using joint response functions and data vectors and utilizing (unit area) window functions corresponding in shape and width to the peak of the response function for each experimental data bin. Figure 1.7.1 illustrates the result as lines drawn joining the upper and lower two-thirds confidence limits for the integral of the true underlying gamma spectrum weighted by each window. The points are from the preliminary work of ref. 1. This representation of the spectrum retains the experimental resolution (slightly broadened by the convolution over the pulse-height bin width) while removing the adverse effects of nonunique spectrometer response and correcting for the variation of the spectrometer efficiency with energy. The confidence intervals include the propagated counting statistics and the uncertainties inherent in the analysis process, but not the systematic uncertainties of perhaps 6%. Table 1.7.1 gives the corresponding intensities integrated over broad energy groups. Integrals were obtained by using "boxcar" windows of the given mean breadth, smoothed by the spectrometer resolu-

Table 1.7.1. Fission Gamma-Ray Intensities in Broad Energy Groups^a

Energy Range (MeV)	Photons/Fission	MeV/Fission
0.3-1.0	4.55 ± 0.2	2.66 ± 0.1
1.0-1.5	1.18 ± 0.05	1.44 ± 0.06
1.5-2.0	0.570 ± 0.025	0.98 ± 0.04
2.0-2.5	0.314 ± 0.017	0.70 ± 0.04
2.5-3.0	0.194 ± 0.009	0.531 ± 0.026
3.0-4.0	0.161 ± 0.005	0.551 ± 0.015
4.0-5.0	0.0586 ± 0.0023	0.256 ± 0.010
5.0-6.0	0.0197 ± 0.0023	0.107 ± 0.012
6.0-7.2	0.0093 ± 0.0020	0.060 ± 0.012
7.2-10.5	0.0005 ± 0.0012	0.005 ± 0.012
0.3-10.5	7.14 ± 0.23	7.17 ± 0.10

^aListed uncertainties do not include systematic effects of perhaps 6%.

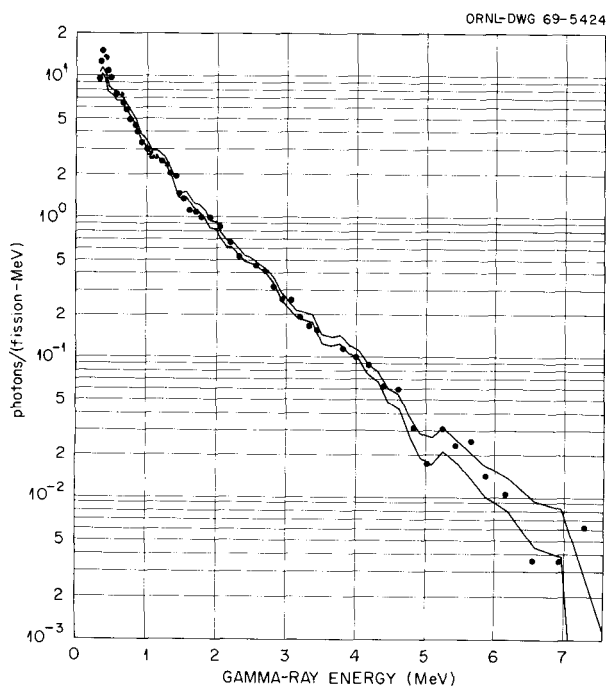


Fig. 1.7.1. The Spectrum of Prompt Gamma Rays from Fission of ^{235}U by Thermal Neutrons. The lines indicate two-thirds confidence limits on the spectrum reported here. The points represent a 1958 preliminary analysis of partial results from the same experiment.

tion. In this case analysis difficulties account for a greater share of the uncertainties, since the response functions cannot be combined to fit the boxcar shapes exactly. In the overlap region between pair and Compton spectra, results from narrow windows corresponding to the pair spectrometer are plotted for energies above 1.9 MeV, and results from the broader windows corresponding to the Compton spectrometer response are shown at lower energies. The points from the lowest energies (about 1.4 to 1.6 MeV) obtained from the pair spectrometer would fall very considerably above the curve shown, but they are thought to be less reliable because of the very low and rapidly varying pair spectrometer efficiency in this region. The new results in Fig. 1.7.1 and Table 1.7.1 should be used in preference to those of ref. 3.

Analysis is now proceeding on the 10-to-800-keV data obtained using a single NaI(Tl) scintillator with flight-time discrimination against pulses caused by fission neutrons. Although the pulse-height spectrum has long been available,^{4,7} the interpolation of a response matrix is just now being completed. Measured peak efficiencies down to ~ 20 keV have been shown to agree within a few percent with values calculated from gamma-ray cross sections, the experimental geometry, and

published peak/total ratios. A joint analysis will shortly be attempted of the pulse-height spectra from all three spectrometers.

References

- ¹Work funded by Los Alamos Scientific Laboratory under Purchase Order No. CM9-6111-1.
²Civil Defense Research Project.
³F. C. Maienschein *et al.*, *Proc. U.N. Intern. Conf. on Peaceful Uses of Atomic Energy, Second Geneva Conference* **15**, 366 (1958).
⁴R. W. Peelle *et al.*, *Pile Neutron Research in Physics*, p. 273, IAEA, Vienna, 1962.
⁵R. W. Peelle, W. Zobel, and F. C. Maienschein, *Neutron Phys. Div. Ann. Progr. Rept. May 31, 1968*, ORNL-4280, p. 104.
⁶W. R. Burrus, *Utilization of A Priori Information by Means of Mathematical Programming in the Statistical Interpretation of Measured Distributions*, ORNL-3743 (1965); W. R. Burrus *et al.*, *Neutron Phys. Div. Ann. Progr. Rept. May 31, 1966*, ORNL-3973, vol. 1, p. 61.
⁷T. A. Love, F. C. Maienschein, and R. W. Peelle, *Neutron Phys. Div. Ann. Progr. Rept. 1959*, ORNL-2842, p. 93.

1.8 OAK RIDGE ELECTRON LINEAR ACCELERATOR (ORELA)

A. L. Boch¹ F. C. Maienschein
 J. A. Harvey² N. C. Pering⁴
 T. A. Lewis³ H. A. Todd³

Varian Associates has made progress which was steady but slower than anticipated in putting into operation and testing the electron linear accelerator (ORELA). Installation of the accelerator was completed in August 1968, and the first beam was obtained in September 1968. Low-power (~1 kw) acceptance tests started in December 1968 and were completed in February 1969. The results obtained, summarized in Table 1.8.1, are in substantial accordance with the specifications.

Section 1.9 is an abstract of a paper which describes the low-power tests. Figure 1.8.1, taken from that paper, shows the variation of peak electron current at the target position ~22 ft beyond the end of the accelerator as a function of pulse width, determined as the full width at half maximum.

Table 1.8.1. Results of Low-Power Tests

Pulse Width, FWHM ^a (nsec)	Peak Current (A)	Average Energy (MeV)
2.0	7.5	
2.5	13.2	146
4.0	17.5	150
7.0	18.5	141
16.0	15.2	139
26.0	13.8	139
33.0	11.8	

Miscellaneous Performance Data	
Jitter, external trigger to beam	<2 nsec
Peak dark current, rf on, gun filament hot, grid not pulsed	<10 μ A
Average energy, at pulse width of 950 nsec	116 MeV
Current in 5% energy spread, pulse width of 950 nsec	60%
Rise time, typical for 16 to 26 nsec	3.5 nsec
Fall time, typical for 16 to 26 nsec	3.5 nsec
Beam spot size at output window, 22 nsec, ~13 A	~80% current within 1.3 \times 3 cm rectangle

^aFull width at half maximum.

High-power tests continue to this time (May 12, 1969), having reached the specified peak power at 24 nsec of 50 kW. The major remaining tests are those of reliability and dark current. The dark current indicated in Table 1.8.1 is quite low, but especially important for neutron time-of-flight measurements is the requirement that the electron pulse have no appreciable tail (area less than 2% of peak area). Observation of the counting rate in an organic scintillator adjusted to respond only to high-energy gamma rays from a target struck by the electron beam will be made as a function of time in order to determine the tail magnitude.

The intense pulsed neutron source made available at ORELA will allow neutron cross-section measurements in the energy region between 1 keV and 1 MeV, a region of the greatest interest for the fast breeder reactor program. For such measurements one requires, in addition to the linac, a

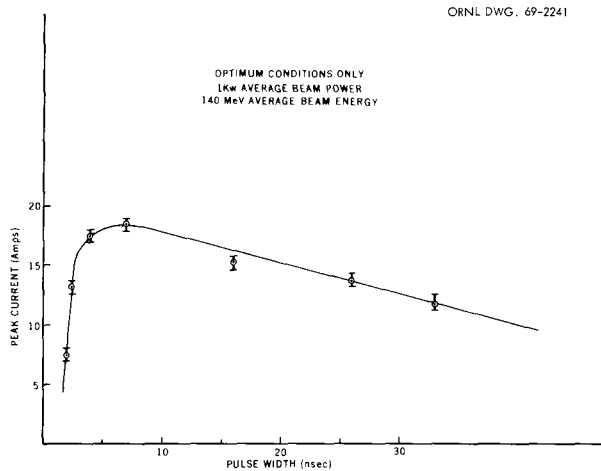


Fig. 1.8.1. Peak Current vs Pulse Width.

target, flight paths with neutron-beam collimators, detectors, and data-handling systems.

Suitable targets and accompanying moderators have been constructed by ORNL. Collimators, beam stops, and related equipment, also designed and fabricated by ORNL, have been installed in four flight paths. These will be used as follows:

Flight Path No.	Length (m)	Experiment(s)
6	40	a) Neutron cross-section measurements using scintillation tank b) Total cross-section measurements for fissile materials at low temperatures
5	20	a) Measurement of γ near thermal energies b) Preliminary experiments for flight path 6
7	40	Neutron capture cross sections for nonfissile materials in the keV range
1	80	a) Total neutron cross sections b) Angular distributions of elastically scattered MeV neutrons

Work is under way to equip seven other flight stations for use within the next year, including an extension of flight path 1 to 200 m. The major new detector constructed for use at ORELA is described in Sect. 1.11. Detectors for other experiments are, in general, already available.

The initial data-acquisition equipment at ORELA (phase I) consists of two small computers with fixed-head disks, CRT's with light pens, and peripherals (magnetic tape drives, plotters, etc.). This equipment was accepted from the manufacturer, Systems Engineering Laboratories, during April, and a programming course attended by 25 scientists and engineers was held during that month. A maintenance course is now under way, and use of the system for data taking is expected in June. Section 1.10 consists of an abstract of a paper describing this system.

Bids have been received and examined for the phase II Immediate Analysis System with the intention of ordering this equipment in fiscal year 1970.

References

- ¹Director's Division.
- ²Physics Division.
- ³Instrumentation and Controls Division.
- ⁴Varian Associates, Palo Alto, Calif.

1.9 PERFORMANCE OF 140-MeV HIGH-CURRENT SHORT-PULSE LINAC AT ORNL¹

N. C. Pering² T. A. Lewis³

High-current results of a 140-MeV electron traveling wave *L*-band linear accelerator are discussed. The 150-kV gridded gun injector has demonstrated pulse currents in excess of 30 A and pulse widths as narrow as 2.3 nsec at 1000 Hz. The accelerator wave-guide sections are of non-uniform impedance design, 4.3 m each, and are driven by 24-MW, 67.5-kW *L*-band klystrons. Uniform solenoidal focusing is employed over the accelerating beam transport. Short-pulse current exceeding 16 A has been observed at the target position within an area of less than 4 cm².

References

¹Abstract of paper presented at 1969 Particle Accelerator Conference, Washington, D.C., Mar. 5-7, 1969.

²Varian Associates.

³Instrumentation and Controls Division.

1.10 RAPID DATA ACQUISITION INTO MORE THAN 10^5 CHANNELS AT ORELA¹

N. A. Betz² J. W. Reynolds³
G. G. Slaughter⁴

A data-acquisition system which combines the high data rates (to 10^4 events per second) made possible by the Oak Ridge Electron Linear Accelerator (ORELA) and the large number of channels (to 10^6) needed for multiparameter neutron cross section measurements has been designed and implemented. The system consists of a digital data multiplexer interface, a fixed-head disk for channel and program storage designed specifically for rapid semirandom access of individual channels, a CRT with light pen for data examination, and a small fast general-purpose computer (SEL 810B). Each experimental event is tested to determine whether it is to be ignored or mapped into a channel address whose contents are then incremented. The ability to access individual words from the disk allows the experimental events to determine which channels are read into core memory for updating. This avoids the constant manipulation of unwanted channels and allows easy handling of in excess of 10^9 channel events per second (total number of channels times number of events per second) by the system.

References

¹Summary of paper presented at the Conference on Computer Systems in Experimental Nuclear Physics, Skytop, Pa., Mar. 3-6, 1969.

²Mathematics Division.

³Instrumentation and Controls Division.

⁴Physics Division.

1.11 ASSEMBLY AND INITIAL OPERATION OF THE ORELAST

E. G. Silver J. H. Todd¹
J. Lewin

During the past year the system located on flight path 6, including the ORELAST at the 40-m station, has been completed and is ready to be used for σ_c and α measurements. Figure 1.11.1 shows the ORELAST at the 40-m station.

A fairly elaborate support system for the thirty-two 5-in.-diam RCA-4522 photomultipliers was designed and fabricated. As shown in Fig. 1.11.2, each tube is mounted in a yoke which presses it against an O-ring with enough force to make a liquid-tight seal. A separate cover provides both the light seal and an airtight containment envelope. The space inside this cover is flushed continuously with inert gas. This arrangement is intended to prevent the loss of the scintillator fluid and the possibility of a fire due to the high voltage on the tube if a tube should fracture. The entire tube-yoke-cover assemblies are attached to the ORELAST as a unit with an O-ring seal, and in case of need would be replaced as a unit.

The tank interior has been coated with NE-561, a titanium oxide reflector in an epoxy vehicle. The through tube installed for initial work is of aluminum, 7 in. in inside diameter, with walls nominally 0.015 in. thick. Inserted in this is a cylindrical 5-ft.-long, 1-in.-thick liner of ⁶LiH. The liner is made of pressed material coated with a sprayed-on plastic film.

The neutron beam collimation system has been designed, fabricated, and installed. The detail design was done by F. C. Davis.² The system uses copper to scatter the unwanted neutrons into the earth and concrete. The largest (last) collimator has an outer section of cast iron and a lead gamma absorber at its rear face. The collimator system is designed to make it possible to obtain any beam diameter up to 6 in. by use of relatively light inserts into stepped outer portions.

The present collimator inserts are designed to give a 2.6-in.-diam beam with a 3.25-in. penumbra. A shadow bar, rectangular in cross section, made of copper followed by lead, has been installed at the first collimator position in the target room wall. This bar shields the sample from the unmoderated neutrons and the gamma rays coming from the central portion of the linac target. At



Fig. 1.11.1. View of ORELAST at the 40-m Station of ORELA.

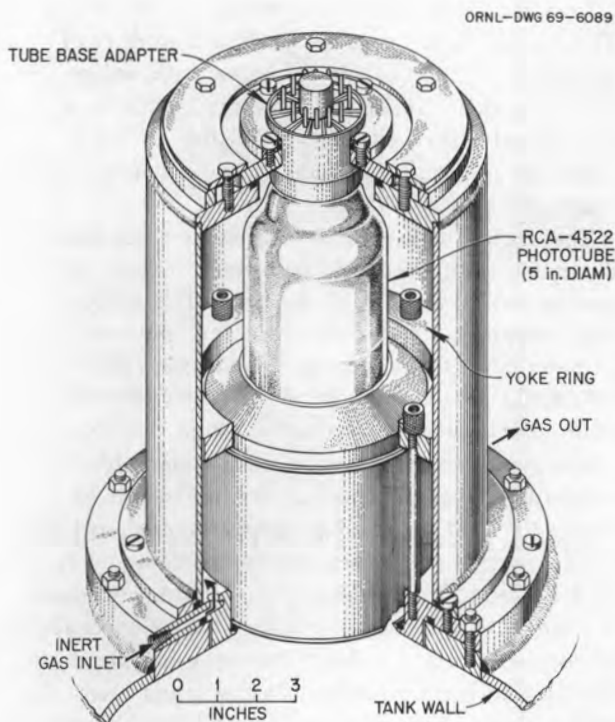


Fig. 1.11.2. Photomultiplier Tube Support and Mounting Assembly for ORELAST.

the 5-m station there is also a beam stop and a ten-section filter positioner, both of which are operated by air pressure and remotely controllable. Figures 1.11.3 and 1.11.4 depict the beam collimation and filtering system.

A thin-beryllium-walled BF_3 beam-monitor chamber, to be mounted in the beam where it enters the 40-m station, is under construction. There is also a helium-filled "tail pipe" which carries the neutrons into the beam catcher.

The Helmholtz coil pair for eliminating the vertical component of the earth's field has been installed and operates satisfactorily.

After considerable difficulty with leaks and contamination, the liquid-transfer and storage system has been made operable, and the scintillator in the ORELAST can be stored if necessary.

An optical separation system for the ORELAST has been designed, which will allow dividing the tank into four segments around the beam axis. The mounting components for it have been fabricated. The separator will be made of 0.002-in. Mylar coated with aluminum. This system has not yet been installed in the ORELAST.

A program to adjust and test the signal output of the ORELAST was carried out after completion

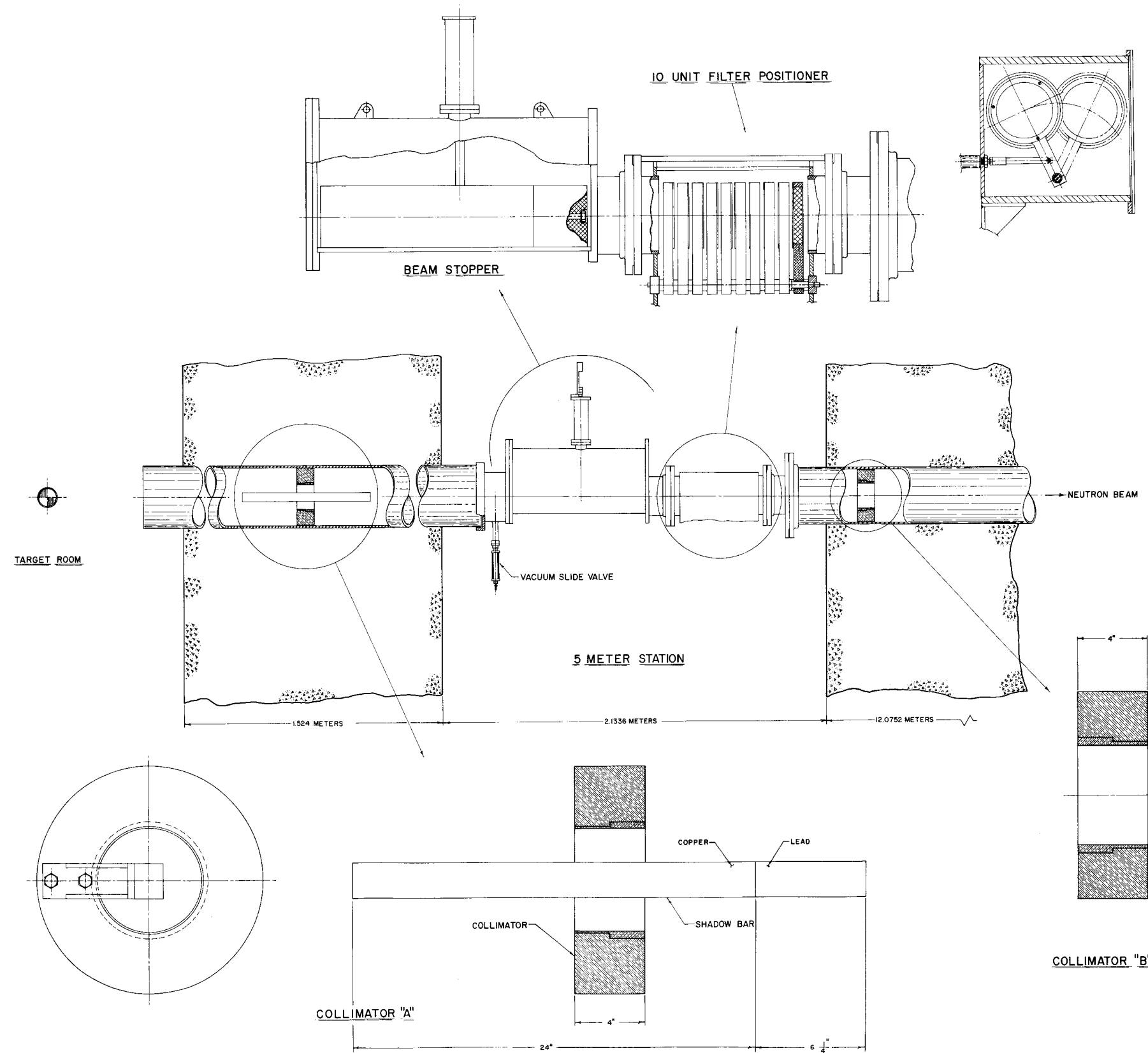


Fig. 1.11.3. Flight Path No. 6. Diagram of first two collimators and 5-m Station components including beam stop and 10-section filter positioner.

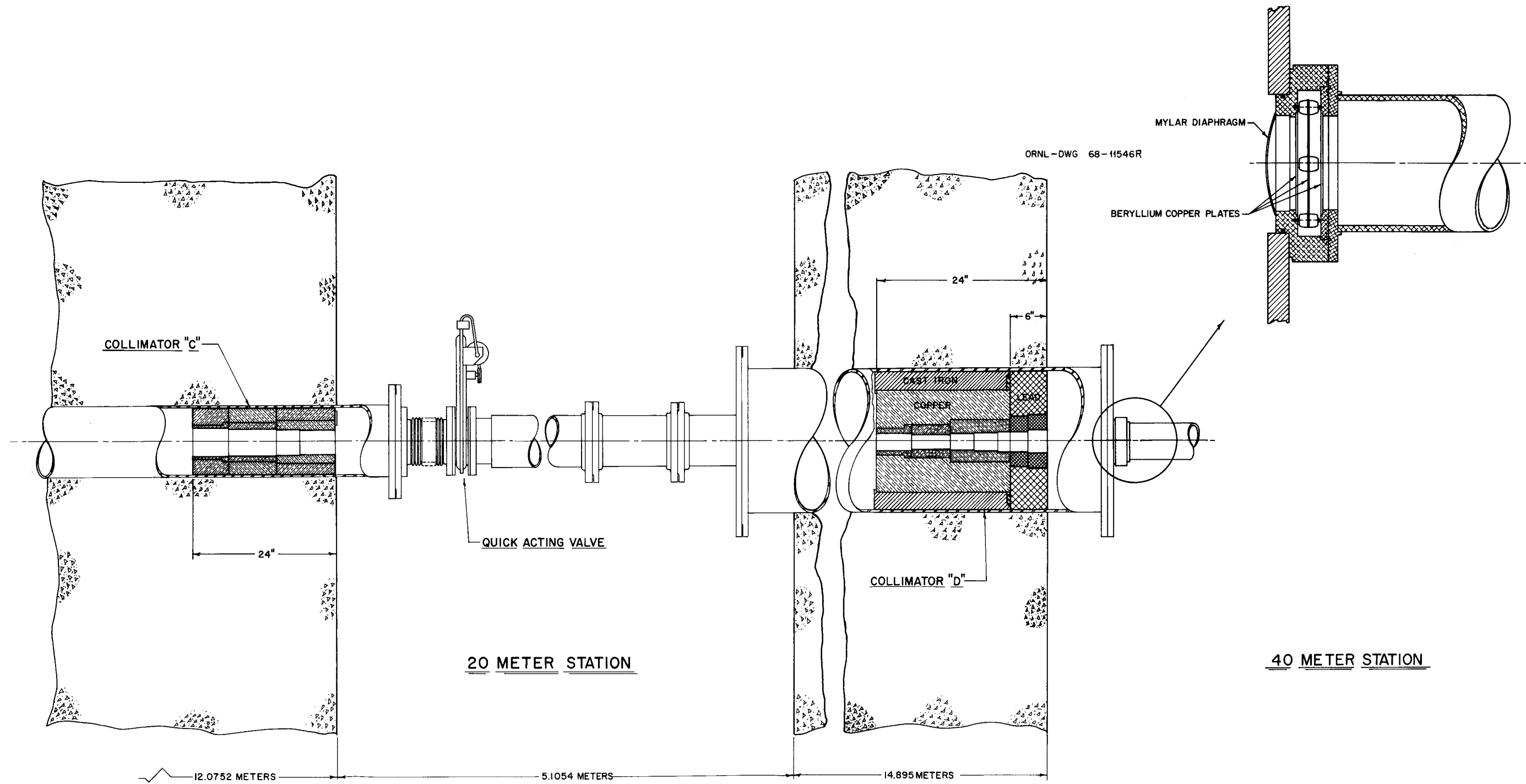


Fig. 1.11.4. Flight Path No. 6. Diagram of third and fourth collimators and 20-m Station components.

of the assembly of the system. Operation of the tubes at a gain level such that the combined gain from all tubes would be in the desired range ruled out the use of radioactive sources for gain calibration and the use of fission chambers for time resolution. Hence cosmic rays, and their attendant showers, were used to equalize the gains of the phototubes. After gain equalization the pulse-height resolution of the ^{60}Co sum peak was 27.7% and the resolution of the ^{24}Na peak was 24.4%.

The time resolution measurements were also made utilizing cosmic ray showers. One tube was used as a reference. The maximum transit time variation between tubes was found to be 6.6 nsec. Without correcting for these differences between individual tubes (which can be done by cable length adjustments) the composite time resolution (FWHM) was found to be 5.7 nsec.

If future needs for timing resolution become more severe, this value can probably be reduced by careful delay adjustments.

References

¹Instrumentation and Controls Division.

²General Engineering Division.

1.12 STATUS OF THE NEUTRON TIME-OF-FLIGHT DATA

W. E. Kinney F. G. Perey

The following is a summary of the status of the neutron elastic and inelastic scattering data.

1. Data completely reduced and being edited for publication:
 - a) Elastic scattering angular distributions at 5.44, 6.37, 7.60, and 8.52 MeV from C, Na, Mg, Al, Si, S, Ca, V, Fe, Co, and Y.
 - b) Inelastic scattering cross sections at 4.19, 4.46, 5.0, 5.18, 5.50, 6.37, 7.60, and 8.52 MeV from C, Na, Mg, Al, Si, S, Ca, V, Fe, Co, and Y.
2. Data acquired and undergoing data reduction:
 - a) Elastic and inelastic scattering angular distributions at 6.01, 6.44, 7.03, 7.54, 8.04, and 8.66 MeV from C, N, and O.
 - b) Elastic and inelastic scattering angular distributions at 6.44, 7.54, and 8.56 MeV from Sc, Ti, ^{nat}Cr , ^{52}Cr , ^{nat}Ni , ^{60}Ni , W, and U.

- c) Inelastic scattering at 9.5, 11, and 12 MeV from C, Na, Mg, Al, Si, S, Ca, V, Fe, Co, and Y.

1.13 IMPROVEMENTS TO THE NEUTRON TIME-OF-FLIGHT EXPERIMENT

W. E. Kinney J. W. McConnell²
C. O. LeRigoleur¹ F. G. Perey

Several improvements were made during the past year on the data-acquisition system:

1. A modular collimator system for inelastic neutron scattering was designed and built to enable data taking at three angles simultaneously. The collimators are built of paraffin and are of the reentrant throat type. The maximum scatterer size which can be accommodated is 1 in. by 1 in. The modular construction allows the angular separation between the detectors to be varied with a minimum angle of 7.5° between each detector.

2. The shielding wall of the 5.5-MeV Van de Graaff analyzing magnet room was moved to allow measurements to be made up to 140° instead of 120° . Our present system on both the 3- and the 5.5-MeV Van de Graaff enables us to make measurements from 10 to 140° .

3. The new photomultipliers, XP-1041 with bialkali photocathode, were investigated. Because of the increased photocathode efficiency and lower dark current, our neutron-gamma discrimination circuit was capable of operating over a wider dynamic range. We are converting our system to use these phototubes instead of the XP-1040's, since this will allow us to lower our neutron threshold by almost a factor of 2.

4. Minor modifications were made to the PDP-7 on-line data-acquisition system, which operated very reliably during the past year. Our digital interface was expanded to include three more analog-to-digital converters of eight bits each. The display interface was modified slightly to allow the two oscilloscopes attached to it to be programmed independently and display different information at the same time. Experience with the data-acquisition system indicates that more thorough and complete checks on the quality of the data as well as the status of the Van de Graaff beam pulse are feasible and would relieve the experimenters of many of the tedious checks performed during the experiment. At present such

checks are not possible due to memory size limitations. The addition of a disk to our system would relieve us of the memory size limitation and improve the quality of the data.

References

¹Commissariat a L'Energie Atomique, Centre D'Etudes Nucleaires de Cadarache.

²Instrumentation and Controls Division.

1.14 DATA REDUCTION CODES FOR THE NEUTRON TIME-OF-FLIGHT EXPERIMENT

F. G. Perey W. E. Kinney

Because of the large number of spectra accumulated in the neutron inelastic scattering work, a series of computer programs was developed to facilitate the data-reduction process. The basic idea behind these codes is to use the large computer (CDC-1604) to do all of the off-line computations and graphical presentations but use the PDP-7 on-line data-acquisition system to perform all of the input and major decision processes, which are required by the large code, via the interactive display. Both computers have input and output IBM compatible seven-track magnetic tapes. Each code uses as input the output of the previous code, regenerates it as output, and adds to the file the information it has processed. In this fashion, bookkeeping is kept at a minimum, the final tape contains a complete record of the treatment of the data, and results of any intermediate step in the process may be reproduced if desired.

We have found it necessary to develop five different codes to complete the data reduction:

1. JETSAM (PDP-7). – Time-of-flight spectra for both sample in and sample out are retrieved from the experimental data tapes. Monitor areas are extracted as well as the centroid of calibration peaks in the time-of-flight sample-in spectrum.

2. TRA (CDC-1604). – Corrections are performed for sample out and efficiency of the detector. The time-of-flight spectrum is transformed to a cross section per 25 keV of excitation energy per channel, and the variance of this spectrum is generated.

3. JETSIG (PDP-7). – Peak areas are determined and backgrounds traced under the continuum.

4. XFINAL (CDC-1604). – Information on peak areas and background is analyzed to determine the cross sections and errors for both discrete levels and the continuum. The cross sections are then corrected for finite sample size and multiple scattering.

5. EDIT. – This program edits the output tape of XFINAL to provide the final cross sections in tabular or graphical form.

Most of the manipulations of the data in these programs are straightforward, with two exceptions: (1) the treatment of the corrections for finite-sample effects, which has been written and included in a paper for publication (see abstract in Sect. 1.15); (2) the treatment of the propagation of errors when the backgrounds are traced with the program JETSIG; this treatment will be described in an ORNL report in preparation.

1.15 THE CORRECTION OF NEUTRON SCATTERING CROSS SECTIONS FOR FINITE-SAMPLE EFFECTS

W. E. Kinney

In reducing the data from a neutron time-of-flight experiment to elastic and inelastic neutron scattering cross sections, there are three effects due to the finite size of the scattering sample which must be corrected for: neutron attenuation in the sample, angular spread in single scattering, and multiple scattering.

An excellent approximation to the attenuation which is less than 1% in error for solid cylindrical samples less than 0.3 of a total mean free path in radius and having height-to-diameter ratios less than 3 can be obtained by considering the sample to be a disk with a parallel beam incident edge-on and with neutron paths restricted to be parallel to the faces of the disk.¹ This approximation gives

$$\exp \left[- \left(\frac{\pi}{4} + \frac{8}{3\pi} \right) \Sigma_T R \right]$$

for the attenuation factor, where Σ_T is the total macroscopic cross section and R is the sample radius.

Typical samples subtend an angle of 5 to 10° at the neutron source, so that the angular spread in single scattering requires a correction which

approaches the multiple scattering correction in magnitude at angles where the cross section is rapidly changing, for example, in the first minimum of elastic scattering.

If the differential cross section is known or reasonably well approximated, both the attenuation and the angular spread factors may be calculated without approximation by numerical integration.

Cox² suggested a method of combining general Monte Carlo calculations with analytic methods to calculate multiple-scattering contributions. A somewhat different formulation was found to be more useful than his, however. Monte Carlo was used to calculate probabilities for first, second, and third collisions, collision orders higher than the third occurring with negligible probability in samples less than 0.5 of a total mean free path in radius. The probabilities were expressed as functions of the sample radius, height-to-diameter ratio, and average cosine of scattering. The functions were then used in analytic expressions for the multiple-scattering contributions.

The above correction methods were found to save a factor of 40 over standard Monte Carlo multiple-scattering correction techniques in correcting elastic scattering cross sections and to allow the correction of isotropic inelastic cross sections in the same calculation that heretofore reduced stripped spectrum peak areas to uncorrected cross sections.

References

¹The approximation was suggested by F. G. Perey.

²S. A. Cox, *Nucl. Instr. Methods* **56**, 245 (1967).

1.16 THE $^{14}\text{N}(n,xy)$ REACTION FOR $5.8 \leq E_n \leq 8.6 \text{ MeV}^1$

J. K. Dickens F. G. Perey

We have obtained gamma-ray spectra for the reactions $^{14}\text{N}(n,n'\gamma)^{14}\text{N}$, $^{14}\text{N}(n,p\gamma)^{14}\text{C}$, and $^{14}\text{N}(n,\alpha\gamma)^{11}\text{B}$ for incident mean neutron energies $E_n = 5.8, 6.4, 7.4, 8.0,$ and 8.6 MeV . The gamma rays were detected using a coaxial Ge(Li) detector of 30 cc active volume. The detector was placed at 55 and 90° with respect to the incident neutron

direction and was 77 cm from the sample; time of flight was used with the gamma-ray detector to discriminate against pulses due to neutrons and background gamma radiation. The sample was 100 g of Be_3N_2 in the form of a right circular cylinder. Data were also obtained using a 75-g beryllium sample to provide an estimate of the background. The incident neutron beam was produced by bombarding a deuterium-filled gas cell with the pulsed deuteron beam of appropriate energy from the ORNL 6-MV Van de Graaff. The resulting neutron beam was monitored using a scintillation counter; a time-of-flight spectrum from this detector was recorded simultaneously with the gamma-ray data. These data have been studied to obtain absolute cross sections for production of gamma rays from ^{14}N for the incident neutron energies quoted above. The cross sections have been compared, where possible, with previously measured values with good agreement. However, there are several important differences with previous data, and these are discussed. In particular, summing the partial cross sections yields a value for the total nonelastic cross section which is approximately half the total nonelastic cross section obtained from the difference between the total cross section and the total elastic cross section.

Reference

¹Abstract of paper accepted for publication in *Nuclear Science and Engineering*.

1.17 THE $^{14}\text{N}(n,xy)$ REACTION FOR $8.6 \leq E_n \leq 11 \text{ MeV}^1$

J. K. Dickens F. G. Perey

Measurements of gamma-ray production cross sections due to neutron interactions with nitrogen, fully reported for $E_n \leq 8.6 \text{ MeV}$ (see Sect. 1.16), have been extended to 11 MeV. For these measurements a pulsed deuteron beam was obtained from the ORNL tandem Van de Graaff; otherwise, the experimental system was that used for the lower-energy work and discussed fully in the report of that work.² Spectra have been obtained for $\theta_\gamma = 55$ and 90° , and for $E_n = 8.6, 9.0, 9.5, 10.0, 10.5,$ and 11.0 MeV . The desired cross sections are being extracted from the spectra.

This work is pertinent to requests 40, 41, and 43 of WASH-1078.³

References

¹Research sponsored by the Defense Atomic Support Agency under Task No. PC068.

²J. K. Dickens and F. G. Perey, sect. 1.16, this report.

³A. B. Smith, *Compilation of Requests for Nuclear Cross-Section Measurements*, WASH-1078 [EANDC (US)-103 "U"], Argonne National Laboratory (June 1967).

1.18 THE $^{16}\text{O}(n,xy)$ REACTION FOR $6.7 \leq E_n \leq 11 \text{ MeV}$ ¹

J. K. Dickens F. G. Perey

The gamma rays produced by neutron interaction with nuclei of oxygen have been studied for neutron bombarding energies between 6.7 and 11 MeV. Spectra were obtained for $\theta_\gamma = 55$ and 90° for $E_n \approx 7.0, 7.5, 8.0, 8.6, 9.0, 9.5, 10.0, 10.5,$ and 11.0 MeV, and for $\theta_\gamma = 55^\circ$ for $E_n \approx 6.7, 6.8, 7.4, 7.7, 7.9, 8.1,$ and 8.3 MeV. For $E_n \leq 8.6$ MeV, the same experimental arrangement reported for the $^{14}\text{N}(n,xy)$ work² (see Sect. 1.16) was used. For $E_n \geq 8.6$ MeV, the only change was to obtain the pulsed deuteron beam from the ORNL Tandem Van de Graaff.

The spectrum shown in Fig. 1.18.1 was obtained for $\theta_\gamma = 55^\circ$, $E_n = 10.5$ MeV, using a 30-cc Ge(Li) detector. The upper portion of the figure exhibits the response to the 3.68- and 3.85-MeV gamma rays from the $^{16}\text{O}(n,\alpha)^{13}\text{C}$ reaction; the principal gamma rays from $^{16}\text{O}(n,n')^{16}\text{O}$ at $E_\gamma = 6.13, 6.92,$ and 7.12 MeV are indicated in the lower portion of the spectrum. Because of the good resolving power of the Ge(Li) detector, the Doppler effect upon the detected gamma-ray energy (due to the motion of the excited ^{13}C or ^{16}O ion) is clearly exhibited in this figure. The ^{16}O excited

states at 6.92 and 7.12 MeV have half-lives of $\approx 10^{-14}$ sec (ref. 3), and the ^{16}O ion requires $\sim 10^{-12}$ sec to come to rest in the BeO medium; thus the peaks for the 6.92- and 7.12-MeV state in ^{16}O have $t_{1/2} \approx 10^{-11}$ sec,³ and so a narrow peak is seen representing the 6.13-MeV gamma ray. The effect is even more pronounced for the gamma rays from the $^{16}\text{O}(n,\alpha)^{13}\text{C}$ reaction. The 3.86-MeV excited state in ^{13}C has $t_{1/2} \sim 10^{-11}$ sec,⁴ and the result is a narrow peak in the spectrum. The 3.68-MeV state in ^{13}C has $t_{1/2} < 26 \times 10^{-15}$ sec,⁴ with the gamma response in the Ge detector spread over 25 channels in the spectrum for $E_n = 10.5$ MeV.

Figure 1.18.2 shows the detector response to the 3.68-MeV double-escape peak in more detail. A study of this response seemed necessary to ensure that there was only one gamma ray involved; if it were necessary to postulate contributions from two (or more) gamma rays in order to reproduce the experimental spectrum, the extra gamma ray would have to be associated with a heretofore unreported yet energetically possible transition. Therefore, response spectra were computed for various likely $^{16}\text{O}(n,\alpha)$ angular distributions (since no experimental angular distributions have been reported) with the principal result that, as shown in Fig. 1.18.2, the experimental response can be associated with detection of a single 3.68-MeV gamma ray provided that the half-life of the 3.68-MeV state in ^{13}C is $\approx 10^{-15}$ sec and that the postulated $^{16}\text{O}(n,\alpha)$ angular distribution is strongly peaked at large and small scattering angles, for example, as shown in the inset of Fig. 1.18.2.

Cross sections for the strong gamma transitions have been extracted. Those for the 6.13-MeV gamma ray are in reasonable agreement with those previously reported;⁵ our values for the 6.92- and 7.12-MeV gamma rays are larger than previously reported. The resonant structure of the excitation function for the 6.13-MeV gamma ray for E_n between 6.7 and 8 MeV⁵ is generally confirmed by our data. The work is pertinent to request No. 50 in WASH-1078.⁶

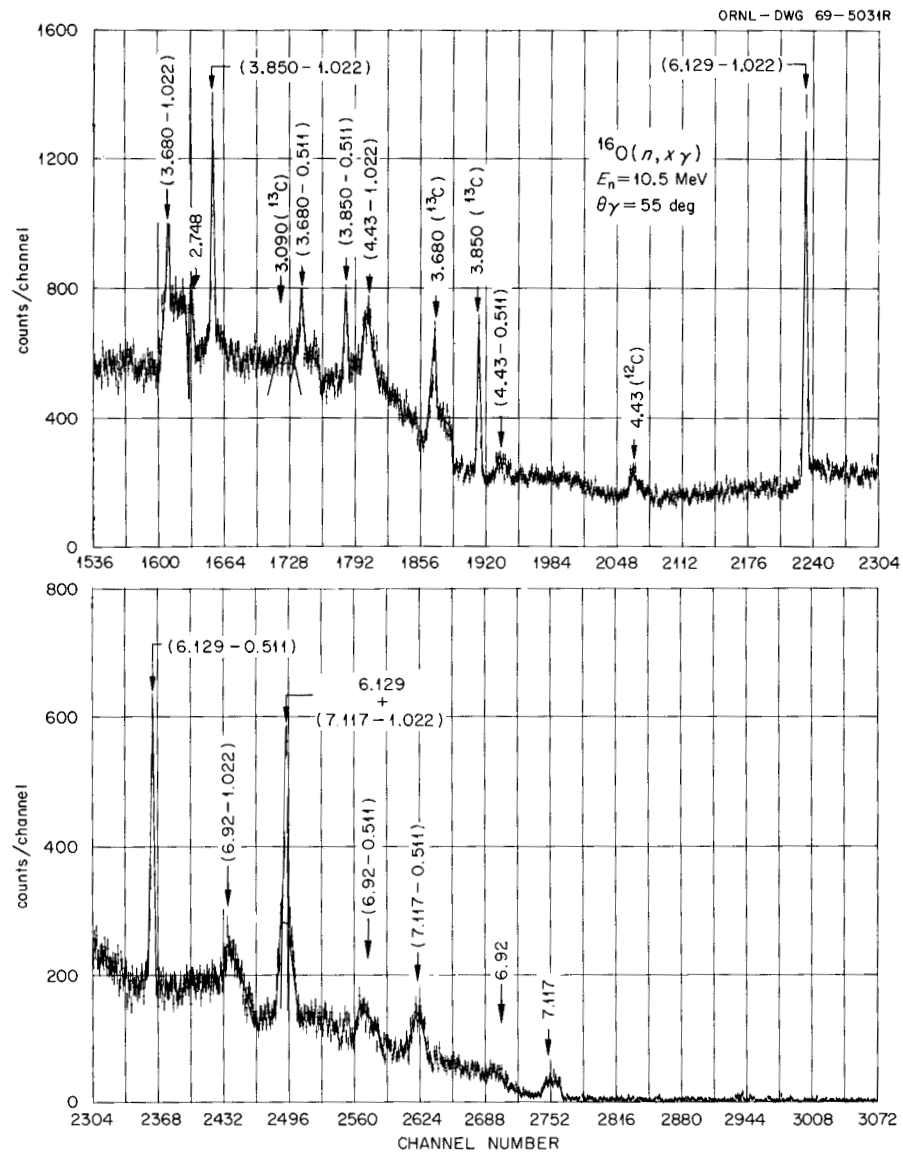


Fig. 1.18.1. Spectrum of Gamma Rays for 10.5-MeV Neutron Bombardment of ^{16}O , $\theta_\gamma = 55^\circ$. Peaks are labeled with the energy of the detected gamma ray. Escape peaks are indicated by $(E_\gamma - 0.511)$ and $(E_\gamma - 1.022)$ labels. Isotope symbols indicate gamma radiation emanating from nuclei other than ^{16}O .

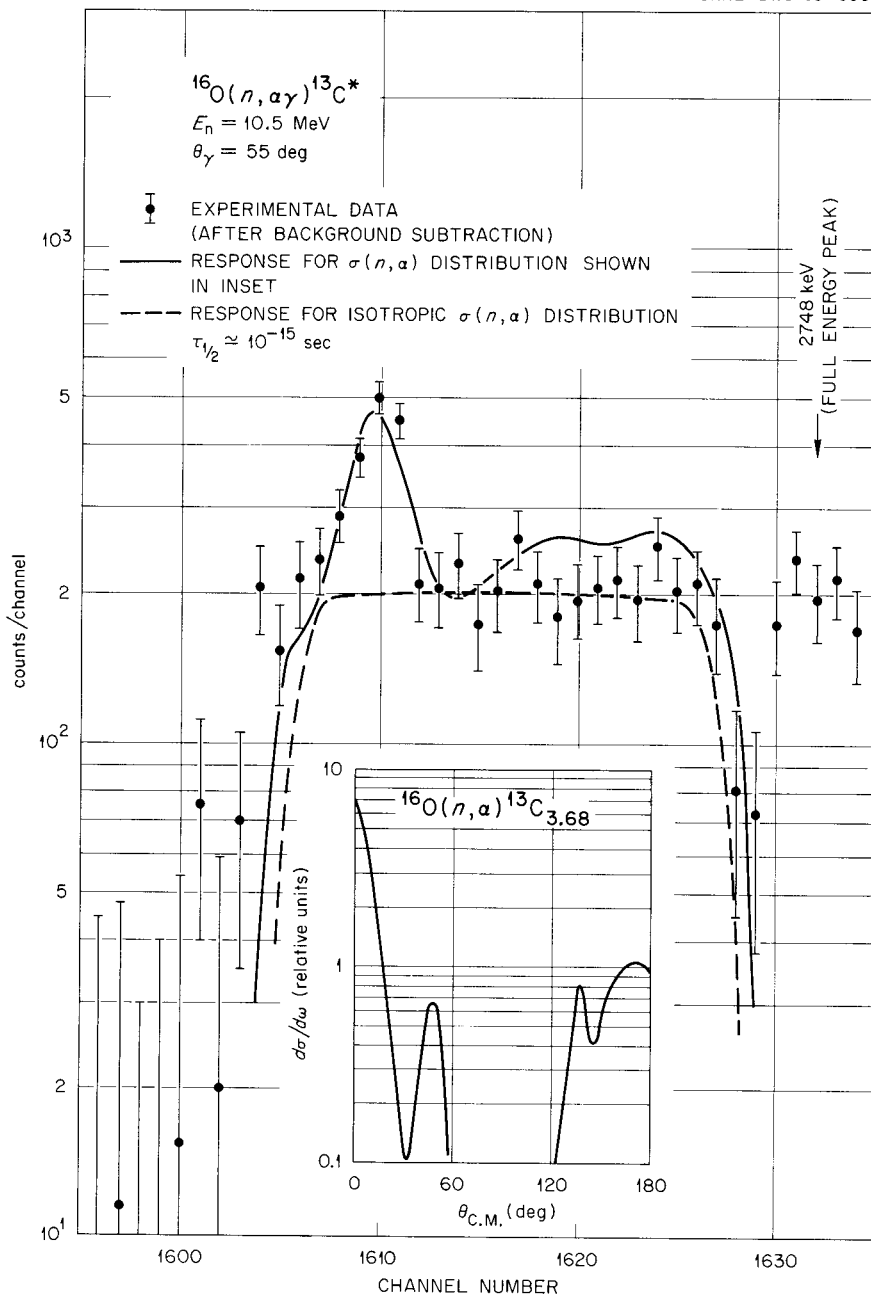


Fig. 1.18.2. Details of the Spectrum of Gamma Rays for 10.5-MeV Neutron Bombardment of ^{16}O , Showing the Response Associated with the Double Escape Peak of the 3.68-MeV Gamma Ray. The Compton background has been subtracted, and the error bars include the effect of the subtraction. The solid curve is the response calculated for 3.68-MeV radiation from the 3.68-MeV state in ^{13}C if the half-life of this state is 10^{-15} sec and the $^{16}\text{O}(n, \alpha)$ angular distribution is that shown in the inset. The dashed curve is the response calculated assuming an isotropic $^{16}\text{O}(n, \alpha)$ distribution. The peak labeled "2748 keV full energy" is due to deexcitation of the 8.88-MeV excited state in ^{16}O .

References

- ¹Research sponsored by the Defense Atomic Support Agency under Task No. PC068.
- ²J. K. Dickens and F. G. Perey, sect. 1.16, this report.
- ³F. Ajzenberg-Selove and T. Lauritsen, *Nucl. Phys.* **11**, 1 (1959).
- ⁴F. Riess *et al.*, *Phys. Rev.* **176**, 1140 (1968).
- ⁵H. E. Hall and T. W. Bonner, *Nucl. Phys.* **14**, 295 (1959).
- ⁶A. B. Smith, *Compilation of Requests for Nuclear Cross-Section Measurements*, WASH-1078 [EANDC (US)-103 "U"], Argonne National Laboratory (June 1967).

1.19 (n,xy) STUDIES ON SAMPLES OF ALUMINUM, SILICON, AND IRON FOR $5.5 \leq E_n \leq 11 \text{ MeV}^1$

J. K. Dickens F. G. Perey

The gamma rays produced by neutron interaction with nuclei of aluminum, silicon, and iron are being studied for neutron bombarding energies between 5.5 and 11 MeV. Spectra obtained thus far are summarized in Table 1.19.1. These data are being reduced to differential cross sections; preliminary results for the 1.78-MeV gamma transition indicate good agreement with differential cross sections previously obtained in the overlapping energy region of 5.5 to 7.5 MeV.² The work is pertinent to requests 65, 66, 71, 100, 101, 102, and 103 of WASH-1078.³

References

- ¹Research sponsored by the Defense Atomic Support Agency under Task No. PC068.
- ²D. M. Drake, J. C. Hopkins, C. S. Young, H. Conde, and A. Sattler, private communication to be published).
- ³A. B. Smith, *Compilation of Requests for Nuclear Cross-Section Measurements*, WASH-1078 [EANDC(US)-103 "U"], Argonne National Laboratory (June 1967).

Table 1.19.1. Compilation of Gamma-Ray Spectra Obtained for (n,xy) Reactions Produced by Neutron Interaction with Natural Samples of Aluminum, Silicon, and Iron

E_n (MeV)	θ_γ (deg)	Aluminum	Silicon	Iron
5.5	55	x	x	x
	90		x	x
6.0	55	x	x	x
	6.5			
6.5	55	x	x	x
	75	x	x	x
	90	x	x	x
7.0	55	x	x	x
	7.5			
7.5	35	x	x	x
	55	x	x	x
	75	x	x	x
	90	x	x	x
8.0	55	x	x	x
	8.6			
8.6	55	x	x	x
	90	x	x	x
9.0	55	x	x	x
	90	x		x
10.5	55			x
	90			x
11.0	55	x	x	

1.20 (n,xy) STUDIES ON SAMPLES OF SODIUM, CHROMIUM, AND NICKEL FOR $E_n = 7.5 \text{ MeV}^1$

J. K. Dickens F. G. Perey

We have initiated experiments to obtain gamma-ray production cross sections related to neutron interaction with nuclei of sodium, chromium, and nickel. Gamma-ray spectra have been obtained for $\theta_\gamma = 55^\circ$, $E_n = 7.5 \text{ MeV}$ for samples of Na, ^{nat}Cr , ^{52}Cr , ^{nat}Ni , and ^{60}Ni . The work is pertinent to requests 60, 88, 115, and 116 of WASH-1078.² Study of these spectra indicates that the concurrent use of samples of separated isotopes (^{52}Cr and ^{60}Ni) is required for accurate analysis of the spectra obtained using the samples of natural abundance. We intend to continue this study for E_n between 5 and 11 MeV and other scattering angles.

References

¹Research sponsored by the Defense Atomic Support Agency under Task No. PC068.

²A. B. Smith, *Compilation of Requests for Nuclear Cross-Section Measurements*, WASH-1078 [EANDC(US)-103 "U"], Argonne National Laboratory (June 1967).

1.21 11-MeV PROTON OPTICAL-MODEL ANALYSIS¹

C. M. Pery² F. G. Pery
J. K. Dickens R. J. Silva³

An optical-model analysis of elastic scattering of 11-MeV protons from 24 nuclei in the mass range ⁴⁵Sc to ⁷⁶Ge is presented. The data analyzed include 18 angular distributions which we have measured and the previously published 10.5-MeV elastic polarization data. An average set of geometrical parameters is determined for the data, and the real radius parameter of this potential is substantially larger than normally

used at higher energies. The analysis performed with a fixed geometry, but allowing the well depths to be readjusted independently for each nucleus, reveals a very smooth dependence of the real well depth as a function of mass number. However, the real well depths fail to follow the expected isospin dependence of the optical potential.

References

¹Abstract of *Phys. Rev.* **175**, 1460 (1968).

²Consultant.

³Oak Ridge Associated Universities, Oak Ridge, Tenn.

1.22 THE ^{64,66,68}Zn(*d,n*)^{65,67,69}Ga REACTIONS

R. G. Couch¹ J. A. Biggerstaff²
F. G. Pery S. Raman³

The (*d,n*) reactions on ^{64,66,68}Zn have been studied by the time-of-flight method. A 10-MeV

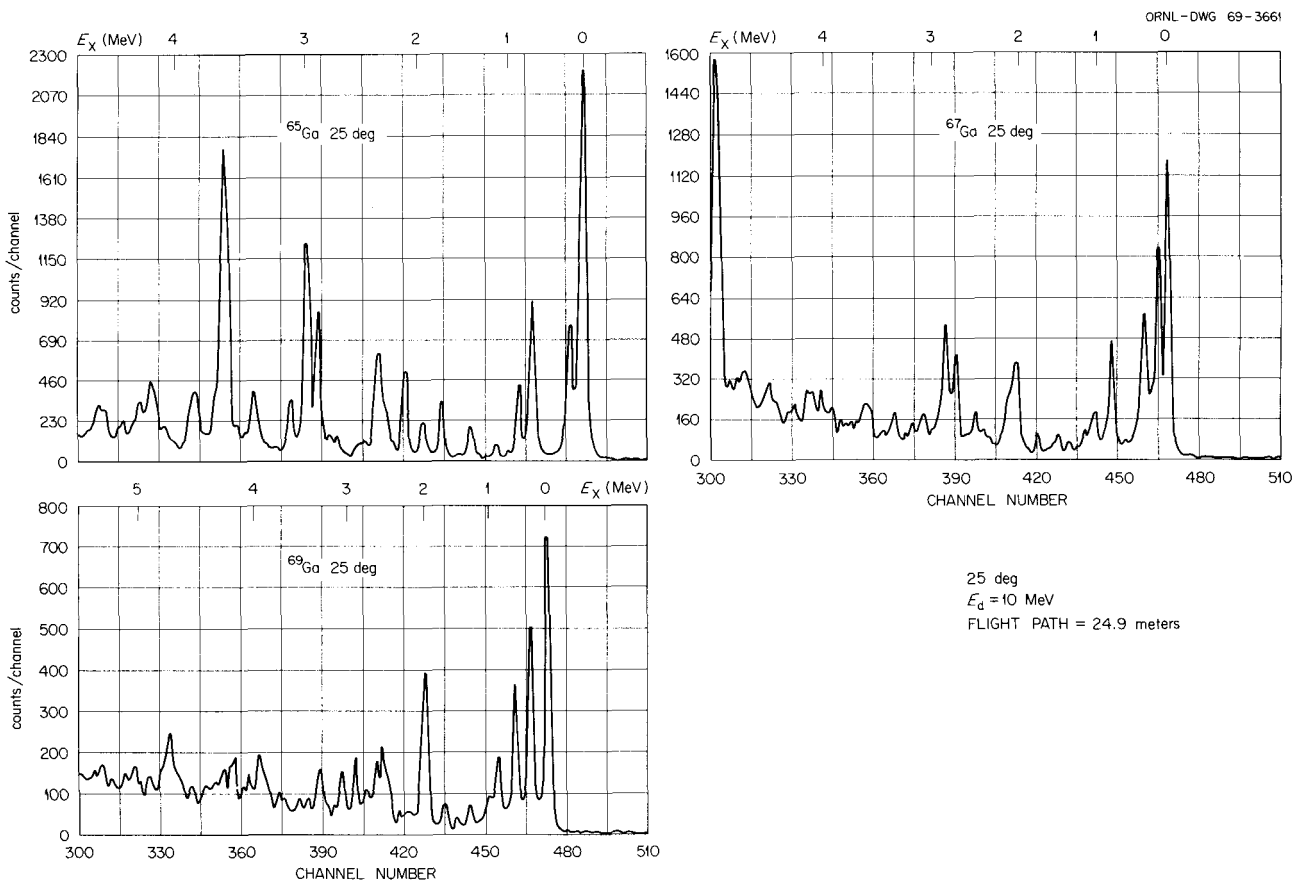


Fig. 1.22.1. Typical Neutron Time-of-Flight Spectra.

pulsed deuteron beam from the ORNL tandem Van de Graaff was used. Absolute differential cross sections were measured in the range from 18 to 70°. Several previously unreported levels were excited by this reaction. As shown in Fig. 1.22.1, they are at 1.344 and 3.046 MeV in ^{65}Ga , 2.531 and 2.851 MeV in ^{67}Ga , and 2.932 and 3.092 MeV in ^{69}Ga . The only known levels below 1.5 MeV excitation energy which were not seen are those at 0.905 and 1.450 MeV in ^{67}Ga .

A DWBA analysis was performed. In order to reproduce the angular distributions it was necessary to include finite-range and nonlocality corrections. Similarities were observed in the level schemes of the three residual nuclei. Although the spins of the levels cannot be determined, the l transfers observed indicate that the order of the spins for the first six levels in each nucleus may be the same.

References

¹Oak Ridge Graduate Fellow from Northwestern University.

²Physics Division.

³Nuclear Data Project of Director's Division.

1.23 MEASUREMENTS OF (d,n) REACTIONS ON ^{58}Ni , ^{60}Ni , ^{62}Ni , AND ^{64}Ni AT 5 AND 10 MeV¹

A. L. Marusak²

Absolute differential cross sections for $^{58}\text{Ni}(d,n)^{59}\text{Cu}$, $^{60}\text{Ni}(d,n)^{61}\text{Cu}$, $^{62}\text{Ni}(d,n)^{63}\text{Cu}$, and $^{64}\text{Ni}(d,n)^{65}\text{Cu}$ at 5 and 10 MeV were measured by time-of-flight techniques in order to obtain energy levels, l values, and spectroscopic strengths for the odd- A copper isotopes, and in order to compare these results with those obtained from the ($^3\text{He},d$) and (α,t) proton stripping reactions.

Pulsed deuteron beams with pulses of 1 nsec FWHM and currents of 1 to 2 μA were obtained from the Oak Ridge National Laboratory 5.5-MV Van de Graaff and the Tandem Van de Graaff accelerators. Neutrons were detected in 2-in.-thick liquid scintillators optically coupled to phototubes. Gamma rays were discriminated against to reduce background, and the deuteron beam was monitored by measuring elastically scattered

deuterons with a silicon surface-barrier detector. Measurements were made at angles ranging from 15 to 120° with flight paths varying from 7 to 34 m. Flight times for ground-state neutrons from $^{58}\text{Ni}(d,n)^{59}\text{Cu}$ were measured with a resolution of about 2 nsec.

All data were accumulated in a PDP-7 computer. Peak areas and centroids were extracted by means of a light pen which interacted with the PDP-7 by detecting light from an oscilloscope display. Absolute efficiency of the neutron detectors was calculated with a Monte Carlo computer program.

Angular distributions were compared with predictions of DWBA theory using optical-model potentials of the Woods-Saxon form, taking into account nonlocality, spin-orbit terms, and finite-range effects in the (p,n) interaction. Optical-model parameters were obtained from elastic scattering of deuterons on ^{60}Ni . Angular distributions predicted by DWBA analysis agreed well with the 10-MeV data but poorly with the 5-MeV data.

Spectroscopic strengths were obtained for 14 levels in ^{59}Cu , 19 levels in ^{61}Cu , 10 levels in ^{63}Cu , and 9 levels in ^{65}Cu . Agreement with spectroscopic strengths obtained from ($^3\text{He},d$) measurements was good.

Relative spectroscopic strengths of the first few low-lying levels in the odd- A copper isotopes are in marked disagreement with those predicted by the simple excited-core model, but in fair agreement with predictions of more extended models.

References

¹Abstract of ORNL-TM-2472 (in press).

²Present address: Los Alamos Scientific Laboratory, Los Alamos, N.M.

1.24 ^{120}Sn OPTICAL-MODEL ANALYSIS

F. G. Perey T. A. Love
F. E. Bertrand N. Baron¹
J. K. Dickens

Tin-120 is a frequent target for the study of proton optical-model parameters. We performed some measurements² on this nucleus in order to obtain more complete data in the energy range 20 to 40 MeV. We have completed an optical-

model analysis of all of the data on ^{120}Sn from 10 to 40 MeV. Using the optical-model search code GENOA, all of the data from 14.5 to 40 MeV are well reproduced by the following potential:

$$\begin{aligned} V_S &= 60.93 - 0.322 E, \\ r_S &= 1.184 \text{ F}, \\ a_S &= 0.726 \text{ F}, \\ W_D &= 15.92 - 0.525 E + 0.00665 E^2 \text{ MeV}, \\ W_S &= -5.92 + 0.498 E - 0.00618 E^2 \text{ MeV}, \\ V_D &= 1.289 \text{ F}, \\ a_D &= 0.705 \text{ F}, \end{aligned}$$

$$\begin{aligned} V_{SO} &= 6.17 \text{ MeV}, \\ r_{SO} &= 1.102 \text{ F}, \\ a_{SO} &= 0.729 \text{ F}. \end{aligned}$$

The quality of the fit is shown in Figs. 1.24.1, 1.24.2, and 1.24.3. The elastic scattering data at 9.8 MeV were rather poorly fitted by the above potential, as shown by the dashed curve in Fig. 1.24.4. However, good agreement with the data was obtained if one only allowed the imaginary diffuseness, a_D , to decrease from 0.705 to 0.53 F. Various attempts were made to study the varia-

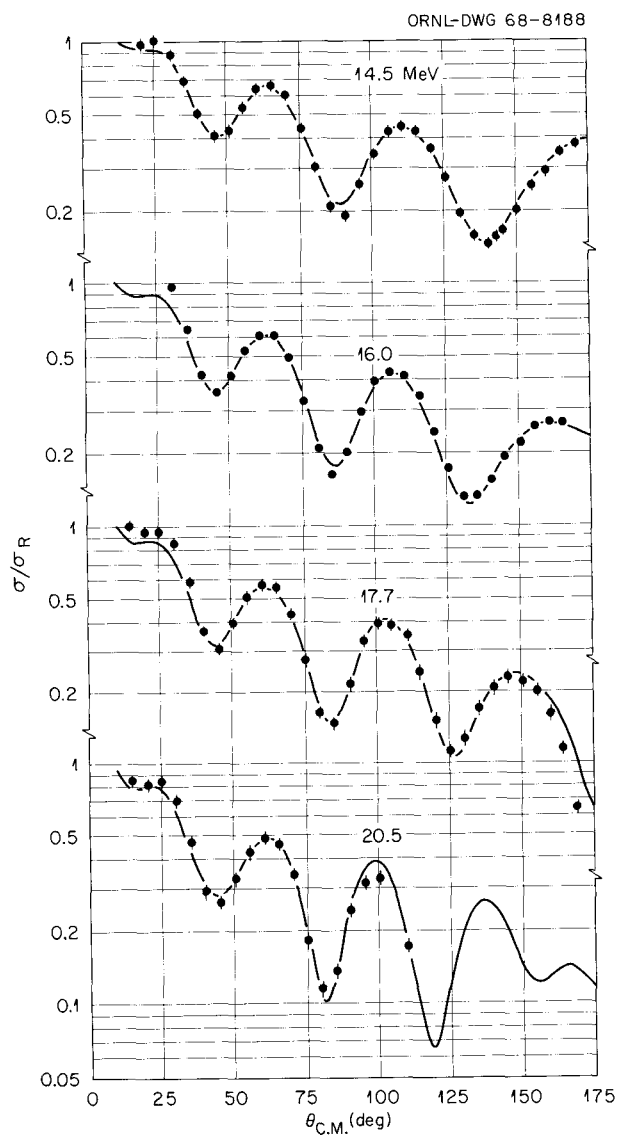


Fig. 1.24.1. Optical-Model Fits to the Elastic Scattering of Protons from ^{120}Sn .

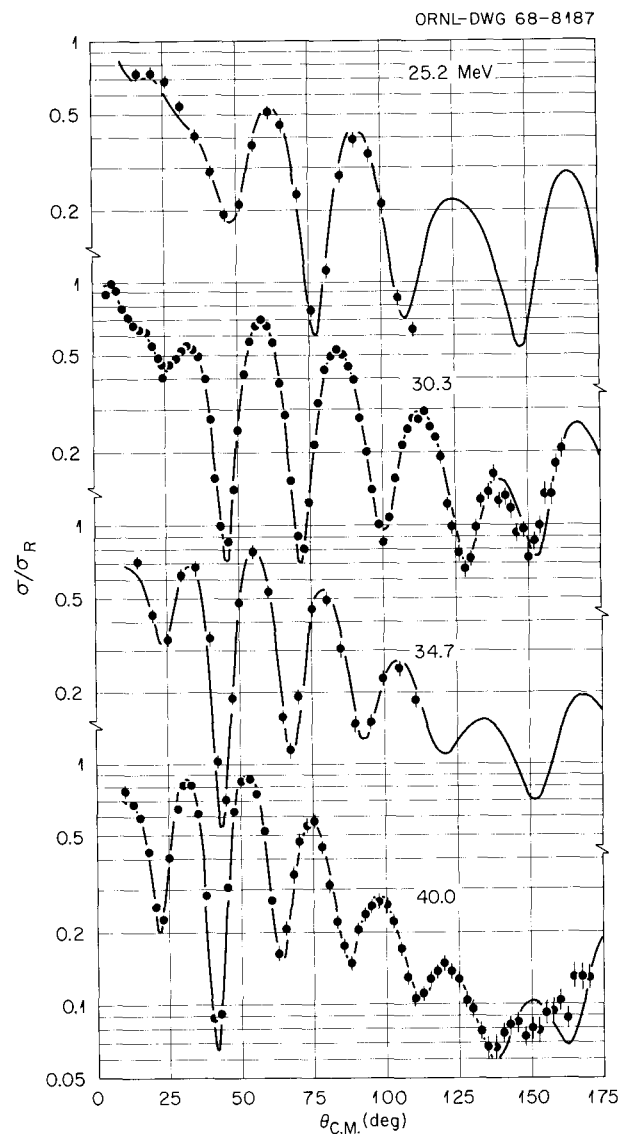


Fig. 1.24.2. Optical-Model Fits to the Elastic Scattering of Protons from ^{120}Sn .

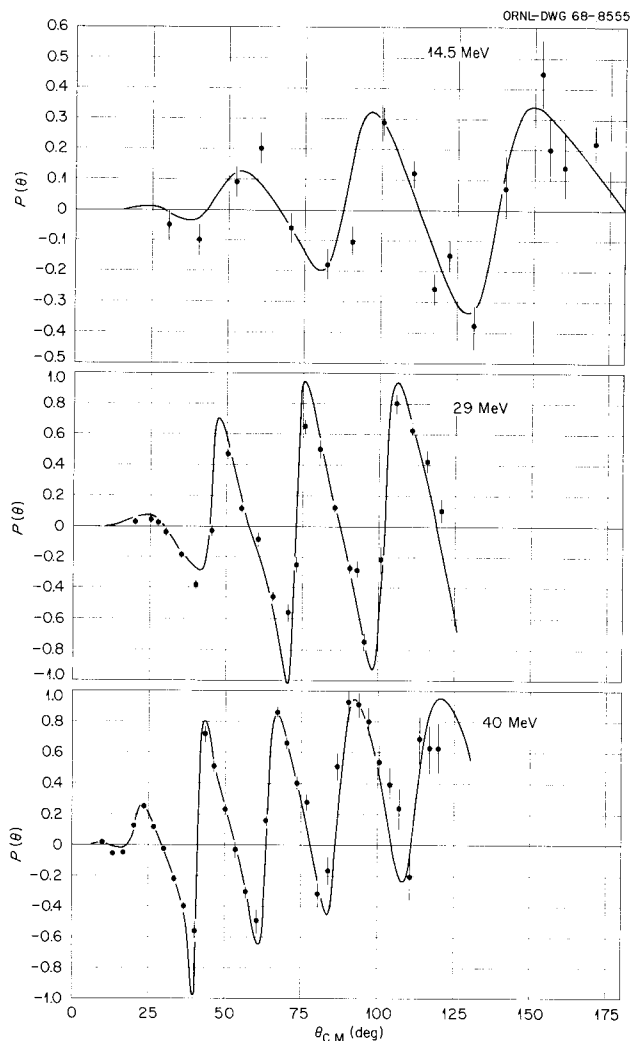


Fig. 1.24.3. Optical-Model Fits to the Polarization of Protons Elastically Scattered from ^{120}Sn .

tion of the geometrical parameters as a function of energy, but they were unsuccessful in yielding convincing systematic changes for energies greater than 10 MeV.

The observed change in a_D for low energy is supported by some recent studies³ of the reaction cross section on the tin isotope between 2.5 and 5.5 MeV, which required an imaginary diffuseness a_D of 0.25 F.

References

¹National Aeronautics and Space Administration, Lewis Research Center, Cleveland, Ohio.

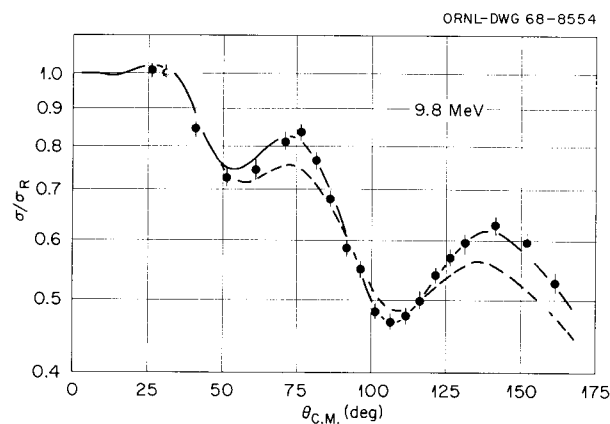


Fig. 1.24.4. Optical-Model Fit to the Elastic Scattering of 9.8 MeV Protons from ^{120}Sn . The dashed curve is the fit predicted from the analysis at higher energy and the full curve the fit when the imaginary diffuseness is reduced from 0.705 to 0.53 F.

²F. E. Bertrand *et al.*, *Elastic and Inelastic Scattering of Protons from ^{120}Sn for $E_p = 20.6, 25.2, 30.6, \text{ and } 36.2 \text{ MeV}$: Tabulated Differential Cross Sections*, ORNL-4252 (May 1968).

³C. H. Johnson and R. L. Kernell, private communication and to be published.

1.25 ^{60}Ni OPTICAL-MODEL ANALYSIS

C. M. Perey¹

F. G. Perey

Various recent analyses of proton elastic scattering seem to indicate that the geometrical parameters of the effective local optical-model potential may vary as a function of bombarding energy. Since most neutron optical-model analyses are performed at an energy lower than the proton analyses, this fact may explain why the neutron and proton optical-model potentials are not compatible with the simple isotopic spin dependence normally found from proton optical-model analyses. In an effort to understand better the optical-model potential for nucleon scattering and, in particular, the relationship between neutron and proton optical-model potentials, we are performing an extensive investigation of the optical-model parameter space for proton scattering from ^{60}Ni as a function of energy from 11 to 40 MeV. The nucleus ^{60}Ni was selected because it is a typical middle-weight nucleus for which there are considerable complete sets of proton scattering data, differential cross

section and polarization, and its z value is low enough to allow meaningful analyses to be performed at incident proton energies which overlap the neutron data energy range.

Reference

¹Consultant.

1.26 MEASUREMENTS OF THE LIFETIMES OF ISOMERS OF ⁹²Nb AND ⁹⁴Nb

R. Kuebbing¹ E. Eichler²
J. K. Dickens

We have continued our studies of the reactions $Zr(p,n\gamma)Nb$ and $Mo(p,n\gamma)Tc$, which were first reported two years ago.³ The object of these

studies is to deduce the energy level structures of the residual nuclei and to compare these level structures with theoretical predictions obtained from the nuclear shell model. Two lifetime measurements in the niobium nuclei have been made. Both of these measurements concern transitions between low-spin negative parity levels (simply described by a wave function consisting principally of the odd neutron in a $d_{5/2}$ orbit and the odd proton in a $p_{1/2}$ orbit) and low-spin positive parity levels (odd neutron in $d_{5/2}$ orbit as before, but odd proton in $g_{9/2}$ orbit).

The experiment used a pulsed proton beam from the ORNL 6-MV Van de Graaff. The time response for the gamma ray of interest was obtained, and details of the experimental procedure have been published.⁴ Figure 1.26.1 shows the spectrum obtained for the 99.4-keV transition in ⁹⁴Nb.

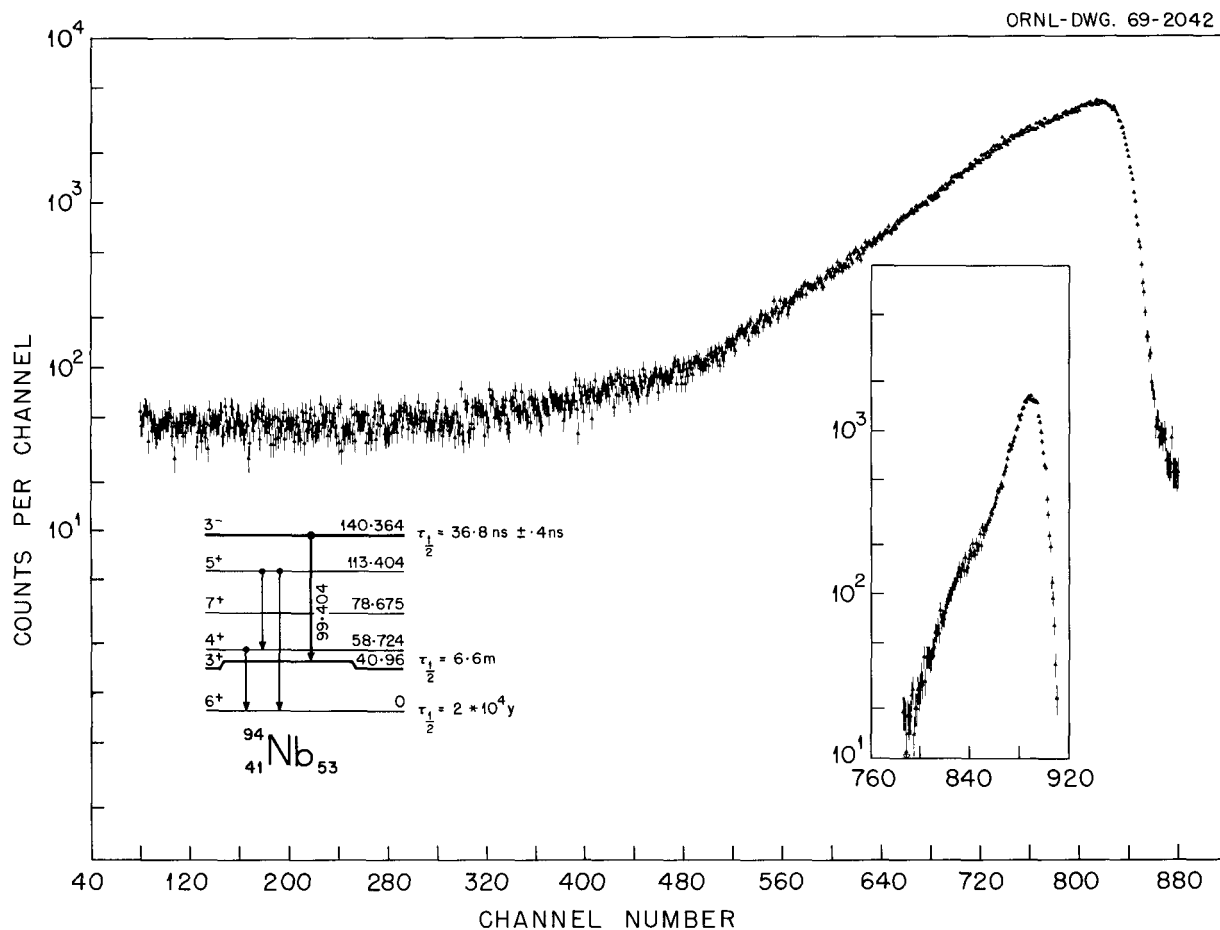


Fig. 1.26.1. Time Response for the 99.4-keV Transition in ⁹⁴Nb. The spectrum consists principally of three components: (a) prompt events, (b) time-independent background events, and (c) 99.4-keV gamma events of interest. The insert shows the time response obtained for prompt events.

The measured half-life is 36.8 ± 0.4 nsec for the 140.4-keV level of ^{94}Nb . A similar experiment for the 91-keV transition in ^{92}Nb yielded a half-life of 5.2 ± 0.7 μsec , which is in good agreement with the previously reported value⁵ of 5.9 ± 0.5 μsec , for the 226-keV second excited state in ^{92}Nb .

References

¹Graduate student, Physics Department, Case Western Reserve University, Cleveland, Ohio.

²Chemistry Division.

³J. K. Dickens *et al.*, *Neutron Phys. Div. Ann. Progr. Rept. May 31, 1967*, ORNL-4134, p. 22; see also J. K. Dickens *et al.*, *Neutron Phys. Div. Ann. Progr. Rept. May 31, 1968*, ORNL-4280, p. 22.

⁴E. Eichler *et al.*, *Nucl. Phys.* **A120**, 622 (1968).

⁵R. B. Duffield and S. H. Vegors, Jr., *Phys. Rev.* **112**, 1958 (1958).

1.27 THE EXPERIMENTAL ASPECTS OF NEUTRON WAVE AND PULSE PROPAGATION¹

R. B. Perez

The purpose of this paper is to discuss how a neutron wave or pulse experiment is performed. This class of experimentation deals with the determination of the damping coefficient and phase shift of a disturbance of the neutron field produced at one of the boundaries of the assembly. The

necessary localized source of thermal neutrons can be obtained by a variety of means, such as the thermal column of a reactor or from the combination of a small accelerator and a thermalizer tank. The time-dependent behavior of the source is impressed upon the neutron source by several methods like pulsing the reactor, neutron choppers, or electrical modulation of the ion beam in the accelerator. Standard detection techniques and electronic equipment are used in this field of experimentation. Careful consideration has to be given to proper normalization of the data obtained at the various frequencies, with the usual precautions regarding counting losses and statistics. To obtain the real and imaginary parts of the inverse complex relaxation length, $\alpha(\omega)$ and $\xi(\omega)$, respectively (ω = angular frequency of the wave), one fits the plots of the amplitude and phase shift vs distance traveled by the wave to exponential and linear functions respectively. The end result is the measurement of the inverse complex relaxation length, $k(\omega) = \alpha(\omega) + i\xi(\omega)$, as a function of the frequency, that is, the dispersion law of the nuclear assembly under investigation.

The comparison of the experimental dispersion law with the one obtained from a given theoretical model allows the determination of relevant parameters of neutron physics.

Reference

¹Abstract of an invited paper published in *Transactions of the American Nuclear Society*, Toronto, June 10–13, 1968, p. 41.

2. Reactor and Weapons Radiation Shielding

2.0 INTRODUCTION

C. E. Clifford

The objectives of the ORNL shielding program, which is largely supported by the Space Nuclear Auxiliary Power (SNAP) project and the Defense Atomic Support Agency (DASA), are the development of basic methods for solving radiation transport problems, the testing of these methods by comparison with experimental results, and the development of data and techniques that engineers can use with a high degree of confidence in designing shields to meet their requirements. Further, the intent is to provide design techniques that are general in nature so that shields can be optimized not only with respect to weight, as required for the SNAP program, but also with respect to cost, radiation heating, radiation damage, or any other requirement or constraint that may be imposed by the design engineers.

The experimental effort in support of the program has been concerned primarily with neutron and gamma-ray transport in heavy-metal shields and with the measuring of secondary gamma rays produced in various shielding materials. The majority of the effort at the TSF has been in support of the SNAP shielding program. About one-fourth of the effort has been supported by DASA and has been concerned with the measurement of secondary gamma-ray spectra in good-geometry experiments, and one month of TSF time has been devoted to LMFBR shielding problems. A Benjamin-type neutron spectrometer has been put into operation at the TSF, which permits a measurement of neutron spectra between 2 MeV and 10 keV. In addition to work at the TSF, the program has supported measurements of the secondary gamma rays produced in tungsten and ^{238}U for a number of broad neutron energy groups between thermal and 100 keV at the Gulf General Atomic linac facility.

The nuclear data evaluation program has been concerned with the application of the previously developed gamma-ray cascade model to the calculation of neutron-energy-dependent capture gamma-ray production cross sections. Thermal capture gamma-ray spectra for many elements have been calculated, the capture gamma-ray spectra from copper for epithermal neutrons have been calculated and found to compare well with measurements, and the spectrum for tungsten has been calculated and compared with the TSF and GGA results. The calculational ability is being extended to include the generation of inelastic gamma-ray yields and has been extended to provide the calculation of the differential cross sections for scattering and reactions which proceed through a compound nucleus. Calculated results for tungsten and copper agreed quite well. The calculation of the neutron capture gamma-ray yield for ^{238}U is now in progress. Reliable data for a comparison of absolute intensities in ^{238}U are lacking. Analysis of thermal capture gamma-ray spectra in good geometry at the TSF and the GGA measurements can be expected to improve this situation.

During the past year the emphasis in the theoretical shielding work was on the development of time-dependent discrete ordinates codes and the development of a multigroup Monte Carlo code, MORSE. Significant improvements in methods have resulted from the application of the discrete ordinates and Monte Carlo methods to problems of particular interest. The one- and two-dimensional discrete ordinates codes ANISN and DOT were greatly improved in efficiency. A procedure has been developed which optimizes, with respect to minimum weight, shields of lithium hydride and heavy metal for the SNAP-8 reactor for a manned space station concept. Results from DOT and ANISN calculations have been compared extensively with experimental data from the Tower Shielding Facility experimental program. In the

DASA program, which is concerned with protection against radiation from nuclear weapons bursts, DOT calculations were completed for steady-state weapons radiation transport from neutron sources at a number of altitudes relatively near to the air-ground interface. This completed the description of the radiation environment at the ground surface for all weapons burst altitudes. The DOT code was also used to calculate radiation transport in silo configurations and to evaluate the shielding of the AURORA accelerator which is being designed for DASA use.

Monte Carlo development work included a revision of the 05R programs to provide additional features such as albedo scattering, time dependence, better banking logic, and more efficient cross-section manipulation. The revised code 06R was used as the starting point for the development of the multigroup Monte Carlo code. The multigroup Monte Carlo code was developed because it offers the possibility of solving three-dimensional problems with the advantages that can be gained through the use of the multigroup cross-section sets. These advantages include the availability of directly coupled neutron and secondary gamma-ray group cross-section sets, an adjoint capability, and additional options in biasing. It has been demonstrated that the multigroup Monte Carlo code gives results that are comparable with those given by ANISN and DOT and that running times are less when multigroup cross sections are used rather than the 06R point cross-section data. Monte Carlo codes have also been used to predict the experimental results obtained at the Tower Shielding Facility. The neutron spectra transmitted through lithium hydride shields up to 30 cm thick were calculated. Other Monte Carlo calculations were performed to carry out a comprehensive study of time-dependent neutron and secondary gamma-ray transport through the atmosphere for the case of a source at several altitudes.

2.1 REACTOR AND WEAPONS RADIATION SHIELDING PROGRAM AT THE TOWER SHIELDING FACILITY

F. J. Muckenthaler	K. M. Henry
J. L. Hull	L. B. Holland
J. J. Manning	L. W. Gilley
J. W. Paul	

The experimental program was continued at the TSF to generate accurate data for use in evaluation

of the current techniques for obtaining solutions to radiation transport problems. The evaluation of the techniques can best be realized through a comparison of the measured and calculated neutron and gamma-ray energy spectra.

The majority of the measurements taken during the past year have been concerned with the SNAP shielding program. The work has included additional measurements of the neutron spectra being emitted by the SNAP reactor; also, dose profiles beneath the reactor were obtained in order to check the accuracy of the predicted spatial distribution of the neutron environment.

Following this, measurements were made of the neutron spectra above 1 MeV transmitted through typical SNAP shielding materials placed directly beneath the SNAP reactor. The measurements were taken with the NE-213 spectrometer at a distance of approximately 28 ft below the reactor. The detector was collimated and surrounded by a lead and water shield. Additional shielding was provided by placing the detector and its collimator on the bottom of the drained reactor handling pool, which is 25 ft deep and 20 ft square. The pool was covered with a slab of concrete 2 ft thick, and the reactor and shield were viewed through a hole in the slab approximately 5 ft in diameter.

Additional shielding was provided between the hole through the slab and the shield beneath the reactor in order to prevent scattered neutrons from reaching the detector. Shielding samples for which neutron spectra measurements were obtained included slabs of lead, ^{238}U , tungsten powder, Hevimet, and lithium hydride and laminated slabs of lead, lithium hydride, and ^{238}U . The heavy-metal samples varied in thickness from 2 to 6 in., and the lithium hydride samples were 6 and 12 in. thick.

In addition to measurements on shielding samples beneath the SNAP reactor, gamma-ray spectra measurements from thin samples¹ were made in a "good" geometry configuration. Samples used in these measurements have included ^{235}U , for which thermal capture and fission gamma-ray spectra were measured. Uranium-238 was also measured,² along with lead, Hevimet, nickel, and iron; analysis has been performed with the discrete-ordinates method.³

The DASA experimental program at the TSF is also concerned with measurement of gamma-ray spectra in good geometry for three neutron spectra obtained from the TSR-II reactor. The samples were, in most cases, thin, and 14 elements were measured. The experimental results have been analyzed and reported in part by Maerker.¹

A short experiment, which consisted of the measurement of neutron spectra through samples up to 2 ft thick of sodium and iron and through arrays of iron rods immersed in sodium, was also completed in support of the LMFBR program. These samples were placed beneath the SNAP reactor and were surrounded by an oil bath to eliminate scattered neutrons. Fast-neutron spectra were measured with the NE-213 spectrometer in the same geometry described previously, and, in addition, Benjamin spectrometers were beneath the samples. Measurements were obtained to aid in designing the FFTF grid plate shield which is required to minimize radiation damage.

References

¹R. E. Maerker and F. J. Muckenthaler, *Gamma-Ray Spectra Arising from Thermal-Neutron Capture in Elements Found in Soils, Concretes, and Structural Materials*, ORNL-4382 (to be published).

²See paper 2.9 of this section.

³See paper 2.22 of this section.

2.2 INTENSITIES OF GAMMA RAYS FROM THE RADIATIVE CAPTURE IN NATURAL TUNGSTEN OF NEUTRONS FROM 0.02 eV TO 100 keV^{1,2}

V. Orphan³

J. John³

This annual summary report describes the work performed on a program of capture gamma-ray measurements from October 1, 1967, through September 30, 1968, under subcontract 3032 with the Union Carbide Corporation. Yost⁴ has shown that significant changes in dose penetrating an LiH-W space reactor shield result if the epithermal capture gamma-ray spectrum differs from the thermal capture gamma-ray spectrum. Currently, thermal capture spectra are assumed in shielding calculations, even if a significant fraction of the flux is epithermal, since very few or no epithermal capture data exist. This demonstrated need for the accurate knowledge of the epithermal capture gamma-ray intensities for several space shield materials, tungsten, and depleted uranium was the principal motivation for our measurements.

Section 2 of this report describes the facility which was used at the Gulf General Atomic linac installation to measure capture gamma-ray spectra

and the experimental apparatus and measurement techniques. Section 3 contains a description of the two-parameter data acquisition and sorting computer codes. Tungsten capture gamma-ray spectra measured with a Ge(Li)-NaI spectrometer, and a description of the method employed to obtain capture gamma-ray intensities are given in Sect. 4. Finally, results are presented for the gamma-ray intensities from neutron capture in natural tungsten over the neutron energy range 0.02 eV to 100 keV.

References

¹Abstract of GA-9121 (Dec. 31, 1968).

²This work prepared under Subcontract 3032 for Union Carbide Corp. with Gulf General Atomic, Inc., San Diego, Calif.

³Gulf General Atomic, Inc., San Diego, Calif.

⁴K. J. Yost and M. Solomito, "Sensitivity of Gamma-Ray Dose Calculations to the Energy Dependence of Gamma-Ray Production Cross Sections," *Proc. Neutron Cross Sections and Technology Conference*, NBS Special Publication 299, vol. 1, p. 53 (1968).

2.3 MEASUREMENTS OF THE ABSOLUTE POWER AND FISSION DISTRIBUTION IN THE TSF-SNAP REACTOR AND COMPARISON WITH MONTE CARLO AND DISCRETE-ORDINATES CALCULATIONS^{1,2}

E. A. Straker

The relative power distribution in the TSF-SNAP Reactor was determined by scanning individual fuel elements for fission product gammas, and the absolute fission rate was determined from uranium-foil activation. Numerical integration of the fission density over the core volume gave an absolute power calibration for detectors and foils external to the core. Calculations of both the axial and radial power distributions by Monte Carlo and discrete-ordinates methods were in excellent agreement with the measured distributions.

References

¹Abstract of paper submitted to *Nuclear Applications* (March 1969).

²Abstract of ORNL-TM-2265 (Sept. 3, 1968).

2.4 COMPARISONS OF MONTE CARLO CALCULATIONS WITH MEASUREMENTS OF NEUTRON LEAKAGE FROM THE TSF-SNAP REACTOR^{1,2}

V. R. Cain

The TSF-SNAP reactor is being used at ORNL as a realistic source for investigations of the light-weight shields required for space power systems. As part of this program, experimental and analytical determinations have been made of the energy and angular distribution of neutrons leaving an area roughly equal to 10% of the reactor lower surface. The agreement between experiment and Monte Carlo calculations was found to be quite good when the reactor was described in sufficient detail in the calculations.

References

¹Abstract of ORNL-TM-2586 (to be published).

²Submitted for publication in *Nuclear Applications*.

2.5 MODIFICATIONS TO THE MONTE CARLO CODES USED TO CALCULATE POWER DISTRIBUTION AND NEUTRON LEAKAGE FROM THE TSF-SNAP REACTOR¹

K. D. Franz² V. R. Cain

Earlier calculations of power distribution and neutron leakage from the TSF-SNAP reactor assumed that a small amount of beryllium was uniformly distributed throughout the core and that the reactor control drums were fully inserted. These calculations were repeated with the distributed beryllium removed, with a central cylinder of beryllium inserted, and with two of the four control drums rotated out 30°. Listings are given of all the necessary changes in computer programs and their inputs.

References

¹Abstract of ORNL-TM-2562 (to be published).

²Computing Technology Center, Union Carbide Corp., Oak Ridge, Tenn.

2.6 FAST-NEUTRON COLLIMATOR STUDIES AND THE DESIGN OF THE TSF-SNAP CORE MAPPING COLLIMATOR^{1,2}

E. A. Straker

The Monte Carlo technique has been used to determine some general properties of fast-neutron collimators for the cases in which the sources and detectors were finite disks. Based on these results a collimator was designed to be used in determining the angular and spatial-dependent neutron leakage spectrum from the TSF-SNAP reactor with a minimum distortion of the measured results. The detector-collimator response functions were then calculated for use in a separate Monte Carlo calculation of the leakage from the SNAP core. The adequacy of the response functions was determined by comparing the measured and calculated values of detector counts for a number of PoBe source locations off the axis of the collimator.

References

¹Abstract of *Nucl. Appl.* 6, 168 (1969).

²Abstract of ORNL-TM-2299 (Aug. 26, 1968).

2.7 COMPARISONS OF DISCRETE-ORDINATES CALCULATIONS WITH NEUTRON AND GAMMA-RAY SLAB TRANSMISSION DATA FOR THE TSF-SNAP REACTOR

F. R. Mynatt¹ M. L. Gritzner¹
R. J. Rodgers¹

An important part of the theoretical program for SNAP shielding applications is the comparison of calculations with the experimental results obtained at the Tower Shielding Facility. These comparisons provide an indication of the adequacy of the basic cross-section data and the accuracy of this particular application of the transport codes.

All of the discrete-ordinates calculations were performed with the two-dimensional transport codes DOT and DOT-II. The calculations performed thus far include neutron and gamma-ray spectra calculations for a detector position approximately 28 ft below the bare reactor and also at this location with homogeneous slab shields placed directly beneath the reactor.

The bare-core power distribution calculation was performed with a 21-group cross-section library, S_{10} quadrature, and a P_2 approximation for the anisotropic scattering. The calculated power shape agreed very well with experimental data and with a Monte Carlo calculation.² Using this power shape, a subsequent calculation was performed for 30 energy groups in the range of 0.8 to 15 MeV using an S_{130} quadrature³ with a P_3 approximation for the anisotropic scattering. The absolute neutron spectrum at the detector position was then obtained from the surface angular fluxes in this high-resolution calculation using the SPACETRAN⁴ code. Figure 2.7.1 shows the results of this calculation compared with the unfolded experimental data and a Monte Carlo calculation.⁵ The agreement is generally good, but below 2 MeV the calculated results range up to 30% higher than the measurements.

Calculations also were performed for neutron spectra transmitted through homogeneous slabs of lithium hydride, depleted uranium, lead, and tung-

sten (Hevimet) slabs. The transport calculations for these slabs were all S_{130} - P_3 30-group problems which had the surface angular fluxes of the reactor as a source. The example shown in Fig. 2.7.2 is for a 12-in. slab of lithium hydride. The agreement is fairly good, with the calculation being somewhat low at the higher energies and high at the lower energies.

The gamma-ray spectrum from the bare core was calculated using 60 gamma groups with an S_{130} - P_3 approximation. The gamma source tape was obtained from the 21-neutron-group core calculation using secondary gamma yield data processed by an early version of the POPOP4 code.⁶ The gamma-ray pulse-height distribution was obtained by first calculating the absolute spectrum at the face of the 5-in. NaI crystal 28 ft below the core and then folding this with the scintillator response functions.⁷ The nonlinear amplifier response is incorporated in the transformation to the energy scale.

G-69-596

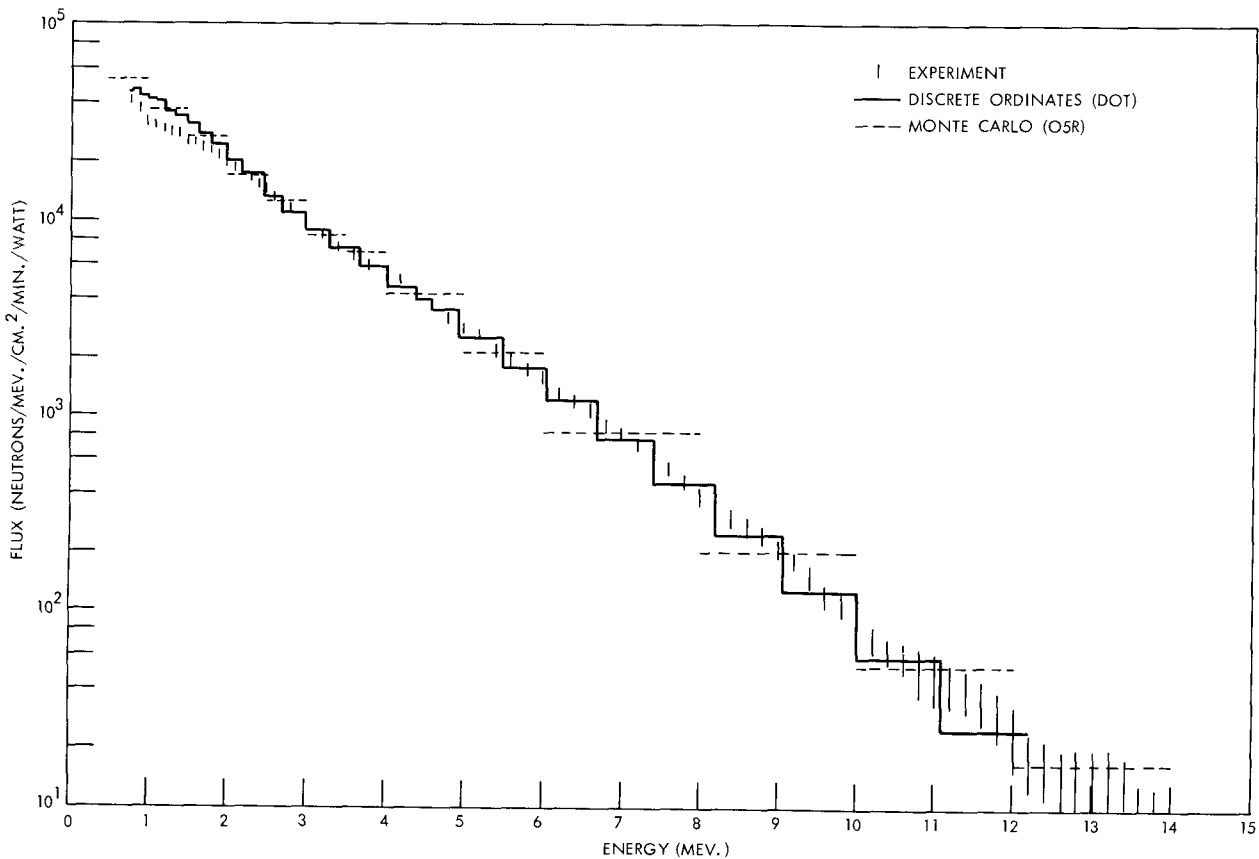


Fig. 2.7.1. Comparison of Calculations with the Measured Neutron Spectrum Below the TSF-SNAP Reactor.

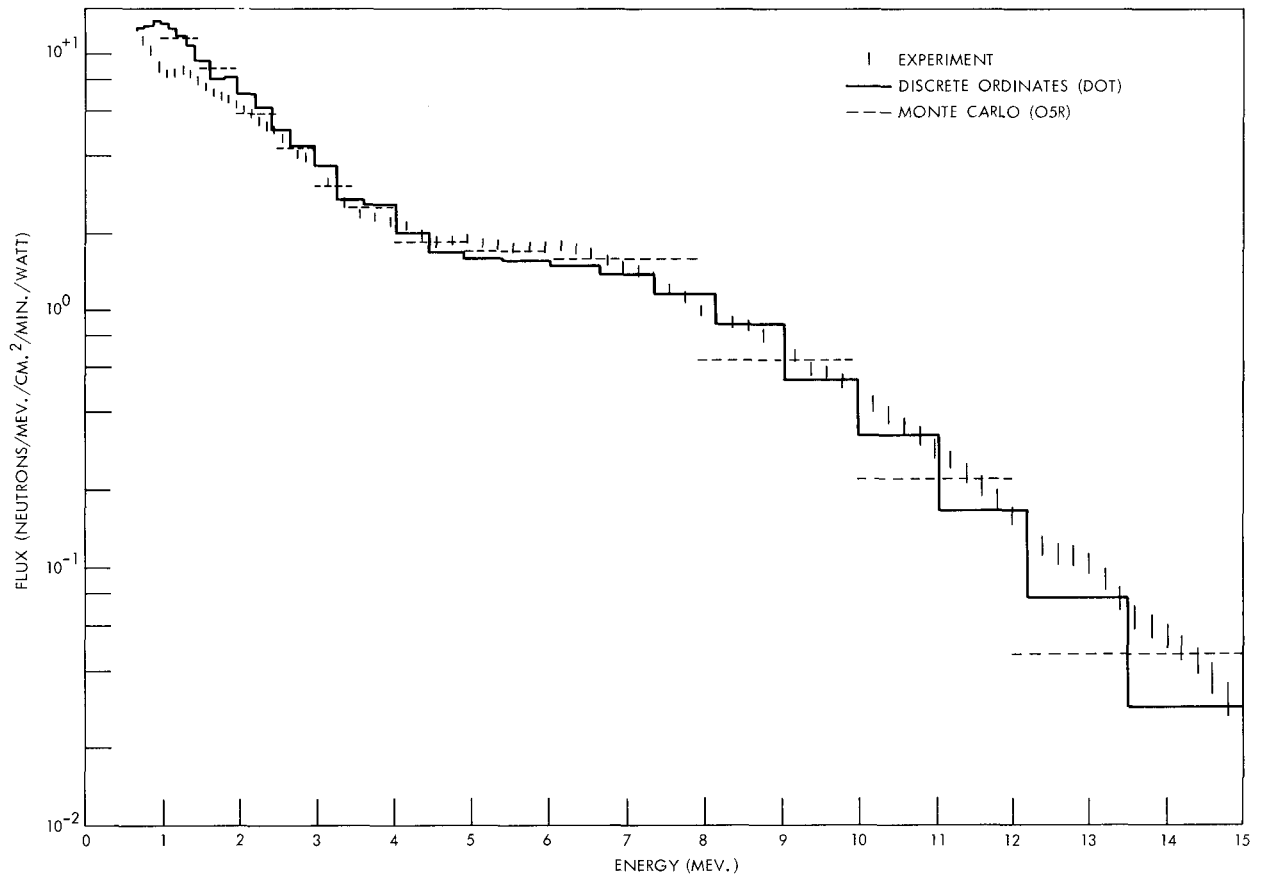


Fig. 2.7.2. Comparison of Calculated and Measured Neutron Spectra Transmitted Through 12 in. of Lithium Hydride Under the TSF-SNAP Reactor.

Figure 2.7.3 shows the comparison of calculated and measured pulse-height distributions. The disagreement at higher energies is presently thought to be due to inadequate secondary gamma-ray yield data.

Gamma-ray spectra transmitted through the slabs of depleted uranium, lead, and tungsten have been determined using $S_{130}-P_3$ coupled neutron-gamma-ray calculations (27 neutron and 60 gamma groups) with the neutron and gamma-ray angular flux distribution from the bare reactor as the source. For thick slabs the calculated results were consistently lower than measurements. For a time this was believed to be due to resonance self-shielding. However, subsequent calculations using resonance self-shielded cross sections obtained by the GAM-II

method⁸ indicated that large changes in the self-shielding result in small changes in the gamma-ray transmission. This is presently explained by the observation that most of the captures were occurring at neutron energies above the resolved resonance region, where self-shielding is not very important. It was later found that, by including both the reactor and depleted uranium slab in one problem and calculating both the perturbed fission power distribution in the reactor and in the uranium slab, the gamma-ray leakage was increased more than a factor of 2, which gave better agreement with the experiment (see Fig. 2.7.4). The disagreement in shape is partly due to the fact that a thermal neutron capture gamma-ray spectrum was used for captures at all energies.

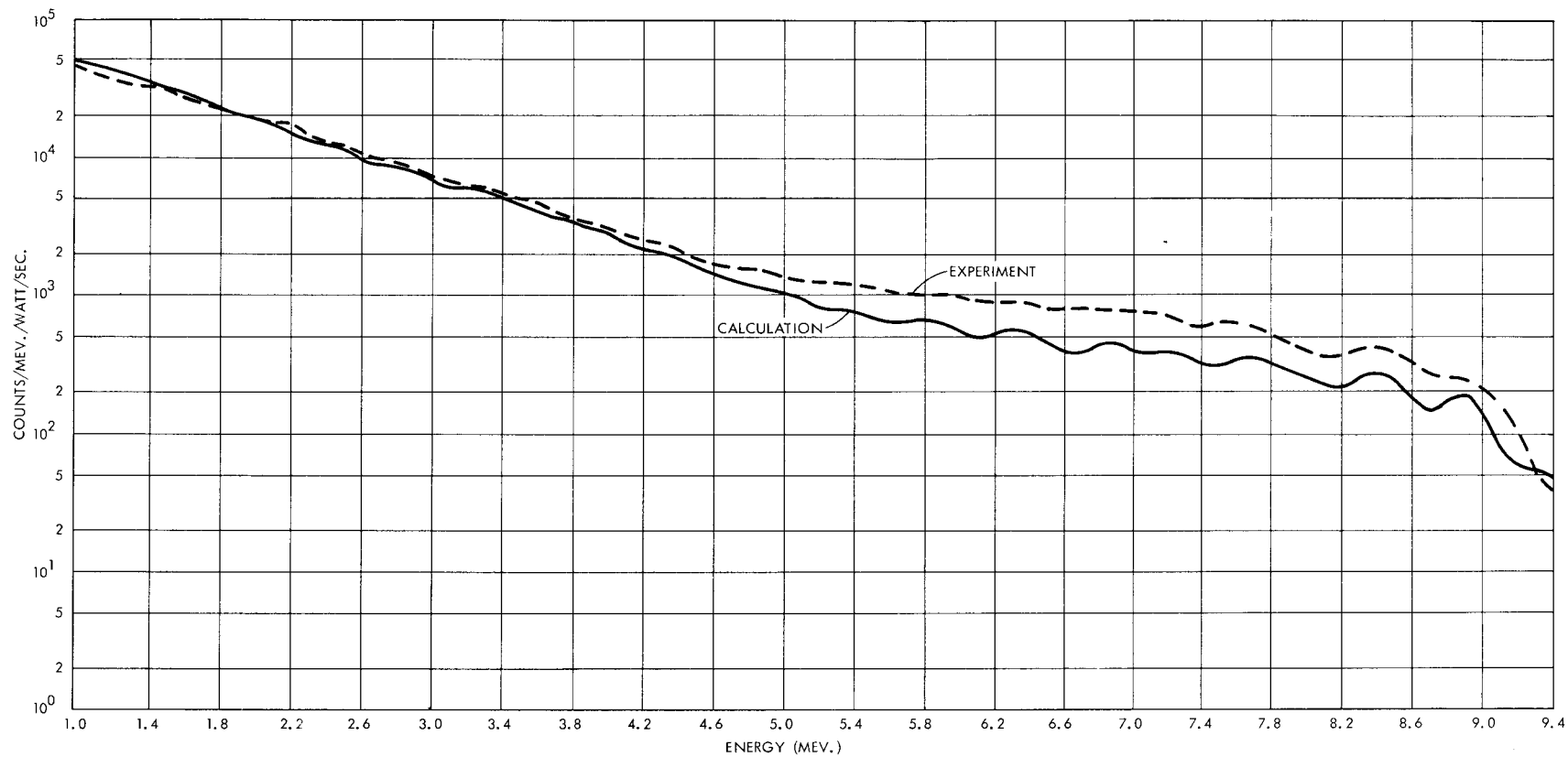


Fig. 2.7.3. Comparison of Calculated and Measured Gamma-Ray Pulse-Height Spectra Below the TSF-SNAP Reactor.

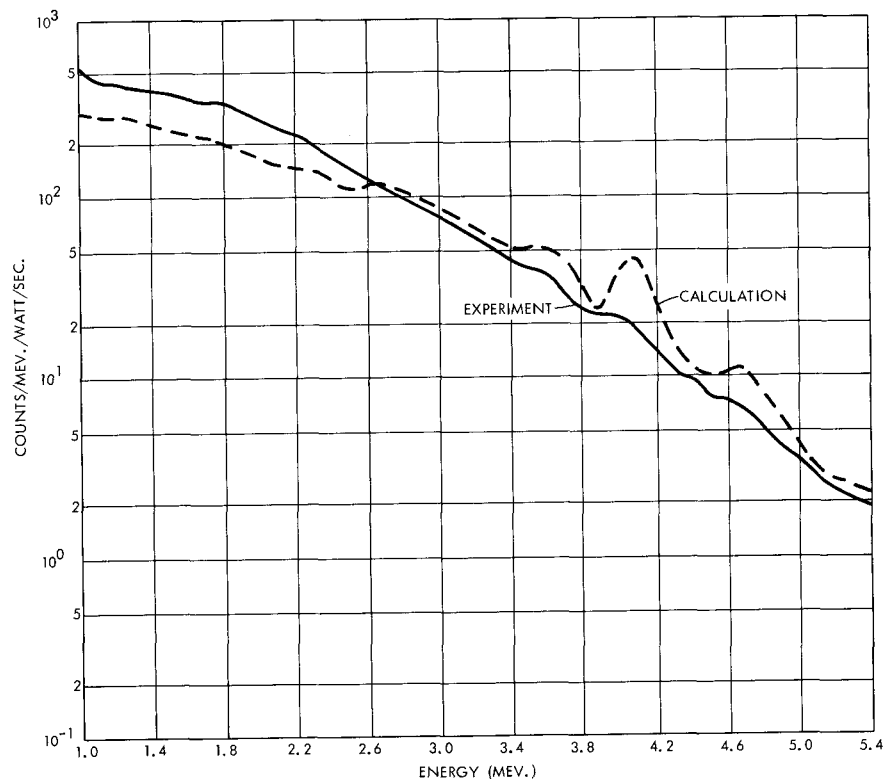


Fig. 2.7.4. Comparison of Calculated and Measured Gamma-Ray Pulse-Height Spectra Transmitted Through a $4\frac{1}{2}$ in. Depleted Uranium Slab Under the TSF-SNAP Reactor.

References

¹Computing Technology Center, Union Carbide Corp., Oak Ridge, Tenn.

²E. A. Straker, *Measurements of the Absolute Power and Fission Distribution in the TSF-SNAP Reactor and Comparison with Monte Carlo and Discrete Ordinates Calculations*, ORNL-TM-2265 (Sept. 3, 1968).

³F. R. Mynatt, F. J. Muckenthaler, and P. N. Stevens, *Development of Two-Dimensional Discrete Ordinates Transport Theory for Radiation Shielding*, CTC-INF-952 (to be published).

⁴F. R. Mynatt et al., *Neutron Phys. Div. Ann. Progr. Rept. May 31, 1967*, ORNL-4134, pp. 51-52.

⁵E. A. Straker, private communication.

⁶W. E. Ford III and D. H. Wallace, *POPOP4 - a Code for Converting Gamma-ray Spectra to Secondary Gamma-Ray Production Cross Sections*, CTC-12 (May 23, 1969).

⁷R. E. Maerker, *Neutron Phys. Div. Ann. Progr. Rept. May 31, 1967*, ORNL-4134, pp. 68-71.

⁸G. D. Joanou and J. S. Dudek, *GAM-II, a B_3 Code for the Calculation of Fast-Neutron Spectra and Associated Multigroup Constants*, GA-4265 (1963).

2.8 COMPARISON OF MONTE CARLO CALCULATIONS WITH MEASUREMENTS OF FAST-NEUTRON DOSE TRANSMITTED FROM A BEAM SOURCE THROUGH A SNAP-2 LiH SHIELD¹

V. R. Cain

K. D. Franz²

Measurements and calculations were made of fast-neutron dose rates transmitted through an LiH SNAP shield surrounded by a collar shield of iron and oil. This was done in order to evaluate the

Monte Carlo techniques used to design the experimental configurations for SNAP shielding experiments at the Tower Shielding Facility. Comparisons were made for a number of typical configurations, and the calculated and measured fast-neutron dose rates for neutrons leaving both the LiH shield and the collar shield are in excellent agreement. This establishes the validity of this technique for analyzing future experiments.

References

¹Abstract of ORNL-TM-2423 (Dec. 18, 1968).

²Computing Technology Center, Union Carbide Corp., Oak Ridge, Tenn.

2.9 EXPERIMENTAL GAMMA-RAY SPECTRA ABOVE 1 MeV FROM THERMAL-NEUTRON ABSORPTION IN ²³⁵U¹

R. S. Booth F. J. Muckenthaler

The object of this experiment was to determine the energy spectrum above 1 MeV of the total gamma intensity resulting from neutron interactions with ²³³U, ²³⁵U, ²³⁸U, and ²³⁹Pu. The incident neutron energy spectra used were: (1) the TSR-2 spectrum, (2) the TSR-2 spectrum filtered by 32 mils of cadmium, and (3) the TSR-2 spectrum filtered with 2.58 g/cm² of ¹⁰B. Presented here are the thermal-neutron gamma yield spectra for ²³⁵U.

In this experiment the sample was placed in a collimated beam of neutrons from the TSR-2, and gamma rays from the sample were observed with a collimated and shielded sodium iodide detector. The detector was placed 30 ft from the sample at a right angle to the neutron beam. This arrangement is similar to that described by Muckenthaler² with the following modifications: Smaller foils were used than in the typical Maerker experiment, and the collimator located between the sample and the detector was rebuilt. A total of 12 in. of lithium hydride encased in aluminum was placed between the sample and the detector to ensure that neutrons "born" in the sample did not reach the detector. A 4-in. thickness of lead was placed on both sides of the lithium hydride to shield from the detector all but uncollided photons from the sample. The ratio of foreground counts (sample exposed to the col-

limited reactor beam) to background counts (sample removed) was increased through additional shielding of the detector.

The thermal-neutron gamma yield spectra were determined by subtracting foreground data obtained with spectrum 2, corrected for neutron absorption above 0.4 eV, from foreground data obtained with spectrum 1 after the background data had been subtracted from both of these measurements. The absolute intensity of the thermal flux incident on the sample was determined by exposing a copper foil of the same dimensions as the sample to the same flux as was incident on the sample, measuring the resulting photon energy spectrum, and then normalizing these data to copper measurements for which the absolute thermal source was known.³ Unfolding of the data, including error estimates, was accomplished by the use of the FERD unscrambling code of Burrus.⁴

Preliminary analysis of these data is complete. Shown in Fig. 2.9.1 is the total photon energy spectrum per absorption⁵ resulting from thermal-neutron interactions with ²³⁵U during a 400-min irradiation time. Also shown are the components of the total spectrum as presented by Claiborne.⁶

References

¹This work funded by the Defense Atomic Support Agency under Subtask A2-11.037.

²F. J. Muckenthaler *et al.*, *Determination of Response Functions of a 5-in. NaI Crystal to Gamma Rays with Energies Above 1 MeV*, ORNL-4280 (October 1968).

³R. E. Maerker and F. J. Muckenthaler, *Gamma-Ray Spectra Arising from Thermal-Neutron Capture in Elements Found in Soils, Concretes, and Structural Materials*, ORNL-4382 (to be published).

⁴W. R. Burrus, *Utilization of A Priori Information by Means of Mathematical Programming in the Statistical Interpretation of Measured Distributions*, ORNL-3743 (June 1965); W. R. Burrus *et al.*, *Neutron Phys. Div. Ann. Progr. Rept. May 31, 1966*, ORNL-3973, vol. 1, p. 61.

⁵The data are normalized on an absorption basis rather than a capture basis because, for fissionable materials, absorption and capture are not equivalent ($\sigma_a = \sigma_c + \sigma_f$).

⁶H. C. Claiborne, "Gamma Energy Released per Fission of ²³⁵U," Intra-Laboratory Correspondence, ORNL, Jan. 29, 1968.

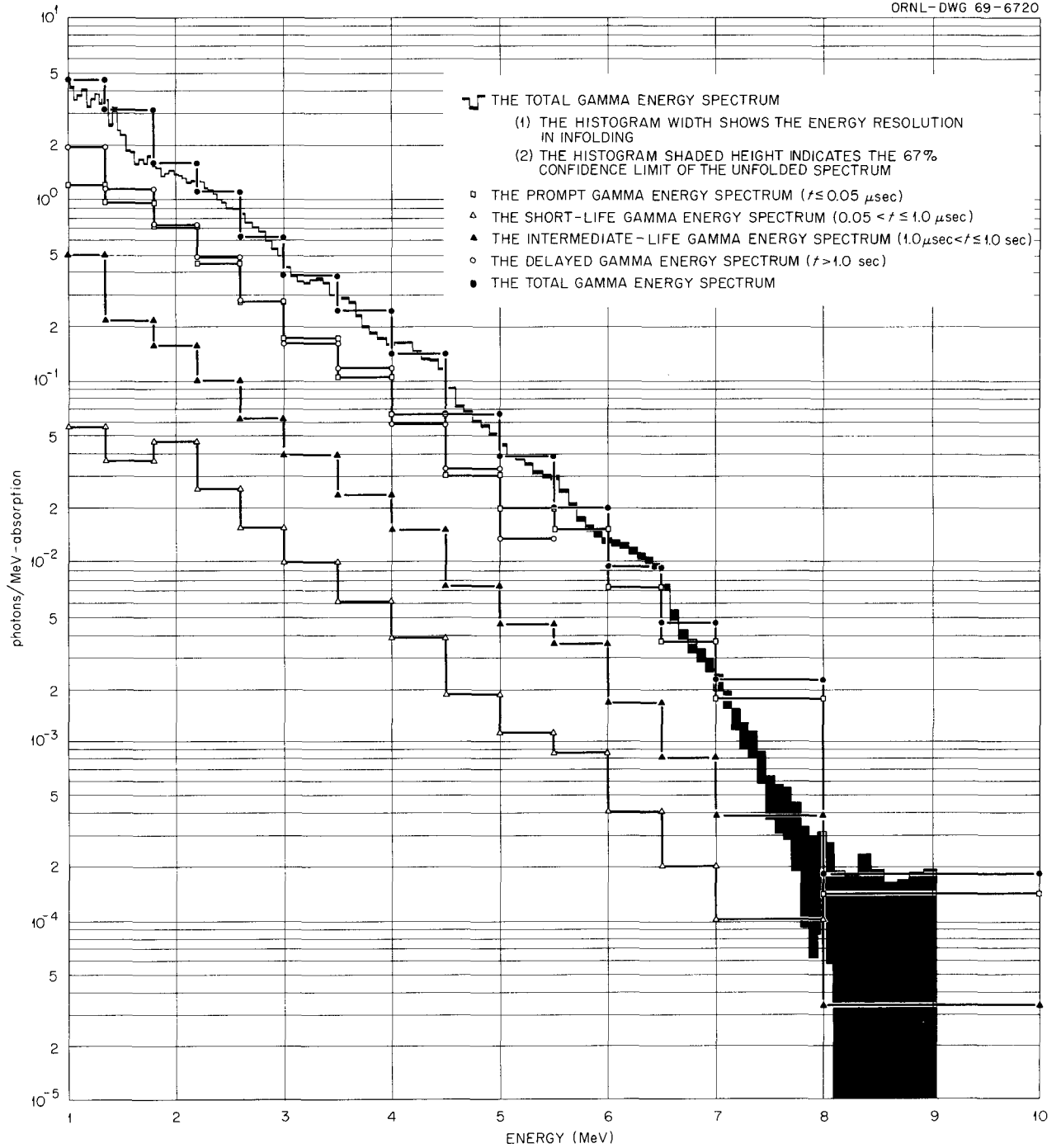


Fig. 2.9.1. The Total Gamma Energy Spectrum Above 1 MeV Due to Thermal Neutron Absorption in ^{235}U . (Photons/MeV absorption.)

2.10 GAMMA-RAY SPECTRA ARISING FROM THERMAL-NEUTRON CAPTURE IN ELEMENTS FOUND IN SOILS, CONCRETES, AND STRUCTURAL MATERIALS^{1,2}

R. E. Maerker F. J. Muckenthaler

Gamma-ray spectra arising from the capture of thermal neutrons are presented for iron, aluminum, copper, zinc, titanium, nickel, silicon, calcium, potassium, sodium, barium, chlorine, sulfur, and stainless steel. The spectral intensities in photons per 100 captures are presented both as individual lines and as sums of these lines over 0.5-MeV intervals which are intended for use in shielding calculations. The latter results have an estimated accuracy of $\pm 15\%$ and include the contributions from both discrete and continuum gamma rays. Comparisons of these spectra are made with previously determined spectra, as well as with values reported in the *Reactor Handbook*, and considerable revision in the latter is concluded to be necessary. The present results do not go below 1 MeV, but when the relatively small contributions from energies less than 1 MeV are added to them, binding energy checks within $\pm 5\%$ are obtained.

The measurements were made at the Tower Shielding Facility with a carefully calibrated 5×5 in. NaI(Tl) detector.

References

¹This work funded by the Defense Atomic Support Agency under Subtask A2-11.037.

²Abstract of ORNL-4382 (to be published).

2.11 EXPERIMENTAL EVALUATION OF MINIMA IN THE TOTAL NEUTRON CROSS SECTIONS OF SEVERAL SHIELDING MATERIALS¹⁻³

E. A. Straker

Neutron total cross sections in the energy range from 1 to 11 MeV have been experimentally evaluated for several shielding materials by comparing calculations and measurements of the spectra of the collided flux transmitted through thick samples. This technique provides a critical test of the minima in the cross sections but yields little information about the resonance regions. Special emphasis has been placed on evaluating the total

cross sections in the Evaluated Nuclear Data File (ENDF/B). In most cases the ENDF/B cross sections are the best available, the exceptions being for iron and tungsten.

References

¹This work funded by the Defense Atomic Support Agency under Subtask No. RRP-5037.

²Abstract of ORNL-TM-2242 (June 6, 1968).

³Abstract of *Nucl. Sci. Eng.* **34**, 114-21 (1968).

2.12 AN ON-LINE DATA ACQUISITION, DISPLAY, AND ANALYSIS SYSTEM FOR THE TOWER SHIELDING FACILITY

R. M. Freestone, Jr. K. M. Henry

A data acquisition system centered around a small on-line digital computer offers significant advantages in the conduct of large-scale shielding experiments such as are carried out at the ORNL Tower Shielding Facility (TSF). Probably the most important of these advantages is that of flexibility or versatility – the capability of rapid and fairly easy adaptation to the differing demands of a variety of experiments. A second advantage is the possibility of performing a significant amount of preliminary processing of the data as it is being acquired.

With these advantages in mind a system based upon a Digital Equipment Corporation (DEC) PDP-9 computer has been installed at the TSF. The PDP-9 has a memory capacity of 8192 18-bit words (readily expandable in units of 8192 words to 32,768 if a need arises), a cycle time of $1 \mu\text{sec}$, and extended arithmetic for hardware multiply, divide, and long shifts. Most single operations are completed in two cycles, with the extended arithmetic instructions requiring a maximum of 19 cycles.

Peripheral portions of the system include an ASR-33 Teletype, a DEC high-speed optical paper-tape reader and mechanical punch, three DEC TU55 Dectape (magnetic tape) transports and their associated TC02 controller, a TECTRONIX RM503 oscilloscope with light pen, two Nuclear Data model TC-2200 analog-to-digital converters (ADC's), and, perhaps most interesting, a specially designed and constructed ADC-computer interface having the capability of simultaneously handling the inputs

of up to seven ADC's, in all possible combinations and modes (coincidence, anticoincidence, singles, etc.).

The system was installed early in December 1968. A number of early difficulties in its operation were encountered, both in the areas of system (manufacturer-furnished) software and in regions of the hardware. However, considerable progress has been made toward making the system on-line operative. Programs now exist to accept data from an experimental configuration, utilizing the existing ADC's to display the data in either linear or semi-logarithmic mode, to output the data in typewritten form or as punched paper tape (or both simultaneously), to make Teletype plots of the data as linear or semilog graphs, including options for smoothing the data by binning, and to store and retrieve the data on Dectape.

2.13 RESPMG: A RESPONSE MATRIX GENERATION CODE PACKAGE¹

W. R. Burrus² R. M. Freestone, Jr.

In the unfolding of the complex pulse-height spectra resulting from the interaction of neutrons with an organic scintillator such as NE-213, an accurate and detailed matrix of monoenergetic response functions is needed.

RESPMG is a package of 15 FORTRAN codes which operate on a relatively small number of input response functions, generated by the Monte Carlo code 05S or otherwise, to produce such a matrix.

Input to RESPMG, other than the response functions, is simple and straightforward. Output consists of tabulations of the results, page-printer plots of selected responses, and a deck of punched cards suitable for input, in particular, to the unfolding codes COOLC and FERDOR.

This report contains complete descriptions of all subroutines, including flow charts, plus a users' manual or "cookbook" section giving detailed instructions for using the codes.

References

¹Abstract of report ORNL-TM-2594 (to be published).

²Present address: Tennecomp, Inc., P.O. Box J, Oak Ridge, Tenn.

2.14 GAMMA-RAY RESPONSE OF THE NE-213 LIQUID SCINTILLATION DETECTOR^{1,2}

C. Y. Fu³ E. A. Straker
V. R. Cain P. N. Stevens³
F. J. Muckenthaler

The response of an NE-213 scintillation counter to gamma rays has been calculated with the OGRE-G Monte Carlo gamma-ray transport code modified to include the transport of Compton electrons. Since the calculation model did not explicitly include statistical fluctuations due to variations in the intensity of light produced by the scintillator, nonuniformities in the transmission of the light pulse to the photomultiplier, nonlinearities in the conversion of the light pulse into an electrical pulse by the photomultiplier, and variation in the amplification of the pulse, the application of two correction factors to the Monte Carlo results was required. The resulting calculated responses were in excellent agreement with experimental data. Comparisons of the calculated responses with experimental data are presented for gamma-ray source energies from 0.66 to 6.13 MeV.

References

¹This work partially funded by the Defense Atomic Support Agency under Subtask No. RRP-5037.

²Abstract of ORNL-TM-2273 (Aug. 1, 1968).

³University of Tennessee.

2.15 A UNIFIED NUCLEAR MODEL FOR THE GENERATION OF NUCLEAR DATA¹

K. J. Yost P. H. Pitkanen
C. Y. Fu²

A nuclear model pertinent to the generation of certain classes of nuclear data is described. The analysis is structured so as to minimize difficulties in its numerical implementation. The model involves the simultaneous treatment of particle excitations in a deformed potential well, together with rotational and vibrational collective excitations. Details of certain aspects of the theory are presented with comparisons of calculated and measured level structures of several nuclei of interest in shielding technology.

References

- ¹Abstract of *Nucl. Sci. Eng.* **36**, 189–201 (1969).
²University of Tennessee.

2.16 THE APPLICATION OF A GAMMA-RAY CASCADE MODEL TO THE CALCULATION OF NEUTRON-ENERGY-DEPENDENT CAPTURE GAMMA-RAY PRODUCTION CROSS SECTIONS^{1,2}

K. J. Yost S. M. Kremer³

A simplified cascade model for the calculation of neutron capture gamma-ray spectra is compared with experiment. In the context of the model the simplifying assumptions involve extrapolations of measured multipole transition probabilities and equal spin-branching probabilities. Calculated and measured neutron capture gamma-ray spectra are compared for 25 elements spanning virtually the entire mass scale. Substantial agreement between calculated and measured spectra is obtained for medium and heavy nuclei. An analytical method for obtaining neutron-energy-dependent capture gamma-ray production cross sections is developed. A comparison between calculated and measured epithermal capture gamma-ray yields in ⁶⁴Cu is presented.

References

- ¹Abstract of *Nucl. Sci. Eng.* **36**, 220–31 (1969).
²Abstract of ORNL-TM-2404 (Nov. 6, 1968).
³University of Tennessee.

2.17 A NUCLEAR MODEL FOR DATA GENERATION AND ANALYSIS IN LIGHT NUCLEI¹

K. J. Yost P. H. Pitkanen
 C. Y. Fu²

Nuclear data for the light elements constitute an important part of the overall data requirements of shielding technology. A nuclear model pertinent to the description of nuclear level schemes and radiative transition probabilities in light elements has been programmed for the purpose of generating and/or analyzing nuclear data of interest in shield design.

The present model, similar to one investigated by Malik and Scholz,³ is a modification of one described in an earlier paper.⁴ The latter is based in part on the extreme single-particle model of Nilsson.⁵ It thus has primary application to heavier nuclei whose properties are essentially determined by the state of a single extra-core unpaired nucleon. This approach is unrealistic for light nuclei, in part due to the relatively wider energy spacing of the Nilsson orbitals. It is frequently the case that less energy is required to break a nucleon pair and excite one member to pair off with the odd nucleon than is required to excite the odd nucleon to the next highest Nilsson orbital. For such a particle configuration the nuclear characteristics are those of the newly unpaired nucleon or "hole." Thus one is concerned in essence with configuration rather than strictly single-nucleon wave functions in analyzing light nuclei. The total energy corresponding to a particular nucleon configuration is given by⁶

$$E_c = \sum_k n_k \left[\frac{3}{4} E_k - \frac{1}{4} \langle Cl \cdot s + nl^2 \rangle \right],$$

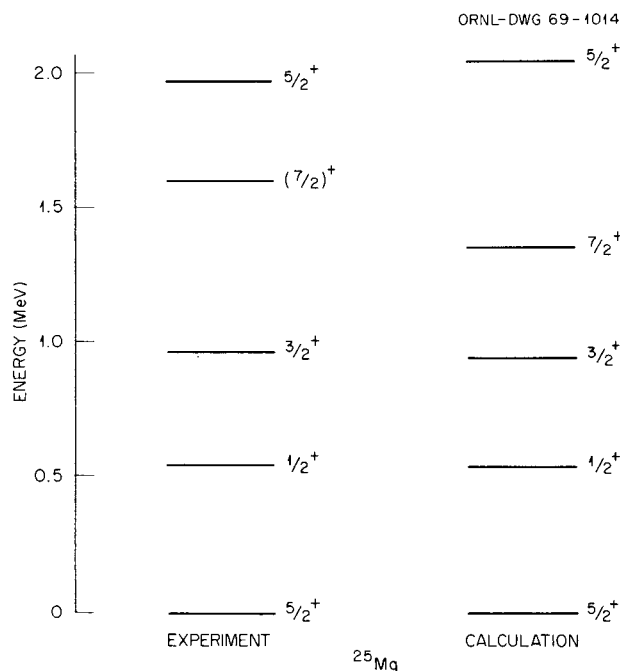


Fig. 2.17.1. Comparison Between Measured and Calculated Energy Levels for ²⁵Mg.

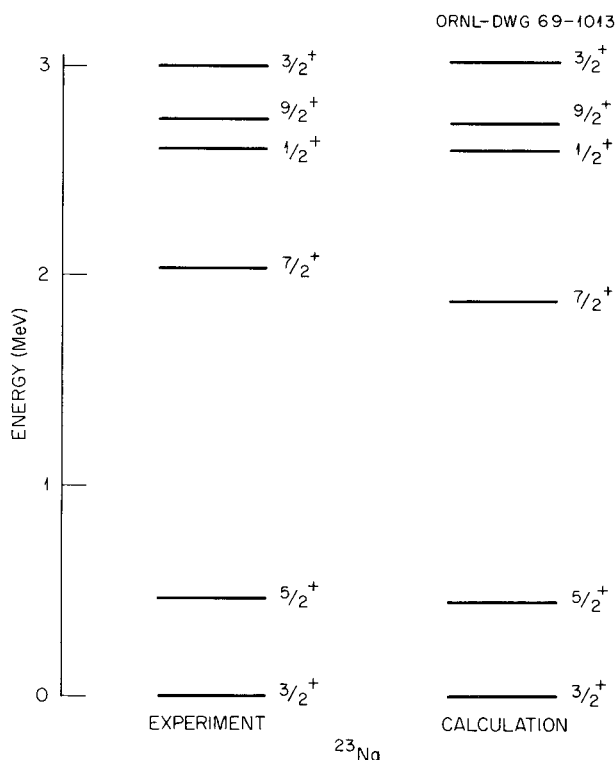


Fig. 2.17.2. Comparison Between Measured and Calculated Energy Levels for ^{23}Na .

where n_k and E_k are respectively the occupation number and energy of the k th Nilsson orbit. The expression represents a correction to the potential energy term of the nuclear Hamiltonian which compensates for the fact that single-nucleon potential energy terms are counted twice in a simple sum over nucleons.

In light nuclei where hole states are not directly observed in the low energy level spectrum, their inclusion in model calculations is still essential due to the fact that rotation-particle coupling is a determining factor in the level structure. Inclusion of hole states by way of rotation-particle coupling provides a means for the participation of the nuclear core in the determination of radiative transition probabilities.

Figures 2.17.1 and 2.17.2 exhibit comparisons between measured and calculated level schemes for ^{25}Mg and ^{23}Na .

References

¹Abstract of paper to be published in proceedings of Annual Meeting of American Nuclear Society, Seattle, Wash., June 15–19, 1969.

²University of Tennessee.

³F. B. Malik and W. Scholz, *Phys. Rev.* **150**, 919 (1966).

⁴K. J. Yost, P. H. Pitkanen, and C. Y. Fu, *Nucl. Sci. Eng.* **36**, 189–201 (1969).

⁵S. G. Nilsson, *Kgl. Danske Videnskab. Selskab. Mat.-Fys. Medd.* **29**, 16 (1955).

⁶T. D. Newton, *Energy Levels of a Completely Anisotropic Oscillator*, CRT-886, Atomic Energy of Canada Limited (1960).

2.18 HELENE: A COMPUTER PROGRAM TO CALCULATE NUCLEAR CROSS SECTIONS EMPLOYING THE HAUSER-FESHBACH MODEL, PORTER-THOMAS WIDTH FLUCTUATIONS, AND CONTINUUM STATES¹

S. K. Penny

A computer code was written with which one may calculate the differential cross sections for scattering and reactions which proceed through a compound nucleus. The code is limited to binary reactions such as (n, n') , (n, α) , etc., but includes a means of calculating capture and a kind of "partial disappearance" to take into account fission, etc. Continuum states can be included in competition with discrete states.

The Hauser-Feshbach model² is employed with Porter-Thomas width fluctuation corrections³ for scattering and reaction widths and for the capture width,⁴ a chi-squared distribution with an infinite number of degrees of freedom.

The penetrabilities are calculated via an optical model with no spin-orbit interaction. This is accomplished through subroutines obtained from Wilmore⁵ which utilize the standard optical-model potential where the imaginary part can be of the forms Saxon-Woods, or its derivative, and Gaussian. The analog of the penetrability for capture is the product of 2π , the radiative width, and a level density. This product is limited in the code to vary slowly after it reaches a certain input value, similar to the manner of Fricke and Lope⁶.

The level densities needed for the continuum states and capture are an extension of the composite scheme of Gilbert and Cameron.⁷

References

¹Abstract of ORNL-TM-2590 (to be published).

²W. Hauser and H. Feshbach, *Phys. Rev.* **87**, 366 (1952).

³C. E. Porter and R. O. Thomas, *Phys. Rev.* **104**, 483 (1956).

⁴L. Dresner, *The Effect of Fluctuations in the Widths on Neutron Reaction Cross Sections*, Oak Ridge National Laboratory Report CF-57-6-2 (1957).

⁵D. Wilmore, *A Computer Program for the Calculation of Compound Nuclear Cross Sections by the Hauser-Feshbach Theory*, AERE-R5053 (1966).

⁶M. P. Fricke and W. M. Lopez, Gulf General Atomic, Inc., San Diego, Calif., private communication.

⁷A. Gilbert and A. G. W. Cameron, *Can. J. Phys.* **43**, 446 (1965).

2.19 CALCULATION OF NEUTRON CAPTURE AND INELASTIC GAMMA-RAY YIELDS USING A MODIFIED VERSION OF THE COMPUTER CODE DUCAL

S. K. Penny K. J. Yost
 J. White¹

The spin-dependent cascade code DUCAL, described by Yost,² has been modified in order to provide more sensitive control over input parameters and to automatically calculate the gamma-ray yields from neutron inelastic scattering and neutron-induced charged-particle emission. An interim code, AVA, was written to average the neutron-

energy-dependent yields obtained from DUCAL over neutron energy groups. These group-averaged yields could then be used directly in a transport code.

The program DUCAL has been modified so that deexcitation to individual discrete levels from the continuum is parameterized. This was necessary because it is well known that the transition strengths to states with the same spin and parity, but belonging to different rotational bands, differ appreciably. The program was also altered to perform automatically all the deexcitation spectrum calculations necessary for inelastic scattering and charged-particle emissions for a given neutron energy. The program has also been modified to include the composite level density scheme of Gilbert and Cameron.³

The program DUCAL requires parameters which are obtained either from theoretical calculations⁴ or from the fitting of experimentally determined primary lines⁵ (see Fig. 2.19.1). The yields obtained from a DUCAL calculation can be used in a number of ways, according to Fig. 2.19.1. The yields can be placed directly in the ENDF/B format,⁶ used as input to group-averaging programs, used as input to a gamma-ray production cross-section program, used directly as input to a Monte Carlo program, etc.

A gamma-ray production cross-section program, HELGA, based on the program HELENE,⁷ is now being written. It will accept DUCAL output spectra

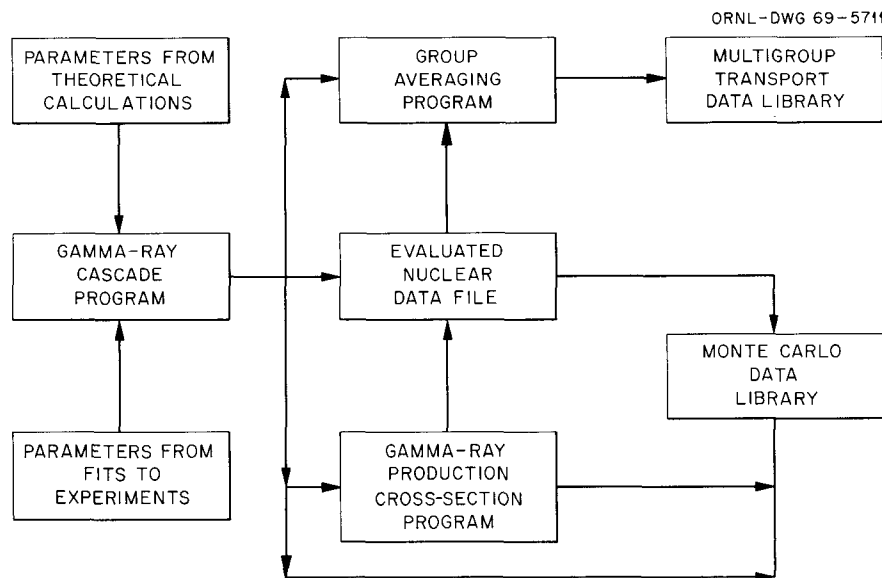


Fig. 2.19.1. Relationship of the Gamma-Ray Cascade Program to Other Programs and Data Files.

and weight them with the appropriate (n, n') , (n, α) , (n, p) , (n, γ) cross sections to produce $(n, n' \gamma)$, $(n, \alpha \gamma)$, $(n, p \gamma)$, (n, γ) , and $(n, x \gamma)$ spectra.

The program AVA averages the neutron capture gamma-ray yields over Breit-Wigner Line shapes in the resonance region and averages with a statistical model similar to that of HELENE above the resonance region. Since it is known that resonance self-shielding effects can be very important, use is being made, with the collaboration of the Reactor Division,⁸ of the more elaborate programs for treatment of resonances. This is important because the gamma-ray spectra from capture in adjacent resonances can be quite different. This new program, along with HELGA, will make AVA obsolete.

Primary lines from thermal-neutron capture in natural tungsten were reported by Bartholomew *et al.*⁹ These lines were matched to within 10% by

adjusting the DUCAL input parameters. These spectra were used except for energies above 60 eV for ^{183}W and for energies below 60 eV for ^{182}W , where minor adjustments were made. Resonance parameters were taken from Goldberg *et al.*¹⁰ up to 1 keV, except that a bound state was added and the spin of the 101.3-eV resonance was changed to 1 for ^{183}W . Above 1 keV, *s*-, *p*-, and *d*-wave gamma-ray spectra were used. Yields were calculated using the program AVA and compared with the experimental data of Orphan and John.¹¹ The comparison is shown in Table 2.19.1, where the experimental numbers are in parentheses. The measured binding energies (B.E.) do not include energies below 1 MeV, as the calculated binding energies do. The agreement is reasonable. The primary lines from thermal-neutron capture in tantalum reported by Bartholomew *et al.*⁹ were also

Table 2.19.1. Comparison of Neutron-Energy-Dependent Gamma-Ray Yields from Capture in Tungsten
Calculations vs experiment (in parentheses)

E (MeV)	En(eV)										
	0-1	1.5-2.5	2.5-6.0	6.0-9.0	9.0-25	25-60	60-120	120-300	300-500	500-1000	1000-100 keV
1.0-1.5	21.3 (57.5)	19.2 (29.9)	11.4 (14.2)	38.1 (21.8)	18.6 (18.1)	38.3 (22.5)	16.1 (30.2)	23.6 (38.4)	21.5 (53.5)	23.0 (47.9)	27.7 (43.9)
1.5-2.0	23.0 (59.0)	21.7 (26.8)	17.3 (11.6)	35.5 (17.0)	20.3 (18.9)	36.4 (17.9)	18.8 (21.2)	26.7 (32.0)	23.1 (38.8)	24.1 (40.6)	29.0 (36.2)
2.0-2.5	29.9 (70.3)	29.2 (31.7)	25.1 (14.9)	29.1 (24.4)	29.9 (22.3)	29.2 (24.2)	23.1 (24.4)	27.2 (33.4)	24.9 (43.6)	26.7 (35.2)	27.3 (30.4)
2.5-3.0	34.6 (38.1)	23.9 (29.9)	28.6 (19.7)	24.5 (24.1)	37.5 (24.0)	25.2 (21.4)	28.2 (20.6)	30.0 (33.3)	27.5 (39.2)	29.7 (20.6)	27.4 (20.6)
3.0-3.5	19.7 (20.6)	21.0 (26.6)	26.7 (23.2)	21.1 (26.2)	19.4 (25.2)	21.9 (32.4)	14.4 (19.0)	19.8 (27.4)	21.8 (30.8)	20.5 (18.8)	23.4 (16.7)
3.5-4.0	16.2 (12.1)	18.3 (17.4)	26.3 (19.6)	10.9 (13.6)	15.1 (16.9)	13.5 (19.9)	16.8 (13.6)	14.3 (19.5)	15.1 (19.9)	14.4 (15.1)	18.8 (12.6)
4.0-4.5	14.1 (6.7)	14.0 (12.9)	14.0 (11.5)	18.7 (12.0)	13.0 (11.1)	18.3 (18.8)	13.7 (9.5)	14.6 (13.7)	14.6 (13.8)	14.6 (9.9)	15.4 (8.9)
4.5-5.0	8.6 (5.3)	7.4 (7.5)	7.1 (5.2)	12.1 (9.8)	6.8 (7.8)	12.8 (10.3)	8.0 (7.4)	8.9 (13.1)	8.9 (11.1)	8.7 (8.2)	8.7 (6.5)
5.0-5.5	10.5 (7.6)	10.0 (13.4)	7.3 (13.9)	7.9 (8.2)	11.5 (11.0)	8.1 (9.8)	7.6 (10.5)	8.4 (8.4)	7.2 (7.4)	8.0 (8.1)	5.8 (4.6)
5.5-6.0	1.5 (0.8)	1.4 (1.3)	1.3 (0.8)	3.5 (2.6)	1.9 (1.5)	4.0 (5.0)	5.6 (4.5)	4.7 (5.8)	5.8 (7.0)	5.2 (6.7)	5.0 (3.1)
6.0-6.5	5.8 (5.7)	7.7 (13.6)	16.3 (11.7)	8.8 (12.0)	5.2 (4.2)	8.2 (6.4)	13.0 (6.4)	4.9 (8.1)	8.2 (8.2)	5.5 (5.6)	5.0 (4.8)
6.5-7.0	0.34 (0.3)	0.23 (1.8)	0.007 (0.4)	2.2 (1.4)	0.003 (1.0)	2.0 (3.2)	3.9 (3.7)	4.2 (4.8)	4.8 (5.2)	3.9 (4.9)	2.8 (3.5)
7.0-7.5	1.1 (1.2)	0.73 (3.2)	0.02 (1.0)	7.9 (9.2)	0.01 (1.0)	7.0 (5.2)	2.7 (2.8)	3.0 (3.7)	3.4 (4.3)	2.8 (2.5)	2.1 (1.6)
B.E.	6.02 (6.95)	6.03 (6.78)	6.24 (5.09)	7.31 (6.31)	5.79 (5.08)	7.41 (6.61)	6.51 (5.41)	6.35 (7.41)	6.50 (8.14)	6.30 (6.33)	6.46 (5.21)

matched, and neutron-group-averaged yields were calculated using AVA. Primary lines from thermal capture in uranium reported by Sheline *et al.*¹² and from capture in seven resonances reported by Price *et al.*¹³ were matched and calculations performed with AVA.

References

- ¹Computing Technology Center, Union Carbide Corp., Oak Ridge, Tenn.
- ²K. J. Yost, *Nucl. Sci. Eng.* **32**, 62 (1968).
- ³A. Gilbert and A. G. W. Cameron, *Can. J. Phys.* **43**, 1446 (1965).
- ⁴K. J. Yost *et al.*, *Nucl. Sci. Eng.* **36**, 189 (1969).
- ⁵K. J. Yost and S. M. Kremer, *Nucl. Sci. Eng.* **36**, 220 (1969).
- ⁶H. C. Honeck, *ENDF/B - Specifications for an Evaluated Nuclear Data File for Reactor Applications*, BNL-50066 (T-467), ENDF 102 (May 1966); D. J. Dudziak, *ENDF/B Format Requirements for Shielding Applications*, LA-3801, ENDF 111 (December 1967).
- ⁷See paper 2.18 of this section.
- ⁸C. W. Craven, Jr., *et al.*, private communication (1969).
- ⁹G. A. Bartholomew *et al.*, *Nucl. Data A5*, 243 (1969).
- ¹⁰M. D. Goldberg *et al.*, *Neutron Cross Sections*, BNL-325, 2d ed., Suppl. 2, vol. IIC, Z = 61 to 87 (August 1966).
- ¹¹V. J. Orphan and J. John, *Intensities of Gamma Rays From the Radiative Capture in Natural Tungsten of Neutrons from .02 eV to 100 keV*, GA-9121 (1968).
- ¹²R. K. Sheline *et al.*, *Phys. Rev.* **151**, 1011 (1966).
- ¹³D. L. Price *et al.*, *Nucl. Phys.* **A121**, 630 (1968).

2.20 CALCULATION OF NEUTRON INELASTIC SCATTERING CROSS SECTIONS FOR IRON AND URANIUM

S. K. Penny

Inelastic cross sections for level excitation in ⁵⁶Fe and ²³⁸U were calculated using the statistical-model computer program HELENE¹ and the distorted-wave Born approximation (DWBA) computer program JULIE.² The neutron energy range

for the ⁵⁶Fe calculations was 0.88 to 7.6 MeV, where 41 discrete levels up to 5.243 MeV were used. The neutron energy range for the ²³⁸U calculations was 0.1 to 10 MeV, where 23 discrete levels up to 1.298 MeV were used. The results agree well with Schmidt's tabulations,³ with the results of Towle and Owens for iron at 7 MeV,⁴ and with Kinney's results⁵ for iron at 4.19, 4.46, 5.00, 5.18, 5.5, 6.00, 6.37, and 7.6 MeV.

Competition from the (*n,α*) and (*n,p*) reactions was included in the ⁵⁶Fe calculations for energies above 4 MeV. Above 5.25 MeV continuum states in the neutron exit channels were included in the competition. The optical-model parameters needed for calculation of the penetrabilities in the neutron channels were those derived by Kinney.

The direct-interaction calculations were essentially the same as reported by Kinney for the 0.846-MeV level, that is, ~80 mb above 4 MeV. The direct-interaction cross section for the 3⁻ 4.531 level varied from 7 mb at 4.19 MeV to 16 Mb at 7.6 MeV.

The ²³⁸U calculations were performed with competition from capture and from a "partial disappearance" which included fission and the (*n,2n*) reaction. Continuum states were included above 1.3 MeV in the neutron exit channels, and, of course, continuum states were needed for the ²³⁹U compound nucleus states with which the capture, fission, and (*n,2n*) competition was calculated. The optical-model parameters for the neutron channels were the same as for the ⁵⁶Fe calculations.

Unique comparisons with Perey's and Kinney's experiments can be performed by means of a computer code, GUSSY.⁶ This program smears the calculated differential cross sections for a given incident neutron energy and a given exit angle over Gaussians whose widths are roughly consistent with experiment. The result is a differential cross section as a function of excitation energy which has peaks and valleys nearly identical with those of experiment. The cross section can thus be compared directly with the experimental cross section on the cathode-ray display device of the PDP-7 computer.⁷ Figure 2.20.1 is a Calcomp plot, made at the PDP-7, of such a comparison for 6.37-MeV neutrons and an angle of 52.5°. The direct-interaction components are not included; therefore the elastic and first excited state should not, and indeed do not, compare well. Also, the experimental results cut off at 1 MeV exit neutron energy. However, the results between these two extremes compare very well.

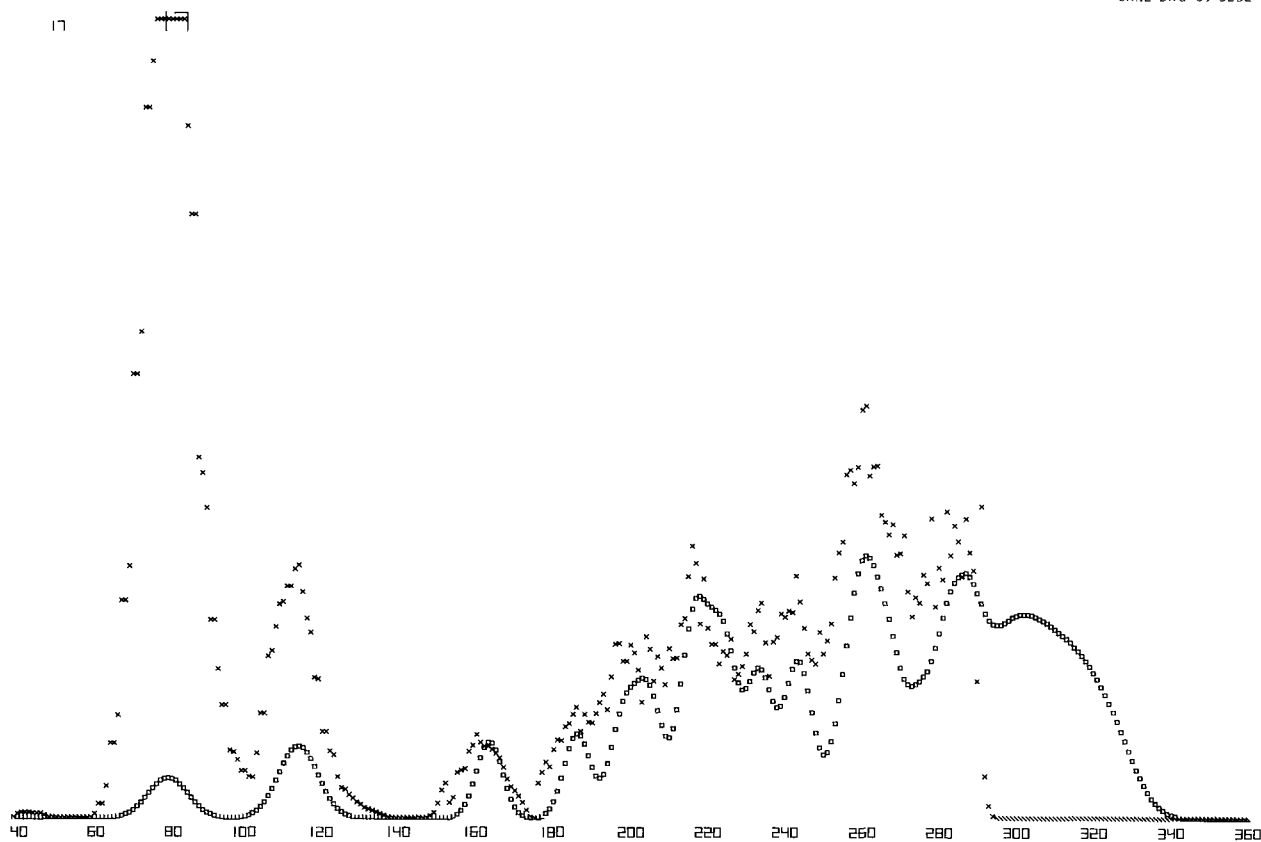


Fig. 2.20.1. Comparison of the Inelastic Scattering Excitation Spectrum at 52.5° for 6.37-MeV Neutrons Incident on Iron as Measured by Kinney with Calculations Smeared with Gaussian Distributions. x, experiment; \square , calculation.

Results for neutrons of 7 MeV incident on ^{56}Fe are shown in Table 2.20.1, comparing calculations with the experiment of Towle and Owens. Above 5.3 MeV the calculation is for exciting continuum states. Table 2.20.2 presents a comparison of Kinney's experiment with calculations for 5.5-MeV neutrons. Figure 2.20.2 presents the calculated inelastic cross sections for exciting the 0.846-MeV level. Figure 2.20.3 presents the calculated inelastic cross sections for exciting the 3.119 + 3.122 MeV levels, the 3.600 + 3.601 + 3.605 MeV levels, and the 100-keV band centered about 5.6 MeV in the continuum.

Figure 2.20.4 presents calculated inelastic cross sections for exciting in ^{238}U the 0.680, 0.925, and 1.167 + 1.170 + 1.209 + 1.270 + 1.298 MeV levels respectively. Figure 2.20.5 presents the calculated inelastic cross section for exciting the 100-keV band centered about 6.05 MeV in the continuum.

References

- ¹See paper 2.18 of this section.
- ²R. H. Bassel, R. M. Drisko, and G. R. Satchler, *The Distorted Wave Theory of Direct Nuclear Reactions*, ORNL-3240 (1962).
- ³J. J. Schmidt, *Neutron Cross Sections for Fast Reactor Materials, Part I: Evaluation*, KFK-120 (1966).
- ⁴J. H. Towle and R. O. Owens, *Nucl. Phys.* **A100**, 257 (1967).
- ⁵W. E. Kinney, *Neutron Elastic and Inelastic Scattering from ^{56}Fe from 4.60 to 7.55 MeV* (thesis), ORNL-TM-2052 (January 1968); and private communication (1969).
- ⁶GUSSY was programmed by M. B. Emmett of the Mathematics Division with liberal advice given by F. G. Perey.
- ⁷Use of the PDP-7 and associated equipment was guided by W. E. Kinney.

Table 2.20.1. Comparison of Calculated Results with Inelastic Scattering Data of Towle and Owens for 7-MeV Neutrons Incident on Iron

$$4\pi \frac{d\sigma}{d\Omega} (\theta = 90^\circ) (t^2/\text{MeV})$$

Energy Range (MeV)	Towle and Owens	Calculated	Energy Range (MeV)	Towle and Owens	Calculated
0.65-1.05	24.2 ± 1	23.4	5.45-5.55	35.0 ± 1.5	48.0
2.00-2.30	13.1	18.6	5.55-5.65	47.8	47.8
2.30-3.00	6.83 ± 0.5	8.87	5.65-5.75	48.4	47.4
3.00-3.55	17.0	24.0	5.75-5.85	43.5	46.5
3.55-4.00	21.2	26.7	5.85-5.95	41.9 ± 2	45.2
4.00-4.35	22.5 ± 1	24.2	5.95-6.05	45.1	43.6
4.35-4.65	33.4	45.9	6.05-6.15	49.3	41.6
4.65-4.90	38.0	44.4	6.15-6.25	44.9	39.2
4.90-5.10	30.9	30.6	6.25-6.35	47.4 ± 3	36.6
5.10-5.30	37.0	44.7	6.35-6.45	43.4 ± 5	33.8
5.30-5.45	47.8	47.8			

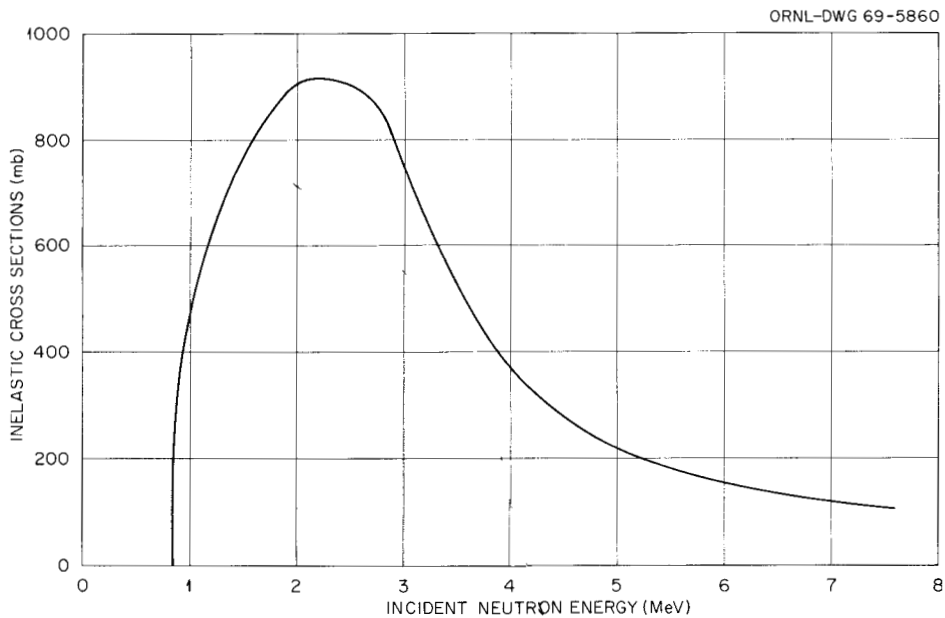


Fig. 2.20.2. Calculation of the Neutron Inelastic Scattering Cross Section for Excitation of the 0.846-MeV Level of ^{56}Fe .

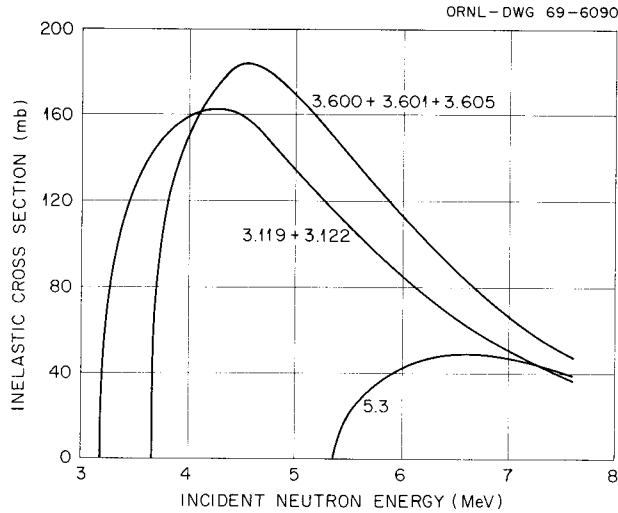


Fig. 2.20.3. Calculation of the Neutron Inelastic Scattering Cross Section for Excitation of the 3.119 + 3.122, 3.600 + 3.601 + 3.605 MeV Levels of ^{56}Fe and of the 100-keV Band Centered About 5.3 MeV in the Continuum of ^{56}Fe .

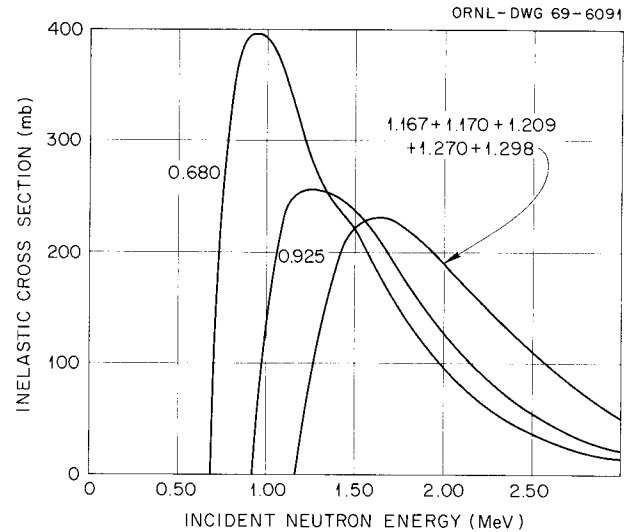


Fig. 2.20.4. Calculation of the Neutron Inelastic Scattering Cross Section for Excitation of the 0.680, 0.925 and 1.167 + 1.170 + 1.209 + 1.270 + 1.298 MeV Levels of ^{238}U .

Table 2.20.2. Comparison of Calculated Results with Inelastic Scattering Data of Kinney for 5.5-MeV Neutrons Incident on Iron

Level (MeV)	Total Cross Section (mb)	
	Kinney	Calculated
0.846	190	185
2.084	66	71
2.654	80	81
2.939	87	100
2.957		
3.119	96	111
3.122		
3.368	190	197
3.888		
3.445		
3.450		
3.600	120	145
3.601		
3.605		
3.747	100	123
3.829		
3.856		
4.046	130	119
4.099		
4.166		

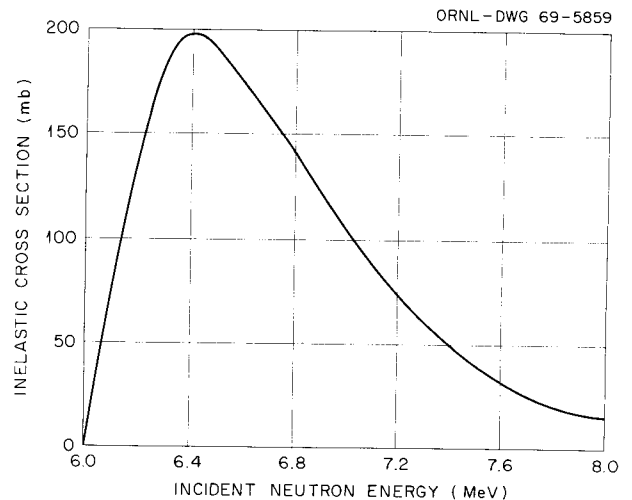


Fig. 2.20.5. Calculation of the Neutron Inelastic Scattering Cross Section for Excitation of the 100-keV Band Centered About 6.05 MeV in the Continuum of ^{238}U .

2.21 POPOP4: A CODE FOR CONVERTING GAMMA-RAY SPECTRA TO SECONDARY GAMMA-RAY PRODUCTION CROSS SECTIONS¹

Walter E. Ford III² David H. Wallace²

POPOP4 is a FORTRAN IV program which converts gamma-ray spectra from neutron-induced re-

actions to a required neutron-gamma energy group structure. If the spectra are given in terms of gamma intensity per reaction, POPOP4 will multiply the converted spectra by input reaction cross sections to produce secondary gamma-ray production cross sections. The code will also convert secondary gamma-ray cross sections from a given neutron-gamma energy group structure to a required neutron-gamma energy group structure. POPOP4 will make, update, or read a hexadecimal library tape of spectral data.

The conversion technique used in POPOP4 is described for the various forms of spectra which are found in the literature. The input data required to execute the various options are also described. The input and output for a sample problem are shown.

Using another code, secondary gamma-ray production cross sections calculated by POPOP4 can be coupled with the P_0 components of the neutron and gamma-ray cross sections for the nuclides of interest. The coupled multigroup cross sections can then be used with codes such as ANISN, DOT, and 05R.

References

¹Abstract of CTC-12 (May 23, 1969).

²Computing Technology Center, Union Carbide Corp., Oak Ridge, Tenn.

2.22 DISCRETE-ORDINATES CALCULATION OF SECONDARY GAMMA-RAY SPECTRA FOR COMPARISON WITH TOWER SHIELDING FACILITY EXPERIMENTS

Walter E. Ford III D. H. Wallace¹

Secondary gamma-ray data in multigroup form are being checked by comparing discrete-ordinates calculations of secondary gamma-ray pulse-height spectra with measurements at the Tower Shielding Facility.^{2,3} The calculational scheme required the development of a FORTRAN IV code for converting gamma-ray yield data for (n,γ) , $(n,x\gamma)$ reactions to secondary gamma-ray production cross sections. This code, POPOP4, calculates the cross sections in multigroup form to be coupled with multigroup

neutron and gamma-ray cross-section sets.⁴ A library of secondary gamma-ray yield data for use with POPOP4 is being assembled. The neutron cross sections for this study are from GAM-II, and the gamma-ray multigroup cross sections are calculated with MUG.^{5,6} Cross sections are used in an 87-energy-group structure [27 neutron groups (0.9–14.9 MeV) and 60 gamma groups (0.01–11.0 MeV)].

The secondary gamma-ray spectra resulting from exposure of slabs to neutron beams from the TSR-II reactor are calculated with the one-dimensional discrete-ordinates transport code, ANISN.⁷ Measured spectra for the bare beam, the cadmium-filtered beam, and the boron-filtered beam from the TSR-II reactor are used as the sources in ANISN. A relatively high order of angular quadrature, S_{96} , is used to obtain a source angle representative of the 45° inclination of the material slab with respect to the TSR-II beams.

A FORTRAN IV code, LINFOLD, was developed to compare calculated with measured spectra. LINFOLD incorporates the response functions which were experimentally determined and programmed for an "in house" code by Maerker.⁸ The calculated spectra are folded with the response functions for comparison with measured pulse-height distributions. LINFOLD includes provisions for incorporating the geometrical attenuation of the neutron shields for the detector. It also can correct for the characteristics of the experiment electronics. The code subtracts backgrounds and produces Calcomp plots of the calculated and measured results.

Comparisons have been made with iron, nickel, tungsten, and depleted uranium. As an example of the results, three calculated spectra and the measured spectra for thermal capture are shown in Fig. 2.22.1 for a 2.54-cm slab of nickel. The orientation of the nickel slab with respect to the beam and the detector is shown in the figure. The sources of the (n,γ) secondary gamma-ray yield data used in POPOP4 are listed in Table 2.22.1.

Comparisons of calculated and measured spectra for 5.08 cm of Hevimet encased in 0.635 cm of aluminum are shown in Fig. 2.22.2 for the bare beam case. (Hevimet is composed of tungsten, nickel, and copper.) The sources of the secondary gamma-ray yield data and the number densities of the constituents of the slab are shown in Table 2.22.2.

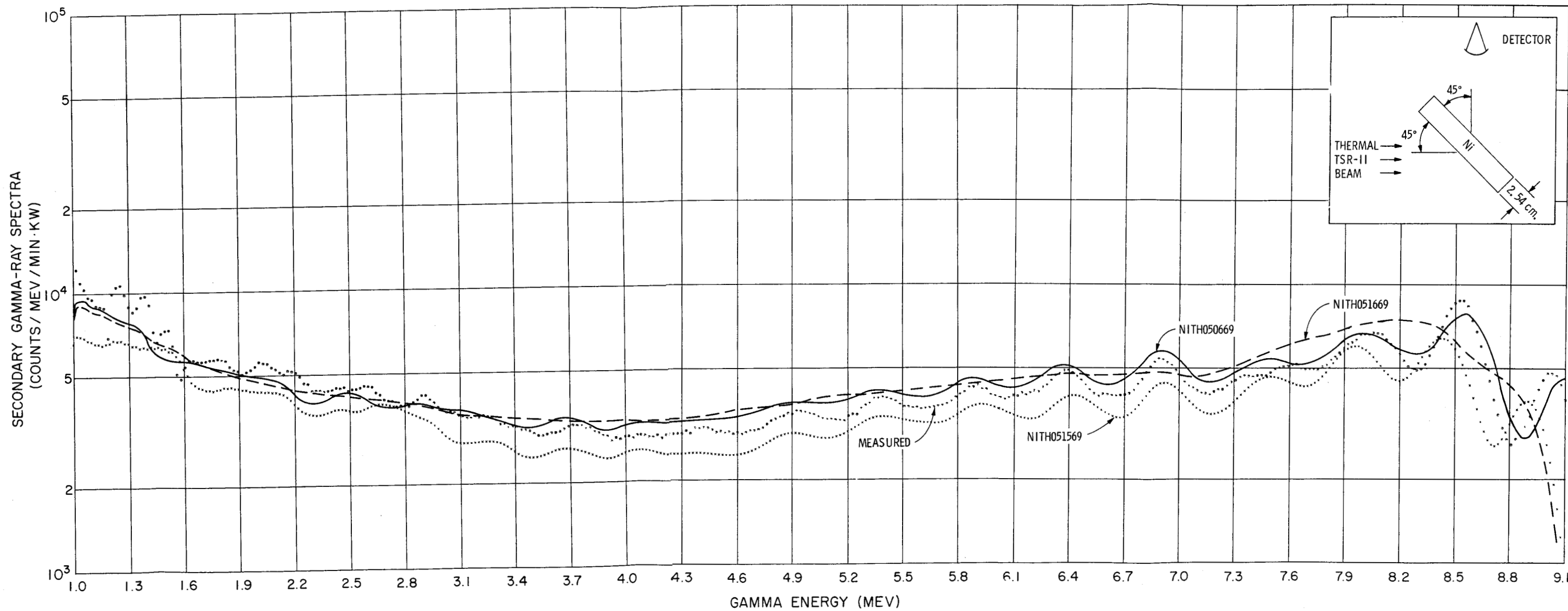


Fig. 2.22.1. Comparison of Calculated and Measured Nickel Secondary Gamma-Ray Spectra for the TSR-II "Thermal Beam."

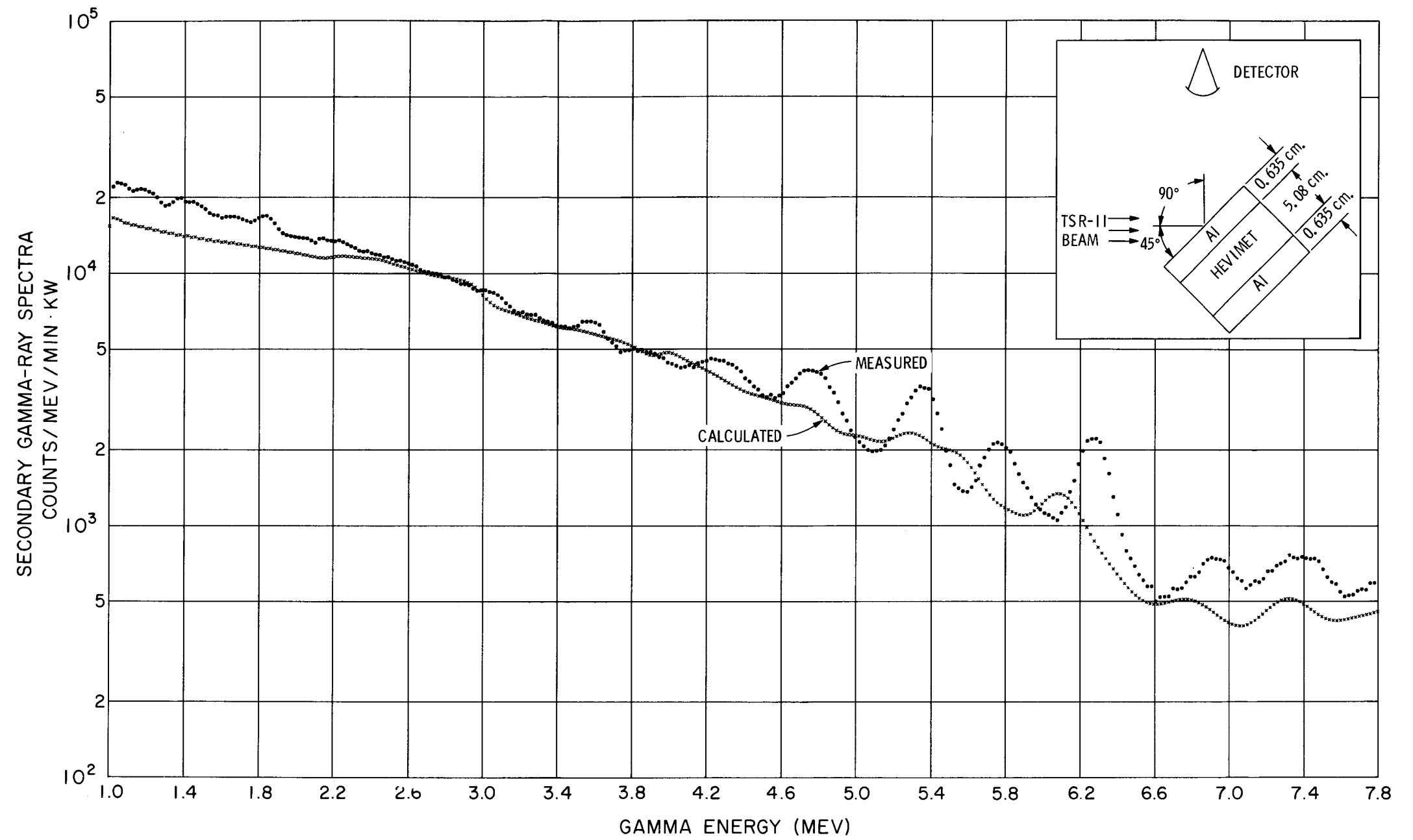


Fig. 2.22.2. Comparison of Calculated and Measured Hevimet Secondary Gamma-Ray Spectra for the TSR-II Bare Beam.

Table 2.22.1. Sources of (n,γ) Secondary Gamma-Ray Yield Data Used in Nickel Calculations

Calculation Identification	Yield Data Source	Remarks
NITH051569	Ref. 9, p. 524	Thermal-neutron capture gamma-ray yields for 52 discrete gamma energies
NITH051669	R. E. Maerker, private communication	Thermal-neutron capture gamma-ray yields given in 16 gamma energy groups for the range $1.0 \leq E_\gamma \leq 9.0$ MeV
NITH050669	R. E. Maerker and F. J. Muckenthaler, ref. 2, p. 158	Thermal-neutron capture gamma-ray yields for 55 discrete gamma energies above 1 MeV

Table 2.22.2. Composition of Laminated Slab and Sources of Secondary Gamma-Ray Yield Data Used in Hevimet Calculations

Element	Number Density (nuclei $\text{b}^{-1} \text{cm}^{-1}$)	(Reaction): Yield Data Source	Remarks
Aluminum	0.0603	(n,γ) : R. E. Maerker, ref. 10, p. 702	Thermal-neutron capture gamma-ray yields given in 14 gamma energy groups for the range $1.0 \leq E_\gamma \leq 8.0$ MeV
		$(n,n'\gamma)$: ref. 11, p. 75	Yields given in 13 neutron energy groups ($0.897 \leq E_n \leq 18.02$ MeV) and 15 gamma energy groups ($0.25 \leq E_\gamma \leq 9.0$ MeV)
Nickel	0.01308	(n,γ) : R. E. Maerker, private communication	Thermal-neutron capture gamma-ray yields given in 16 gamma energy groups for the range $1.0 \leq E_\gamma \leq 9.0$ MeV
		$(n,n'\gamma)$: ref. 12, p. 38	Yields given in 11 neutron energy groups ($1.059 \leq E_n \leq 18.017$ MeV) and 12 gamma energy groups ($0.25 \leq E_\gamma \leq 11.25$ MeV)
Copper	0.004028	(n,γ) : R. E. Maerker, ref. 10, p. 702	Thermal-neutron capture gamma-ray yields given in 14 gamma energy groups for the range $1.0 \leq E_\gamma \leq 8.0$ MeV
Tungsten	0.05012	(n,γ) : S. K. Penny, ref. 13	Yields given in 12 neutron energy groups ($2.0 \times 10^{-2} \leq E_n \leq 1.0 \times 10^5$ eV) and 30 gamma energy groups ($0.0 \leq E_\gamma \leq 7.5$ MeV)
		$(n,n'\gamma)$: ref. 12, p. 42	Yields given in 14 neutron energy groups ($0.12 \leq E_n \leq 18.0$ MeV) and 11 gamma energy groups ($0.0 \leq E_\gamma \leq 6.0$ MeV)

References

- ¹Computing Technology Center, Union Carbide Corp., Oak Ridge, Tenn.
- ²R. E. Maerker and F. J. Muckenthaler, *Gamma-Ray Spectra Arising from Thermal Neutron Capture in Elements Found in Soils, Concretes, and Structural Materials*, ORNL-4382 (to be published).
- ³F. J. Muckenthaler *et al.*, *Neutron Phys. Div. Ann. Progr. Rept. May 31, 1968*, ORNL-4280, pp. 114-17.
- ⁴W. E. Ford III and D. H. Wallace, *POPOP4 - a Code for Converting Gamma-Ray Spectra to Secondary Gamma-Ray Production Cross Sections*, CTC-12 (May 23, 1969).
- ⁵G. D. Joanou and J. S. Dudek, *GAM-II - a B₃ Code for the Calculation of Fast-Neutron Spectra and Associated Multigroup Constants*, GA-4265 (Sept. 16, 1963).
- ⁶J. R. Knight and F. R. Mynatt, *MUG - a Program for Generating Multigroup Photon Cross Sections*, CTC-17 (to be published).
- ⁷W. W. Engle, Jr., *A User's Manual for ANISN*, K-1693 (Mar. 30, 1967).
- ⁸R. E. Maerker, *Neutron Phys. Div. Ann. Progr. Rept. May 31, 1968*, ORNL-4280, pp. 110-14.
- ⁹K. Way (ed.), "Compendium of Thermal-Neutron-Capture Gamma-Ray Measurements, Part I, Z = 46," *Nucl. Data* 3, Nos. 4-6 (December 1967).
- ¹⁰R. E. Maerker and F. J. Muckenthaler, *Trans. Am. Nucl. Soc.* XI (Winter 1968), pp. 701-2.
- ¹¹J. H. Ray, G. Grochowski, and E. S. Troubetzkoy, *Neutron Cross Sections of Nitrogen, Oxygen, Aluminum, Silicon, Iron, Deuterium, and Beryllium*, UNC-5139 (Nov. 15, 1965).
- ¹²J. Celnik and D. Spielberg, *Gamma Spectral Data for Shielding and Heating Calculations*, CR-54794 (UNC-5140) (November 1965).
- ¹³See paper 2.19 of this section.

2.23 THE USE OF KERNELS IN STUDYING NEUTRON TRANSPORT PROBLEMS¹⁻³

S. N. Cramer⁴

V. R. Cain P. N. Stevens⁴
R. R. Coveyou E. A. Straker

In the study of neutron transport in an air medium by the Monte Carlo technique, excessive computer time is required in following the neutrons through the keV and eV energy ranges due to the small

energy loss per collision. At these energies, neutron scattering in air is elastic and isotropic in the center-of-mass system, the cross sections are slowly varying in energy, and absorptions are negligible. It is these conditions which make an analytic solution possible but cause a Monte Carlo solution to become time consuming. An analytic time-, space-, and energy-dependent kernel is derived for an infinite homogeneous medium with constant cross sections assuming continuous slowing down of neutrons. This kernel is coupled with a Monte Carlo solution creating an estimator from collisions in the keV energy range to lower energies. In addition to the analytic development, a general investigation of transport model coupling techniques is performed by solving the Boltzmann transport equation for two regions of phase space. It is shown that the coupling of the Monte Carlo and analytic models is a special case of the general coupling approach. Results from the analytic model and its combination with the Monte Carlo solution give excellent agreement with results from a complete Monte Carlo solution in the entire energy range. Considerable machine time is also saved in obtaining answers having comparable statistical error with the complete Monte Carlo solution.

References

- ¹This work partially funded by the Defense Atomic Support Agency under Subtask No. RRP-5037.
- ²A dissertation presented to the Graduate Council of the University of Tennessee in partial fulfillment of the requirements for the degree of Doctor of Philosophy.
- ³Abstract of ORNL-TM-2508 (1969).
- ⁴University of Tennessee.

2.24 EVALUATION OF THE TOTAL CROSS SECTION OF IRON

D. C. Irving E. A. Straker

Since 1965 there have been several measurements of the total cross section of iron.¹⁻⁶ In addition, measurements made at the Tower Shielding Facility at ORNL^{7,8} provided a check on the cross-section data. Since this check emphasizes the valleys in the cross section, it is especially relevant to the

validity of a cross-section set for use in a shielding calculation. Comparison of the iron evaluation available in the ENDF file with the TSF data showed that the transmission would be greatly underestimated in thick shields.⁸ To obtain an improved cross-section set for use in shielding calculations, an evaluation of the iron cross section was begun in early 1968. Unfortunately the data available at that time¹⁻⁴ were not very satisfactory. There were disagreements of as much as 25% between the different experimental measurements. Comparison of the measurements was often hindered by energy shifts in the data. A comparison of each data set with the TSF data indicated the best agreement in the 2-to-40-MeV range was with the one measurement which was 25% lower than all other measurements. This one measurement did not extend below 2 MeV, and no agreement could be obtained in that region.

Finally in mid-1968 we were able to obtain the data from a new measurement made at Karlsruhe.⁵ The resolution in this experiment was an order of magnitude better than in previous measurements. Since the iron cross section has an enormous amount of structure, this resulted in an increase in the number of peaks and valleys which could be detected. This increase was so great as to render the Karlsruhe data almost unrecognizable in comparison with the earlier measurements. Unfortunately, comparison of the Karlsruhe data with the TSF experiment did not provide much better agreement than had been achieved previously.

Several attempts were made to check the TSF data and the calculations necessary to compare the other experimental data with it. The experiment was rerun completely using the SNAP reactor with its somewhat different spectrum as a source. The number of points used in the calculation were increased, and integration meshes were made finer. The net result was a slight improvement, but a major disagreement still remained.

In early 1969 a new measurement of the iron total cross section was completed at Gulf General Atomic.⁶ These data compared excellently with the data obtained at Karlsruhe. The energy shift was almost nonexistent; the same structure, peaks, valleys, etc. were seen in both measurements; and the cross sections were on the average the same. The GGA data did have slightly better resolution than the Karlsruhe data, at least at the lower en-

ergies. This means that in the GGA data the peak values are higher and the valleys are lower, significantly lower in several cases. These lowered valleys are apparently significant for shielding calculations. In a comparison with the TSF measurement, the GGA data showed good agreement. A cross-section set based on the GGA measurement would seem to be adequate for calculations involving deep penetration in iron.

The GGA experiment produced 3726 data points between 0.5 and 9 MeV. In addition, several hundred points are needed to represent the total cross section outside this range. For computational use it is desirable to reduce this mass of data to as few points as possible while still providing an adequate representation of the cross section. In addition, the ENDF format has a restriction to a maximum of 3000 points allowed for any single cross section. Many of the experimental data points represented statistical fluctuations and not real detail. Many other points could be eliminated since they were adequately represented by straight-line interpolation between the remaining data points. The reduction of this mass of data by hand would have been a formidable task had there not been available an IBM-1800 computer with an on-line display device and light pen. Use of this facility simplified the mechanical aspects of the elimination of data points, but, more importantly, it promoted an interactive approach to the reduction of data points. Displays of the data were easily obtained. Scale factors for the display could readily be changed, revealing many structural details which would otherwise have been overlooked. Smoothing operations were used to examine structure previously hidden in areas of much statistical variation. Details which vanished or changed significantly with the elimination of a single point were deemed to be due to the statistical fluctuation of that point; those details which were due to the average behavior of many points were held to be significant and were retained in the final data set. The light pen was also used to construct lines connecting data points. This facilitated the removal of points where straight-line interpolation would be sufficient.

The evaluation of the iron total cross section produced in this study will be combined with an evaluation of the other cross sections of iron made by the Westinghouse Atomic Power Division to produce a new file of iron data for the ENDF library.

References

- ¹M. D. Goldberg *et al.*, *Neutron Cross Sections, Z = 21 to 40*, BNL-325, 2d ed., Suppl. 2, vol. IIA (February 1966).
- ²A. D. Carlson and H. H. Barschall, *Phys. Rev.* **158**, 1142 (1967).
- ³R. B. Schwartz, private communication.
- ⁴J. M. Ferguson, private communication.
- ⁵S. Cierjacks *et al.*, *High Resolution Total Neutron Cross Sections Between 0.5–30 MeV*, KFK-1000 (June 1968).
- ⁶R. J. Cerbone, private communication.
- ⁷C. E. Clifford *et al.*, *Nucl. Sci. Eng.* **27**, 299–307 (1967).
- ⁸E. A. Straker, *Nucl. Sci. Eng.* **34**, 114–21 (1968).

2.25 NUCLEAR DATA REQUIREMENTS AND ACQUISITION FOR SHIELDING APPLICATION¹

K. J. Yost J. R. Beyster²

This paper was intended as a survey of nuclear models and their application to the generation and analysis of nuclear data of interest in shielding technology. It was one of a series of papers covering various aspects of shielding technology which appeared in the February 1969 issue of *Nuclear News*.

References

- ¹Abstract of *Nucl. News* **12**(2), 37–41 (February 1969).
- ²Gulf General Atomic, Inc., San Diego, Calif.

2.26 RECENT DEVELOPMENTS IN TRANSPORT SOLUTIONS TO SHIELDING PROBLEMS^{1,2}

C. E. Clifford F. R. Mynatt³
E. A. Straker

This paper presents a review of the development of the modern techniques being applied to solve radiation transport problems. The state of the art of the discrete ordinates and Monte Carlo methods is described in some detail. It was one of a series of six papers covering all aspects of shielding

technology which were prepared for the purpose of stimulating interest in shielding technology.

References

- ¹This work partially funded by the Defense Atomic Support Agency under Subtask A2-11.037.
- ²Abstract of *Nucl. News* **12**(2), 51–56 (February 1969).
- ³Computing technology Center, Union Carbide Corp., Oak Ridge, Tenn.

2.27 THE MORSE CODE: A MULTIGROUP NEUTRON AND GAMMA-RAY MONTE CARLO TRANSPORT CODE¹

E. A. Straker D. C. Irving
P. N. Stevens² V. R. Cain

The Multigroup Oak Ridge Stochastic Experiment code (MORSE) is a multipurpose neutron and gamma-ray Monte Carlo code. Some of its features include: the ability to treat the transport of either neutrons or gamma rays or a coupled neutron and secondary-gamma-ray problem; the option of solving either the forward or adjoint problem; the incorporation of multigroup cross sections; one-, two-, or three-dimensional geometry description; modular input-output, cross-section, analysis, and geometry packages; time dependence for both shielding and criticality problems; albedo option at any material boundary; and optional importance sampling.

The basic logic of the O6R code³ was modified to incorporate the features of the MORSE code. When multigroup cross sections are read from cards (the same input used by ANISN⁴ and DOT⁵) there are no tapes required. (The use of ANISN-type cross sections makes it possible to utilize the vast efforts that have been devoted to multigroup cross-section preparation.) The batch processing feature of O6R is retained for the determination of statistical estimates; however, a particle is followed from birth to death without being banked.

To aid in the development and debugging of the many options in the code, ten or more transport problems are being investigated. Presently, the options now available in MORSE have been checked on the following problems. The point

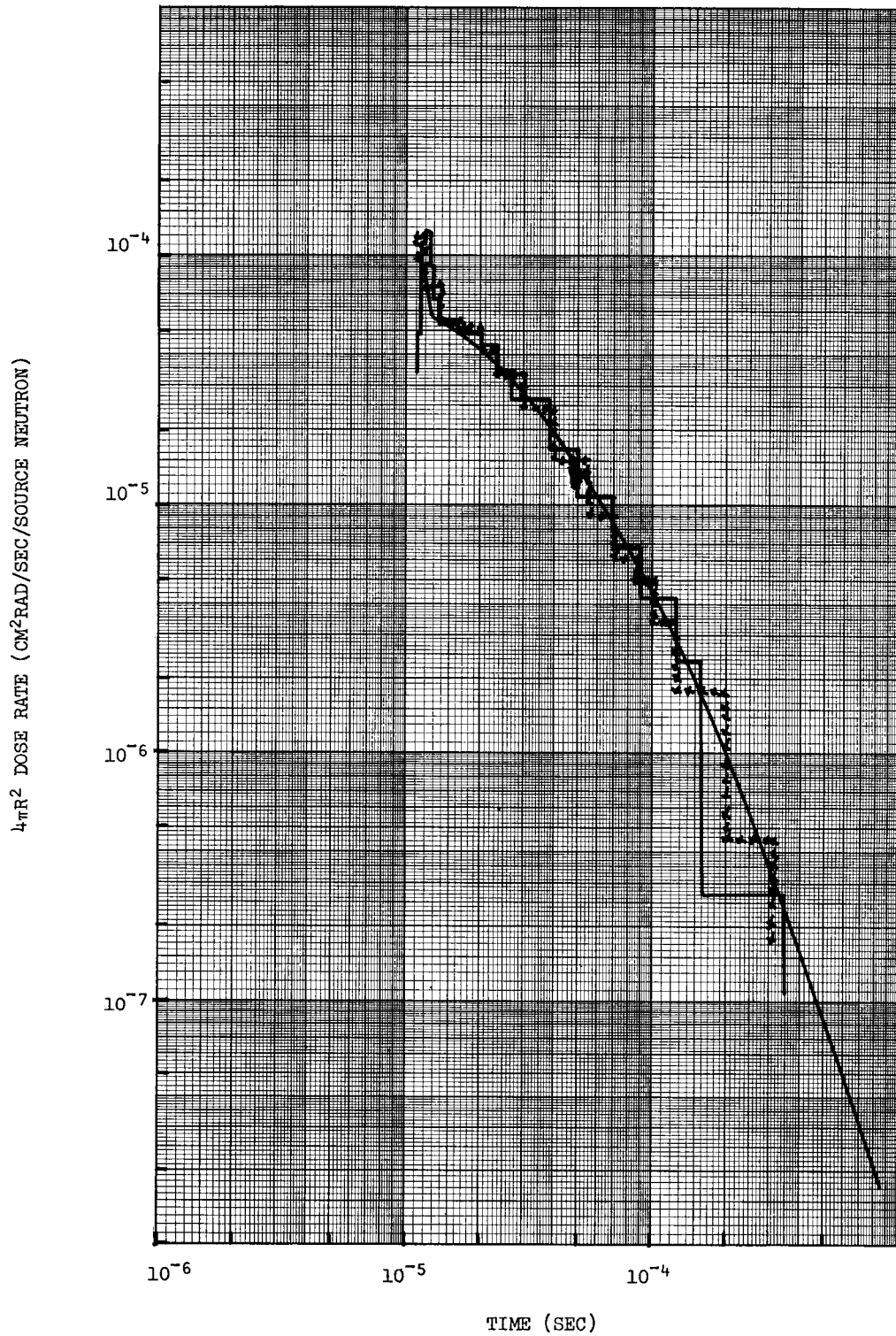


Fig. 2.27.1. $4\pi R^2$ Dose Rate vs Time at 600 m for a 12.2- to 15-MeV Neutron Source in Infinite Homogeneous Air. Curve: ANISN, \square : 05R, xx: MORSE.

fission and 12.2- to 15-MeV source in infinite air benchmark problem⁶ has been calculated and extended to include some time-dependent results.⁷

Figure 2.27.1 shows a typical comparison between O5R,⁸ ANISN-T1,⁹ and MORSE. The dose vs range for this problem has also been calculated by using the adjoint option of MORSE. A gamma-ray source problem in air has been calculated and compared with ANISN results.

Work is continuing in developing the coupled neutron-gamma option, the albedo option, the next event and the once more collided estimators, and the calculation of criticality. The incorporation of optional importance sampling, including the exponential transform, source biasing, and energy biasing, is also being pursued.

References

¹This work partially funded by the Defense Atomic Support Agency under NWER Subtask 6.044.

²Consultant, University of Tennessee.

³See paper 2.28 of this section.

⁴W. W. Engle, Jr., *A User's Manual for ANISN, a One-Dimensional Discrete Ordinates Transport Code with Anisotropic Scattering*, K-1693 (1967).

⁵F. R. Mynatt, *A User's Manual for DOT, a Two-Dimensional Discrete Ordinates Transport Code with Anisotropic Scattering*, K-1694 (to be published).

⁶A. E. Profio (ed.), *Shielding Benchmark Problems*, ORNL-RSIC-25 (1969).

⁷E. A. Straker, W. W. Engle, Jr., and P. N. Stevens, *Some Calculated Milestone Solutions to Time-Dependent Radiation Transport Problems*, ORNL-TM-2499 (1969).

⁸D. C. Irving *et al.*, *O5R, a General Purpose Monte Carlo Neutron Transport Code*, ORNL-3622 (1965).

⁹See paper 2.33 of this section.

2.28 O6R: AN IMPROVED VERSION OF THE O5R MONTE CARLO CODE

D. C. Irving E. A. Straker
C. L. Thompson¹

Extensive changes are being made to the general-purpose neutron Monte Carlo program, O5R.² To distinguish this revised code from its parent, the

new program will be referred to as O6R. The major changes made in this revision are discussed below.

1. A direct linkage of O6R to the ENDF/B cross-section format has been provided. New programs were written to replace the XSECT code of O5R. These programs use the ENDF cross-section tapes to produce the macroscopic data tapes used in O6R. This eliminates the older O5R cross-section format in favor of the more general ENDF/B format and makes the present ENDF library and new cross-section evaluations produced in that format immediately available for use in O6R.

2. The energy boundaries of supergroups were made variable instead of being fixed. This added flexibility will improve the usefulness of the code in the resonance region while increasing the overall efficiency of cross-section storage and handling.

3. The handling of cross-section data has been revised to allow more than one supergroup in memory at a time. The advantage of this modification will be felt in problems requiring a moderate amount of cross-section data which are run on a computer with a large memory size. In these problems it will be possible to store all the cross-section data in memory at one time. This will save a great amount of computer time that is normally devoted to the repeated reading of cross sections from magnetic tape. When all the cross sections are in core, O6R will follow each particle history through from birth to death instead of interrupting the history at each supergroup boundary, thus reducing the time spent in the banking of particle data. The histories will still be grouped in batches to facilitate the estimation of statistics.

This change and the preceding one were made at the expense of a small amount of additional bookkeeping in the main subroutines of O6R. They will, however, result in significant time savings for those problems which can make most use of them.

4. To make optimum use of the storage area for the neutron bank in problems using importance sampling through Russian roulette and splitting, a change was made in the logic involving the banking of neutrons. Whenever a neutron history is terminated, its space in the bank is made available for new particles created by splitting.

5. An energy cutoff may be specified below which isotropic scattering is used rather than the Coveyou anisotropic technique. This saves time in the scattering routine at low energies. It also reduces the amount of cross-section data needed and the time spent in reading the cross-section tape.

6. An additional parameter, the time elapsed since the start of the history, has been added to the parameters of each neutron. This will greatly facilitate the calculation of time-dependent problems.

7. A change in the geometry routines allows the specification of certain boundaries as ones where reflection rather than transmission occurs. This was added to permit the use of albedo techniques in O6R calculations. Generality is achieved by relying on a user-written routine for the angular distribution of neutrons reflected from such a boundary.

8. The output from the O6R program has been greatly expanded from that produced by O5R. Since O6R itself produces neutron histories but provides no analysis, this output is not the direct answer to a desired problem. However, the information provided about the histories can prove very useful in debugging the particular problem and its analysis. The data now provided include: the average parameters of the neutrons at their source, the number of pseudocollisions of each type, the number of real collisions with each scatterer in each medium, the number of real collisions in each energy group, the method of termination of each history, and the number of Russian roulette and splitting events.

9. Patch stretching, a form of the exponential transform, has been added as a variance reduction technique.

The first version of O6R, containing the above modifications with one restriction, has been completed and each feature debugged. The single restriction is that the linkage to ENDF/B does not treat the resonance parameters of the ENDF/B library. Work is under way on a second version of O6R, which will not have this restriction and will have some additional features.

References

¹Mathematics Division.

²D. C. Irving *et al.*, *O5R, a General Purpose Monte Carlo Neutron Transport Code*, ORNL-3622 (1965).

2.29 APPLICATIONS OF ADJOINT FLUX CALCULATIONS TO MONTE CARLO BIASING¹

F. A. R. Schmidt² E. A. Straker
V. R. Cain

A review of the use of the adjoint flux in the biasing of Monte Carlo calculations is presented. A detailed discussion is given of the application of discrete-ordinates adjoint calculations to obtain a priori importance sampling parameters and the relative importance of energy, angle, and spatial biasing for a realistic three-dimensional shield. More than an order of magnitude gain in efficiency over empirical biasing was obtained by the use of modified source energy selection, an energy-, angular-, and spatial-dependent exponential transform, and the application of spatial-, energy-, and angular-dependent weight standards for Russian roulette and splitting.

References

¹Abstract of ORNL-TM-2454 (Dec. 26, 1968).

²Institut für Kernenergetik, Universität Stuttgart, Germany.

2.30 A GENERAL METHOD OF BIASING THE ANGLE OF SCATTERING IN MONTE CARLO CALCULATIONS¹

C. E. Burgart²

The application of the Monte Carlo method to the study of deep-penetration radiation transport problems requires the use of "importance sampling." A systematic approach to obtaining an importance function is to calculate the solution of the inhomogeneous adjoint equation (using the Monte Carlo estimator of the answer of interest as the source term) and to use this adjoint flux (or value function) as the importance function. In many cases the adjoint flux is calculated for a simplified geometry using one-dimensional S_n (discrete-ordinates) methods.

In three-dimensional deep-penetration Monte Carlo calculations the alteration of both the collision kernel and transport kernel is desirable. However, the alteration of the collision kernel is much the more difficult task. The approach taken here is to introduce an angular grid with 30 discrete directions fixed in the laboratory coordinate

system, along which particles are required to travel. After determining appropriate scattering probabilities and values of the importance function for each of the discrete directions, the selection of the outgoing direction and, hence, energy from the resulting discrete distribution is easily performed.

The effects of the discrete angular grid have been investigated for neutrons by comparison with standard Monte Carlo and discrete-ordinates calculations, experiment, and exact analytic solutions for several configurations and media. The problems investigated were: (1) infinite air with a 14-MeV point isotropic source,³ (2) air over ground with a 14-MeV point isotropic source located 15.15 m above the air-ground interface,⁴ (3) a hypothetical infinite homogeneous medium with an infinite-mass isotropic scatterer and a plane isotropic source,⁵ and (4) the SNAP-2 LiH collar shield with a beam source.⁶ In all cases, the discrete grid alone was observed to have no significant effect on the results.

The capability of angular-biased Monte Carlo calculations using the discrete grid was investigated in problems 3 and 4. Monte Carlo calculations were performed utilizing the following previously developed forms of importance sampling: exponential transform, source energy biasing, nonescape biasing, Russian roulette, and splitting. Angular-biased Monte Carlo calculations were then performed utilizing all of the above forms of importance sampling plus the angular biasing.

The results of several calculations for problem 3 are illustrated in Fig. 2.30.1. (All error bars are one standard deviation.) Two cases are presented. The upper results are for a scattering-to-total cross-section ratio (c) of 0.9. The lower results are for $c = 0.55$. Scalar flux times $\exp K_c z$ is plotted vs z in mean free paths, where $K_{0.9} = 0.525$ and $K_{0.55} = 0.936$. Thus for $c = 0.9$ the attenuation of the scalar flux is approximately 10^{23} at 100 mean free paths, and for $c = 0.55$ it is 10^{41} at 100 mean free paths. The solid lines indicate the exact analytic solutions. The solid circles along the $c = 0.55$ results indicate Monte Carlo results when the exponential transform is utilized. The path-length stretching parameters for a particular region in space are given by

$$B = \frac{1}{1 - \text{XNU} \cdot \text{DIRECT}},$$

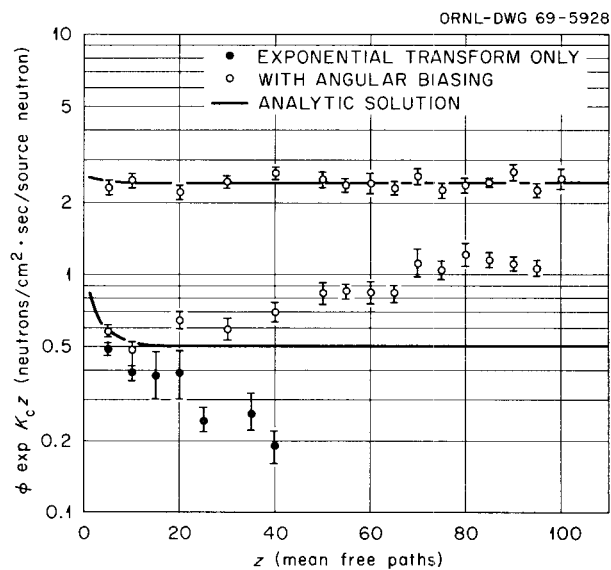


Fig. 2.30.1. Flux Times $e^{K_c z}$ vs Distance for Infinite-Mass Problem.

where XNU is the biasing parameter for a given region and DIRECT is the cosine of the angle between the particle direction and the outward normal to the plane source. The results when only the exponential transform is utilized are for 16,000 histories. (Only results with less than 25% variance are plotted in all cases.) Meaningful results are not obtained for distances greater than 30 mean free paths. The open circles indicate Monte Carlo results when angular biasing, as well as directionally dependent path-length stretching, is utilized. For $c = 0.9$, the angular-biased results (for 500 histories) agree very well with the analytic solution out to 100 mean free paths. For $c = 0.55$ the angular-biased results (for 2000 histories) agree well out to 30 mean free paths, and they are high by about a factor of 2.4 at 100 mean free paths. This discrepancy does not appear to be due to statistics, as many runs have been made, all of which yield approximately the same results. Thus either the discrete grid or the biasing seems to be causing this effect. However, it should again be noted that at 30 mean free paths the attenuation is already 10^{-12} .

The results of these calculations illustrate the general usefulness of this discrete-grid approach to angular biasing in two ways. First, for problem 3, meaningful results were obtained with angular biasing at much greater distances from the source than were practically possible with the earlier

biasing techniques. For problem 4, the answers, variances, and computer times were all on the same order or better than those obtained with the earlier biasing techniques. Second, this method utilizing the discrete grid to incorporate angular biasing requires very little human interaction once the adjoint configuration is selected.

References

¹Summary of work done in partial fulfillment of the requirements for the degree of Doctor of Philosophy for the Department of Nuclear Engineering, University of Tennessee.

²University of Tennessee.

³A. E. Profio (ed.), *Shielding Benchmark Problems*, ORNL-RSIC-25 (June 1969).

⁴E. A. Straker, *Time-Dependent Neutron and Secondary Gamma-Ray Transport in an Air-over-Ground Geometry*, ORNL-4289 (September 1968).

⁵K. M. Case, F. DeHoffman, and G. Placzek, *Introduction to the Theory of Neutron Diffusion, Vol. I*, U.S. Government Printing Office (1953).

⁶V. R. Cain and K. D. Franz, *Comparison of Monte Carlo Calculations with Measurements of Fast-Neutron Dose Transmitted from a Beam Source Through a SNAP-2 LiH Shield*, ORNL-TM-2423 (December 1968).

2.31 MONTE CARLO PATH-LENGTH SELECTION ROUTINES BASED ON SOME SPECIFIC FORMS OF THE IMPORTANCE FUNCTION^{1,2}

V. R. Cain E. A. Straker
G. Thayer³

One of the more fruitful techniques for importance sampling in Monte Carlo calculations is that of modifying the path-length selection in the random walk. The simplest practical approach is usually referred to as the "exponential transform" and assumes that the value, or importance, function (which gives the value of a collision in the random walk to the answer of interest) is a simple exponential in space. In many cases of interest, more detailed information is available about the actual value function, and a more complicated form

of the importance function can be assumed. The formalisms and computer listings are given for some of these specialized importance functions which have been implemented in the path-length selection routines of the O5R Monte Carlo code.

References

¹This work partially funded by Defense Atomic Support Agency under Orders EO-802-65 and EO-800-64.

²Abstract of ORNL-TM-1967 (Feb. 6, 1969).

³University of Illinois.

2.32 AN AMPLIFICATION OF SELECTED PORTIONS OF THE O5R MONTE CARLO CODE USER'S MANUAL¹

D. C. Irving V. R. Cain
R. M. Freestone, Jr.

The original report describing the O5R neutron transport code² was a rather complete documentation. However, intensive use of the code has revealed areas in which a more detailed presentation was desirable, or, conversely, a more general approach was convenient. In addition, some portions of the code, notably the geometry routines, were treated as "black boxes" in the original report. The present report presents a rather miscellaneous collection of material which the authors have found useful in using, modifying, and understanding the O5R code. It is roughly grouped into three sections. The first section presents logic flow charts (supplementing the FORTRAN flow charts of the original report) for the important subroutines of O5R. The second section presents logic flow charts for XSECT, the cross-section handling program. The final section is comprised of logic flow charts and other material describing the operation of the general geometry package, GEOM.

References

¹Abstract of ORNL-TM-2601, to be published.

²D. C. Irving *et al.*, *O5R, a General Purpose Monte Carlo Neutron Transport Code*, ORNL-3622 (1965).

2.33 THE DEVELOPMENT OF A TIME-DEPENDENT ONE-DIMENSIONAL DISCRETE-ORDINATES CODE - ANISN-TI¹

W. W. Engle, Jr.² F. R. Mynatt²
R. S. Booth

By treating the time derivative in the Boltzmann equation in a manner analogous to the treatment of the space and angle derivatives,³ the one-dimensional discrete-ordinates code ANISN⁴ has been modified to include the time-dependent behavior of the particles or radiation of interest.

Preliminary calculations with the new code were focused on a hypothetical single-velocity problem having an infinite isotropic scattering medium with an instantaneous point source. Since the most difficult problems for the time-dependent code are those concerned with pulse propagation, this simple problem was appropriate for the test calculations. The discrete-ordinates calculations were compared with a detailed Monte Carlo calculation of the same problem.⁵ In order to accurately describe the propagation of the pulse of uncollided particles without imposing severe restrictions on the space and time mesh spacings, an analytic first-collision source was implemented. Concurrent with the use of the first-collision source, a new spatial difference model was introduced for use in that space interval containing the pulse of uncollided particles. This model may be considered as a moving boundary condition which assures that the flux in space intervals beyond the uncollided pulse is identically zero while maintaining particle balance. The combination of these techniques prevented a buildup of particles beyond the uncollided pulse which had been observed in earlier calculations, and the results obtained compared well with a Monte Carlo calculation of the pulse propagation.

Calculations of the single-velocity problem with various space-time mesh combinations and multi-group simultaneous neutron-gamma calculations revealed occasional oscillations in the particle flux with respect to space and time. The instabilities appeared to be related to the ratio of the distance traveled by a particle in a time interval to the distance across a space interval, $v \Delta t / \Delta r$, and the oscillations were always larger when $v \Delta t / \Delta r$ was near 1. Use of a step-differencing scheme in space and angle instead of the usual diamond-step model³ removed the oscillations but, as expected, reduced the ac-

curacy of the calculations. An alternate difference model, suggested by characteristic schemes and dependent on $v \Delta t / \Delta r$, was implemented and proved to be adequate in most cases.

Since the new model was not entirely successful in removing the instabilities in the more severe cases, a weighted diamond-difference model suggested by Lathrop and Carlson⁶ was programmed. The model ensures positive fluxes (assuming positive sources) and allows a continuous variation between the diamond and step schemes independently in space, time, and angle. Examination of the weighting coefficients has shown that the near-step-function models are used more frequently, particularly in space and angle. Even so, accuracy has been maintained with respect to Monte Carlo comparisons, and flux oscillations are no longer apparent.

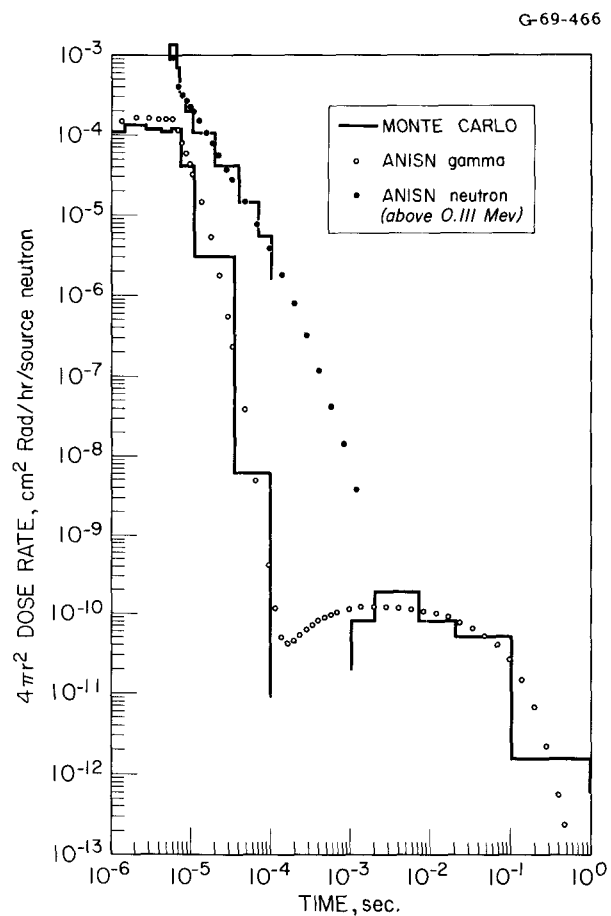


Fig. 2.33.1. Fast Neutron and Gamma Dose Rates 300 m from a Point 12.2- to 15-MeV Neutron Source in Air.

Figure 2.33.1 shows the fast-neutron and total gamma dose rates as a function of time 300 m from a point 12.2- to 15-MeV source in infinite air as calculated by time-dependent ANISN using the weighted diamond model and by Monte Carlo.⁵

References

- ¹This work funded by the Defense Atomic Support Agency under NWER Subtask 6.044.
- ²Computing Technology Center, Union Carbide Corp., Oak Ridge, Tenn.
- ³F. R. Mynatt, "The Discrete Ordinates Method Problems Involving Deep Penetrations," *A Review of the Discrete Ordinates S_n Method for Radiation Transport Calculations*, ORNL-RSIC-19 (March 1968).
- ⁴W. W. Engle, Jr., *A User's Manual for ANISN*, K-1693 (Mar. 30, 1967).
- ⁵E. A. Straker, W. W. Engle, Jr., and P. N. Stevens, *Some Calculated Milestone Solutions to Time-Dependent Radiation Transport Problems*, ORNL-TM-2499 (Apr. 22, 1969).
- ⁶K. D. Lathrop, *User's Guide for the TWOTRAN (x, y) Program*, LA-4058 (February 1969).

2.34 FEATURES IN THE DOT-II CODE

F. R. Mynatt¹ W. W. Engle, Jr.¹
R. J. Rodgers¹

A revised version of the DOT code known as DOT-II has been made operational. Although development is continuing, it was judged desirable to make this improved version of the two-dimensional discrete-ordinates code as of January 1, 1969, available through RSIC. The following is a brief description of the new features:

1. Three methods are available for the acceleration of the convergence of the inner iterations. In addition to the usual normalized power iteration, the user may select successive overrelaxation, a semi-iterative method based on Chebyshev polynomials, or a space-dependent normalized power iteration. With the latter procedure, which is recommended, some very difficult problems have been accelerated by factors of from 10 to 20.
2. A zone-of-interest convergence criterion is provided as an option. With this criterion the

average normalized flux error is computed for the specified spatial zone. One may thus specify the convergence requirement for the spatial zone which is most important for a particular problem. The value of this convergence indicator is printed for each iteration for each group.

3. The maximum number of inner iterations allowed can be specified as a function of energy group. This option is often useful when restarting problems for various reasons.
4. As an additional output option, the fission distribution can be punched on cards on completion of the calculation.
5. As standard procedure the DOT-II program will attempt to store the entire flux array in the fast memory. If this is not possible the data storage will be reallocated so that only the fluxes for one group will be in the fast memory. The latter storage allocation can be forced by input option.
6. A source tape containing the scalar and higher angular moments of the source for each space point and group can be used. This is the method of using the results of an analytic first-collision program.
7. An asymmetric angular quadrature can be used; the quadrature is specified by the total number of angles rather than the traditional n of S_n .

Reference

- ¹Computing Technology Center, Union Carbide Corp., Oak Ridge, Tenn.

2.35 DEVELOPMENT OF TWO-DIMENSIONAL DISCRETE-ORDINATES TRANSPORT THEORY FOR RADIATION SHIELDING¹

F. R. Mynatt² F. J. Muckenthaler
P. N. Stevens³

The discrete-ordinates (S_n) method, which is also known as the second version of the S_n method, was first introduced by B. G. Carlson. The two-dimensional discrete-ordinates method has until recently been successful only for relatively easy problems such as criticality calculations for

highly enriched uranium cylinders. The purpose of this study is to extend the capabilities of the two-dimensional discrete-ordinates method in order to provide accurate calculations for deep-penetration radiation transport problems. The basic method is generalized and improved, a complete technique for application is developed, and a comprehensive comparison with experiment is performed.

The generalized discrete-ordinates difference equation is derived by applying an integral operator to each term of the transport equation in a consistent manner. In the convection term the coefficients for ray-to-ray streaming in cylindrical geometry are obtained directly, in contrast with older derivations where they are defined due to flow balance conservation only. In the total collision term a transformation is performed such that an assumption of flux separability is not required. In the scattering integral the angle dependence of the scattering cross section is approximated by a Legendre polynomial series, the addition theorem is used to transform from the collision coordinate system to the laboratory coordinate system, and the final difference form is given by straightforward application of the integral operator. The instability which is inherent in the diamond-difference technique when steep flux gradients occur is removed by a combination of the diamond-difference and step-difference techniques. An example of the effect of mesh size on problem stability is shown.

The inner-iteration procedure is examined from both a physical and analytical viewpoint. Power iteration and normalized power iteration are discussed, and two convergence acceleration techniques, the Chebyshev method and a space-dependent normalized power iteration, are developed. The problem of determining a convergence criterion is discussed, and a zone-of-interest criterion is proposed for two-dimensional calculations. Two test problems are studied, and it is shown that the Chebyshev method can reduce the number of iterations by one-half and that the space-dependent scaling can reduce the number of iterations by one-seventh. These improvements in the inner-iteration procedure make it possible to obtain converged solutions to deep-penetration problems within reasonable computational times.

Three additional improvements in the method are developed. An analytic first-collision source is developed for use in point-source problems

which may have "ray effects" and for problems with monodirectional beam sources in which the collided and uncollided components must be separated. The question of preferred quadrature sets is examined, and a method for using tailored quadratures is developed. The problem of calculating the flux at arbitrary points external to the system is considered. Three techniques are developed: two of these involve a surface integration of the angular flux, and the third involves a last-flight response based on an adjoint solution.

In order to provide an unequivocal test of the methods, a clean-geometry experiment was designed and executed, and the results are compared with calculations. The experiment comprises large slab shields exposed to a collimated reactor beam source. The emergent angle-dependent spectra were measured with the NE-213 liquid organic scintillator-FERDOR spectra unfolding system which gives spectra in the energy range from 0.8 to 15.0 MeV. Fast-neutron dose measurements were also made, including dose profiles at the exit faces of the slabs. Lead, polyethylene, laminated lead and polyethylene, and depleted uranium slabs were included in the study. A large number of calculations were performed, and many comparisons are shown.

References

- ¹Abstract of CTC-INF-952 (to be published).
- ²Computing Technology Center, Union Carbide Corp., Oak Ridge, Tenn.
- ³University of Tennessee.

2.36 A USER'S MANUAL FOR ASOP - ANISN SHIELD OPTIMIZATION PROGRAM¹

W. W. Engle, Jr.²

ASOP is a one-dimensional shield optimization program based on the one-dimensional discrete-ordinates code, ANISN.³ The code was written for the IBM/360 and will compile on the IBM/FORTRAN-IV-H compiler.

The user's manual describes only that portion of the ANISN input which is applicable to the optimization process. As an aid to data preparation, selected input and output of a typical problem are presented.

References

- ¹Abstract of CTC-INF-941 (to be published).
²Computing Technology Center, Union Carbide Corp., Oak Ridge, Tenn.
³W. W. Engle, Jr., *A User's Manual for ANISN*, K-1693 (Mar. 30, 1967).

2.37 AVKER: A PROGRAM FOR DETERMINING NEUTRON KERMA FACTORS FOR USE IN ENERGY DEPOSITION CALCULATIONS^{1,2}

M. Solomito J. J. Ritts³
 H. C. Claiborne

The FORTRAN code AVKER calculates neutron kerma factors which may be used to determine dose or heat generation rates in materials. The program allows the evaluation of the kerma factors for any desired composition that can be made up from elements presently available in the kerma library and for any arbitrary group structure within the energy limits of 19.2 MeV to 0.023 eV.

References

- ¹This work supported by Defense Atomic Support Agency under Task No. RRP-PE037.
²Abstract of ORNL-TM-2558 (Apr. 15, 1969).
³Reactor Division.

2.38 SPACETRAN: A CODE TO CALCULATE DOSE AT DETECTORS AT VARIOUS DISTANCES FROM THE SURFACE OF A CYLINDER^{1,2}

S. N. Cramer³ M. Solomito

Program SPACETRAN is a FORTRAN code designed to calculate the energy-dependent total flux, or some proportional quantity, due to the radiation leakage from the surface of a right circular cylinder at detector positions away from the surface. Two versions of the SPACETRAN code are described. One uses the surface angular fluxes calculated by the S_n code ANISN as the input; the other uses the surface angular flux as described by a cosine distribution. Both versions of the code permit an arbitrary energy group structure and any number of detectors at any position away from the surface.

References

- ¹This work partially funded by the Defense Atomic Support Agency under Task No. PE037.
²Abstract of ORNL-TM-2592 (to be published).
³Computing Technology Center, Union Carbide Corp., Oak Ridge, Tenn.

2.39 SHIELD ANALYSIS AND DESIGN SERVICES

H. C. Claiborne M. Solomito

The function of the Shield Design and Analysis Group is to give assistance in the design of radiation shields, either by solving specific problems or by recommending methods of solution. This has led to the development of new computer codes for use in design and to the improvement of these codes. (An example of the former is the SPACETRAN codes discussed in this report.) In addition, close interaction with the developers of shielding codes is maintained in order to make them more aware of the user's problems and also so that new techniques can be applied to design problems with no delay. Such assistance in the past year has been given to a number of reactor projects at the Laboratory and at nine other government agencies and contractors in weapons reactor and accelerator projects.

2.40 SOME CALCULATED MILESTONE SOLUTIONS TO TIME-DEPENDENT RADIATION TRANSPORT PROBLEMS^{1,2}

E. A. Straker W. W. Engle, Jr.³
 P. N. Stevens⁴

In developing time-dependent transport computer codes it is helpful to have some typical problems for which the answers are believed to be known. Thus reproducibility of these results provides confidence in the use of new techniques. Some time-dependent results are presented for three problems: (1) one-speed isotropic scatterer with nonabsorption probabilities of 0.3 and 0.9; (2) a point 12.2- to 15-MeV neutron source in infinite homogeneous air; and (3) a point fission neutron source in infinite homogeneous air. Both Monte Carlo and discrete-ordinates techniques were used in determining time-dependent results

at three, six, and nine mean free paths for problem 1 and at 300, 600, and 900 m for problems 2 and 3.

References

¹Abstract of ORNL-TM-2499 (Apr. 22, 1969).

²This work funded by the Defense Atomic Support Agency under Subtask No. RRP-2050.

³Computing Technology Center, Union Carbide Corp., Oak Ridge, Tenn.

⁴Consultant, University of Tennessee.

2.41 TIME-DEPENDENT NEUTRON AND SECONDARY GAMMA-RAY TRANSPORT IN AN AIR-OVER-GROUND GEOMETRY. VOLUME II. TABULATED DATA^{1,2}

E. A. Straker

This report presents the tabulated results of Monte Carlo and discrete-ordinates calculations of neutron fluxes and doses and secondary gamma-ray fluxes and doses resulting from an isotropic neutron source located 50 ft above the ground surface. Sources of various energies up to 15 MeV are considered, and in addition the sources are folded together to simulate a fission source. The Monte Carlo data are tabulated as time-energy and time-dose distributions integrated over angle and as time-angle distributions integrated over energy for ranges from the source up to approximately 1500 m. The discrete-ordinates data are tabulated as energy spectra and as angular dose at the various ranges, and also as angular distributions of the thermal, intermediate, fast, and total neutron flux and of the low, high, and total gamma-ray flux.

References

¹This work supported by the Defense Atomic Support Agency under Task No. RRP-2050.

²Abstract of ORNL-4289, vol. II (September 1968).

2.42 NEUTRON AND SECONDARY GAMMA-RAY TRANSPORT IN INFINITE HOMOGENEOUS AIR^{1,2}

E. A. Straker M. L. Gritzner³

The detailed energy, angular, and spatial distribution of neutrons and their secondary gamma

rays is given for nine source energy groups, a fission spectrum, and a typical thermonuclear spectrum. Results for ranges to 2000 m for the ten sources are supplemented with results to 5000 m for a fission and 12.2- to 15-MeV source. In addition to the detailed description of the radiation field, the angular distributions of Henderson dose, Snyder-Neufeld dose, tissue kerma, midphantom dose, concrete kerma, air kerma, ionizing silicon kerma, and nonionizing silicon kerma are given for neutrons, and the Henderson dose, concrete kerma, air kerma, and silicon kerma are given for secondary gamma rays. Some comparisons with air-over-ground results are given.

References

¹This work funded by the Defense Atomic Support Agency under NWER Subtask 6.044.

²Abstract of ORNL-TM-2503 (to be published).

³Computing Technology Center, Union Carbide Corp., Oak Ridge, Tenn.

2.43 SHIELD DESIGN STUDY FOR A SPACE STATION CONCEPT

F. R. Mynatt¹ W. W. Engle, Jr.¹
L. R. Williams¹

Extensive calculations have been performed with the ASOP² one-dimensional shield optimization program and the DOT-II³ two-dimensional discrete-ordinates transport code for the nuclear design of a radiation shield for a manned space station concept. The shield design is determined by both the source and the dose constraints. In this case the source is the reference-design 600-kW zirconium hydride-moderated SNAP reactor,⁴ which may be contained in a cylindrical envelope approximately 30 in. long and 22 in. in diameter, and the converter equipment gallery, which may be contained in a truncated cone 24 in. high with a base 64.5 in. in diameter and a top 56 in. in diameter containing approximately 260 Ci of ²⁴Na activity. The design dose limits are specified as 1.82 millirems/hr on a 46-ft-diam dose plane located 117 ft from the reactor and 200 rems/hr on a spherical surface centered at the reactor and having a 100-ft radius.

The first calculations were for the unshielded reactor. DOT calculations were performed to ob-

tain the multiplication factor and fission power distribution. The fission distribution was then used as the source for a 21-neutron-group and 18-gamma-ray-group DOT calculation which gave the neutron and gamma-ray leakage from the reactor.

Numerous ASOP calculations were performed to obtain end and side shield configurations which were optimum with respect to weight. In the ASOP code the radiation transport calculation uses a spherical geometry approximation, but the weight function is that of the actual two-dimensional assembly. In the optimization of the side shield, the end shield does not change, and, in the optimization of the end shield, the side shield is constrained to a minimum thickness. In this design the fixed-size converter gallery heavily influences the shield design. Thus the resulting shield is not optimum for the reactor source only.

When a shield design is obtained from the ASOP, the complete reactor-gallery-shield assembly is calculated with the DOT code. The neutron and gamma-ray dose distributions can be obtained from the DOT calculation for all detector points. In addition the neutron and gamma-ray heating distribution is obtained for the entire assembly. The results from the DOT calculation are used to adjust the dose constraints in the geometrically approximate ASOP calculations so that the distributions from the final two-dimensional DOT calculations are very near the design criteria.

The selection of materials is part of the optimization process. In this study lithium hydride, lead, depleted uranium, and tungsten were considered. The fact that the shields using each material combination are individually optimized with respect to weight greatly mitigates the effects of changing materials. In many cases, when the heavy metal is changed the optimum zone thicknesses will be noticeably changed, but the total shield weight will be relatively constant.

Figure 2.43.1 shows a schematic diagram of a shield design obtained from these procedures for the conditions given above. This shield weighs approximately 11,130 lb. In the DOT calculation the reactor was fully described, including the active fuel region, upper and lower fuel grid plates, three control drum regions, upper and lower coolant plenums, and pressure vessel. Also included were the containment vessel for the lead and the reactor support ring. In this design the fixed diameter of the gallery and the minimum thickness for the side shield heavily

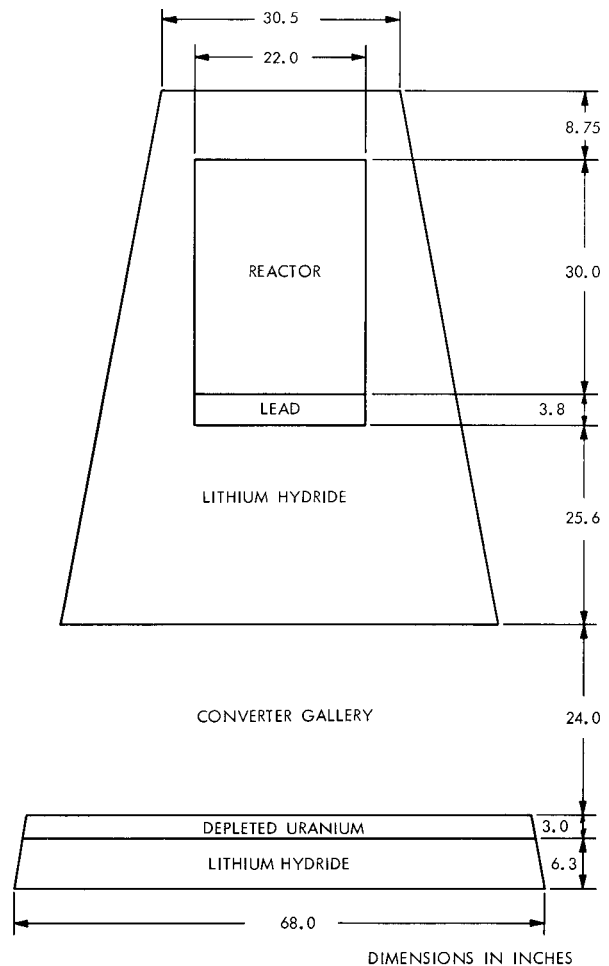


Fig. 2.43.1. Schematic Diagram of an OWS-SNAP Shield Design.

influence the end shield composition. This accounts for the large thickness of the first lithium hydride zone and small thickness of the second lithium hydride zone.

Table 2.43.1 contains the dose values obtained from the DOT calculation of this assembly. For the angle-dependent data on the 100-ft spherical surface, the angles are measured from the z axis in the direction of the crew. The maximum value on the 100-ft surface is 1% over the design criteria, and the maximum dose on the plane 117 ft from the reactor is 5.5% over the design criteria.

This design procedure appears to work quite well in terms of giving an efficient shield for a given set of circumstances. Since the optimization step does not yet include a two-dimensional transport model, there is still a great need for

Table 2.43.1

Detector Angle	Dose Rate		
	Neutron	Gamma	Total
Dose Rates (rems/hr) on the 100-ft-radius Spherical Surface			
13°	0.243	0.08	0.323
30°	6.67	5.10	11.8
47°	20.5	21.8	42.3
64°	50.0	47.3	97.3
81°	93.7	69.7	163.0
99°	122.0	79.8	202.0
116°	113.0	77.4	191.0
133°	87.3	68.9	156.0
150°	82.7	79.4	162.0
167°	93.9	96.9	191.0
Dose Rates (millirems/hr) on the 46-ft-diam Dose Plane Located 117 ft from the Reactor			
	0.200	1.73	1.93

judgment based on experience in the operation of this procedure. However, since the calculational tools used in the evaluation of the design are identical to those used in the analysis of the experiments, the degree of uncertainty in the final results may be quite low.

References

¹Computing Technology Center, Union Carbide Corp., Oak Ridge, Tenn.

²W. W. Engle, Jr., *A User's Manual for ASOP, ANISN Shield Optimization Program*, CTC-INF-941 (to be published). See paper 2.36 of this section.

³F. R. Mynatt, W. W. Engle, Jr., and R. J. Rogers, "Features in the DOT-II Code," paper 2.34 of this section.

⁴Private communication from Atomics International.

2.44 ANALYSIS OF VOID STREAMING EFFECTS IN A MISSILE SILO COVER SHIELD

F. R. Mynatt¹ L. R. Williams¹

Figure 2.44.1 shows a hypothetical design for a missile silo closure shield. The cover con-

sists of a concrete cylinder that is enclosed in steel on the bottom and sides and supported on a steel-lined concrete ledge. A relatively thin 1-in. air gap separates the cylindrical cover from the steel-lined concrete wall and provides the necessary clearance for movement.

The typical one-dimensional analysis of the radiation protection afforded by this cover approximates the geometry with an infinite slab. Although the air gap is not contiguous with or in line with the air space under the cover, the large attenuation of the concrete cover is such that the streaming in the air gap is important.

A calculation of the cover design was performed with the two-dimensional discrete-ordinates code DOT, using a coupled 27-neutron-group and 18-gamma-group cross-section library, a typical S_{10} (70 angles) quadrature, and P_3 approximation of the scattering cross section. The source was the initial radiation from a weapon and was approximated with isotropic and direct angular components. It was observed that the flux in the slit decreased faster than the uncollided flux which could be obtained from an analytical calculation. This difficulty was traced to the requirements placed on the quadrature by the void streaming. To a point at the bottom of the slit the source appears

G-69-502

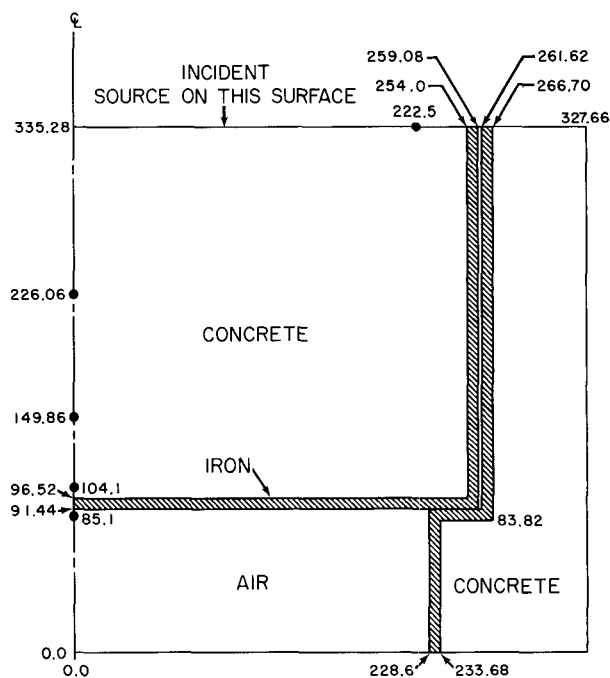


Fig. 2.44.1. A Possible Silo Closure Shield Design.

to be a curving line source of decreasing strength because of the large radius of curvature.

In order to calculate accurately the void streaming in the discrete-ordinates code, the quadrature must be such that the entire source can "see" a point at the bottom. In terms of the quadrature there must be several polar angle levels between 0 and 20°, each with several azimuthal angles which can connect points at the top and bottom

Table 2.44.1. The Effect of Quadrature on the Uncollided Flux in the Slit

Quadrature	Attenuation Factor for Uncollided Flux
Analytic	3.21×10^{-4}
S-100	8.9×10^{-6}
S-147	1.45×10^{-5}
S-189	1.21×10^{-4}
S-315	3.11×10^{-4}
S-525	3.19×10^{-4}

of the slit. Asymmetric quadratures with 100 to 525 angles were used, and the results were compared with the analytical results for the uncollided flux. Table 2.44.1 shows that essentially the correct answer is obtained with the 315-angle set. A calculation including scattering in the slit also showed that an acceptable answer can be obtained by using the 315-angle set only for the first iteration (giving the uncollided flux) followed with the 100-angle set for the subsequent iterations.

Figure 2.44.2 shows the axial distributions of the total (neutron and gamma) dose for the problem with a source elevation of 16°. The dose in the slit follows the uncollided flux except for a slight upturn at the bottom caused by secondary gammas in the iron. The dose at the center of the cover follows the one-dimensional result to a distance approximately 120 cm from the bottom, below which it increases to a value approximately 40 times the one-dimensional result. Larger streaming effects were obtained at higher source elevations.

Future work will include analysis of other possible designs, an evaluation of the applicability of multigroup transport calculations for

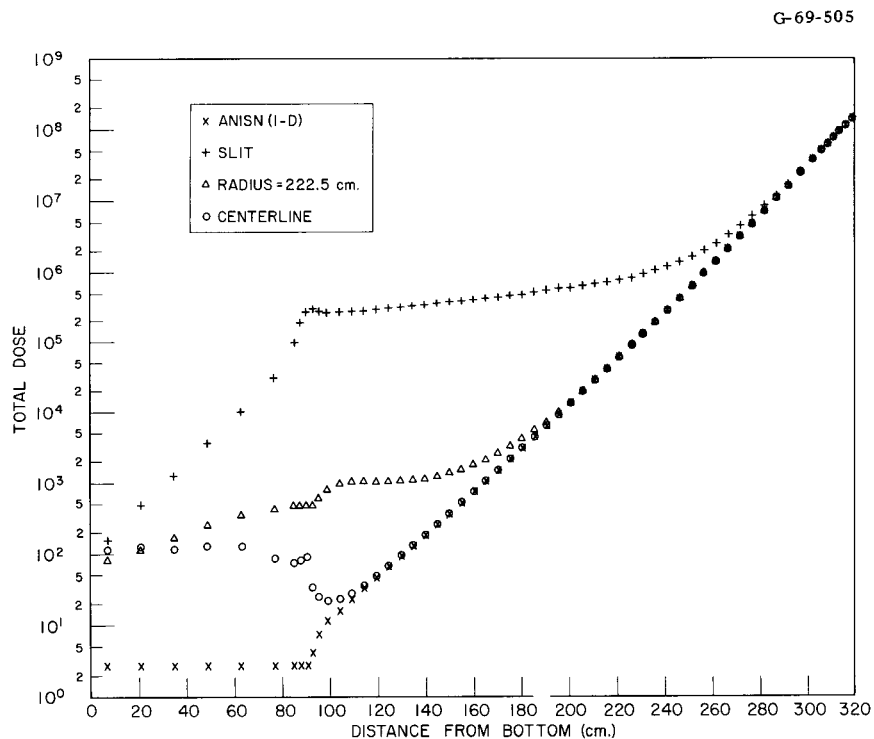


Fig. 2.44.2. Axial Distributions of the Total Dose at Three Radial Locations for a 16° Source Elevation.

the iron-concrete slit problem, and calculations of the time-dependent radiation environment under the cover.

Reference

¹Computing Technology Center, Union Carbide Corp., Oak Ridge, Tenn.

2.45 SENSITIVITY OF NEUTRON TRANSPORT IN OXYGEN TO VARIOUS CROSS-SECTION SETS¹⁻³

E. A. Straker

The effect of several input cross-section sets on the results of neutron transport in an infinite medium of oxygen is determined. The detail with which the minimum in the cross section is represented significantly affects the neutron intensity at deep penetration. The importance of using angular distributions and total cross sections determined with approximately the same energy resolution is demonstrated by results obtained by combining parts of two different cross-section sets. In addition, the effect of various amounts of smoothing of the input cross sections over energy is also shown. In general, the slope of the $4\pi R^2$ dose curves at deep penetration is determined by the minimum in the total cross section as used in the code.

References

¹This work supported by the Defense Atomic Support Agency under Subtask No. RRP-2050.

²Abstract of ORNL-TM-2252 (June 26, 1968).

³Abstract of Technical Notes, *Nucl. Sci. Eng.* (1968).

2.46 GROUND HEATING DUE TO A POINT SOURCE OF 12.2- TO 15-MeV NEUTRONS AT AN ALTITUDE OF 50 ft^{1,2}

E. A. Straker M. B. Emmett³
C. L. Thompson³

The heat transferred to structural concrete due to the neutrons and their secondary gamma rays from a

12.2- to 15-MeV neutron source at an altitude of 50 ft has been determined as a function of range, concrete depth, and time. Both Monte Carlo and discrete-ordinates methods were used to transport the neutrons and gamma rays through the atmosphere and into the ground. The importance of low-energy neutrons and the secondary gamma rays to the total heat deposited is shown.

References

¹Abstract of ORNL-TM-2587 (to be published).

²This work funded by the Defense Atomic Support Agency under NWER Subtask 6.044.

³Mathematics Division.

2.47 HEAT TRANSFER STUDY OF A LITHIUM HYDRIDE SPACE SHIELD¹

J. Lewin R. D. Sabin²
J. D. White² K. Yamada²

Temperature distributions were calculated in a "4 π " shield surrounding a zirconium hydride compact reactor operating at 600 kW (thermal). Heat generation rates within the shield were available from DOT calculations of radiation interactions in the shield. The configuration is shown in Fig. 2.47.1. The heat conduction code HEATING, first written by the ASTRA Corp., was used to perform the calculations on the IBM-360/75 computer at ORNL.

The components of heat generation within the shield are: ²³⁸U fissions in the uranium around the reactor, gamma-ray absorption in the uranium, neutron elastic moderation in the lithium hydride, neutron capture in the ⁶Li of the lithium hydride, and gamma-ray absorption in the lithium hydride. A measure of the relative magnitudes of these contributions to internal heating are provided by the following values on the reactor axis, below the reactor.

At the inner surface of the 0.6-in.-thick uranium: 1.4 W/cc ²³⁸U fissions; 0.73 W/cc gamma absorption. At the interface of the uranium and the lithium hydride, in the lithium hydride: 0.0465 W/cc neutron moderation; 0.023 W/cc ⁶Li(*n,α*)*T* reactions; 0.0075 W/cc gamma absorptions in lithium hydride.

A sampling of the most significant temperature profiles obtained along the axis is given in Fig.

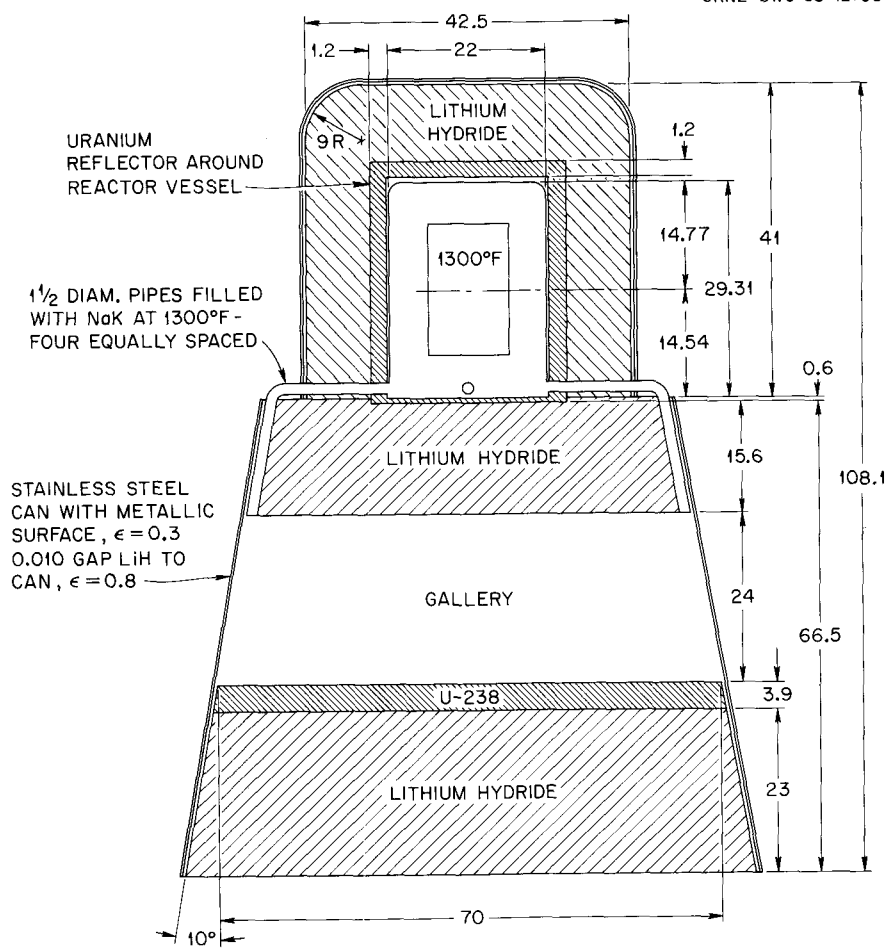


Fig. 2.47.1. "4 π " Shield for Man-Rated SNAP System.

2.47.2. The four cases are for the following four physical situations:

Case 1 – As shown in Fig. 2.47.1. Contact between uranium and lithium hydride; 0.010-in. gap between lithium hydride and stainless steel can that radiates to space with an emissivity of 0.3 and shape factor of 1.

Case 2 – Same as in Fig. 2.47.1 except: (a) a $\frac{1}{16}$ -in. layer of insulation of $K = 0.08 \text{ Btu hr}^{-1} \text{ ft}^{-1} (\text{°F})^{-1}$ between the uranium and lithium hydride, below the reactor only; (b) the 0.010-in. gap between the lithium hydride and the stainless steel can is filled with a material whose conductivity is $20 \text{ Btu hr}^{-1} \text{ ft}^{-1} (\text{°F})^{-1}$.

Case 3 – Same as case 2 except the 0.010-in. gap between lithium hydride and stainless steel was assigned an equivalent conductivity to simu-

late the radiative transfer from the hydride to the can.

Case 4 – Same as case 2 except for a $\frac{1}{8}$ -in. layer of insulation of $K = 0.08 \text{ Btu hr}^{-1} \text{ ft}^{-1} (\text{°F})^{-1}$ between the uranium and lithium hydride, below the reactor only.

The results, subject to some qualifications, indicate that:

1. acceptable operating temperatures for lithium hydride are exceeded in all cases, save possibly case 4;
2. the peak temperatures are insensitive to conditions at the shell.

Therefore it is the heat generation internal to the shield, plus the conductivity of the lithium hydride, that dominates the peaking of temperatures.

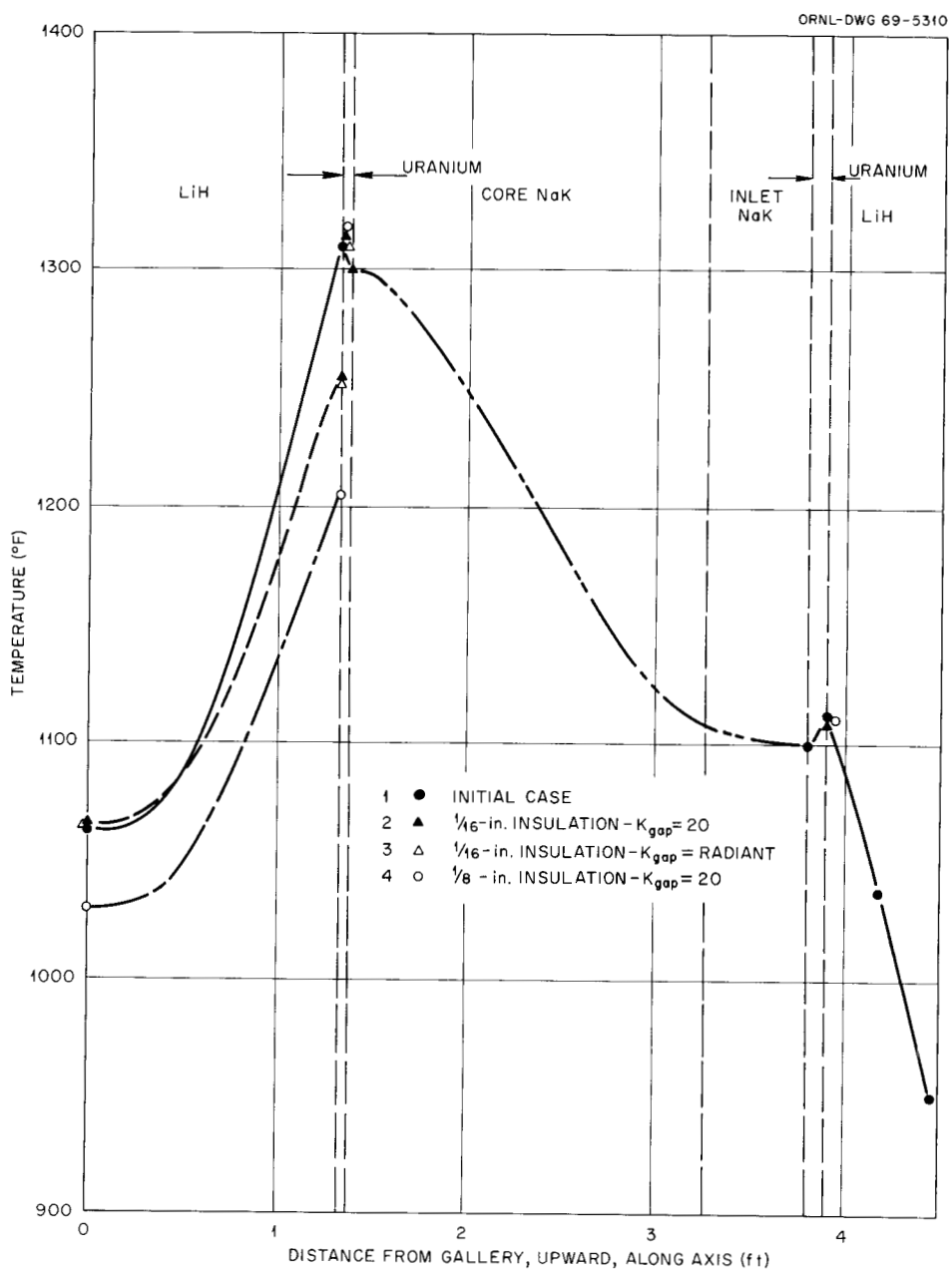


Fig. 2.47.2. Temperatures Along Axis for Steady-State 600-kW Operation of Reactor.

References

- ¹Abstract of ORNL-OREPS-7.
²University of Tennessee—Oak Ridge Engineering Practice School.

2.48 DOSE RATES IN A SLAB PHANTOM FROM MONOENERGETIC GAMMA RAYS^{1,2}

H. C. Claiborne D. K. Trubey

Gamma-ray flux-to-dose conversion factors obtained with a philosophy consistent with that used for neutron conversion factors have not been available for use in design work. To eliminate this inconsistency and develop more realistic gamma-ray conversion factors, gamma-ray dose rate distributions were determined in a slab phantom of a standard man composition.

Calculations were made with the discrete-ordinates code ANISN with some checks by the Monte Carlo code OGRE. Based on these results, a recommended curve to convert gamma-ray flux to maximum dose rate delivered to a body was prepared for design use.

It is also recommended that a new unit, the maximum exposure dose (MED), be used in shield design work to express the product of the flux, dose-rate conversion factor, and quality factor for both gamma rays and neutrons.

References

- ¹This work partially funded by the Defense Atomic Support Agency under Subtask No. RRP-5033.
²Abstract of ORNL-TM-2574 (Apr. 28, 1969).

2.49 A SIMPLE METHOD FOR DETERMINING A LEAD-STEEL SHIELD FOR SHIPPING CASKS THAT IS EQUIVALENT TO A LEAD SHIELD¹

M. Solomito H. C. Claiborne

A simple method is provided for determining the combined steel-lead shield thickness of casks for shipping spent fuel elements when the required lead shield thickness is known. Curves are given which relate the shielding provided by lead alone to an equivalent shield of lead followed by steel. This allows the designer to take into account quickly and simply the shielding effect of the

structural steel which is normally used in shipping cask design.

Reference

- ¹Abstract of ORNL-TM-2591 (to be published).

2.50 OGRE-CDE: A MONTE CARLO CODE FOR CALCULATING RESPONSE FUNCTIONS OF A COMPTON DIODE DETECTOR TO GAMMA RAYS^{1,2}

C. Y. Fu³ R. W. Roussin⁴
 V. R. Cain

OGRE-CDE, a computer program based on the OGRE-G Monte Carlo code, was developed to calculate the contribution to the response of a Compton diode detector due to the net number of Compton electrons transferred to the collector element. Comparisons of several calculations with experimentally determined responses using three diodes of equal size for source energies from 0.66 to 2.76 MeV are presented and exhibit reasonable agreement, which suggests that the transfer of Compton electrons across region boundaries is a major source of the detector response. Computational results for a five-diode detector of different heights and source energies ranging from 0.66 to 8.0 MeV are also given.

References

- ¹This work supported by USAMC Harry Diamond Laboratories under Agreement 40-76-66.
²Abstract of ORNL-CF-68-6-61 (June 28, 1968).
³University of Tennessee.
⁴Summer student, University of Illinois. At present, in Neutron Physics Division, Oak Ridge National Laboratory.

2.51 THE SHIELDING EFFECTIVENESS OF SINGLE-COMPARTMENT ABOVE-GROUND CONCRETE STRUCTURES AGAINST THE INITIAL RADIATION FROM NUCLEAR WEAPONS^{1,2}

L. G. Mooney³

The radiation dose inside hardened above-ground concrete structures that results from the initial radiation produced by a nuclear weapons detonation

has been calculated for weapons detonated as surface bursts and for ranges greater than 300 m. Predictive methods have been applied to define the neutron, nitrogen capture gamma, and fission product gamma distributions along the air-ground interface for weapons categories formulated to be representative of nuclear weapons of all types and yields. Calculations were performed to determine the various components of the total dose inside structures due to the initial radiation incident on the walls and roof of the structures. These components include the doses resulting from neutrons, nitrogen capture gamma rays, and fission product gamma rays penetrating the walls and roof, the neutrons scattered by the inside surfaces of the structure, and capture gamma rays produced within the concrete walls, roof, and floor of the structures. Attention has also been given to the dose contribution resulting from entranceway streaming of neutrons and gamma rays. The outside incident nitrogen capture gamma rays and concrete capture gamma rays were found to contribute the major portion of the dose inside the structure.

References

¹This work sponsored by the Defense Atomic Support Agency for performance under subcontract with Oak Ridge National Laboratory, operated by Union Carbide Corp. under contract with the U.S. Atomic Energy Commission.

²Abstract of RRA-T93 (to be published).

³Radiation Research Associates, Inc., Fort Worth, Tex.

2.52 ANALYSIS OF INITIAL RADIATION PROTECTION ABOARD SHIP^{1,2}

R. L. French³

J. M. Newell³

A system using three machine codes was developed to compute the shielding effectiveness of naval vessels against initial radiation from nuclear weapons. The new code system accepts arbitrary free-field neutron and gamma-ray energy and angle distributions (including secondary gamma rays) and transforms the radiation incident upon the major external surfaces of a ship into a fixed set of energy and angle groups. These distributions are

then folded with transmission data (including secondary gamma production) computed for a fixed set of iron slab thicknesses by the ANISN code.⁴ The emerging energy and angle distributions are treated as effective sources on the inner surface of the ship's hull and deck. The above operations are performed by the "source" code, and the results are transferred to the "integration" code.

The "geometry" code sets up an integration mesh over the inner surface of the hull and deck and traces the line of sight between each differential area and specified detector positions. The angle between each line of sight and the differential area is computed, and the slant thicknesses through partitions and compartment contents along each line of sight are accumulated. These data, along with the exterior iron thickness associated with each differential area, are transferred to the integration code.

Input data for the geometry code are taken directly from a ship description tape produced by a USNRDL code system called the "ship vulnerability model."⁵ This model represents the ship as a three-dimensional array of rectangular parallelepipeds, each corresponding to a compartment. The tape includes the thickness of each partition and identifies the function of each compartment.

The integration code interpolates the effective source energy and angle distribution data for the iron thicknesses of each section of the ship's hull and deck. A dimensionless attenuation factor, based on ANISN⁴ data giving the fraction of the radiation which would be transmitted to a corresponding mass depth in a semi-infinite iron medium, is applied to the radiation along each line of sight in integrating over the effective sources. This "mush" concept precisely accounts for the uncollided radiation and provides an approximation of that scattered in by materials off the line of sight, including backscatter from material beyond the detector position. Secondary radiation produced in the interior of the ship is treated in a like manner.

The modular design of the code system allows the source code and the geometry code to be completely independent of one another. Thus source data for various nuclear weapon attack situations may be processed and held on file for later application to a given ship. Likewise, geometry analyses for a variety of ships may be held on file for processing with one or more attack situations.

References

¹Summary of paper to be presented at Annual ANS Meeting in Seattle, Wash., June 15-19, 1969.

²This work sponsored by the Defense Atomic Support Agency for performance under subcontract with Oak Ridge National Laboratory, operated by Union Carbide Corp. under contract with the U.S. Atomic Energy Commission.

³Radiation Research Associates, Inc., Fort Worth, Tex.

⁴W. W. Engle, Jr., *A User's Manual for ANISN*, K-1693 (1967).

⁵J. Manganaro, *The Ship Vulnerability Model (SVM)*, NRDL-TR-68-31 (1968).

2.53 A REVIEW OF CURRENT TECHNOLOGY FOR PREDICTING THE INITIAL NUCLEAR RADIATION ENVIRONMENTS PRODUCED BY NUCLEAR WEAPONS¹

R. L. French²

A review is being made of the available information and data (both calculated and measured) on the initial radiation environment produced by nuclear weapons to identify those data and methods which best represent the state of the art. The end product of the review is to be a report which discusses the physics of initial radiation transport and presents a selection of data suitable for use in updating the report entitled *Capabilities of Atomic Weapons* (TM-23-200, Department of the Army, November 1959).

To date, the study has centered on determining the types of data, that is, which specific quantities and which weapon types should be included in the report, and on evaluating recent neutron transport and secondary gamma data for sources near the air-ground interface.

References

¹This work sponsored by the Defense Atomic Support Agency for performance under subcontract with Oak Ridge National Laboratory, operated by Union Carbide Corp. under contract with the U.S. Atomic Energy Commission.

²Radiation Research Associates, Inc., Fort Worth, Tex.

2.54 SHIELDING ANALYSIS OF MILITARY STRUCTURES¹

R. L. French²

As a result of an invitation extended at a 1967 meeting of the Shielding Panel of the Defense Atomic Support Agency (DASA), several requests from military commands were made to ORNL for shielding analysis of specific structures. The purpose of the analyses was twofold: (1) to test the adequacy of the data and methods being incorporated into the DASA Weapons Radiation Shielding Handbook and (2) to provide assistance to the military in solving specific shielding problems.

Initial and fallout radiation analyses were performed for four different structures, and the results were given in informal reports.³⁻⁶ The analyses indicated that considerable improvisation was required to apply the handbook methods and data to real structures. In particular, the handbook as originally conceived was deficient in methods for treating above-ground structures and structures that contained significant amounts of materials other than concrete. The fallout shielding methodology was generally adequate for the tasks.

References

¹This work sponsored by the Defense Atomic Support Agency for performance under subcontract with Oak Ridge National Laboratory, operated by Union Carbide Corp. under contract with the U.S. Atomic Energy Commission.

²Radiation Research Associates, Inc., Fort Worth, Tex.

³R. L. French and J. M. Newell, *Shielding Analysis of a Naval Communications Tower*, RRA-N72 (Apr. 7, 1967).

⁴R. L. French, J. M. Newell, and J. H. Price, *Shielding Analysis of a Blast Resistant Shelter*, RRA-N73 (May 12, 1967).

⁵R. L. French, J. M. Newell, J. D. Marshall, and W. E. Selph, *Shielding Analysis of a Hardened Naval Communications Tower*, RRA-N77 (Aug. 11, 1967).

⁶R. L. French and L. G. Mooney, *Shielding Analysis of a Protective Structure*, RRA-N78 (Aug. 23, 1967).

2.55 CALCULATIONS OF THE RADIATION LEAKAGE INTO MISSILE SILOS EXPOSED TO NUCLEAR WEAPONS INITIAL RADIATION¹

M. B. Wells²J. D. Marshall²

A study was performed to evaluate the effect on the radiation doses inside the silo of radiation streaming in the air gap formed between the cover shield and wall of a missile silo for the silo geometry illustrated by Mynatt and Williams.³ The incident radiation environment considered in the calculations consisted of the prompt gammas, air capture gammas, air inelastic gammas, and neutrons produced by the detonation of a nuclear weapon at elevation angles of 16 and 90°. The energy and angular distributions of each of the components of the neutron and gamma-ray fluence incident on the closure shield were taken from ref. 4.

Both the ANISN⁵ and DOT⁶ codes were used to study the effects of streaming of radiation in the air gap formed between the cover shield and silo wall.⁷ The ANISN calculations were used to give transmitted doses for the case where there was no air gap, and DOT was used to evaluate the transmitted doses when the air gap was present.

The neutron cross sections were obtained from the GAM-II library and the gamma-ray cross sections from the MUG code. The gamma-ray production cross sections for gamma rays produced by neutron capture and inelastic scattering were taken from the *Reactor Handbook*. Gamma-ray production cross sections for gamma rays produced by inelastic scattering with Ti, Mg, Ca, Na, K, P, and S were not available in the format needed for input to DOT and ANISN, and since this contribution would be small, it was neglected.

Comparisons between the DOT and ANISN calculations for each of the weapon burst elevation angles revealed that the presence of a 1.0-in. air gap between the closure shield and the silo wall results in significant increases in the neutron and gamma-ray doses at the bottom of the closure shield over that calculated without a gap (using ANISN). The neutron and gamma-ray doses were computed by use of DOT and ANISN at depths greater than 210 cm below the top of the closure shield.⁸ The presence of the air gap causes the neutron and gamma-ray doses on the center line at the bottom of the closure shield to be higher than

those computed neglecting the air gap by factors of about 670 and 18 respectively. For the case where the burst angle of elevation was 90°, the presence of the air gap increased the neutron and gamma-ray doses by factors of 2500 and 8600 respectively. The neutron and gamma-ray doses along a radial at the bottom of the shield varied by factors of about 6 and 3, respectively, as the radial distance was increased from 0 to 222.5 cm.

An increase in the burst angle of elevation from 16 to 90° results in an increase in the total transmitted dose on the center line by a factor of 620 when the 1-in. air gap is considered, whereas only a factor of 2.2 increase was found in the ANISN calculated total transmitted dose. The DOT calculations indicate that the gamma dose at receiver position near the bottom of the closure shield results almost entirely from neutron interactions within the concrete and steel.

The results of these calculations indicate that a serious shielding problem exists for silos having an air gap between the closure shield and wall if the closure shield design was for a minimum shield thickness based on infinite slab penetration calculations.

References

¹This work sponsored by the Defense Atomic Support Agency for performance under subcontract with Oak Ridge National Laboratory, operated by Union Carbide Corp. under contract with the U.S. Atomic Energy Commission.

²Radiation Research Associates, Inc., Fort Worth, Tex.

³See Fig. 2.44.1 of this section.

⁴*Attachment 3, Input Characteristics, Closure Analysis and Tests (U)* revised May 17, 1967, SA67/0000-2488 (SRD-1).

⁵W. W. Engle, Jr., *A User's Manual for ANISN*, USAEC report K-1693.

⁶F. R. Mynatt, F. J. Muckenthaler, and P. N. Stevens, *Development of Two-Dimensional Discrete Ordinates Transport Theory for Radiation Shielding*, CTC-INF-952, to be published. Also see paper 2.35 of this section.

⁷E. P. Blizard (ed.), *Reactor Handbook*, 2d ed., vol. III, Part B, *Shielding* (1962).

⁸See Fig. 2.44.2 of this section.

2.56 CALCULATIONS OF NEUTRON AND SECONDARY GAMMA-RAY DOUBLY DIFFERENTIAL ALBEDO DATA FOR STEEL-COVERED CONCRETE SLABS¹

M. B. Wells²J. D. Marshall²

DOT calculations³ of neutron and secondary gamma-ray reflection from a 2-ft-thick concrete slab covered with a 1-in.-thick steel layer have been analyzed to obtain neutron and secondary gamma-ray number albedo data as a function of the incident energy, the incident polar angle, the reflected energy, the reflected polar angle, and the reflected azimuthal angle. The DOT calculations gave the number of neutrons reflected in each of 35 different solid-angle directions for each of 27 incident neutron energy groups between 14.9 MeV and 0.0253 eV. The reflected neutron data were sorted into the same energy intervals as those used for the incident neutron energies. The reflected secondary gamma rays were sorted into 18 energy intervals between 10.0 and 0.01 MeV and five polar-angle directions for each incident neutron energy group and polar angle.

The number albedo data were folded with single-collision neutron fluence-to-dose conversion factors and gamma-ray fluence-to-dose conversion factors to obtain dose reflection factors.

The neutron dose reflection factor data were compared with Monte Carlo data generated by Allen *et al.*,⁴ and in all cases it was found that the DOT-calculated dose reflection factors as a function of the incident neutron energy were slightly lower than Allen's. Both sets of data have a noticeable minimum at an incident energy of about 1.1 MeV, with the dip in the pure iron data from Allen's calculations being more predominant. The angle distributions of the dose reflection factors were found to be in reasonably good agreement with those computed by Allen *et al.*⁴ and Burrell and Cribbs.⁵ The calculated neutron reflection factor for 1 in. of iron backed by a 2-ft-thick concrete slab was slightly less than those computed by Burrell and Cribbs for a 5-in.-thick iron slab. Most of the iron-concrete results lie between the results calculated by Burrell for 2-in.- and 3-in.-thick iron slabs.

The thermal-neutron number albedo was found to vary approximately with incident angle as that found by Maerker and Muckenthaler⁶ for concrete, but to be about a factor of 2 less.

The thermal-neutron capture gamma-ray dose albedo as a function of incident angle for an iron-covered concrete slab was generally a factor of 2 greater than that calculated by Wells⁷ for concrete alone.

References

¹This work sponsored by the Defense Atomic Support Agency for performance under subcontract with Oak Ridge National Laboratory, operated by Union Carbide Corp. under contract with the U.S. Atomic Energy Commission.

²Radiation Research Associates, Inc., Fort Worth, Tex.

³F. R. Mynatt, Computing Technology Center, Union Carbide Corp., private communication. See also paper 2.44 of this section.

⁴F. J. Allen, A. Futterer, and W. Wright, *Neutron Reflection and Flux Versus Depth for Iron*, Ballistic Research Laboratories Report No. 1199 (March 1963).

⁵M. O. Burrell and D. L. Cribbs, *A Monte Carlo Calculation of Neutron Penetration Through Iron Slabs*, Lockheed Aircraft Corporation Report NR-82, vol. III (May 1960).

⁶R. E. Maerker and F. J. Muckenthaler, *Nucl. Sci. Eng.* **26**, 33 (1966).

⁷M. B. Wells, *Reflection of Thermal Neutrons and Neutron-Capture Gamma Rays From Concrete*, Radiation Research Associates, Inc., Report RRA-M44 (June 1964).

2.57 WEAPONS RADIATION SHIELDING HANDBOOK: STATUS REPORT¹

L. S. Abbott, H. C. Claiborne, and
C. E. Clifford, Editors

As the editing of the *Weapons Radiation Shielding Handbook* has progressed, it has become apparent that changes in the order of the chapters would both improve the continuity of the handbook and increase its usefulness. As a result what was to have been Chap. 2 has been published as Chap. 6. Now titled "Methods for Predicting Radiation Fields Produced by Nuclear Weapons," the chapter gives detailed descriptions of the various sources of radiation produced by a nuclear weapons burst

and presents techniques for calculating the transport of the radiations from the point of burst to the surface of a shield. Typical spectra of the various sources are presented, including weapons emission spectra. The calculational procedures recommended vary from simplified methods, which yield estimates for certain classes of weapons, to sophisticated machine techniques. Basic transport data which can be applied to specific weapons spectra are supplied for the latter techniques.

Chapter 6 will serve as the connecting link between four basic shielding chapters applicable to all low-energy radiation shielding problems and three or more chapters prepared specifically for engineers charged with the responsibility of designing shields to protect military equipment and personnel in the vicinity of nuclear weapons bursts. As now conceived the chapters of the entire Handbook will be as follows:

- Chapter 1. Introduction
- Chapter 2. Basic Shielding Concepts
- Chapter 3. Methods for Calculating Neutron and Gamma-Ray Attenuation (published, 114 pages)
- Chapter 4. Neutron and Gamma-Ray Albedos (published, 50 pages)

- Chapter 5. Methods for Calculating Effects of Ducts, Access Ways and Holes in Radiation Shields (published, 47 pages)
- Chapter 6. Methods for Predicting Radiation Fields Produced by Nuclear Weapons (published, 322 pages)
- Chapter 7. Engineering Methods for Designing Underground Initial Radiation Shelters
- Chapter 8. Engineering Methods for Designing Above-Ground Initial Radiation Shelters
- Chapter 9. Engineering Methods for Designing Fallout Radiation Shelters

Of the remaining chapters, Chap. 7 is in the final stages of publication, and Chap. 2 is undergoing final editing. Drafts of Chaps. 8 and 9 are awaiting editing. At least one additional chapter, on time-dependent effects of weapons radiation, may be added at a later date.

Reference

¹Work funded by Defense Atomic Support Agency under DASA Task No. PEO33.

3. Radiation Shielding Information Center

3.1 RECENT DEVELOPMENTS IN RSIC OPERATIONS¹

D. K. Trubey Betty F. Maskewitz
R. W. Roussin

The Radiation Shielding Information Center continues to serve the technical community engaged in radiation shielding research and development.² This community represents a wide variety of interests, as indicated by the fact that RSIC is supported by three agencies: the Atomic Energy Commission, the National Aeronautics and Space Administration, and the Defense Atomic Support Agency. The people served by RSIC generally have interests in parallel with or are doing work for one of those agencies.

The internal operation of the Center changed markedly as a result of the move to Building 6025. Previously, the staff was located in three separate locations, which made effective communication difficult. Being located together has made it possible to sufficiently increase efficiency to support the ever-increasing work load.

3.1.1 Data Libraries

The performance of machine calculations, in general, may be thought of as a three-part process which can be associated with three components. The first phase is the acquisition and preparation of a data base to be processed. The second is the development and use of a computer program to operate on the input data, perform certain logical operations, and finally produce output data. The output data, the third component, are then analyzed, often with the aid of machine manipulation. The data, after reduction, finally appear in reports and journal articles.

In shielding calculations, the three components normally take the form of (1) cross-section libraries, (2) shielding computer codes, and (3) shielding (output) data.

Since inception, RSIC has actively acquired, packaged, and distributed computer codes. We have also acquired and indexed published literature which contains shielding data. The available input cross-section data have never been entirely satisfactory, because each code requires its own format, and so adequate libraries have depended on users developing their own libraries to satisfy their own requirements.

With the development of the Evaluated Nuclear Data File (ENDF) by the Cross-Section Evaluation Working Group (CSEWG) and the National Neutron Cross Section Center (NNCSC) at Brookhaven National Laboratory, we now have the opportunity to proceed in an orderly fashion to develop a reliable, well-documented set of data available to all. With the development of suitable processing routines, each radiation transport code will be able to utilize data in the standard formats.

Since we feel these developments are so important, RSIC is working closely with NNCSC to assist in getting data of interest to shielders into the ENDF system. The 1968 versions of the codes CHECKER, PLOTFB, CRECT, and DAMMET were received from NNCSC and implemented and extended at Oak Ridge. The extension was mainly the implementation of PLOTFB to edit and plot File 23, photon interaction cross sections. Several sets of "shielding" data were edited, plotted on the ORNL CRT plotter, and examined. Appropriate follow-up actions are being taken. The April 1969 versions of the codes have been received, and implementation has been initiated.

It was obvious that a well-documented fine-group neutron library with high-order angular expansion coefficients was badly needed by the shielding community. Consequently, when the Oak Ridge code

SUPERTOG³ became available, a 99-group $\leq P_8$ set of neutron cross sections based on ENDF/B Cat. I (1968) data was made available on tape. A retrieval program allows the user to select nuclides and expansion order to produce input for ANISN, DOT, DTF, MORSE, or other transport codes.

Output shielding data will also be made available. RSIC is cooperating with the American Nuclear Society in the development and publishing of benchmark problems (see Sect. 3.3). Milestones, or state-of-the-art data, for many more problems will also be compiled and published. Some of these may become benchmarks as data accumulate.

In some cases, the volume of data from a problem may be so great that it is not feasible to publish it all. One can then publish samples of the results but place the entire output on magnetic tape for distribution, as needed, by RSIC. Processing codes for performing editing, plotting, interpolation, and certain integrations would accompany the data. An example is the Hallmark data, which are available in differential form, 5 times more voluminous than the 500-page report.⁴

Data libraries are now being packaged and organized by RSIC in a manner analogous to the RSIC code collection. Each data set carries a Data Library Collection (DLC) number and is packaged as a unit. As with the code packages, a particular data package will not remain static but will be subject to revision, updating, and expansion as required. As of April 30, 1969, nine sets of data have been packaged.

3.1.2 New Class of Codes Distributed by RSIC

A new class of codes has been designated to permit packaging useful routines that are not shielding codes but may be of interest to those doing shielding research. In order to distinguish between complex shielding programs designated as CCC's (Computer Code Collection), these peripheral codes are packaged and designated as such. In the published abstracts, when such a code is useful to a given code package it is labeled an "auxiliary routine." Where it cannot be tied to a specific package, it is packaged alone and carried under a PSR (Peripheral Shielding Routine) number. As of April 30, 1969, eight separate programs have been so packaged.

3.1.3 Electron Transport Theory Seminar – ETRAN Workshop

Fifty-three participants from 24 separate installations were in attendance at the Seminar-Workshop held at the Oak Ridge National Laboratory in January 1969. Cosponsored by RSIC and the Center for Radiation Research, National Bureau of Standards, Dr. Martin J. Berger presented the theory and operation of the electron and photon transport program, RSIC code package CCC-107/ETRAN.

ETRAN is a Monte Carlo computer program which performs the following calculations: (1) the reflection and transmission of electrons and photons by a target, (2) the production of secondary bremsstrahlung and characteristic x-ray photons in the target and their emergences from it, (3) the deposition of energy and charge by electrons as a function of depth in the target, and (4) the flux of electrons as a function of depth in the target.

Dr. Thomas M. Jordan, ART Research Corporation, presented a paper entitled "BETA, a Monte Carlo Computer Program for Bremsstrahlung and Electron Transport Analysis," describing a code which is now available from RSIC.

3.1.4 Literature Store

The three sets of literature files – reactor-weapons, space-accelerator, and computer codes – have continued to increase. The reactor-weapons shielding indexed bibliography was reissued, and the loose-leaf abstracts were updated.

3.1.5 Concrete for Shielding of Neutrons

A review of the use of concrete as a shield for neutrons up to 14 MeV is in preparation. The work is essentially complete and is being reported in a journal article (see Sect. 3.4) and, in a more complete form, as an RSIC report.⁵ The report will not only include a review of previous work but will report results of new calculations of neutron transmission by concrete. The new calculations embody the latest cross sections available and include coupled neutron-secondary-gamma-ray calculations. The cross-section set compiled is being made available on tape as DLC-9.

3.1.6 RSIC Newsletter

As of April 30, the newsletter was being sent to 1086 subscribers, most of whom are individual shielding specialists. Several issues of the newsletter have been used to transmit and publicize recently available basic data of great interest. These were thermal-neutron capture and fission gamma-ray spectra. Other uses of the newsletter have been to publicize conferences and short courses of interest, to list the report numbers used in the shielding field, to outline RSIC policies, and to announce personnel changes of address, as well as to publish the RSIC literature accessions.

The computer-based system was used to produce cards for subscribers to return to verify the distribution list.

3.1.7 General Information Services

The Center provides a variety of information services, such as personal conferences regarding shielding problems, computer searches of bibliographic material, computer-produced abstracts, microfiche copies of difficult-to-obtain reports, and inquiries regarding RSIC services or reports. During the seven months ending April 30, 320 requests were processed in addition to those requests connected with computer codes. (For statistics on computer code services, see below.)

One by-product of the computer file of shielding specialists who receive RSIC material is the referral to shielding specialists in the company of the person making an inquiry. There have been many occasions when we have informed an engineer, newly faced with a shielding problem, of several experienced people who could aid him and who were located at his own installation.

3.1.8 Codes Center Operations

With the entire staff in one location, it has been possible to effect more efficient procedures in the processing of codes, code requests, code information requests, and other services of the RSIC code center. With no addition in staff, new service areas were introduced, which has added to the overall work load. The PSR class of codes and the DLC data libraries are processed, maintained, and distributed by the code center staff.

The computer codes collection^{6,7} has continued to grow, both in number of packages and in additional code development being reflected in those packaged in prior years. The year ending April 30, 1969, was characterized by activity usually designated as feedback. For example, many leads to shielding programming efforts were given to us so that RSIC staff members could follow efforts leading toward codes which would be likely to be acquired later. In 28 instances, a requester received a particular code package, made it operable on hardware different from that for which it was designed, and returned the new version to RSIC. In at least 9 instances, improvements to code packages were made and offered to the Center. In several cases, in response to need, RSIC staff members have improved the usefulness of a code package.

As of April 30, 115 CCC numbers have been assigned to code packages. In many cases the package may contain from one to five different versions, the difference usually due to the hardware on which each is operable. Currently, 43% of the codes packaged are written in FORTRAN-IV, 30% in FORTRAN-II, 11% in FORTRAN-63, and 16% in mixtures of FORTRAN and assembly language.

In the year ending April 30, 950 separate letters of request were received and processed by the code center. Domestic requesters accounted for 90% of these, and 10% of the requests were foreign. Action taken on the requests resulted in the following: 165 complete code packages shipped, 226 additional documents mailed, 61 data tapes sent, and 265 miscellaneous additional requests processed which required time spent by RSIC staff members.

References

¹Work partially supported by National Aeronautics and Space Administration under NASA Order W-12792 and by Defense Atomic Support Agency under DASA Task No. PE055.

²D. K. Trubey, "The Radiation Shielding Information Center - a Technical Information Service for Nuclear Engineers," *Nucl. Eng. Design* (1969).

³R. Q. Wright, J. L. Lucius, N. M. Greene, and C. W. Craven, Jr., *SUPERLOG: A Program to Generate Fine-Group Constants and P_N Scattering Matrices from ENDF/B*, ORNL Technical Memorandum, to be published.

⁴E. A. Straker, *Time-Dependent Neutron and Secondary Gamma-Ray Transport in an Air-over-*

Ground Geometry, Vol. II, Tabulated Data, ORNL-4289, vol. II (September 1968).

⁵F. A. R. Schmidt, *Concrete for Shielding of Neutrons up to 14 MeV*, ORNL-RSIC-26 (to be published).

⁶B. F. Maskewitz, *Abstracts of Digital Computer Code Packages Assembled by the Radiation Shielding Information Center*, ORNL-RSIC-13, vols. I and II (January 1968).

⁷B. F. Maskewitz and D. K. Trubey, *The Radiation Shielding Information Center Computer Codes Collection 1963-1967*, ORNL-TM-1956 (September 1967).

3.2 HANDBOOK ON PROTECTION AGAINST RADIATION IN SPACE¹

J. Wallace Webster

A handbook is being prepared for NASA entitled *Handbook on Protection Against Radiation in Space*. The chapter titles are tentatively as given in Table 3.2.1.

Table 3.2.1. Handbook on Protection Against Radiation in Space

Chapter	Title
I	Space Radiation Environment
II	Radiobiological Factors in Manned Space Flight
III	Effects and Limits for Radiation of Materials and Components
IV	Shielding for Simple Geometries Against Protons and Alpha Particles -- Primary Particles Only
V	Shielding Against Protons, Alpha Particles, and Heavy Galactic Particles for Simple Geometries -- Nuclear Secondaries Included Where Data Are Available
VI	Shielding Against Electrons for Simple Geometries
VII	Shielding Against Electrons and Bremsstrahlung for Simple Geometries
VIII	Shielding Space Vehicles and Shielding Specific Missions

With the help of RSIC's computer system for the selective dissemination of information (SDI), a compilation of document titles and abstracts in the categories relevant to the subject of the handbook was obtained. From the corresponding microfiche, copies of about 600 relevant graphs and tables were compiled. These were then sorted and assigned to the appropriate chapters.

As of May 1, Chaps. I, IV, V, and VIII have received the most study and effort. These chapters or the portions of them that deal with protons, alphas, etc., may be issued separately as Vol. I of the handbook. The material that deals with electrons may be delayed to form a second volume in order to make Vol. I available sooner. Chapters II and III are included in the outline for the sake of completeness. A decision as to whether they will be definitely included will be delayed until the completion of Vol. I.

The sections and subsections of Chaps. I, IV, V, and VIII are tentatively as shown in Table 3.2.2.

Table 3.2.2. Handbook on Protection Against Radiation in Space: Sections and Subsections of Chaps. I, IV, V, and VIII

Chapter I
1 Solar Flares
1.1 Frequency
1.2 Intensity
1.3 Spectra
1.4 Rigidity Studies
1.5 Probability
2 Van Allen Belts
3 Galactic
Chapter IV
1 Protons
2 Alphas
3 Stopping Power and Range Data
Chapter V
1 Monoenergetic Beams
2 Van Allen Belt Spectra
3 Solar Flares
4 Galactic
Chapter VIII
1 Simulated Spacecraft Geometries
2 Long Range Missions
3 Earth Orbiting Missions

Some writing has been done, but final decisions have not been made about how much to include on methods, on interpretation of graphs and tables, etc. About one man-year per year is being expended on the project.

Reference

¹Work funded by National Aeronautics and Space Administration under NASA Order W-12792.

3.3 SHIELDING BENCHMARK PROBLEMS¹

A. E. Profio, Editor²

The Benchmark Problem Group (BPG) of the ANS-6 Standards Committee of the American Nuclear Society, in collaboration with RSIC, has prepared an initial set of benchmark problems for publication. The problem descriptions and data are published in loose-leaf form and distributed by RSIC.

The chairman of the ANS-6 committee is N. M. Schaeffer, Radiation Research Associates. The members of the Benchmark Problems Group are A. E. Profio, Gulf General Atomic, chairman; H. L. Beck, AEC Health and Safety Laboratory; A. H. Foderaro, Pennsylvania State University; A. W. Thiele, Atomics International; and D. K. Trubey, Oak Ridge National Laboratory.

The first benchmark problems are:

- 1.0 Fast Neutron Spectrum from a Point Fission Source in Infinite Graphite, by A. E. Profio
- 2.0 Gamma-Ray Spectrum from a Point ¹³⁷Cs Source in Infinite Water, by H. L. Beck
- 3.0 Neutron Spectrum from Point Fission and 14-MeV Sources in Infinite Air, by E. A. Straker
- 4.0 Gamma-Ray Dose Above a Plane Source of ⁶⁰Co on an Air-Ground Interface, by C. W. Garrett

Considerable thought and discussion have gone into the selection of problems which may serve as computational standards. The four problems chosen for the initial collection were already reasonably well documented and included several configurations of interest in neutron and gamma-ray shielding.

Revisions and extensions are expected as more work is done, more data accumulate for the present problems, and additional benchmarks are chosen. The compilation is being issued by RSIC in loose-leaf form to permit easy updating from time to time.

The primary objective of the benchmark problems effort is to compile in convenient form a limited number of well-documented problems in radiation transport which will be useful in testing computational methods used in shielding.

The compilation and publication of solutions to benchmark problems is expected to accomplish several things: (1) attention will be focused on typical problems where careful work should produce solutions which are representative of the state of the art in solving radiation transport problems, (2) specifications of standard configurations and data will make comparisons more meaningful, (3) discrepancies between calculation and experiment may suggest refinements in the numerical approximations or nuclear data or may suggest new experiments to resolve the disagreement, (4) reliable solutions by several methods will be made available to help judge the precision and efficiency of different codes and to suggest if new codes ought to be developed, (5) transmitted programs and programs converted to new machines may be verified by duplication of the benchmark problem solution, and (6) mistakes in existing or new codes, or their options, can probably be detected by independent calculations of the benchmark problems.

The initial collection is concerned with neutron and gamma-ray transport at energies less than 15 MeV. The committee believes that charged-particle and high-energy radiation problems should be represented, and such problems will be included later.

The committee has decided to include both purely computational problems and theory-experiment comparisons. An effort has been made to compare different theoretical methods in the computational problems and to include enough data so that the solutions can be reproduced at other installations. Results of a single computation, and unverified experiments, are not considered to be sufficiently reliable to serve as benchmarks. In general, solutions by rigorous methods are preferred, although some comparisons with inexact methods may prove interesting.

The purely computational problems serve a somewhat similar purpose as the problems proposed by the Mathematics and Computation Division of the American Nuclear Society, published as ANL-7416.

The Shielding and Dosimetry Division problems are, however, concerned with shielding rather than reactor core physics, and more emphasis is placed on the solution of problems of interest than on mathematical purity or computational detail.

We would like to emphasize the goal of making direct comparisons of calculation with clean, basic, fully documented experiments. The theory-experiment comparisons are intended to serve as tests of computational procedures rather than nuclear data, although there is obviously considerable dependence on nuclear data. We have attempted to mitigate the ambiguity by selecting materials whose cross sections are fairly well known and by making available or referencing the nuclear data so that at least the computational results can be compared by those who wish to use the same data.

The BPG has decided not to define certain configurations for which solutions are desired, but to let them be determined by the current interests of the shielding community at large. However, we believe it would be desirable eventually to include two-dimensional and possibly three-dimensional problems, to attempt to obtain spectra, angular distributions, and secondary gamma-ray production as well as dose, heating, and activation, and to include one or more scattering and albedo-type problems. Possible configurations might include shielding experiments with simple sources in pure materials, laminated iron-water slabs, a space power reactor shielded by heavy metal and lithium hydride, an LMFBR and shield, etc. Space and accelerator shielding problems should be included as well. The ideal would be to have a number of problems of progressively increasing complexity in different areas, all well documented and analyzable, with accurate and complete experimental data if possible.

It is anticipated that the benchmark problems book will be updated from time to time by addition or replacement of pages, in the manner of a loose-leaf notebook, through the Radiation Shielding Information Center. Revisions may be made to existing problems, additional solutions to the same problems added, or new benchmark problems included. These revisions will be announced in the Division news columns of *Nuclear News* and in the RSIC Newsletter.

Inquiries, errata, or additional solutions to the published benchmark problems should be directed to the author of the particular problem concerned,

with an information copy to RSIC for transmittal to the chairman of the Benchmark Problems Group. The author will be responsible for corrections and for review of solutions. He shall recommend to the BPG whether or not a new solution should be added to the benchmark problems book. The BPG will make the final decision. The most important criteria for acceptance are: (1) the solution represents a significant contribution, and (2) it is well documented.

Proposed new benchmark problem descriptions or inquiries about new problems should be directed to RSIC for transmittal to the chairman of the Benchmark Problems Group.

References

¹Summary of introductory material to ORNL-RSIC-25 (June 1969).

²Gulf General Atomic.

3.4 ANALYTICAL RADIATION SHIELDING CALCULATIONS FOR CONCRETE¹

F. A. R. Schmidt²

Formulas for analytical radiation shielding calculations are discussed in view of their applicability to concrete shielding. Based on neutron removal-diffusion theory and gamma-ray buildup factors, they provide a reasonable tool to compare shielding properties of different concretes. Therefore parameters for these formulas were calculated from recent cross sections. A sample calculation is given for the concrete tested at the Oak Ridge National Laboratory (USA) Tower Shielding Facility.

References

¹Abstract of paper submitted to *Nuclear Engineering Design* (1969); work partly funded by Defense Atomic Support Agency under subtask PE055.

²Present address: Institut für Kernenergetik, Universität Stuttgart, Germany.

3.5 AN EXAMINATION OF SEVERAL CALCULATIONAL MODELS FOR USE IN COMPUTING GAMMA-RAY PENETRATION OF STRUCTURES¹

Hisao Yamakoshi²

Two analytical models for treating multiple scattering of gamma radiation are utilized to predict the penetration of slabs for a slant-incident monoenergetic, monodirectional source incident on lead and polyethylene slabs.

Monte Carlo calculations were also performed to check the validity of these two models and to give data for the construction of response functions for transmitted dose.

The first model, the so-called "extended single scattering" model, treats the effect of multiple scatterings beyond the first within a barrier by applying a buildup factor to the first scatter, taken to be a source. The second model is based on the idea of the successive collision model, and formulations of transmitted dose and spectra for up to triple scatterings are derived.

Comparison between the numerical calculation of the first model and the Monte Carlo calculation with the OGRE-P3 code shows that the first model is generally not adequate for the prediction of the transmitted gamma-ray field.

Comparison between the second model and the Monte Carlo results shows fairly good agreement.

References

¹Abstract of ORNL-TM-2520 (1969); work partly funded by Defense Atomic Support Agency under subtask PE055.

²Present address: Ship Research Institute, Tokyo, Japan.

3.6 BIBLIOGRAPHY, SUBJECT INDEX, AND AUTHOR INDEX OF THE LITERATURE EXAMINED BY THE RADIATION SHIELDING INFORMATION CENTER (REACTOR AND WEAPONS RADIATION SHIELDING)¹

D. K. Trubey

J. Gurney

An indexed bibliography is presented of literature selected by the Radiation Shielding Information Center in the area of radiation transport and

shielding against radiation from nuclear reactors, x-ray machines, radioisotopes, nuclear weapons (including fallout), and low-energy accelerators. The bibliography was printed by computer from magnetic tape files. In addition to lists of literature titles by subject category, author and key-word indexes are given.

Most of the literature selected was published in the years 1966-68.

Reference

¹Abstract of ORNL-RSIC-5 (Vol. II) (March 1969); work partly funded by Defense Atomic Support Agency under subtask PE055.

3.7 ABSTRACTS OF THE LITERATURE EXAMINED BY THE RADIATION SHIELDING INFORMATION CENTER (REACTOR AND WEAPONS RADIATION SHIELDING)¹

The abstracts included in this loose-leaf binder cover all the reactor and weapons radiation shielding documents that are in both the literature store of the Radiation Shielding Information Center and the latest edition of the RSIC bibliography. At this writing (September 1968), the latest edition of the bibliography is ORNL-RSIC-5 (Vol. II), *Bibliography, Subject Index, and Author Index of the Literature Examined by the Radiation Shielding Information Center (September 1968)*, which is being issued along with these abstracts. Additional abstracts will be issued for inclusion in this loose-leaf binder when the next bibliography is ready for publication.

Although most of the abstracts included here were taken directly from the published documents, some were written by RSIC staff members. These were limited to documents which either did not contain abstracts or contained abstracts that were not sufficiently informative. Only unclassified abstracts are included; all are subject to revision or replacement. At the left-hand margin next to each abstract is an RSIC accession number for the document itself.

Reference

¹Abstract of ORNL-RSIC-6 (Vol. II) (January 1969); work partly funded by Defense Atomic Support Agency under subtask PE055.

3.8 PROGRAMS FOR THE AUTOMATIC TRANSLATION OF CROSS-SECTION DATA BETWEEN THE ENDF AND UKNDL FORMATS

D. C. Irving R. Q. Wright¹

For many years the storage and processing of evaluated neutron cross-section data was an excessively fragmented operation. Each laboratory and often each calculational program had its own format and data library. In recent years, however, the handling of cross sections has been coalescing into the use of two systems, the ENDF/B² library, developed through a cooperative effort in the United States, and the UKNDL library,^{3,4} developed mainly in the United Kingdom. New programs for neutronics calculations are generally being tied to one or the other of these two systems. New cross-section evaluations are nearly always being put into one of these two formats. Although the initial development of these systems has gone on in two different countries, the increasing international exchange of cross-section data and computer programs has created an interest in both systems on both sides of the Atlantic.

To increase the exchange of data sets, to improve the comparability of calculations and pro-

grams, to make the UKNDL data library available for use in ORNL-developed computer programs (which use the ENDF system), and to eliminate the confusion and useless competition of two mesh cross-section formats, we have been developing a program to translate data from the UKNDL format to the ENDF/B format and vice versa. These programs, with the exception of the data for the unresolved resonance region and for the energy distributions of secondary neutrons, are now complete for the translation of neutron cross-section data. Upon completion of the missing sections, the routines will be turned over to the National Neutron Cross Section Center and to RSIC for use and distribution.

References

- ¹Computing Technology Center, Union Carbide Corp., Oak Ridge, Tenn.
- ²H. C. Honeck, *ENDF/B, Specifications for an Evaluated Nuclear Data File for Reactor Applications*, BNL-50066 (1966).
- ³K. Parker, *The Aldermaston Nuclear Data Library as of May 1963*, AWRE 0-70/63 (1963).
- ⁴D. S. Norton, *The U.K.A.E.A. Nuclear Data Library, February, 1968*, AEEW-M824 (1968).

4. Theoretical Studies for Medium- and High-Energy Radiation Shielding

4.0 INTRODUCTION

Theoretical studies of medium- and high-energy radiation transport are pursued on a continuing basis. The purpose of the program is to provide basic data and to study transport methods that are applicable to the shielding of manned space vehicles and high-energy accelerators. While many of the problems involved in the shielding of manned spacecraft are quite different from those involved in shielding high-energy accelerators, the two disciplines have a sufficient area of overlap that it is efficient for them to be considered under the same general program. An excellent example of the overlap between interests of the National Aeronautics and Space Administration and the U.S. Atomic Energy Commission is provided by the calculations of the radioactive residual nuclei produced in matter by a high-energy nucleon-meson cascade. The ability of the nucleon-meson transport code, developed as part of this program, to predict with some reliability the production of these nuclei has been used extensively during the past year in the design of the shielding around the 200-GeV accelerator under construction at the National Accelerator Laboratory, Batavia, Illinois, and will be used in the forthcoming year to estimate the radioactive nuclei induced in the moon by solar-flare and cosmic-ray bombardment.

One of the fundamental difficulties in the study of medium- and high-energy radiation transport has always been the lack of information concerning particle production from nucleon-nucleus collisions, and therefore a substantial portion of the program is devoted to the calculation of such particle-production cross sections. Because of the very large amount of data required, a reliance on experimental information is not practical, but efforts are continually made to obtain experimental verification of the theoretical cross sections by comparing with available experimental data.

Using these theoretical cross sections, transport methods are studied, and their validity is confirmed by comparisons with experimental data. The purpose of this portion of the program is not only to devise elaborate transport methods that yield results of high accuracy but also to devise approximation methods that are sufficiently accurate and easily applicable to be suitable for routine shield design.

A substantial portion of the program is also directed toward using the best available transport methods to provide design data as required by those groups presently engaged in designing particular shields. In the accelerator shielding program, a large number of calculations have been carried out in the past year to provide the data required to design the shielding around the 200-GeV accelerator under construction at the National Accelerator Laboratory. Also, the transport methods that are developed as part of the shielding program are useful in areas that are only peripherally related to shielding. A small part of the program is directed toward these other applications which are of interest to the National Aeronautics and Space Administration and to the U.S. Atomic Energy Commission.

4.1 INTRANUCLEAR-CASCADE CALCULATION OF THE SECONDARY NUCLEON SPECTRA FROM NUCLEON-NUCLEUS INTERACTIONS IN THE ENERGY RANGE 340 TO 2900 MeV AND COMPARISONS WITH EXPERIMENT^{1,2}

H. W. Bertini Arline H. Culkowski³
Miriam P. Guthrie

Total nonelastic cross sections and the nucleon spectra from continuum-state transitions for protons on complex nuclei are calculated using the intranuclear-cascade approach. Comparisons with experiment are made over the energy range 340–2900

MeV. The diffuseness of the nuclear surface, the energy distribution of the bound nucleons, and the exclusion principle are taken into account in the model of the nucleus, while experimentally determined free-particle elastic, inelastic, and differential cross sections are utilized in the calculation of the particle-particle reactions assumed to take place inside the nucleus. The Sternheimer-Lindenbaum isobar model is used in describing all pion production processes. The calculation is essentially parameter free, and hence all comparisons with experiment can be made on an absolute basis. The theoretical nonelastic cross sections and theoretical secondary-particle spectra resulting from continuum-state transitions are shown to be in reasonable agreement with experimental data over the broad energy range considered.

References

¹Work partially funded by National Aeronautics and Space Administration under Order H-38280A.

²Abstract of ORNL-TM-2361 (Mar. 14, 1969). Submitted for journal publication.

³Mathematics Division.

4.2 PROTONS FROM 2.7-GeV PROTONS ON Ag AND Br^{1,2}

D. T. King³

The cross section for nonelastic collisions of 2.7-GeV protons in silver and bromine nuclei has been determined. Among 3565 such collisions in nuclear emulsions, the tracks of 646 outgoing protons with kinetic energies in the range 80–850 MeV were identified by measurements of ionization and multiple Coulomb scattering. The differential cross sections for proton emission were derived and compared with the predictions of Bertini using the Monte Carlo treatment of the intranuclear cascade. A reasonable agreement has been found.

References

¹Work partially funded by National Aeronautics and Space Administration under Order H-38280A.

²Abstract of ORNL-TM-2536 (Mar. 14, 1969). Submitted for journal publication.

³Consultant, The University of Tennessee, Knoxville, Tenn.

4.3 CALCULATION OF THE CAPTURE OF NEGATIVE PIONS IN LIGHT ELEMENTS AND COMPARISON WITH EXPERIMENTS PERTAINING TO CANCER RADIOTHERAPY^{1,2}

M. P. Guthrie R. G. Alsmiller, Jr.
H. W. Bertini

Reactions resulting from the capture of π^- mesons in carbon, nitrogen, oxygen, and aluminum have been studied using a Monte Carlo intranuclear-cascade model. The calculation predicts the multiplicities of the particles emitted following π^- capture and the residual nuclei remaining after the reaction. The energy distributions of the emitted particles and the residual nuclei have also been calculated. The results of the calculation have been compared with experiments investigating the feasibility of the use of π^- mesons in cancer radiotherapy, and reasonable agreement has been obtained.

References

¹Work partially funded by the National Aeronautics and Space Administration under Order H-38280A.

²Abstract of *Nucl. Instr. Methods* **66**, 29–36 (1968).

4.4 ABSORPTION, CHARGE-EXCHANGE, AND DOUBLE-CHARGE-EXCHANGE REACTIONS OF π MESONS WITH COMPLEX NUCLEI: COMPARISONS OF THEORETICAL PREDICTIONS WITH EXPERIMENTAL RESULTS

H. W. Bertini

The two-step cascade-evaporation approach is used in the calculation of charge-exchange, double-charge-exchange, and absorption reactions of pions with complex nuclei. The cascade and evaporation calculations are described elsewhere.^{1,2} To delineate the pion reactions that can take place, the pions are allowed to scatter and to charge-

exchange scatter from the bound nucleons within the nucleus, and they can be absorbed directly by two-nucleon clusters inside the nucleus. In addition, pions can be absorbed by the nucleus as a whole when their kinetic energy falls below an arbitrary cutoff energy, which is half the Coulomb barrier. The theoretical neutron spectra from pion-absorption reactions, therefore, consists of (1) a high-energy portion that results from the two-nucleon absorption reaction that involves emitted primary nucleons and secondary knock-outs and (2) of a low-energy evaporation portion that results from both the absorption of the pion by the nucleus as a whole and the residual excitation energy remaining in the nucleus after a two-nucleon absorption event.

Comparison of the theoretical neutron spectra with experimental results for slow π^- capture on carbon and lead are shown in Figs. 4.4.1 and 4.4.2. The data have been arbitrarily normalized, as indicated in the figure captions, to illustrate the shapes of the curves. The comparisons of the experimental and theoretical neutron multiplicities

for carbon, lead, and several other elements are shown in Table 4.4.1. The agreement in the shape of the spectrum and in the multiplicities for the light elements is quite good. There is disagreement for the heavy elements in that the total number of neutrons emitted is overestimated while the number of fast neutrons is underestimated. This is manifest in Fig. 4.4.2 also, where the shape of the spectrum is not hard enough. It is possible that absorption of pions by heavy nuclei occurs predominantly through high-angular-momentum states of the π -mesic atom,³ whereas a crude calculation indicates that the theoretical model closely resembles absorptions from the $2p$ state of the π -mesic atom for a lead nucleus. Absorptions from higher-angular-momentum states imply that the absorption reactions take place near the surface of the heavy nuclei, and hence the nucleons that absorb the pion can escape more frequently without scattering. They will then carry away more energy upon escaping and leave the nucleus with relatively little excitation energy.

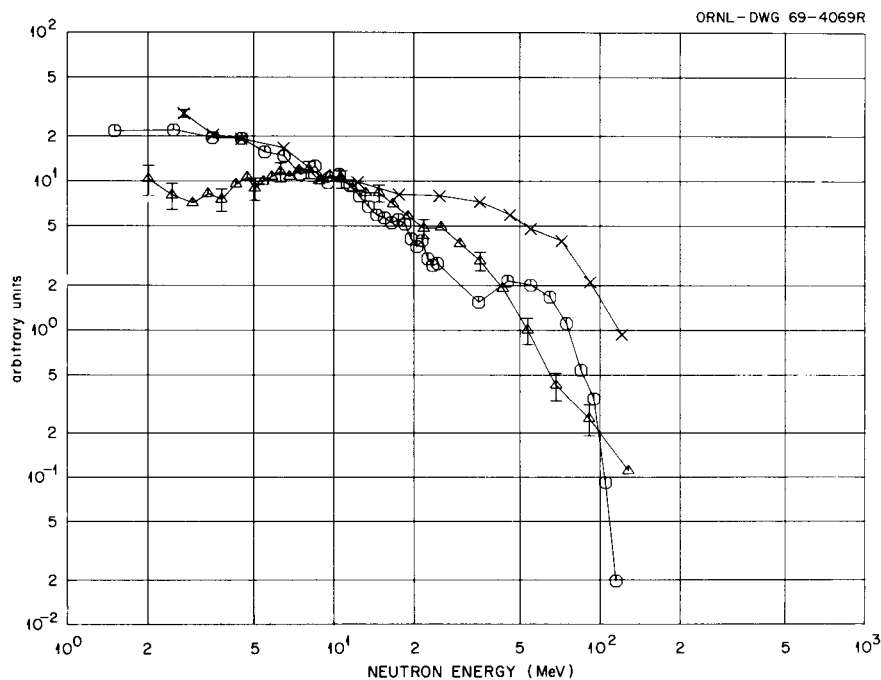


Fig. 4.4.1. Energy Spectra of Emitted Neutrons from π^- -Meson Capture in Carbon. Open circles: theoretical spectrum; triangles: experimental spectrum of H. L. Anderson *et al.* [*Phys. Rev.* 133, B392 (1964)]; x's: experimental spectrum of P. M. Hattersley, H. Muirhead, and J. N. Woulds, [*Nucl. Phys.* 67, 309 (1965)]. The lines connecting the points are drawn to guide the eye. All data have been arbitrarily normalized to the same value at 9.5 MeV.

Table 4.4.1. Experimental and Theoretical Neutron Multiplicities and Neutron Energies Associated with π^- Absorption in Several Targets

Target	Average Value of Total Number of Emitted Neutrons per Pion Absorption		Average Value of the Number of "Direct" Neutrons Emitted per Pion Absorption		Total Kinetic Energy Carried Away by All the Neutrons (MeV)		Kinetic Energy Carried Away by the Evaporation Neutrons (MeV)		Average Excitation Energy Prior to Evaporation (MeV)	
	Experimental	Theoretical ^a	Experimental	Theoretical ^a	Experimental	Theoretical ^a	Experimental	Theoretical ^a	Experimental	Theoretical ^a
C	2.92 ± 0.36^b 2.9 ± 0.3^c	2.7	1.83 ± 0.23^b 2.4^d	1.2	110 ± 11^b 68^d	63	5.84 ± 0.7^b	9		63
O	2.77 ± 0.34^b	3.0	1.74 ± 0.24^b	1.2	105 ± 12^b	61	5.62 ± 0.8^b	15		68
Al	3.07 ± 0.42^b	2.9	1.60 ± 0.23^b	1.1	100 ± 12^b	51	7.70 ± 1.0^b	11		78
	3.6 ± 0.3^c	3.0	2.2^d	1.2	74^d	53		12		77
Cu	5.03 ± 0.62^b 7.4 ± 0.4^e	5.7	2.19 ± 0.3^b 2.1^e	0.95	123 ± 12^b	51	12.4 ± 1.5^b 30 ± 3^e	20	89 ± 5^e	91
	$^{112}_{48}\text{Cd}$ $^{119}_{50}\text{Sn}$	8.1	1.8^d 2.1^e	0.78	80^d	51		25	95 ± 5^e	100
Pb	4.98 ± 0.58^b	11	1.81 ± 0.23^b	0.67	100 ± 12^b	50	13.2 ± 1.5^b	26	88 ± 6^e	107
		11		0.68		50		26		107
	5.0 ± 0.5^c	11	1.9^d	1.0	69^d	49		25		104
	9.4 ± 0.5^e		2.6^e				41 ± 4^e			
U	6.9 ± 0.7^c	13	2.2^d	0.64	100^d	52		30		109

^aTheoretical values listed for Al and Pb are for nuclear models involving different ratios of n - p to p - p absorption and different cutoff energies. The details are described in the text.

^bP. M. Hattersley, H. Muirhead, and J. N. Wouls, *Nucl. Phys.* **67**, 309 (1965).

^cThese numbers were taken from P. H. Fowler and V. M. Moyes, *Proc. Phys. Soc.* **92**, 377 (1967), who extrapolated the spectra of Anderson *et al.* (ref. *d* below) to zero energy.

^dH. L. Anderson, *et al.* *Phys. Rev.* **133**, B392 (1964).

^eG. Campos Venuti, G. Fronterotta, and G. Matthiae, *Nuovo Cimento, Ser. X* **34**, 1446 (1964).

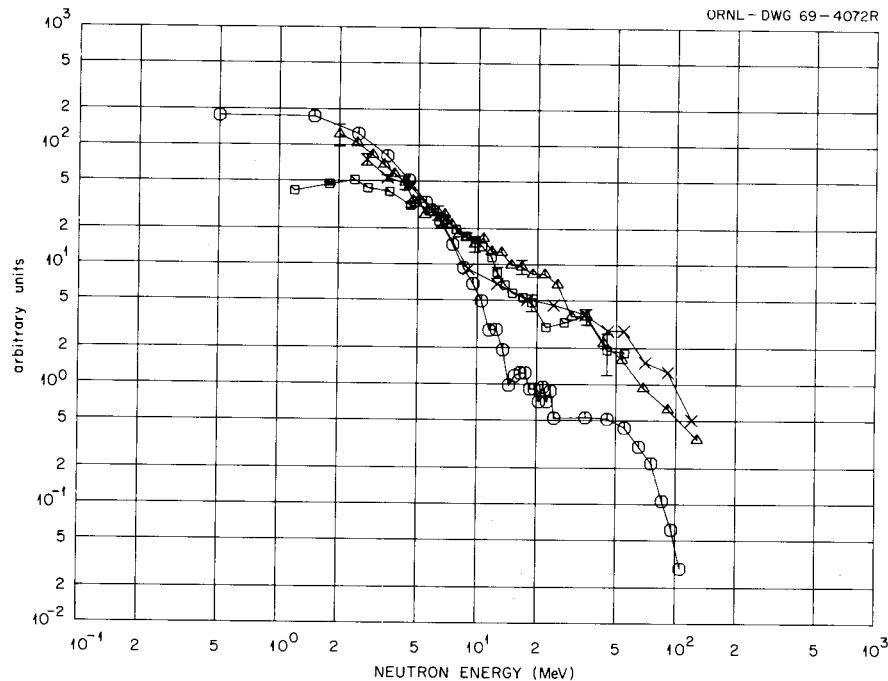


Fig. 4.4.2. Energy Spectra of Emitted Neutrons from π^- -Meson Capture in Lead. Open squares: experimental spectrum of G. Campos Venuti, G. Fronterotta, and G. Matthiae, [*Nuovo Cimento* 34, Ser. X, 1446 (1964)]. Other symbols as defined in Fig. 4.4.1. All spectra have been arbitrarily normalized to the same value at 6 MeV.

There are three entries in the theoretical columns of Table 4.4.1 for aluminum and lead targets. They represent the results when somewhat different nuclear models are used. The first entries for these elements are from the standard model. The second entries are from a model in which the ratio of absorptions by n - p clusters to absorptions by p - p clusters is changed to 5:1 in order to conform to the experimental results of Ozaki.⁴ In the standard model, this ratio is taken to be the number of n - p pairs divided by the number of p - p pairs of nucleons in each nucleus. The third in the group of entries comes from a model in which the cascade cutoff energy for neutrons is taken to be zero, while for protons it is taken to be the full Coulomb barrier. These changes in the physics of the model produce insignificant changes in the results.

There are very few experimental data on the charge-exchange and double-charge-exchange reactions. A comparison of the theoretical and experimental charge-exchange cross sections for 180-MeV π^+ on carbon and oxygen is shown in Table 4.4.2, and the agreement is found to be quite good.

Table 4.4.2. Charge Exchange Cross Sections for 180-MeV Incident π^+

$^{13}\text{C}(\pi^+, \pi^0)^{13}\text{N}$		$^{18}\text{O}(\pi^+, \pi^0)^{18}\text{F}$	
Experimental ^a	Theoretical	Experimental ^a	Theoretical
3.8 mb	2.3 mb	3.1 mb	3.4 mb

^aB. W. Allardice *et al.*, private communication. Quoted by C. Zupancic, *High Energy Physics and Nuclear Structure*, p. 171, ed. by G. Alexander, North-Holland, 1967.

A comparison of the predicted and experimental double-charge-exchange cross sections for π^+ - and π^- -mesons with approximately the same energy is shown in Table 4.4.3. The experimental reactions were selected to investigate the charge symmetry of the double-charge-exchange cross section. The measurements indicate that there is little charge symmetry, while charge symmetry has been built into calculation. The error limits on the theoretical results are statistical errors, and they represent

Table 4.4.3. Double-Charge-Exchange Cross Sections for Various Reactions of Pions on Nuclei

	Incident Particle	Incident Particle Energy (MeV)	Target	Double-Charge-Exchange Cross Sections (mb)
Experimental ^a	π^+	30–80	Emulsion nuclei with $\langle Z \rangle = 21$	0.4 ± 0.1
Theoretical	π^+	55	${}_{21}^{45}\text{Sc}$	2.7 ± 0.5
Experimental ^b	π^-	40–87	Probably emulsion nuclei with $\langle Z \rangle \approx 21^c$	0.09 ± 0.03
		55	${}_{21}^{45}\text{Sc}$	2.1 ± 0.4
Theoretical	π^-	65	${}_{21}^{45}\text{Sc}$	2.9 ± 0.6

^aYu. A. Batusov *et al.*, *Soviet Phys. JETP* **19**, 557 (1964).

^bYu. A. Batusov *et al.*, *Soviet J. Nucl. Phys.* **1**, 271 (1965).

^c $\langle Z \rangle$ not specified, but a description of the experiment is very similar to that given in ref. *a* by the same authors, where the intent was to examine a reaction charge-symmetrical to that measured in ref. *a*.

one standard deviation. In any case, the predicted cross sections are much larger than the measured ones.

It appears to be a characteristic of the theoretical approach that the prediction of events that represent a small fraction ($\sim 10\%$ or less) of all possible events can be in considerable error. In general, however, there is such a paucity of experimental data involving inelastic pion reactions with complex nuclei in the 100-MeV energy region that statements on the accuracy of the model for these reactions cannot be made yet.

References

¹H. W. Bertini, *Phys. Rev.* **131**, 1801 (1963).

²EVAP-2, described by M. P. Guthrie in *EVAP-2 and EVAP-3: Modifications of a Code to Calculate Particle Evaporation from Excited Compound Nuclei*, ORNL-4379 (March 1969).

³In measurements of π -mesic x rays on elements from aluminum to lead, only those coming from the $4f-3d$ and $5g-4f$ transitions are reported for elements heavier than indium. G. Poelz *et al.*, *Phys. Letters* **26B**, 331 (1968), and H. Schmitt *et al.*, *Phys. Letters* **27B**, 530 (1968).

⁴S. Ozaki *et al.*, *Phys. Rev. Letters* **4**, 533 (1960).

4.5 PHENOMENOLOGICAL DETERMINATION OF THE ANGULAR DISTRIBUTION OF ISOBARS PRODUCED IN HIGH-ENERGY NUCLEON-NUCLEON AND PION-NUCLEON REACTIONS¹

H. W. Bertini Arline H. Culkowski²
Miriam P. Guthrie

In the calculation of nuclear reactions by the method of intranuclear cascades,³ one assumes that the nuclear reaction consists of a series of particle-particle reactions that take place inside the nucleus. These reactions are assumed to be essentially free-particle reactions, and hence free-particle elastic and inelastic cross sections are required to determine the type of reaction that will take place. When a reaction is an inelastic reaction, where π mesons are created, the isobar model of Sternheimer and Lindenbaum⁴ is assumed to be valid for the kinematics calculation of the pions that are produced. In this model a pion is created when a nucleon involved in a collision attains an excitation energy and then moves off from the region of collision in an excited state. This excited nucleon, or isobar, subsequently loses its excitation energy by the emission of a π meson which is given off isotropically in the rest system of the isobar. Hence, a three- or

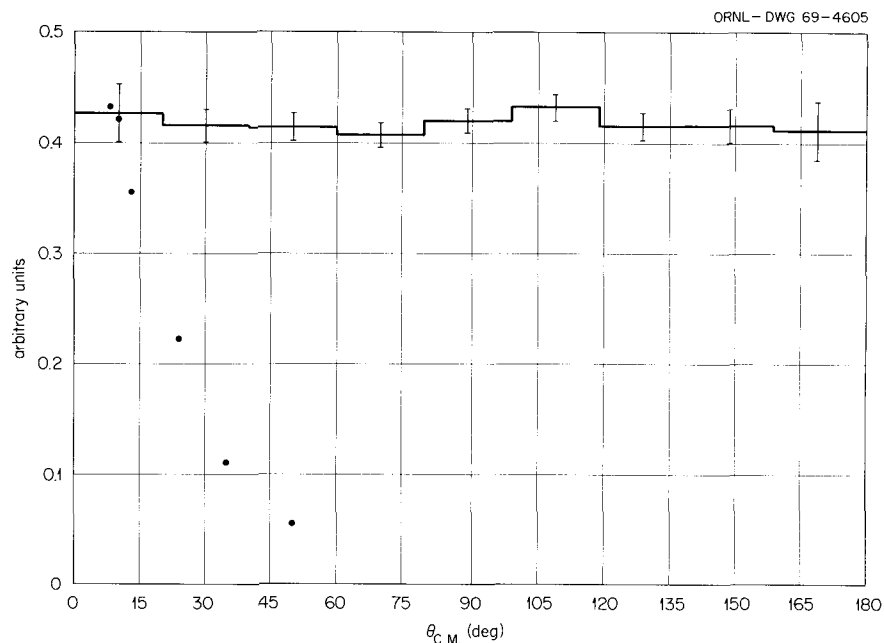


Fig. 4.5.1. Angular Distribution in the Center-of-Mass System for Emission of Recoil Protons with Energies Between 60 and 260 MeV from Single-Pion Production Reactions for 1350-MeV Laboratory Kinetic-Energy Incident Protons on Protons.

four-body problem is reduced to a sequence of two-body problems. The cascade calculation in which this model will be employed is not designed for nuclear reactions at energies higher than about 2500 MeV, and hence it is assumed that only the $\frac{3}{2}, \frac{3}{2}$ isobar is excited.

A major uncertainty in the theory of the isobar model is the center-of-mass angular distribution of the isobars. The theory does not specify this distribution. We will determine it phenomenologically by comparing experimental data with the predicted energy spectra and angular distribution of the reaction particles for various assumed isobar angular distributions. These comparisons will be made for free-particle-particle reactions.

The isobar angular distribution will probably be energy dependent and charge dependent and will depend on whether the initial reaction is a pion-nucleon or nucleon-nucleon reaction. However, no attempt will be made to fit these data with analytic functions, nor will "goodness of fit" or chi-square tests be made. The distributions will be selected by visually comparing results from two extreme distributions with the data and selecting distributions that appear appropriate over large energy ranges and reaction types. Of the extreme

distributions being used, one is isotropic and the other is one in which the isobars go straight forward 50% of the time and straight backward 50% of the time. Examples of the results from these extreme distributions are compared with experimental data⁵ in Figs. 4.5.1 and 4.5.2. The histograms represent the theoretical results, and the open circles represent the experimental data. The experimental data, reported only in the forward direction, are necessarily symmetrical about 90° in p - p reactions. The theoretical results in Fig. 4.5.1 are from the isotropic angular distribution, while those in Fig. 4.5.2 are from the forward-backward distribution. For this specific case, a distribution that is predominantly forward and backward would be appropriate.

References

¹This work partially funded by the National Aeronautics and Space Administration under Order H-38280A.

²Mathematics Division.

³H. W. Bertini, A. H. Culkowski, and M. P. Guthrie, "Intranuclear-Cascade Calculation of the

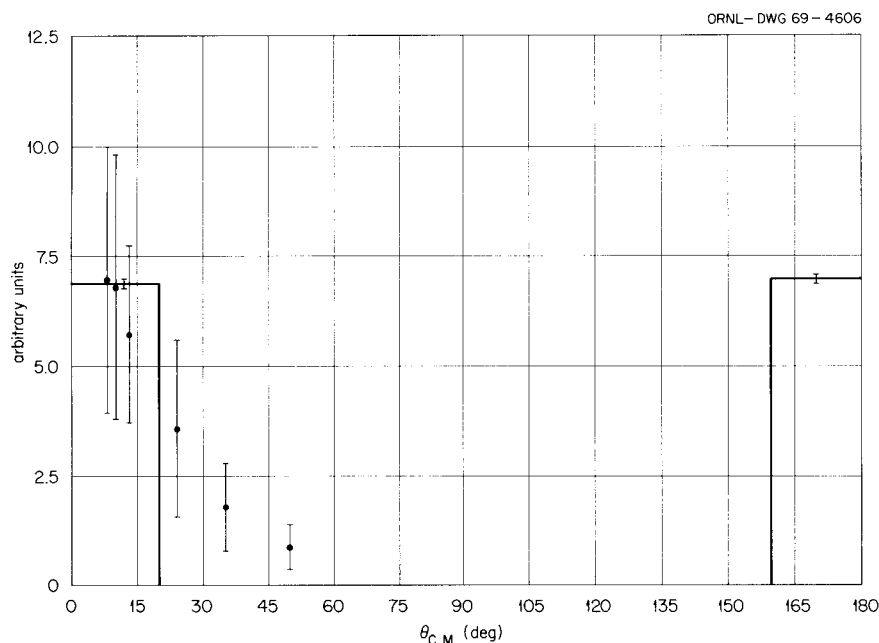


Fig. 4.5.2. Angular Distribution in the Center-of-Mass System for Emission of Recoil Protons with Energies Between 60 and 260 MeV from Single-Pion Production Reactions for 1350-MeV Laboratory Kinetic-Energy Incident Protons on Protons.

Secondary Nucleon Spectra from Nucleon-Nucleus Interactions in the Energy Range 340 to 2900 MeV and Comparisons with Experiment," paper 4.1, this report.

⁴R. M. Sternheimer and S. J. Lindenbaum, *Phys. Rev.* **123**, 333 (1961); *Phys. Rev.* **109**, 1723 (1958); and *Phys. Rev.* **105**, 1874 (1957).

⁵G. B. Chadwick *et al.*, *Phys. Rev.* **128**, 1823 (1962).

4.6 ANALYTIC REPRESENTATION OF NUCLEON- AND PION-EMISSION SPECTRA FROM NUCLEON-NUCLEUS COLLISIONS IN THE ENERGY RANGE 750-2000 MeV^{1,2}

R. G. Alsmiller, Jr. J. Barish³

Analytic fits, obtained by the method of linear least squares, to the intranuclear-cascade data generated by H. W. Bertini are given. For 750-, 1000-, and 2000-MeV protons incident on oxygen, aluminum, and lead, and for 1000-MeV neutrons incident on these same elements, analytic expressions are given for (1) the cascade neutron-, proton-,

π^+ -, π^0 -, and π^- -emission spectra in the laboratory angular intervals 0-30°, 30-60°, 60-90°, 90-180°, and 0-180°, and (2) the evaporation neutron- and proton-emission spectra.

References

¹Work partially funded by the National Aeronautics and Space Administration under Order H-38280A.

²Abstract of ORNL-TM-2277.

³Computing Technology Center, Union Carbide Corp., Oak Ridge, Tenn.

4.7 EVAP-2 AND EVAP-3: MODIFICATIONS OF A CODE TO CALCULATE PARTICLE EVAPORATION FROM EXCITED COMPOUND NUCLEI^{1,2}

Miriam P. Guthrie

The EVAP computer programs calculate the types, multiplicities, and energy distributions of particles evaporated from excited compound nuclei.

The modifications incorporated in EVAP-2 include updating the nuclear masses and shell-plus-pairing energy corrections used as input data, providing for the breakup of ^8Be , and eliminating the possibility of the evaporation residual nucleus having a negative excitation energy. EVAP-3 retains all of the modifications of EVAP-2 and, in addition, calculates the kinetic energies of the recoiling nuclei. The codes are written in FORTRAN IV and operate on the IBM 360 computer. Data cards and the printed output for a sample case are shown.

References

¹Work partially funded by the National Aeronautics and Space Administration under Order No. H-38280A.

²Abstract of ORNL-4379 (March 1969).

4.8 PHOTONUCLEAR DISINTEGRATION AT HIGH (< 350 MeV) ENERGIES^{1,2}

T. A. Gabriel³ R. G. Alsmiller, Jr.

Calculations of high-energy ($40 \lesssim E_\gamma \lesssim 350$ MeV) photon-nucleus ($A \gtrsim 12$) collisions have been carried out. The results of the initial interaction of the photon with the nucleus are obtained either from the quasi-deuteron model of Levinger or, when energetically possible, from one of the four pion-nucleon states formed in photon-nucleon interactions. The effect of nucleon- (pion-) nucleus interactions that follow the initial photon interaction is taken into account by using an intranuclear-cascade model. The results of the calculations are compared with a variety of experimental data, and good agreement is obtained.

References

¹Abstract of ORNL-TM-2481 (Feb. 12, 1969). Submitted for journal publication.

²This paper was submitted by T. A. Gabriel to the University of Tennessee in partial fulfillment of the requirements for the degree of Doctor of Philosophy.

³Work performed while an Oak Ridge Associated Universities Graduate Fellow.

4.9 PHOTONUCLEON AND PHOTOPION PRODUCTION FROM HIGH-ENERGY (50-400 MeV) ELECTRONS IN THICK COPPER TARGETS

T. A. Gabriel R. G. Alsmiller, Jr.

Electron-photon cascade calculations^{1,2} have been carried out for 50-, 100-, 200-, 300-, and 400-MeV electrons on a thick (infinite) copper target. The photon track length per unit energy for photon energies ≥ 22 MeV from these calculations has been used in conjunction with a recently developed model of photonucleon and photopion production from photon-nucleus collisions³ to calculate the energy and angular distribution of high-energy photonucleons (> 15 MeV) and photopions produced by these high-energy electrons. In

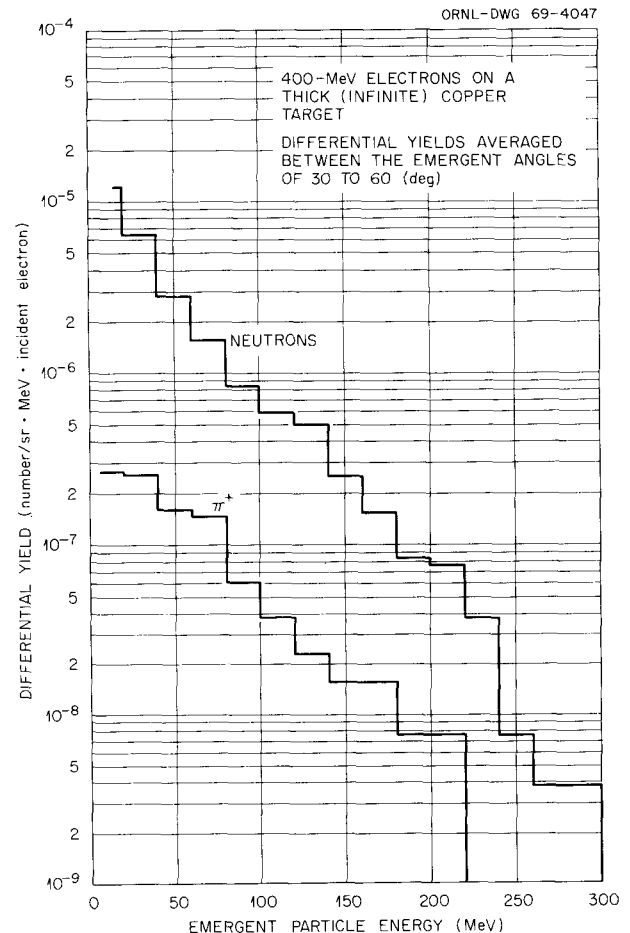


Fig. 4.9.1. Differential Yields of Neutrons and Positively Charged Pions Averaged Over the Angular Interval $30-60^\circ$ from 400-MeV Electrons on a Thick Copper Target.

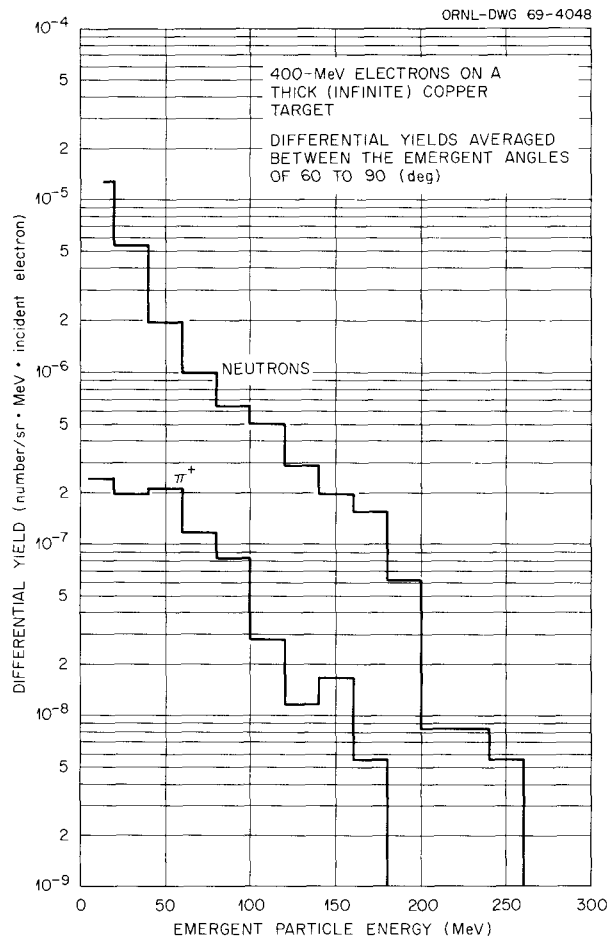


Fig. 4.9.2. Differential Yields of Neutrons and Positively Charged Pions Averaged Over the Angular Interval $60-90^\circ$ from 400-MeV Electrons on a Thick Copper Target.

calculating the angular distribution of the photoparticles, it has been assumed that the angular distribution of the photons with respect to the incident electron may be neglected. It has also been assumed that photoproduction in the target may be equated with emission from the target; that is, the interaction between the photoparticles and the target has been neglected. This is particularly significant in the case of the charged particles, since they may, depending on the size of the target, lose considerable energy before emerging from the target.

For each incident electron energy, calculated results for each type of emitted particle — neutrons, protons, positively charged pions, negatively charged pions, and neutral pions — in the angular intervals $0-30^\circ$, $30-60^\circ$, $60-90^\circ$, $90-120^\circ$, and $120-180^\circ$ have been obtained. Shown in Figs. 4.9.1 and 4.9.2 are the differential yields of the

photoneutrons and positively charged photopions averaged over the angular intervals $30-60^\circ$ and $60-90^\circ$, respectively, from 400-MeV electrons.

All of the calculated differential yields are obtained using the photon track length per unit energy corresponding to an infinite target. However, photon track lengths per unit energy at various depths (greater than two radiation lengths) in the target have also been obtained, and from these results it is possible to obtain approximate estimates of the production in copper targets of any thickness greater than two radiation lengths.

In order to make the calculated results readily available for use in the shielding of intermediate-energy electron accelerators and in the design of experiments around such accelerators, analytic fits using the method of linear least squares to all of the differential yields have been obtained.

References

- ¹C. D. Zerby and H. S. Moran, *Studies of the Longitudinal Development of High-Energy Electron-Photon Cascade Showers in Copper*, ORNL-3329 (1962).
- ²C. D. Zerby and H. S. Moran, *A Monte Carlo Calculation of the Three-Dimensional Development of High-Energy Electron-Photon Cascade Showers*, ORNL-TM-422 (1962).
- ³T. A. Gabriel and R. G. Alsmiller, Jr., *Photoneuclear Disintegration at High (<350 MeV) Energies*, ORNL-TM-2481 (1969); also submitted to the *Physical Review*.

4.10 MODIFICATION AND FURTHER DEVELOPMENT OF THE NUCLEON TRANSPORT CODE NTC^{1,2}

D. C. Irving H. S. Moran
W. E. Kinney

Several modifications to the Nucleon Transport Code NTC are described. Also, descriptions are provided for a few portions of the code which had previously been undocumented. Included in the report are the following:

1. the description of PREP, a data preparation routine;
2. a generalized framework for the High-Energy Analysis Program which handles the bookkeeping details and leaves the specialization to a particular problem to a few user-written routines;

3. a listing of improvements made in the treatment of evaporation processes;
4. the replacement of an older and incompletely documented version of O5R by the published version;
5. the description of a general-purpose evaporation model program in O5R to treat inelastic scattering;
6. the preparation of a special version of NTC using a straight-ahead approximation.

References

¹Work partially funded by the National Aeronautics and Space Administration under Order H-38280A.

²Abstract of ORNL-TM-1866 (Mar. 4, 1969).

4.11 CALCULATION OF THE NEUTRON AND PROTON SPECTRA FROM THICK TARGETS BOMBARDED BY 450-MeV PROTONS AND COMPARISON WITH EXPERIMENT^{1,2}

R. G. Alsmiller, Jr. J. W. Wachter
H. S. Moran

Nucleon-meson cascade calculations have been carried out for 450-MeV protons incident on a variety of thick targets. The energy spectra of emitted neutrons and protons at specific angles are compared with experimental measurements.

References

¹Work partially funded by the National Aeronautics and Space Administration under Order H-38280A.

²Abstract of ORNL-TM-2462 (Jan. 6, 1969). Also to be published in *Nuclear Science and Engineering*.

4.12 CALCULATION OF THE ENERGY DEPOSITED BY NUCLEONS IN A SPHERICAL PHANTOM AND COMPARISON WITH EXPERIMENT^{1,2}

D. C. Irving R. G. Alsmiller, Jr.
H. S. Moran

Nucleon transport calculations have been carried out, and the dose from the secondary particles

produced by 160-MeV protons has been computed as a function of position in a water-filled spherical phantom. The calculated results are compared with experimental measurements, and very approximate agreement is obtained.

References

¹Work partially funded by the National Aeronautics and Space Administration under Order H-38280A.

²Abstract of ORNL-TM-2515 (Feb. 10, 1969). Also to be published in *Nuclear Science and Engineering* as a Technical Note.

4.13 CALCULATION OF THE PHOTON PRODUCTION SPECTRUM FROM HIGH-ENERGY NUCLEON-NUCLEUS COLLISIONS¹

Y. Shima R. G. Alsmiller, Jr.

When a high-energy nucleon-nucleus collision occurs, the residual nucleus that remains after particle emission is no longer energetically possible and usually is in an excited state and de-excites by photon emission. The calculation of the photon spectrum from such a collision is possible if the distribution and state of excitation of the residual nuclei, as well as the energy levels and branching ratios of the residual nuclei, are known. By utilizing the distributions of residual nuclei and excitation energies given by the intranuclear-cascade calculation of Bertini^{2,3} and by making simplifying assumptions about nuclear level spacings and branching ratios, the photon emission spectra from proton-nucleus collisions in the energy range 15–150 MeV have been calculated and compared with the experimental results of Zobel *et al.*⁴ For 150-MeV incident protons, the calculations and comparisons are similar to those obtained previously by Hill and Simpson.⁵

The energy levels of the residual nuclei were taken from the compilation of Lederer *et al.*⁶ when given, and when not given they were calculated from the level-spacing formula of Varshni.⁷ The branching ratios were obtained by assuming that all transitions could be characterized as being electric dipole transitions. The Bertini calculations, which are carried out using Monte

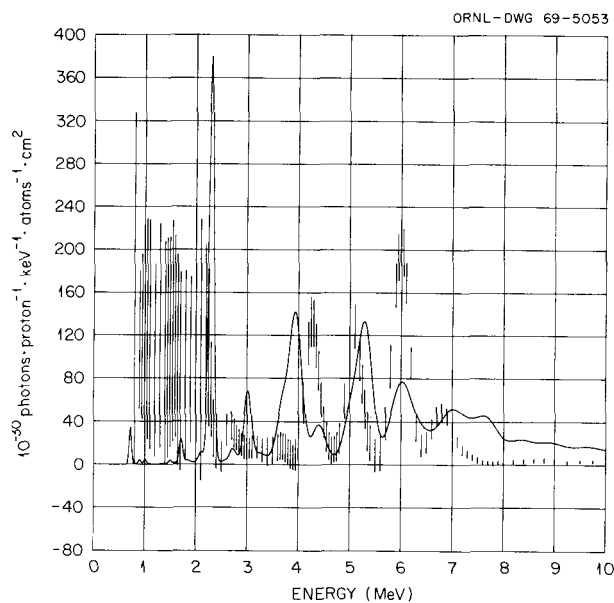


Fig. 4.13.1. Photons from 50-MeV Protons on $^{16}\text{O}_8$. The smooth curve represents the theoretical prediction and the vertical lines represent the experimental data.⁴

Carlo methods, give a discrete number of residual nuclei and an excitation energy for each of these nuclei. In carrying out the calculations, it was assumed that the state of excitation of each residual nucleus was the energy level which most nearly corresponded to the excitation energy given by Bertini.

Calculations have been carried out and compared with experiment for incident proton energies of 15, 25, 50, and 150 MeV on the elements $^{27}\text{Al}_{13}$, $^{16}\text{O}_8$, and $^{12}\text{C}_6$. The calculated and experimental photon spectra for 50-MeV protons on oxygen are compared in Fig. 4.13.1. The smooth curve represents the calculations, and the plotted lines represent the experimental results. The length of the plotted line represents the 67% confidence limits of the experimental data. The agreement shown in Fig. 4.13.1 and in the other cases considered is quite poor. This poor agreement is presumably due to inaccuracies in the distribution and state of excitation of residual nuclei given by the intranuclear-cascade-evaporation model of nuclear reactions.

References

- ¹Work partially funded by the National Aeronautics and Space Administration under Order H-38280A.
- ²H. W. Bertini, *Phys. Rev.* **131**, 1801 (1963), with erratum, *Phys. Rev.* **138**, AB2 (1965).
- ³M. P. Guthrie, *EVAP-2 and EVAP-3: Modifications of a Code to Calculate Particle Evaporation from Excited Compound Nuclei*, ORNL-4379 (1969).
- ⁴W. Zobel et al., *Gamma Rays from Bombardment of ^7Li , Be, ^{11}B , C, O, Mg, Al, Co, Fe, and Bi by 16- to 160-MeV Protons and 59-MeV Alpha Particles*, ORNL-4183 (1967).
- ⁵C. W. Hill and K. M. Simpson, Jr., "Calculation of Proton Induced Gamma-Ray Spectrum and Comparison with Experiment," *Second Symposium on Protection Against Radiations in Space, Gatlinburg, Tennessee, October 12-14, 1964*, NASA SP-71, 351 (1965).
- ⁶C. M. Lederer, J. M. Hollander, and I. Perlman, *Tables of Isotopes*, 6th ed., Wiley, 1968.
- ⁷Y. P. Varshni, *Nuovo Cimento* **22**, 145 (1961).

4.14 HIGH-ENERGY (<400 MeV) NEUTRON TRANSPORT USING THE METHOD OF DISCRETE ORDINATES^{1,2}

R. G. Alsmiller, Jr. J. Barish³
F. R. Mynatt³ W. W. Engle, Jr.³

The energy range of the one-dimensional discrete-ordinates neutron transport code ANISN has been extended to 400 MeV. The validity of the extended code is tested by comparing calculated results obtained with ANISN with calculated results obtained using Monte Carlo methods.

References

- ¹Work partially funded by the National Aeronautics and Space Administration under Order H-38280A.
- ²Abstract of ORNL-TM-2420 (Nov. 1, 1968) and as Technical Note in *Nucl. Sci. Eng.* **36**, 251 (1969).

³Computing Technology Center, Union Carbide Corp., Oak Ridge, Tenn.

4.15 SHIELDING AGAINST NEUTRONS IN THE ENERGY RANGE 50 TO 400 MeV¹

R. G. Alsmiller, Jr. J. Barish²
F. R. Mynatt² W. W. Engle, Jr.²

Neutron transport calculations have been carried out for monoenergetic neutrons normally incident on a semi-infinite slab shield of silicon dioxide with 5% water by weight. For incident neutron energies of 50, 100, 200, 300, and 400 MeV, results are given for the neutron flux per unit energy as a function of depth and energy and for the dose equivalent from neutrons and photons as a function of depth.

References

¹Abstract of ORNL-TM-2554 (Mar. 31, 1969). Also to be published in *Nuclear Instruments and Methods*.

²Computing Technology Center, Union Carbide Corp., Oak Ridge, Tenn.

4.16 THE EFFECTS OF MULTIPLE COULOMB SCATTERING AND RANGE STRAGGLING IN SHIELDING AGAINST SOLAR-FLARE PROTONS^{1,2}

R. G. Alsmiller, Jr. J. Barish³
W. W. Scott⁴

The validity of neglecting multiple Coulomb scattering and range straggling in shielding manned spacecraft against solar-flare protons is tested by comparing calculations including these phenomena with calculations in which they are neglected.

References

¹Work funded by the National Aeronautics and Space Administration under Order H-38280A.

²Abstract of ORNL-TM-2319 (Aug. 12, 1968) and *Nucl. Sci. Eng.* 35, 405 (1969) as Technical Note.

³Computing Technology Center, Union Carbide Corp., Oak Ridge, Tenn.

⁴Professor of Physics and Chairman of Division of Laboratory Sciences and Applied Mathematics at Chattanooga State Technical Institute and Consultant to the Radiation Shielding Information Center of Oak Ridge National Laboratory.

4.17 CALCULATION OF THE RADIATION HAZARD AT SUPERSONIC AIRCRAFT ALTITUDES PRODUCED BY AN ENERGETIC SOLAR FLARE^{1,2}

T. W. Armstrong R. G. Alsmiller, Jr.
J. Barish³

Calculations have been carried out to estimate the absorbed-dose and dose-equivalent rates at various depths in the atmosphere due to the prompt proton spectrum of an energetic solar flare – the flare of February 23, 1956. Although there is some uncertainty associated with the flare spectrum and with the manner in which the dose rates were obtained from the calculated particle spectra, the calculations indicate that in the vicinity of polar latitudes and at the higher altitudes envisioned for supersonic aircraft flights, dose-equivalent rates as high as ~10 rems/hr are possible.

References

¹Work funded by the National Aeronautics and Space Administration under Order H-38280A.

²Abstract of ORNL-TM-2557 (Apr. 11, 1969). Also submitted for journal publication.

³Computing Technology Center, Union Carbide Corp., Oak Ridge, Tenn.

4.18 MONTE CARLO CALCULATIONS OF RESIDUAL NUCLEI PRODUCTION IN THICK IRON TARGETS BOMBARDED BY 1- AND 3-GeV PROTONS AND COMPARISON WITH EXPERIMENT^{1,2}

T. W. Armstrong

Calculations have been carried out for the spatial distribution of certain residual nuclei produced in thick iron targets bombarded by 1-

and 3-GeV protons. Direct comparisons with available experimental results are made, and, in general, the agreement is quite good. In addition, the total production of various nuclei in the entire target and the longitudinal variation of the production of several elements are calculated.

References

¹Work partially funded by the National Aeronautics and Space Administration under Order H-38280A.

²Abstract of ORNL-TM-2287 (July 1, 1968) and *J. Geophys. Res.* **74**, 1361 (1969).

4.19 CALCULATION OF THE RESIDUAL PHOTON DOSE RATE INDUCED IN IRON BY 200-MeV PROTONS

T. W. Armstrong J. Barish¹

Protons that stray from the beam of a high-energy proton accelerator can undergo nuclear interactions in the surrounding materials and produce radioactive residual nuclei. The photons emitted by such radionuclides present a potential radiation hazard after the beam has been shut off. In a previous paper,² calculations were presented for the residual photon dose rate induced in iron by 3- and 200-GeV protons. In the present paper, results are given for the case of 200-MeV protons, and comparisons are made with the 3-GeV results given in ref. 2.

The source-geometry configuration considered is that of a beam of 200-MeV protons traveling along the axis of an iron cylinder of infinite length.³ Cylinders with radii of 20, 40, 60, and 80 g/cm² (~1, 2, 3, and 4 in.) are considered.

As in ref. 2, the calculations were carried out using Monte Carlo methods to determine the nucleon transport, residual nuclei production, and photon transport. The method of calculation used here is identical to that discussed in ref. 2 for the 3-GeV beam.

In Fig. 4.19.1 the radial distributions of the radionuclide production rates are given for a 200-MeV beam and 80 g/cm² radius and are compared with the results from ref. 2 for a 3-GeV beam and 150 g/cm² radius. The error bars represent

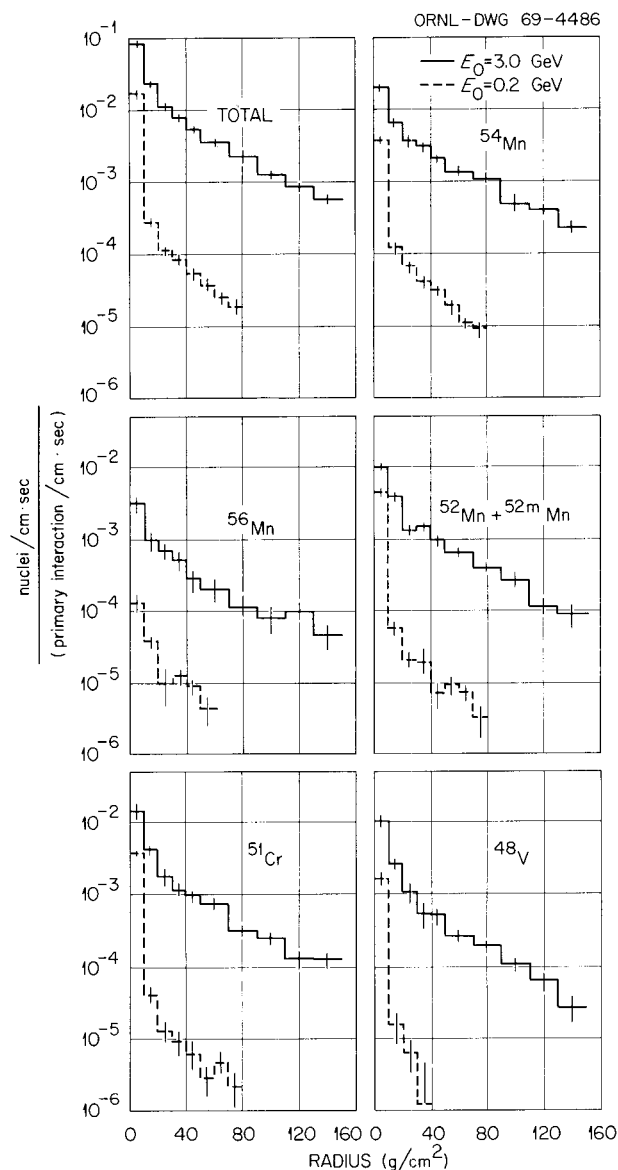


Fig. 4.19.1. Radial Distribution of Production Rates.

statistical errors of one standard deviation. The curves labeled "total" include the contribution of 14 radionuclides which are photon producers; however, essentially all of the total production is contributed by the six radionuclides whose radial distributions are shown. For both beam energies the total production is dominated by ⁵⁴Mn, which has a half-life of 300 days. Consequently, the total photon dose rate as a function of time after

shutdown for long irradiation times is not significantly different for the two beam energies.

Results have also been calculated for the production rate of nuclides other than those shown in Fig. 4.19.1, the neutron leakage spectrum during irradiation, and the photon dose rate as a function of irradiation time, time after shutdown, and cylinder radius.

References

¹Computing Technology Center, Union Carbide Corp., Oak Ridge, Tenn.

²T. W. Armstrong and R. G. Alsmiller, Jr., *Calculation of the Residual Photon Dose Rate Around High-Energy Proton Accelerators*, ORNL-TM-2498 (1969); also submitted to *Nuclear Science and Engineering*.

³This configuration was chosen to aid in the design of the proton accelerator under construction at the National Accelerator Laboratory, Batavia, Ill.

4.20 CALCULATION OF THE RESIDUAL PHOTON DOSE RATE AROUND HIGH-ENERGY PHOTON ACCELERATORS¹

T. W. Armstrong R. G. Alsmiller, Jr.

Calculations have been carried out to determine the time dependence of the residual photon dose rate around a high-energy proton accelerator. The development of the nucleon-meson cascade, the residual nuclei production, and the photon transport are calculated using Monte Carlo methods. Proton beams of 3 and 200 GeV and shields in the form of infinite cylinders of iron and heavy concrete are considered. Although the 3-GeV calculations are carried out with some exactitude, the results for the 200-GeV case must be considered very approximate since the energy and angular distributions of the products from nuclear interactions in this energy range are not well known.

Reference

¹Abstract of ORNL-TM-2498 (Feb. 10, 1969). Submitted for journal publication.

4.21 CALCULATION OF THE RESIDUAL PHOTON DOSE RATE DUE TO THE ACTIVATION OF CONCRETE BY NEUTRONS FROM A 3-GeV PROTON BEAM IN IRON

T. W. Armstrong J. Barish¹

Protons that stray from the beam of a high-energy proton accelerator can, as a result of nuclear interactions, produce radioactive residual nuclei in the surrounding materials. The decay of such radionuclei produces a source of photons after shutdown that presents a potential radiation hazard to personnel requiring entry into the accelerator tunnel. Calculations have been carried out to determine the photon dose rate in an accelerator tunnel as a function of time after shutdown due to photons produced in the material immediately surrounding the beam, such as the magnets, and due to photons produced in the concrete enclosure walls. Of particular interest is the photon contribution due to low-energy neutron capture by the sodium in the concrete since this contribution can, at least to some extent, be controlled either by choosing concrete with low sodium content or by adding appropriate materials, such as boron, to the concrete that will reduce the low-energy neutron flux.

The calculations have been performed for a beam of 3-GeV protons traveling along the axis of an infinitely long cylinder 40 g/cm² in radius. It is assumed that the number of protons per unit distance leaving the beam is constant and that these primary protons have their initial interaction on the beam axis without undergoing energy loss. Surrounding the iron is a void that extends to a radius of 7.5 ft, at which point the concrete begins and extends to infinity. The composition of the concrete is taken to be (in weight percent): O, 48.99; Ca, 37.10; C, 9.47; Al, 1.32; H, 0.80; Si, 0.39; Fe, 0.54; Mg, 0.39; and Na, 1.00.²

The photon dose rate due to photons escaping from the iron has been calculated previously.³ In the present paper, the photon dose rate due to the activity induced in the concrete is calculated and compared with the iron contribution presented in ref. 3. As in ref. 3, the calculations were carried out using Monte Carlo methods to determine the development of the nucleon-meson cascade, residual nuclei production, and the photon transport.

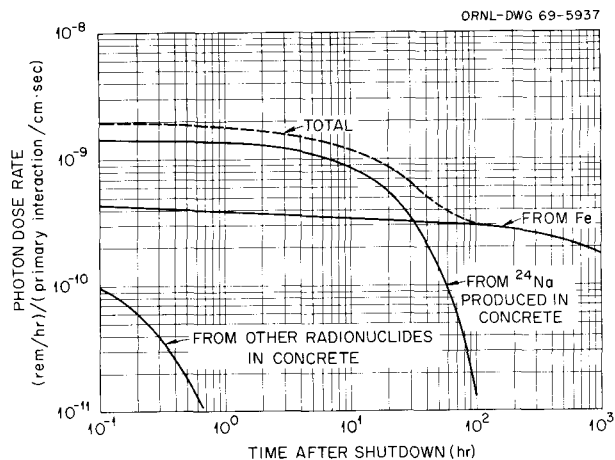


Fig. 4.21.1. Photon Dose Rate at Surface of Tunnel Wall After Infinite Irradiation Time for Concrete with 1% Sodium by Weight.

In Fig. 4.21.1 the photon dose rate at the surface of the concrete is given as a function of time after shutdown. In addition to the total dose rate, the contributions due to photons escaping from the iron, from the sodium in the concrete, and from nuclei other than sodium in the concrete are also given. The sodium contribution is due almost entirely to the ^{24}Na produced by low-energy neutron capture as opposed to the ^{24}Na produced by high-energy spallation interactions. Thus it is possible, either by reducing the sodium content of the concrete or by reducing the low-energy neutron flux, to lower the total photon dose rate by a factor of ~ 5 for shutdown times less than several hours. For shutdown times that are long compared with the 15-hr half-life of ^{24}Na , the total dose rate is dominated by the photons from the ^{54}Mn induced in the iron, which has a half-life of 300 days.

References

¹Computing Technology Center, Union Carbide Corp., Oak Ridge, Tenn.

²The source-geometry configuration was chosen to aid in the design of the proton accelerator under construction at the National Accelerator Laboratory, Batavia, Ill., and the concrete composition was supplied by Dr. Miguel Awschalom of the facility.

³T. W. Armstrong and R. G. Alsmiller, Jr., *Calculation of the Residual Photon Dose Rate Around High-Energy Proton Accelerators*, ORNL-TM-2498 (Feb. 10, 1969), also submitted to *Nuclear Science and Engineering*.

4.22 CALCULATION OF THE ENERGY DEPOSITED IN THICK TARGETS BY HIGH-ENERGY (1 GeV) ELECTRON-PHOTON CASCADES AND COMPARISON WITH EXPERIMENT¹

R. G. Alsmiller, Jr. H. S. Moran

Electron-photon cascade calculations have been carried out for zero-width beams of 1-GeV electrons normally incident on semi-infinite slabs of water and aluminum. The energy deposited as a function of depth and radius is presented and compared with experimental measurements. The calculated and experimental results are in good agreement.

Reference

¹Abstract of ORNL-TM-2559 (Apr. 25, 1969) and to be submitted for journal publication.

4.23 SHIELDING CALCULATIONS FOR A 200-MeV PROTON ACCELERATOR¹

R. G. Alsmiller, Jr. R. T. Boughner³
J. Barish² W. W. Engle, Jr.²

The results of high-energy neutron transport calculations carried out to aid in the design of the radiation shield for a 200-MeV proton accelerator are presented.

References

¹Abstract of ORNL-4336 (December 1968).

²Computing Technology Division, Union Carbide Corp., Oak Ridge, Tenn.

³Formerly with Mathematics Division and now with Technical Division of Y-12.

4.24 THE TRANSPORT OF NEUTRONS PRODUCED BY 3-GeV PROTON-LEAD NUCLEUS COLLISIONS THROUGH A LABYRINTH AND COMPARISON WITH EXPERIMENT¹

R. G. Alsmiller, Jr. E. Solomito

Calculated values of the thermal-neutron flux and the neutron flux above the cadmium cutoff as a function of position in a labyrinth of rectangular concrete ducts are compared with experimental values. In the calculations the approximation of neglecting all incident neutrons with energy greater than 10 MeV and all incident charged particles was made. The results do not give an unambiguous answer concerning the validity of this approximation, because the calculated and experimental values are in good agreement in only one of the three cases considered.

Reference

¹Abstract of ORNL-TM-2560 (Apr. 1, 1969) and to be submitted for journal publication.

4.25 HIGH-ENERGY (< 18 GeV) MUON TRANSPORT CALCULATIONS AND COMPARISON WITH EXPERIMENT¹

R. G. Alsmiller, Jr. J. Barish²

Calculations of the transport of high-energy photomuons through a very thick iron shield have been carried out. Results have been obtained using both Monte Carlo methods and the semi-analytic theory of Eyles. The data obtained by these two different methods of calculation are in very good agreement, but they do not agree well with the experimental data.

References

¹Abstract of ORNL-TM-2439 (Dec. 6, 1968). Also to be published as a Letter to the Editor in *Nuclear Instruments and Methods*.

²Computing Technology Center, Union Carbide Corp., Oak Ridge, Tenn.

4.26 HIGH-ENERGY MUON TRANSPORT AND THE MUON BACKSTOP FOR A 200-GeV PROTON ACCELERATOR¹

R. G. Alsmiller, Jr. M. Leimdorfer²
J. Barish³

High-energy muon transport calculations are presented, and the "shape" of the muon backstop required for a 200-GeV proton accelerator is determined. Results obtained using several different transport approximations are given and compared.

References

¹Abstract of ORNL-4322 (November 1968).
²Industri-Matematik AB, Stockholm, Sweden.
³Computing Technology Center, Union Carbide Corp., Oak Ridge, Tenn.

4.27 HIGH-ENERGY MUON TRANSPORT AND THE MUON BACKSTOP FOR A MULTI-GeV PROTON ACCELERATOR¹

R. G. Alsmiller, Jr. J. Barish²

High-energy muon transport calculations are presented, and the "shape" of the muon backstop required for a 200- and a 500-GeV proton accelerator is determined. The shield material considered is heavy concrete. Results obtained with an energy-dependent and an energy-independent stopping power are presented and compared. The error introduced by using a constant stopping power is clearly evident, but it may be tolerable for some design purposes.

References

¹Abstract of ORNL-4386 (March 1969).
²Computing Technology Center, Union Carbide Corp., Oak Ridge, Tenn.

5. Medium-Energy Nucleon Spectroscopy Studies

5.0 INTRODUCTION

In this section all papers but the first involve neutron spectroscopy using liquid organic scintillators. The neutron energy range to be covered is at least 2 to 40 MeV. The large dynamic range of the corresponding pulses (about 100:1) raises experimental problems, whether the apparatus is in a cyclotron laboratory or swinging gently about at 10^5 ft in the atmosphere. In both cases one must know the pulse-height response functions of the scintillator for the whole energy range in order to analyze the data; but for the balloon work the need is more pressing because the neutron spectrum must be inferred from the pulse-height spectrum, while at the cyclotron one can determine neutron energy by measuring flight time. Monte Carlo calculations of the pulse-height distributions in the scintillator are difficult at energies over 14 MeV because the various reactions of neutrons on carbon have poorly known cross sections. For these reasons a considerable fraction of the work of these groups has centered on scintillator calibration efforts using the (nearly) monoenergetic neutrons from the ${}^7\text{Li}(p,n){}^7\text{Be}(g.s.)$ reaction at forward angles.

There seems yet to be disagreement about the origin of the proton trapped radiation (Van Allen) belt about the earth, and we hope that some firm evidence on the spectrum of fast neutrons near the top of the atmosphere can help settle whether decay of similar escaping neutrons is an important contributor to the radiation belt. Since commercial carriers seem destined to travel at increasingly high altitudes, there are also everyday reasons to better understand this part of our environment.

When all the results have been compiled from the experiment referred to in the first summary, there

will be little room for imagination in the continuum cross sections for charged-particle production from ~ 30 - to 60-MeV protons on nuclei in the range heavier than carbon, other than particle-particle correlations and polarization information. Though in the near-elastic region of the output spectra there are variations in detail from nuclide to nuclide, and though the low-energy "evaporation" peaks vary in strength depending on the position of the target nuclide relative to the nuclear stability line, the results so far show the expected smoothness of behavior with target mass, incident energy, and angle. The Bertini intranuclear cascade model, followed by nuclear evaporation, is able to give about the right general behavior for the proton reactions, but systematic deviations do occur. Deuteron and alpha-particle reactions are not unimportant in carrying off energy, and so far there is no method developed for anticipating their spectra. Perhaps the characteristic overestimates in the proton evaporation spectra are related to this gap in our current theories. To complete our knowledge of the continuum reactions we must know what are the neutron spectra from these reactions; we are not quite assured that neutrons will follow the intranuclear cascade model as well as do the protons. (We are assured that they will behave smoothly.) For this reason our group is hard at work on these neutron cross sections of interest and considerable practical importance.

This year the section includes summaries of miscellaneous instrumentation work incidental to our efforts; previously these were included in separate sections. The quantity of work reported reflects, in delayed time, the series of staff reductions which occurred about two years ago.

5.1 CONTINUUM CHARGED-PARTICLE REACTIONS INDUCED IN NUCLEI BY 29-, 39-, AND 61-MeV PROTONS¹

R. W. Peelle F. E. Bertrand²

Some results have already been made available, for targets of carbon, iron, and bismuth, from an experiment designed to observe and distinguish between differential cross sections for all secondary hydrogen and helium particles from nuclei struck by 30- to 60-MeV protons.³ Events from a three-detector semiconductor telescope were recorded on magnetic tape, including all three pulse heights and flight time in most cases, so a complete delayed analysis is possible. During the past year considerable effort has been expended toward refinement of the data analysis programs employed and the production of final differential cross sections.

The main new refinements in the series of analysis programs have been designed to: (1) improve the ability to evaluate and modify the $\Delta E \times E$ discrimination lines which separate the various particle types, (2) automate the combination of flight-time data with $\Delta E \times E$ data, (3) provide in a general way for computing cross sections integrated over the angular distributions, (4) introduce a correction to identify events in which multiple Coulomb scattering caused protons to miss the third (germanium) detector and redistribute the corresponding cross section with approximately the correct energy distribution, (5) introduce a first-order correction to the spectra to compensate energy loss in the scattering target, (6) include a system to allow correction for events in which the edges of the detector collimator slit were penetrated by the scattered protons, and (7) allow subtraction of data for carbon from those obtained from (Mylar or Kodacel) targets containing both carbon and oxygen. The last proves to be a rather complex system, since one must allow for slight errors in foil weights and composition and also for small shifts in the energy calibration between successive runs. The appropriate factors are obtained in an interactive trial-and-error approach using a PDP-8 computer, while the final calculation is made at the Laboratory Computing Center using averaged parameters determined in this manner. Considerable attention has also been given to redetermination of foil weights and other important experimental parameters.

Final results are now being compiled using the improved analysis procedure and are largely completed for 61-MeV protons on C, O, Al, Y, and Au and for 29-MeV protons on C, O, Al, and Au. Figure 5.1.1 shows the proton spectrum at 50° from 61-MeV protons on ⁸⁹Y, compared with the intranuclear-cascade-plus-evaporation result based on Bertini's MECC-3 (ref. 4) program. Figure 5.1.2 shows data obtained from ²⁷Al at 30° for the same incident energy. In both cases the neutron cutoff energy in the cascade calculation was taken as zero, and the proton cutoff was set at the approximate proton barrier height, 7.0 and 3.3 MeV respectively. Statistical uncertainties in the Monte Carlo results are shown, while those in the experimental plots are unimportant. The

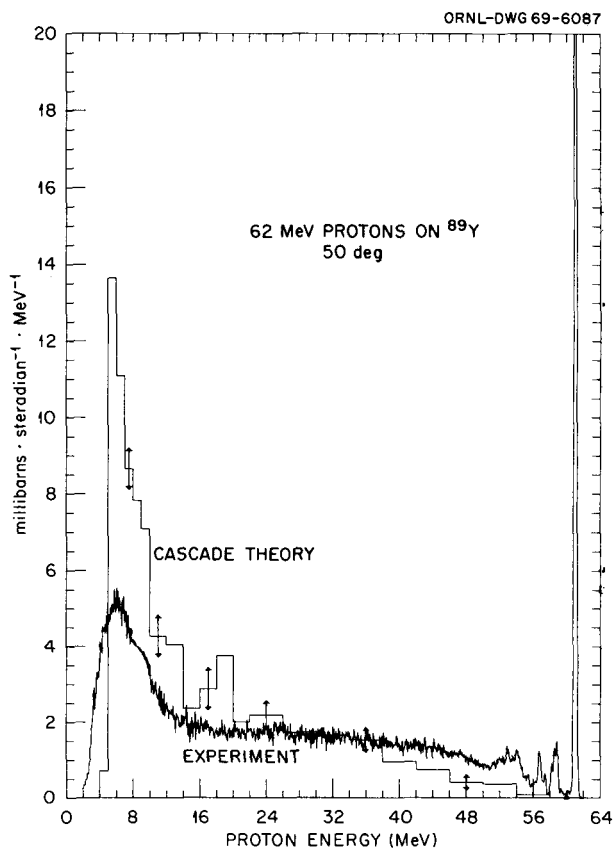


Fig. 5.1.1. Laboratory Differential Cross Sections for Secondary Protons at 50° from 62-MeV Protons on ⁸⁹Y Compared with the Predictions of the Bertini Intranuclear Cascade Theory for the Angular Interval 47–53°. The fluctuations in the experimental data correspond to 50-MeV energy bins.

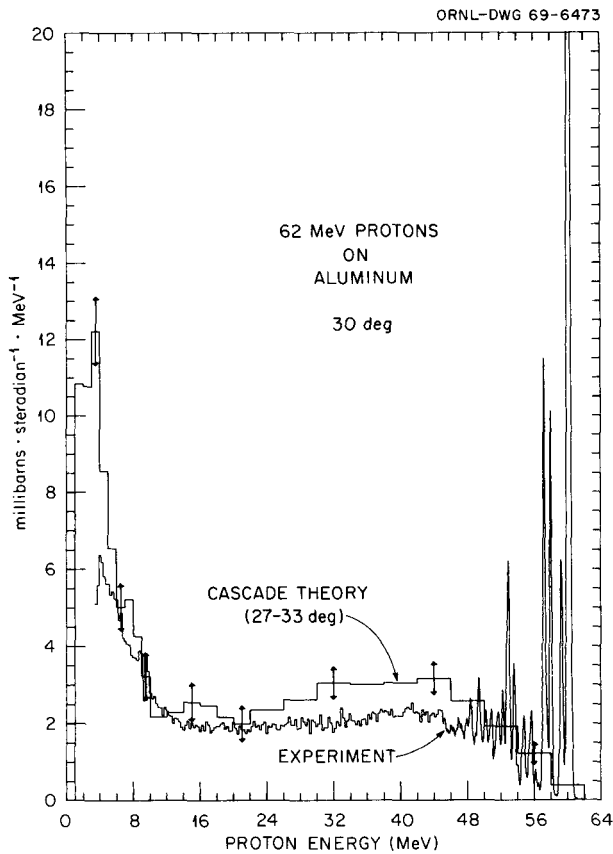


Fig. 5.1.2. Laboratory Differential Cross Sections for Secondary Protons from 61.5-MeV Protons on ^{27}Al Compared with the Predictions of the Bertini Intra-nuclear Cascade Theory for the Angular Interval 27° – 33° .

absolute uncertainty in the experimental curves is tentatively estimated to be about 5%. In Fig. 5.1.1 the dotted region at ~ 9 MeV gives the average result for a region in which protons in the experiment were stopped in a thin nickel foil. The discontinuity in the ^{27}Al theoretical prediction at ~ 3 MeV is caused by the classical treatment of the cutoff energy in the cascade calculation. In each figure the elastic scattering peak is the highest one shown in the figure, and its magnitude should not be included in the theoretical prediction. In the regions of Fig. 5.1.2 where the experimental data are shown as a histogram, many experimental channels have been combined together because statistical tests indicate there is no structure other than counting fluctuations.

Figures 5.1.1 and 5.1.2 are typical of the results obtained so far in that (1) the predicted proton cross sections are considerably higher than

observed in the energy region of the Coulomb barrier; (2) at angles larger than 45° the observed cascade continuum has a more energetic spectrum than the computed one, the effect becoming more marked with increasing scattering angle and atomic weight; and (3) in the region of 30° the calculated cross section is too large in the region of the (badly smeared out) quasi-free scattering peak, at least for all but the heaviest elements.

References

¹Work partially supported by the National Aeronautics and Space Administration under task numbers H-38280A and L-12,186.

²On leave from the University of Southern California.

³F. E. Bertrand *et al.*, *Differential Cross Sections for the Charged Particles Produced by 60-MeV Protons on Carbon, Iron, and Bismuth*, ORNL-4274 (1968). See also sect. 1, *Neutron Phys. Div. Ann. Progr. Rept. May 31, 1968*, ORNL-4280.

⁴In this application, MECC-3 is identical to the earlier low-energy cascade code [H. Bertini, *Phys. Rev.* **131**, 1801 (1963)] except that the cutoff energies can be chosen differently for neutrons and protons. We are indebted to M. Guthrie for aid in the efficient plotting of graphs like Fig. 5.1.1.

5.2 SECONDARY NEUTRON SPECTRA FROM 20. TO 40-MeV PROTONS ON VARIOUS TARGETS¹

J. W. Wachter R. T. Santoro
T. A. Love

An experimental program is in progress to measure the secondary energy spectra from various targets bombarded by 20- to 40-MeV protons. These measurements will cover an incident proton energy range which is of particular interest both because of the relative importance of such neutrons in defining spacecraft shielding effectiveness and because they will complement existing secondary charged-particle and gamma-ray measurements.^{2,3} Preliminary measurements have been performed at an incident proton energy of 40 MeV and are described below.

The experimental apparatus is shown schematically in Fig. 5.2.1. The 40-MeV pulsed proton beam from

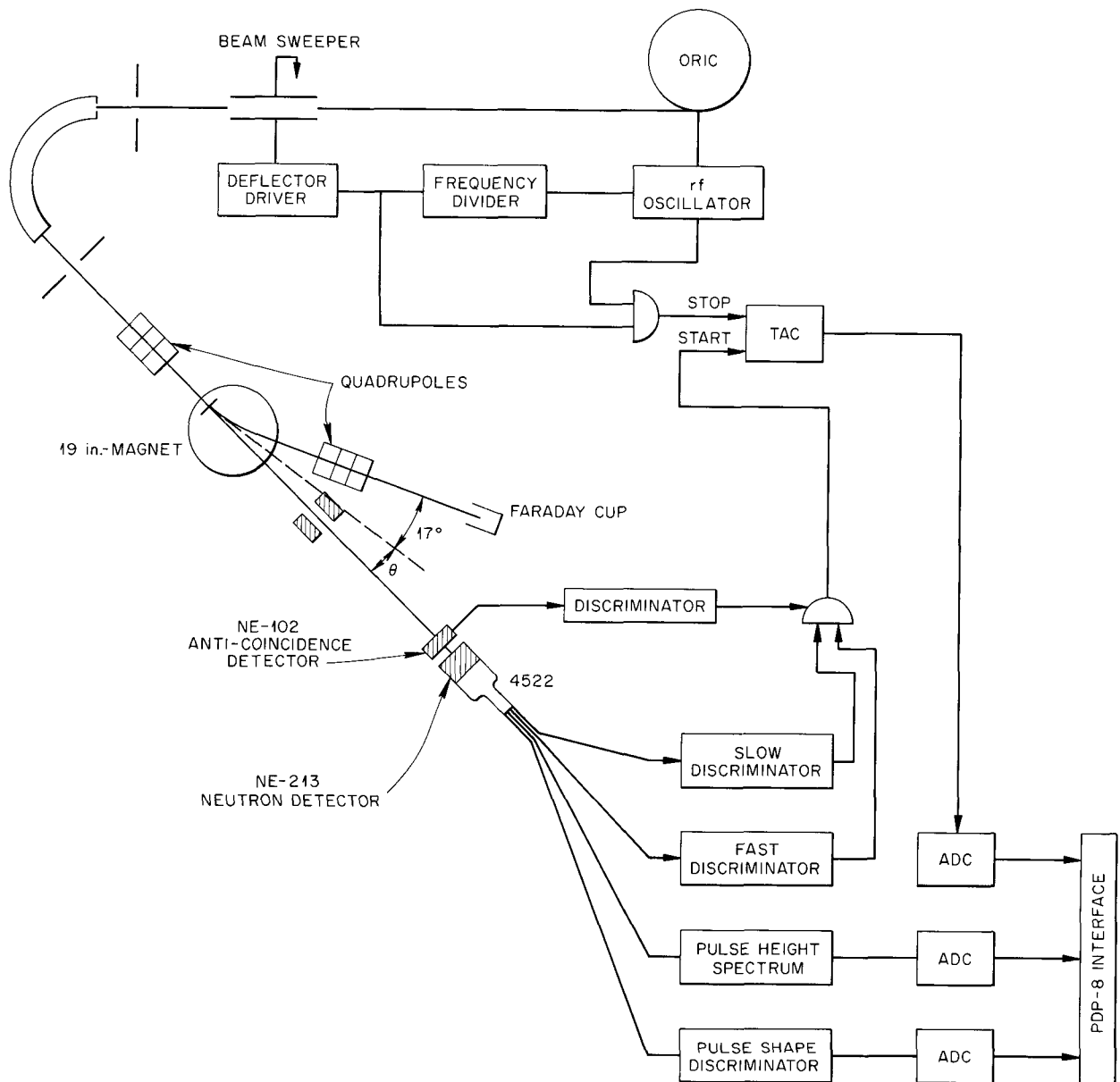


Fig. 5.2.1. Block Diagram of the Experimental Apparatus.

the Oak Ridge Isochronous Cyclotron was directed through parallel metal plates which served as the capacitor of a resonant circuit. The frequency of the circuit was a fixed fraction of the cyclotron rf frequency, so that the electric field of the capacitor deflected four of every five proton bursts away from the entrance slit of the 153° analyzing magnet. The separation of successive proton bursts was thereby increased from 55 to 275 nsec. The analyzed beam was then

focused onto the target at the entrance of a 17° deflection magnet. The primary proton beam was separated from the neutron beam by this clearing magnet and was focused into a Faraday cup, where the integrated proton current was measured. This arrangement, with suitable shielding, is appropriate for observation at detector angles in the range from 0 to 44° .

The neutrons were detected with a 3-in.-diam by 1-in.-thick (or 3 by 3 in.) NE-213 liquid

scintillator centered on the face of an RCA-4522 photomultiplier tube. In this detector, charged particles scattered by the incident neutrons are measured. Charged particles incident on the face of the detector were rejected by means of a thin NE-102 detector. This detector was mounted in front of the NE-213 neutron detector and was operated in anticoincidence with it. Both neutrons and gamma rays are detected in the NE-213, and the slow light emission characteristics of the neutron reactions in the scintillator were used to distinguish between neutron and gamma pulses. The pulse-shape discriminator circuit of Gibson and Santoro⁴ was found to operate well at these energies, and in a later run a system based on pulse crossover timing was employed.

The neutron energy was inferred from its time of flight from the target. The output of a fast-slow coincidence circuit started a time-to-amplitude converter (TAC), which was subsequently stopped by a pulse derived from the rf oscillator of the cyclotron.

In order to minimize errors in the timing circuits and to facilitate data handling, the TAC output, the pulse height from the scintillator, and the output of the pulse-shape discriminator were fed to an on-line PDP-8 computer. Data were continuously recorded on magnetic tape and also displayed for monitoring during the experiment. Retention of these data allows an analysis of the measured time of flight as a function of the light output from the scintillator. This enables an energy-dependent choice of a suitable lower limit for the light output data (the effective bias setting), so that for each time of flight only the portion of the scintillator response for which the efficiency is well determined need be used. Similarly, timing errors depending on pulse height can be evaluated and compensated.

In the first such experiment, targets of Al and ⁷Li were observed at angles of 0 and 15°. Figure 5.2.2 shows the time-of-flight spectrum obtained for ⁷Li at 0°. These data are currently being analyzed. In an experiment just completed, targets of lithium, aluminum, and iron were studied. In the future, it is hoped that measurements will include targets of C, (C₁₂H₁₆O₈)_n, Sn, and Bi and that with the clearing magnet removed, observation can be extended to much larger angles.

Earlier in the year, efforts were concentrated on experiments to ascertain the detector efficiency and pulse-height response for the nearly mono-

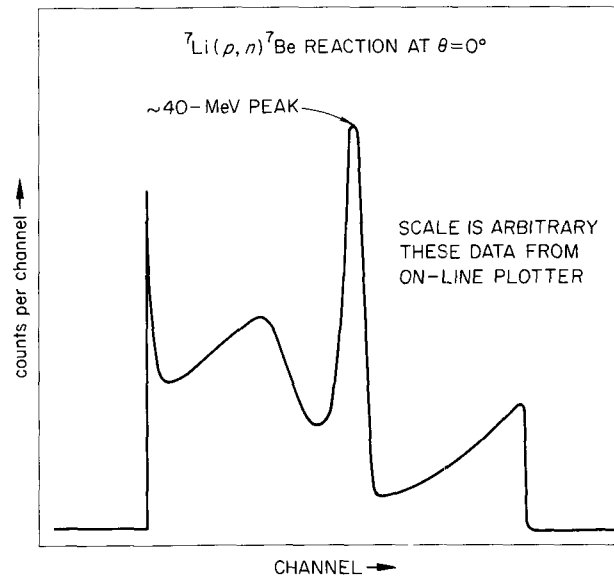


Fig. 5.2.2. Neutron Time-of-Flight Spectrum for the ⁷Li(p,n)⁷Be(g.s.) Reaction at $\theta = 0^\circ$.

energetic neutrons from the ⁷Li(p,n)⁷Be(g.s.)

References

- ¹Work funded by the National Aeronautics and Space Administration under NASA Order L-12,186.
- ²F. E. Bertrand *et al.*, *Differential Cross Sections for the Charged Particles Produced by 60-MeV Protons on Carbon, Iron, and Bismuth*, ORNL-4274 (1968).
- ³W. Zobel *et al.*, *Gamma Rays from Bombardment of ⁷Li, Be, ¹¹B, C, O, Al, Co, Fe, and Bi by 16- to 160-MeV Protons and 59-MeV Alpha Particles*, ORNL-4183 (1967).
- ⁴W. A. Gibson and R. T. Santoro, *Neutron Phys. Div. Ann. Progr. Rept. May 31, 1968*, ORNL-4280, p. 119.

5.3 MEASUREMENT OF NEUTRON SPECTRA IN THE ENERGY RANGE 2 TO 40 MeV IN THE UPPER ATMOSPHERE

W. Zobel J. T. DeLorenzo¹
T. A. Love C. O. McNew, Jr.¹

The neutron spectrometer described in the 1968 Annual Progress Report² was assembled and

tested. A balloon flight was launched from Palestine, Texas, on July 19, 1968, the primary purpose of which was to determine the proper functioning of the spectrometer and associated equipment in the environment at approximately 100,000 ft. The purpose of this flight was accomplished, and the results were very encouraging.

To review briefly, the spectrometer is based on a liquid scintillating proton-recoil detector (NE-213),³ for which extensive calibrations for neutron energies up to 22 MeV exist. The detector and associated photomultiplier tube were surrounded by a plastic scintillator (NE-110)³ with its own photomultiplier tube. This arrangement was chosen to eliminate the background from charged particles striking the liquid scintillator. Separation of events in the liquid scintillator due to neutrons or gamma rays was accomplished by pulse-shape discrimination based on the zero-crossing time of the doubly differentiated pulse.

The detector and surrounding anticoincidence mantle were placed inside a stainless steel can, which was itself enclosed in a thermal insulator. The required electronics were placed in a separate box, also insulated, and located about 3 ft from the detector. The necessary cables from detector can to electronics box were enclosed in Tygon tubing.

Two critical points must be borne in mind with respect to the experiment:

1. The operational temperature range of NE-213 is estimated by the manufacturer as 15 to 80°C, with the proviso that scintillating efficiency will drop with increasing temperature. We must therefore ensure that the temperature of the liquid scintillator does not drop below 15°C. On the other hand, the NE-110 softens at 75°C, and the manufacturer suggests 65°C as an upper limit for continuous operation. This sets an upper limit on the temperature which can be sustained in the detector can.

2. The voltage required for the photomultiplier tubes is of the order of 2000 V. This requires us to keep the high-voltage supplies and the tube bases at ground-level pressure, or pot them to prevent breakdown. It was judged easier to pressurize the detector can and the electronics box, so this was the course chosen.

The flight was launched from Palestine, Texas, at 6:29 AM on July 19, 1968. All systems were operating normally, and data were obtained during

the ascent and float.⁴ Pressure in the detector can and in the electronics box was maintained without trouble. The temperature of the liquid scintillator, a point of great concern as mentioned above, decreased slowly from 27°C at launch to 17°C after about 75 min at float altitude (106,000 ft), then rose again and appeared to stabilize at 19 to 20°C. However, it was noted that the temperature in the electronics box, which had decreased from 36°C at launch to about 28°C shortly before reaching float altitude, started to rise again and showed no sign of leveling off. Since it appeared likely that the temperature of any module was higher than the temperature measured at the top of the box, we were afraid of doing irreversible damage to the modules if the temperature were permitted to continue rising. In addition, we noted a change in the crossover time with temperature which was sufficient to circumvent the pulse-shape discrimination, thus rendering the data meaningless. We therefore terminated the flight after 3.1 hr at altitude, at which time the temperature in the electronics box was 44°C.

During the portion of the float period for which the telemetered data should be correct, we observed neutrons with energies extending to an estimated 70 MeV. The total count rate for neutrons was about 1 to 2 neutrons/sec, and over a period of an hour about three counts were accumulated in each of the higher channels. It should be noted that no account has been taken of background neutrons which might be expected from interactions of cosmic rays in the gondola, particularly in the electronics box and batteries.

The data which are telemetered back are recorded on broad-band video tape. Equipment has been designed and is presently under construction which permits us to read these tapes into our PDP-8. We will then be able either to use the PDP-8 for data analysis or to write the data on IBM-compatible tapes for later analysis on one of the large computers at the Laboratory.

From the above discussion it is apparent that the engineering flight was successful in terms of its mission. We showed that the concept of the spectrometer is viable, that data can be successfully transmitted, and that neutrons are observed.

We are now engaged in preparations for the next flight, tentatively scheduled for June 10, 1969. Certain changes will be made in the system on the basis of the experience gained in the

first flight. The change in the crossover timing, which led to the failure of the pulse-shape discrimination, was traced to changes in the linear amplifier. Substitution of different components eliminated that trouble. To prevent temperature buildup among the electronic components, we propose to fly them without encasing them in an insulated box. To avoid the high-voltage breakdown, we procured new high-voltage power supplies small enough to be incorporated into the detector package, which will still be pressurized and thermally insulated.

To reduce the background expected from the gondola and the equipment carried on it, we propose to lower the detector assembly after launch to about 100 ft below the gondola. We will also thereby approximately double the distance between the balloon and the detector, thus appreciably reducing the solid angle subtended by the balloon.

References

¹Instrumentation and Controls Division.

²W. Zobel, T. A. Love, and J. T. DeLorenzo, *Neutron Phys. Div. Ann. Progr. Rept. May 31, 1968*, ORNL-4280, p. 178.

³Product of Nuclear Enterprises, Inc., San Carlos, Calif.

⁴We wish to gratefully acknowledge the efforts of Mr. H. W. Parker, NASA-MSFC, Huntsville, Ala. and his assistants who procured, installed, and operated the required telemetry equipment.

5.4 CALIBRATION OF AN NE-213 DETECTOR WITH 40-MeV NEUTRONS

L. D. Cohen¹ R. T. Santoro
T. A. Love J. W. Wachter
 W. Zobel

As mentioned elsewhere (see paper 5.3 in this section), we are using a 1.8-in.-diam by 1.8-in.-high cylindrical NE-213² liquid scintillator as a detector to measure the spectrum of neutrons with energies up to 40 MeV at balloon altitudes, and we have plans to extend this energy range to 60 MeV. In order to unscramble the pulse-height data resulting from the interaction of neutrons

with the detector to obtain neutron spectra, it is necessary to know the response of the scintillator to monoenergetic neutrons. Our detector had previously been calibrated over the range from 0.2 to 22 MeV,³ and it was the purpose of this experiment to extend the calibration by measuring the response function at 40 MeV. A Monte Carlo program (O5S) exists⁴ which can calculate the response functions for NE-213 detectors. To check on the adequacy of the Monte Carlo calculation, we also attempted to measure the absolute efficiency of the spectrometer for detection of 40-MeV neutrons.

The NE-213 detector was the same one used in the previous calibration.³ It was mounted on an RCA type 8575 photomultiplier tube and located with its center 2.12 m from the neutron source. Approximately 7.62 cm behind this detector was the front element of a neutron telescope consisting of two NE-102² detectors, each of which was of 7.62 cm diameter and 1.5 cm thick, separated by 13.74 cm. The thickness of the telescope elements was chosen so that each was equal to the range of a 40-MeV proton in the NE-102. A sketch of the arrangement can be seen in Fig. 5.4.1.

The neutron source was a target of either ⁷Li or ²H, the former in a thin (0.001-in. wall thickness) aluminum capsule, the latter in the form of deuterated polyethylene. The targets were approximately 400 keV and 500 keV thick respectively. Protons with energy of 39.04 MeV from the Oak Ridge Isochronous Cyclotron (ORIC) produced neutrons with energies of 37.40 MeV and 36.81 MeV, respectively, at 0° to the direction of the incident proton beam. The protons were swept out of the neutron beam by a magnetic field and directed into a Faraday cup so we could measure the beam strength.

Interactions in the NE-213 were identified by the time of their occurrence and, using pulse-shape discrimination, as to their nature, that is, neutron interactions or gamma-ray interactions. Events from the telescope, that is, the pulse heights from both elements, were recorded only if there was a coincidence between the two elements, and then the time of occurrence was also recorded. No distinction between neutron and gamma-ray events was made in the telescope. A flag was also provided to identify which instrument (NE-213 detector or telescope) initiated the recording of the event.

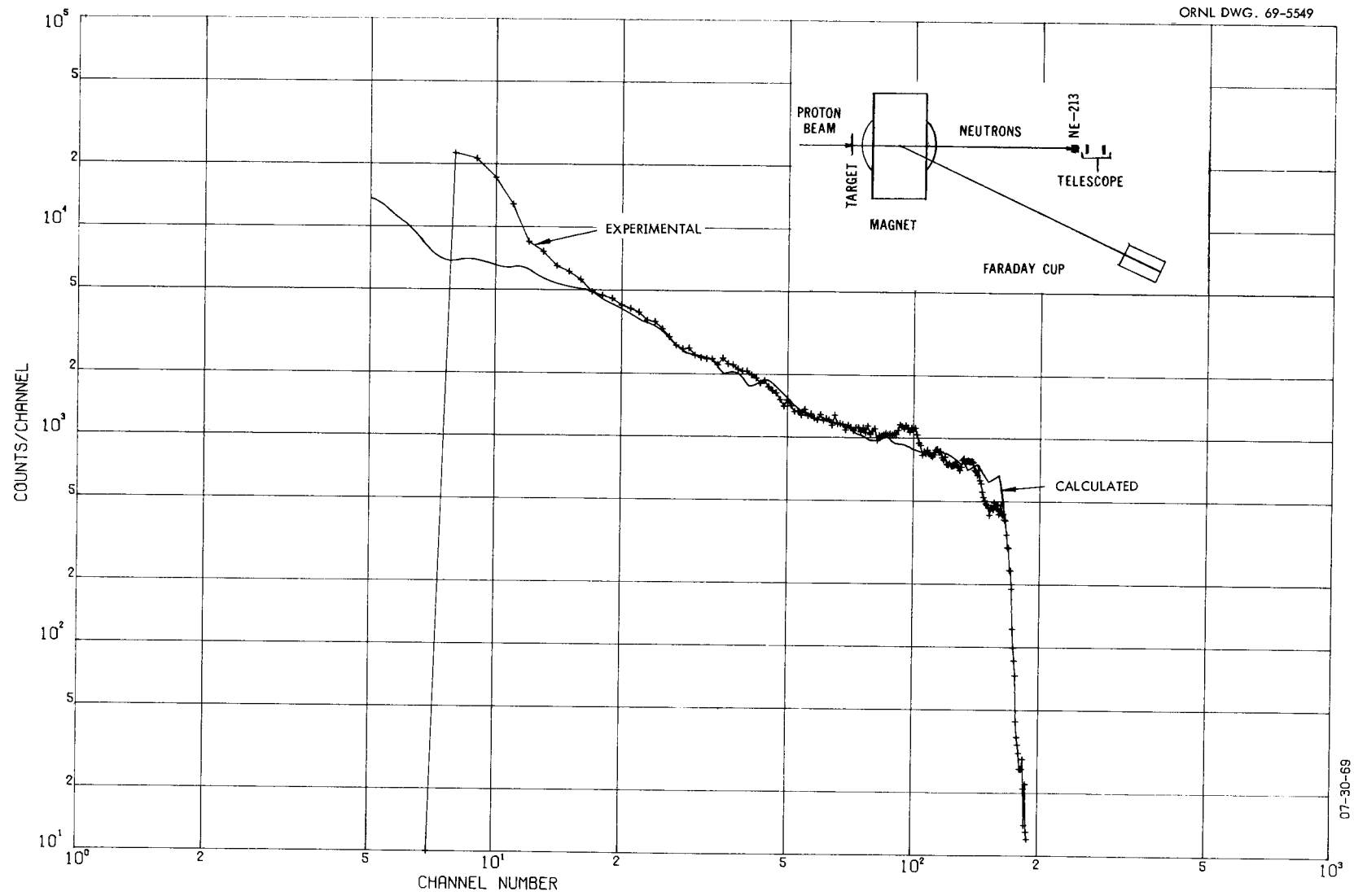


Fig. 5.4.1. Response Function of a 1.8-in.-Diam by 1.8-in.-High NE-213 Detector for 40-MeV Neutrons. The inset shows the experimental arrangement.

All events were recorded on magnetic tape by an on-line PDP-8 computer. In addition, the time-of-flight spectra for the NE-213 detector and for the telescope were separately accumulated, as were the neutron and gamma-ray spectra in the NE-213. A two-dimensional array was accumulated for the telescope data; its primary purpose was to serve as a display to check the proper functioning of the telescope and aid in initial adjustments.

Analysis of the data is in progress. Figure 5.4.1 shows the spectrum calculated with O5S for incident 40-MeV neutrons. Also shown in the figure, and arbitrarily matched to it, is the experimentally determined response function of the NE-213 detector for neutrons with energies above ~ 30 MeV from the ^7Li target. Note that the experimental data are given in counts per channel and the calculated ones in probability per light unit. The light curve for recoil protons with energies above 22 MeV has not been properly established, so that the value used in O5S is an extrapolated estimate. The discrepancy between calculation and experiment at the lower end of the curve is believed due to the uncertainties in the partial cross sections for interactions of neutrons with carbon. A preliminary estimate of the integral efficiency of the NE-213 detector above a bias chosen so as to exclude neutron interactions with the carbon in the scintillator, that is, considering only interactions with the hydrogen for which the cross section is known quite well, results in an efficiency of about 0.5%. A comparable integral efficiency obtained from the O5S calculation is also about 0.5%, lending great confidence to the results expected from the final efficiency calculation for the experimental efficiency of the NE-213.

We hope to be able to continue the calibration, taking several additional points between the previously measured 22 MeV and the 40 MeV of this experiment and extending the calibration to energies as high as 60 MeV.

References

¹Summer research participant from Drexel Institute of Technology, Philadelphia, Pa.

²Product of Nuclear Enterprises, Inc., San Carlos, Calif.

³V. V. Verbinski *et al. Nucl. Instr. Methods* **65**, 8 (1968).

⁴R. E. Textor and V. V. Verbinski, *O5S: A Monte Carlo Code for Calculating Pulse-Height Distributions Due to Monoenergetic Neutrons Incident on Organic Scintillators*, ORNL-4160 (1968).

5.5 CALCULATION OF RESPONSE FUNCTIONS FOR A PROTON-RECOIL TELESCOPE WITH ACTIVE RADIATOR¹

J. W. Wachter

An advantage of proton-recoil neutron spectrometers is that the absolute efficiency can be calculated from knowledge of the (n,p) scattering cross section, the dimensions of the proton radiator, and the geometry of the apparatus. A program to permit computation of the efficiency for such spectrometers has been described.² This program has been extended to enable computation of both the efficiency and the response functions for spectrometers in which the radiator itself is a proton detector.

In a spectrometer, the radiator includes materials other than hydrogen, and the protons generated by neutrons interacting with these materials must be taken into account. In experiments with passive radiators, background runs are made to obtain the response to the nonhydrogenous content of the radiator, and this is then subtracted from the total number of detected events. This is avoided in the case of the spectrometer with an active radiator, because a measurement is made of both the energy lost by the particle in the radiator and also that lost in the detector. Each event is therefore characterized by a pair of energy values. The kinematics of the (n,p) reaction, the dimensions of the spectrometer, and the energy losses suffered by the recoiling proton define a limited range of such paired energy values that can be due to true recoils. A suitable choice of parameters for the spectrometer may then be made so that the corresponding energy values for competing reactions fall outside this range.

The telescope geometry for which the response functions are calculated is shown in Fig. 5.5.1. A neutron is born in the source plane at point S and collides with a proton at point R within the first detector. The recoiling proton traverses the remaining distance within detector 1, the intervening counter, and the slant distance through

detector 2, entering the final detector at point F . In the calculation, the final detector is a geometry-defining plane and may be set to coincide, say, with the face of detector 2, if this detector defines the telescope geometry.

The calculation of the telescope efficiency is essentially the same as for the passive radiator and proceeds as described in detail in ref. 2. Briefly, the method involves a random selection of the source point S , the collision point R within the radiator, and the final point F . A random path being thus chosen, the probability per incident particle of that path is defined from the kinematics of the reaction and the elemental solid angles subtended at S and R . The computed probability is then stored, and another trial is made until the desired number of paths has been traced.

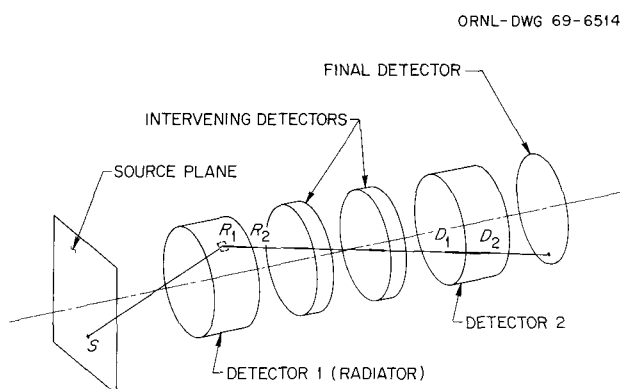


Fig. 5.5.1. Geometry of the Monte Carlo Efficiency Calculations.

In the present calculation a valid path is one in which sufficient energy is deposited in each detector that a corresponding coincidence between them is found experimentally. During the calculation, the energy deposited in each detector is determined for each path using the Bethe-Bloch range-energy formulas, account being taken of losses in the intervening counters. The probabilities for each such energy deposition are binned according to energy and are accumulated to obtain the overall response function.

The method has been used to compute the energy response functions for the proton-recoil telescope described in paper 5.4. A monoenergetic 40-MeV neutron source was assumed to be located at 222 cm from the face of detector 1 and 237 cm from the face of detector 2. Both detectors were 1.5 cm thick and 3.85 cm in radius. The energy losses in the 1-mil aluminum foil covers for the detectors were taken into account, as was the energy loss in traversing the air between detectors.

The response functions are shown in Fig. 5.5.2, in which the probability $N(E_1, E_2)$ is plotted vertically for values of energy deposited in detectors 1 and 2.

References

- ¹Work funded by the National Aeronautics and Space Administration under NASA Order L-12,186.
- ²W. E. Kinney and J. W. Wachter, *Neutron Phys. Div. Ann. Progr. Rept. Aug. 1, 1963*, ORNL-3499, p. 115.

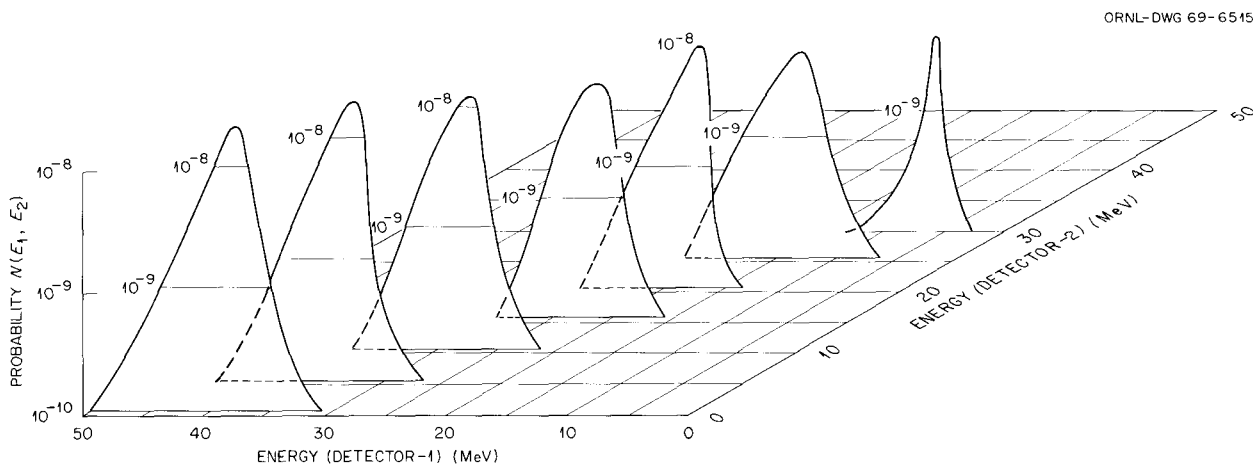


Fig. 5.5.2. Response Functions for 40-MeV Neutrons.

5.6 OBSERVATION OF THE LIGHT OUTPUT FROM AN NE-213 LIQUID SCINTILLATOR FOR 40-MeV PROTONS¹

R. T. Santoro J. W. Wachter
T. A. Love

The comparison of experimental and computed pulse-height response functions for NE-213 liquid scintillators depends on the cross sections for the production of charged particles by neutrons and on the magnitude of the light produced by these particles. In this paper are presented the results of an experiment to compare the light output from 40-MeV protons in NE-213 with the values used in the O5S Monte Carlo code.² The light curve currently in use has been verified experimentally for neutrons up to about 22 MeV.³ Above this energy, the curve has been estimated empirically.

The proton beam from the Oak Ridge Isochronous Cyclotron was directed into a 1-in.-thick by 3-in.-diam NE-213 liquid scintillator viewed by an RCA-4522 photomultiplier tube. The pulse-height spectrum was obtained by integrating the signal from the 9th dynode in a preamplifier (60- μ sec time constant) and analyzing the signal from a Tennelec TC-200 amplifier using double-delay-line shaping of the output pulse (1- μ sec delay line). The analyzer (a PDP-8 digital computer processing a signal from an analog-to-digital converter) was gated by the output from a fast-slow coincidence circuit where the fast signal (14th dynode) determined the timing and the slow signal set the lower bias. The output of the amplifier was 10 V for 40-MeV protons and the lower bias was at 0.1 V. Proton pulses were distinguished from electron pulses by means of a pulse-shape discriminator. The system gain was calibrated using the Compton electrons from a ²²Na gamma-ray source where the extrapolated end point of the upper edge of the pulse-height spectrum defined one light unit. This definition of the light unit depends on the resolution of the detector for the calibration gamma ray. The resolution of the detector used in this experiment is within 10% of the resolution quoted by Verbinski *et al.*³ for the measurements for neutrons up to 22 MeV. Proton pulse-height spectra were obtained as a function of the thickness of copper absorbers placed in the proton beam. The light output from the proton pulses was defined by computing the average peak channel and multiply-

ing by the number of light units per channel from the gamma-ray calibration. The proton energy was determined from the energy loss of the beam in passage through the absorbers and the other intervening materials and upon the beam energy determined by the beam analyzing magnet.

The results of the experiment are shown in Fig. 5.6.1. Also shown is the light curve of Verbinski and points obtained from the integration of Birks' differential light equation.⁴ An unfortunate choice of absorbers produced a nonuniform distribution of the experimental points. The point corresponding to ~ 10 MeV proton energy shows large error bars. This resulted from the uncertainty in the determination of the average channel caused by the broadening of the pulse-height spectrum from straggling of the protons in the thick absorber. For protons above 20 MeV, we observe a difference in the experimental points and the O5S light curve of the order of 10%, with the experimental points yielding the higher light value. The points obtained from Birks' law have been converted to light units

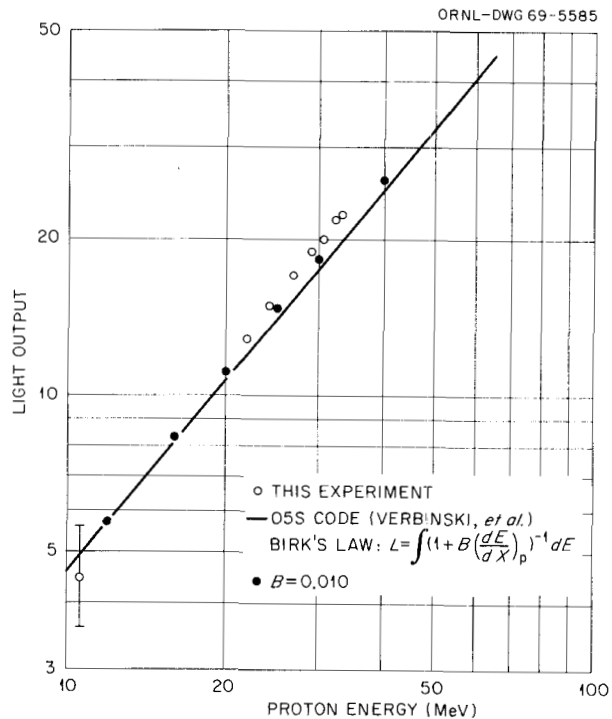


Fig. 5.6.1. Comparison of the Experimental Points from This Experiment with the Light Curve of Verbinski (O5S) and Values Obtained from the Integration of Birks' Law.

using the criterion of Flynn *et al.*⁵ The experimental points and these data are parallel in the proton energy region above 20 MeV, while the O5S curve shows a tendency to drop off. The differences between the experimental points and the O5S light curve may result from several sources. Verbinski's data were obtained using a smaller scintillator where the radiation was incident on the cylindrical surface. Additionally, the gamma-ray calibration might introduce differences which would arise from the fraction of scattered photons escaping the scintillator.

The results of this experiment suggest that the light output from NE-213 scintillators needs further investigation in the energy region above 20 MeV. Similar experiments should be repeated over a wide energy range, and the light output should be measured for different sizes of detectors to observe the light output as a function of detector geometry.

References

¹Work funded by the National Aeronautics and Space Administration under Order L-12,186.

²R. E. Textor and V. V. Verbinski, *O5S: A Monte Carlo Code for Calculating the Pulse-Height Distributions Due to Monoenergetic Neutrons Incident on Organic Scintillators*, ORNL-4160 (1968).

³V. V. Verbinski *et al.*, *Nucl. Instr. Methods* **65**, 8 (1968).

⁴J. B. Birks, *Proc. Phys. Soc.* **A64**, 74 (1952).

⁵K. F. Flynn *et al.*, *Nucl. Instr. Methods* **27**, 13 (1964).

5.7 MONTE CARLO CALCULATIONS TO DETERMINE THE TIME DISTRIBUTION OF SCATTERED NEUTRONS IN TIME-OF-FLIGHT EXPERIMENTS¹

D. I. Putzulu² R. T. Santoro
J. W. Wachter

A calculation has been started to determine the time distribution of secondary neutrons detected in a time-of-flight spectrometer as the result of scattering from the floor, walls, and shielding materials of the experimental area. The method of analysis leading to the scattered neutron fraction is discussed here.

The computation of the scattered neutron time distributions is divided into three phases:

1. the computation of the neutron collision history tape;
2. the analysis of the history tape and the binning of secondary neutron events according to energy, direction of scattering, and time spent in the scattering medium;
3. the determination of the time-distribution functions using intranuclear-cascade cross sections as determined by the MECC-3 program of Bertini.³

The neutron collision history tape is generated using the O5R Monte Carlo code⁴ with subroutine GEOM to simulate the floor-wall configuration shown in Fig. 5.7.1. The composition of the concrete is taken with the same proportions of silicon, oxygen, and carbon used by Maerker and Muckenthaler⁵ in their dose-albedo calculations. Cross sections were taken from the O5R library. Extension of the total, elastic, and integral non-elastic cross sections to higher energies was accomplished using the computer program GENOA.⁶

The collision history tape is written for monoenergetic neutrons incident on the concrete geometry. Six angles of incidence are investigated simultaneously from the boundaries given in Fig. 5.7.1. The neutron is traced through the medium, and each time a boundary is crossed the secondary neutron energy is recorded along with the direction cosines and the coordinates of the emission point. Precautions taken ensure that only one crossing of a boundary is allowed. However, this does not preclude the neutron from having another chance to cross one of the remaining boundaries, provided that boundary had not been previously crossed and is one which is allowed by the geometry. These calculations are run for several values of the incident neutron energy.

The data recorded on the several history tapes are binned according to the incident neutron energy, the scattered neutron energy, and the scattering angles. This gives the set of probability functions that a neutron incident on the concrete interface with energy E and at angle θ is scattered from the concrete with energy E' and in the direction $d\Omega'$ about Ω' after having spent time t' in the scattering medium. These distribution functions are recorded on a second set of tapes.

Finally, the scattered neutron fraction and time distributions will be computed using the Bertini cross sections to simulate the actual neutron

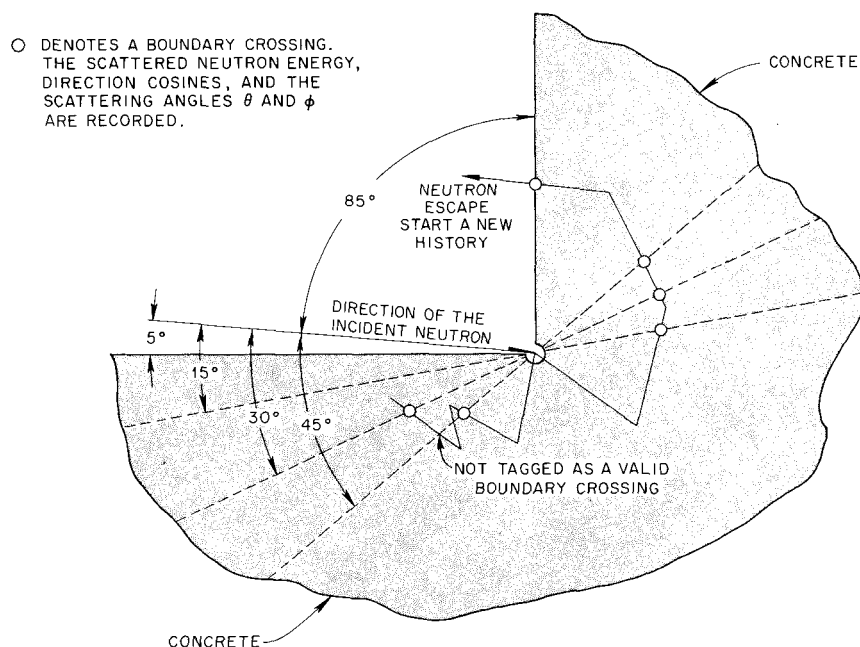


Fig. 5.7.1. Cross Section of the Concrete Configuration Used in Subroutine GEOM. The dashed lines show the several boundaries used in the calculation. The neutron is traced through the concrete, and when one of these boundaries is crossed the scattered neutron energy, direction cosines, and scattering angles are recorded. Note that in one case, two crossings of the same boundary occurred and only one was tagged, since the neutron would have escaped from the concrete for that angle of incidence. If the neutron escapes from the concrete or is degraded in energy below 0.5 MeV, a new history is started.

source. For a neutron emitted from the "target," the energy and direction of emission will be determined. If this neutron has a chance to strike the floor or the walls within a given time interval, it is tagged. A rotation of coordinate system is then performed so that the azimuthal angle is zero, and the new polar angle is recorded. If scattering into the element of solid angle subtended by the detector at the point of emission from the concrete can occur, the total flight time will be recorded. These data are then binned according to the flight time and scattered neutron energy. This is the time distribution of scattered neutrons.

To check the results of the calculation in a partial way, it is proposed to convert the scattered neutron flux to dose and compare the results with the values obtained by Maerker and Muckenthaler for neutron energies up to 10 MeV.

To date, the following progress has been made: the O5R and the associated subroutine GEOM have been demonstrated to be working, and the computer programs have been tested for a few hundred neutron histories. The binning routine is also working properly with coarse energy and scattering angle bins. The application of the Bertini MECC-3 code and the probability distribution functions to obtain the scattered neutron fraction are not yet completely coded.

References

¹Work supported by the National Aeronautics and Space Administration under task Number L-12,186.

²Present address: Virginia Polytechnic Institute, Blacksburg.

³H. W. Bertini, *Preliminary Data from Intra-nuclear-Cascade Calculations of 0.75-, 1-, and 2-GeV Protons on Oxygen, Aluminum, and Lead, and 1-GeV Neutrons on the Same Elements*, ORNL-TM-1996 (1967).

⁴D. C. Irving, R. M. Freestone, Jr., and F. B. K. Kam, *O5R, a General Purpose Monte Carlo Neutron Transport Code*, ORNL-3622 (1965).

⁵R. E. Maerker and F. J. Muckenthaler, *Differential Fast-Neutron Albedos for Concrete. I. Descriptions of Monte Carlo Calculation and TSF Experiment and Comparison of Calculated and Experimental Results*, ORNL-3822 (1965).

⁶F. G. Perey, Program GENOA, unpublished.

5.8 A LIBRARY SYSTEM FOR THE PDP-8 WITH DEC TYPE 580 MAGNETIC TAPE SYSTEM UTILIZING A REDUNDANT RIM RECORD FORMAT¹

J. W. Wachter

Programs for the PDP-8 are described by which program files or data files may be stored on DEC type 580 magnetic tape so that they may be recovered on demand. Each magnetic tape record is written in the TRIM format, a redundant RIM format that may be read either by a short program similar to the RIM or CRIMP programs or by more elaborate programs which check the redundancy features of the records. Locations 0000 and 7777 are used by all programs, and the shortest TRIM loader uses 7756-7777 and 0000. The record format also permits locating records on the tape by a six-character name. A particular system is described in which the bootstrap loader is loaded by the Tennecomp Auto-Loader.² The program uses one page, which may be the upper page of one core, for the loader and swaps various programs into a second page, which may be the upper page of the other core. These programs include: the

library calling program; a program to list descriptive titles of the programs filed on the library tape; a program to dump selected core locations in the TRIM format; and a selection of such utility programs as the binary paper tape loader, the octal dump program, and the paper tape punching program.

References

¹Abstract of ORNL-TM-2609 (in press); work supported by the National Aeronautics and Space Administration under task Number L-12,186.

²Manufactured by Tennecomp, Inc., Oak Ridge, Tenn.

5.9 SMOOTHIE: A PROGRAM FOR SMOOTHING O5S HISTOGRAM OUTPUT^{1,2}

R. T. Santoro R. E. Textor³
W. Zobel

Program SMOOTHIE is an auxiliary routine written to smooth O5S Monte Carlo code histogram data using Gaussian functions with parameters specified by the user. A plot of each smoothed pulse-height spectrum is produced along with a listing of the values of the differential and integral neutron detection efficiency as a function of the light output. Program SMOOTHIE is written in FORTRAN 63 for the CDC-1604 computer.

References

¹Work funded by the National Aeronautics and Space Administration, Order L-12,186, under Union Carbide Corp.'s contract with the U.S. Atomic Energy Commission.

²Abstract of ORNL-TM-2597, to be published.

³Computing Technology Center, Union Carbide Corp., Oak Ridge, Tenn.

Publications and Papers Presented at Scientific Meetings

PUBLICATIONS

ALSMILLER, R. G., Jr., and F. S. ALSMILLER

“High-Energy Accelerator Shielding,” *Nucl. News* **12**, 2, 47 (February 1969).

ALSMILLER, R. G., Jr., and J. BARISH

“High-Energy (<18 GeV) Muon Transport Calculations and Comparison with Experiment,” *Nucl. Instr. Methods* **71**, 121–24 (1969); ORNL-TM-2439 (Dec. 6, 1968).

“High-Energy Muon Transport and the Muon Backstop for a Multi-GeV Proton Accelerator,” ORNL-4386 (March 1969).

ALSMILLER, R. G., Jr., J. BARISH, R. T. BOUGHNER, and W. W. ENGLE

“Shielding Calculations for a 200-MeV Proton Accelerator,” ORNL-4336 (December 1968).

ALSMILLER, R. G., Jr., J. BARISH, and W. W. SCOTT

“The Effects of Multiple Coulomb Scattering and Range Straggling in Shielding Against Solar-Flare Protons,” Technical Note, *Nucl. Sci. Eng.* **35**, 405 (1969); ORNL-TM-2319 (Aug. 12, 1968).

ALSMILLER, R. G., Jr., and R. T. BOUGHNER

“Solar Neutron Transport in the Earth’s Atmosphere,” *J. Geophys. Res.* **73**, 4935 (1968).

ALSMILLER, R. G., Jr., M. LEIMDORFER, and J. BARISH

“High-Energy Muon Transport and the Muon Backstop for a 200-GeV Proton Accelerator,” ORNL-4322 (November 1968).

ALSMILLER, R. G., Jr., and H. S. MORAN

“Calculation of the Energy Deposited in Thick Targets by High-Energy (1 GeV) Electron-Photon Cascades and Comparison with Experiment,” ORNL-TM-2559 (Apr. 25, 1969).

ALSMILLER, R. G., Jr., F. R. MYNATT, J. BARISH, and W. W. ENGLE

“High-Energy (<400 MeV) Neutron Transport Using the Method of Discrete Ordinates,” *Nucl. Sci. Eng.* **36**, 251 (May 1969); ORNL-TM-2420 (Nov. 1, 1968).

“Shielding Against Neutrons in the Energy Range 50 to 400 MeV,” ORNL-TM-2554 (Mar. 31, 1969).

ALSMILLER, R. G., Jr., and E. SOLOMITO

“The Transport of Neutrons Produced by 3-GeV Proton-Lead Nucleus Collisions Through a Labyrinth and Comparison with Experiment,” ORNL-TM-2560 (Apr. 1, 1969).

ALSMILLER, R. G., Jr., J. W. WACHTER, and H. S. MORAN

“Calculations of the Neutron and Proton Spectra from Thick Targets Bombarded by 450-MeV Protons and Comparison with Experiment,” *Nucl. Sci. Eng.* **36**, 291–94 (1969); ORNL-TM-2462 (Jan. 6, 1969).

ARMSTRONG, T. W.

“Monte Carlo Calculations of Residual Nuclei Production in Thick Iron Targets Bombarded by 1- and 3-GeV Protons and Comparison with Experiment,” *J. Geophys. Res.* **74**(6) (Mar. 15, 1969).

- ARMSTRONG, T. W., and R. G. ALSMILLER, Jr.
 "Calculation of the Residual Photon Dose Rate Around High-Energy Proton Accelerators," ORNL-TM-2498 (Feb. 10, 1969).
- "An Estimate of the Prompt Photon Spectrum Arising from Cosmic-Ray Bombardment of the Moon," *Astronaut. Acta* **14**, 143-49 (1969).
- "Monte Carlo Calculations of the Nucleon-Meson Cascade in Iron Initiated by 1- and 3-GeV Protons and Comparison with Experiment," *Nucl. Sci. Eng.* **33**, 291-96 (1968).
- ARMSTRONG, T. W., R. G. ALSMILLER, Jr., and J. BARISH
 "Calculation of the Radiation Hazard at Supersonic Aircraft Altitudes Produced by an Energetic Solar Flare," ORNL-TM-2557 (Apr. 11, 1969).
- ARMSTRONG, T. W., and J. BARISH
 "Calculation of the Residual Photon Dose Rate Induced in Iron by 200-MeV Protons," ORNL-2583 (May 2, 1969).
- BERTINI, H. W., A. H. CULKOWSKI, and M. P. GUTHRIE
 "Intranuclear-Cascade Calculation of the Secondary Nucleon Spectra from Nucleon-Nucleus Interactions in the Energy Range 340 to 2900 MeV and Comparison with Experiment," ORNL-TM-2361 (May 1969).
- BEYSTER, J. R., and K. J. YOST
 "Nuclear Data Requirements and Acquisition for Shielding Application," *Nucl. News* 36-41 (February 1969).
- BIERMAN, S. R., and G. M. HESS (Pacific Northwest Laboratory)
 "Minimum Critical ^{235}U Enrichment of Homogeneous Hydrogenous Uranyl Nitrate," ORNL-CDC-5 (June 1968).
- BURRUS, W. R., and V. V. VERBINSKI
 "Fast-Neutron Spectroscopy with Thick Organic Scintillators," *Nucl. Instr. Methods* **67**, 181-96 (1969).
- CAIN, V. R.
 "Comparisons of Monte Carlo Calculations to Measurements of Neutron Leakage from the TSF-SNAP Reactor," ORNL-TM-2586 (June 1969).
- CAIN, V. R., and K. FRANZ
 "Comparison of Monte Carlo Calculations with Measurements of Fast-Neutron Dose Transmitted from a Beam Source Through a SNAP-2 LiH Shield," ORNL-TM-2423 (Dec. 18, 1968).
- CAIN, V. R., E. A. STRAKER, and G. THAYER
 "Monte Carlo Path Length Selection Routines Based on Some Specific Forms of the Importance Function," ORNL-TM-1967 (Feb. 6, 1969).
- CHAPMAN, G. T.
 "Spectrum of Gamma Rays Emitted by a Stainless-Steel-Clad Pool-Type Reactor (BSR-II)," *Nucl. Sci. Eng.* **34**, 169-80 (1968).
- CLAIBORNE, H. C., and D. K. TRUBEY
 "Dose Rates in a Slab Phantom from Monoenergetic Gamma Rays," ORNL-TM-2574 (Apr. 28, 1969).
- CLIFFORD, C. E., F. R. MYNATT, and E. A. STRAKER
 "Recent Developments in Transport Solutions to Radiation Shielding Problems," *Nucl. News* 52-56 (February 1969).
- COLEMAN, W. A., and R. G. ALSMILLER, Jr.
 "Thermal-Neutron Flux Generation by High-Energy Protons," *Nucl. Sci. Eng.* **34**, 104-13 (1968).
- CRAMER, S. N., V. R. CAIN, R. R. COVEYOU, P. N. STEVENS, and E. A. STRAKER
 "The Use of Kernels in Studying Neutron Problems," ORNL-TM-2508 (April 1969).

CRAMER, S. N., and M. SOLOMITO

"SPACETRAN: A Code to Calculate Dose at Detectors at Various Distances from the Surface of a Cylinder," ORNL-TM-2592 (June 17, 1969).

De SAUSSURE, G., and R. B. PEREZ

"POLLA, a Fortran Program to Convert R-Matrix-Type Multilevel Resonance Parameters for Fissile Nuclei into Equivalent Kapur-Peierls-Type Parameters," ORNL-TM-2599 (June 12, 1969).

DICKENS, J. K., and F. G. PEREY

"The $^{14}\text{N}(n, n\gamma)$ Reaction for $5.8 \leq E_n \leq 8.6$ MeV," *Nucl. Sci. Eng.* **36**, 280 (1969).

EICHLER, E., P. H. STELSON, and J. K. DICKENS

"A New Measurement of the Half-Life of the ^{72}Ge 0^+ State," *Nucl. Phys.* **A120**, 622-24 (1968).

FADER, W. J.

"Energy Response of the Hornyak Scintillation Neutron Detector," ORNL-TM-2274 (June 27, 1968).

FRANZ, K. D., and V. R. CAIN

"Modifications to the Monte Carlo Codes Used to Calculate Power Distribution and Neutron Leakage from the TSF-SNAP Reactor," ORNL-TM-2562 (June 12, 1969).

FU, C. Y., V. R. CAIN, E. A. STRAKER, P. N. STEVENS, and F. J. MUCKENTHALER

"Gamma-Ray Response of the NE-213 Liquid Scintillation Detector," ORNL-TM-2273 (Aug. 1, 1968).

GABRIEL, T. A., and R. G. ALSMILLER, Jr.

"Photonuclear Disintegration at High (<350 MeV) Energies," ORNL-TM-2481 (Feb. 12, 1969).

GRITZNER, M. L., and P. N. STEVENS

"A Comparison of the Building Protection Factor Codes CAPS-2 and PF-COMP," ORNL-TM-2285 (September 1968).

GUTHRIE, M. P.

"EVAP-2 and EVAP-3: Modifications of a Code to Calculate Particle Evaporation from Excited Compound Nuclei," ORNL-4379 (March 1969).

GUTHRIE, M. P., R. G. ALSMILLER, Jr. and H. W. BERTINI

"Calculation of the Capture of Negative Pions in Light Elements and Comparison with Experiments Pertaining to Cancer Radiotherapy," *Nucl. Instr. Methods* **66**, 29-36 (1968); ORNL-TM-2371 (Aug. 1, 1968).

GWIN, R., L. W. WESTON, G. de SAUSSURE, R. W. INGLE, J. H. TODD, F. E. GILLESPIE, R. W. HOCKENBURY, and R. C. BLOCK

"Measurement of the Neutron Fission and Absorption Cross Sections of ^{239}Pu over the Energy Region 0.01 to 30 keV," EANDC (US) 114 "A" (1968); for distribution by the European-American Nuclear Data Center to members of their committee for information purposes.

IANO, P. J., S. K. PENNY, and R. M. DRISKO

"Validity of Perturbation Approach to Two-Step Stripping," *Nucl. Phys.* **A127**, 47-59 (1969).

IRVING, D. C., R. G. ALSMILLER, Jr., and H. S. MORAN

"Calculation of the Energy Deposited by Nucleons in a Spherical Phantom and Comparison with Experiment," ORNL-TM-2515 (Feb. 10, 1969).

IRVING, D. C., V. R. CAIN, and R. M. FREESTONE, JR.

"An Amplification of Selected Portions of the 05R Monte Carlo Code User's Manual," ORNL-TM-2601 (May 29, 1969).

IRVING, D. C., H. S. MORAN, and W. E. KINNEY

"Modification and Further Development of the Nucleon Transport Code, NTC," ORNL-TM-1866 (Mar. 4, 1969).

KING, D. T.

"Protons from 2.7-GeV Protons on Ag and Br," ORNL-TM-2536 (Mar. 14, 1969).

- LEWIN, J., J. GURNEY, and D. K. TRUBEY
"A Survey of Recent Soviet Radiation Shielding Work," ORNL-RSIC-23 (September 1968).
- MAERKER, R. E., and F. J. MUCKENTHALER
"Gamma-Ray Spectra Arising from Thermal-Neutron Capture in Elements Found in Soils, Concretes, and Structural Materials," ORNL-4382 (June 1969).
- MARUSAK, A. L.
"FLOTSAM – a Two-Parameter On-Line Data Acquisition Program for the PDP-7," ORNL-4299 (October 1968).
- MUCKENTHALER, F. J.
"Measurement of the Fast-Neutron Dose Rate Transmitted Through a LiH Shield When Used as a Window in Iron-Oil Shield Mockups," ORNL-TM-2542 (April 1968).
- PEREY, C. M., F. G. PEREY, J. K. DICKENS, and R. J. SILVA
"11-MeV Proton Optical Model Analysis," *Phys. Rev.* **175**, 1460–75 (November 1968).
- RITTS, J. J., M. SOLOMITO, and P. N. STEVENS
"Calculations of Neutron Fluence-to-Kerma Factors for the Human Body," ORNL-TM-2079 (Rev.) (April 1969).
- SCHMIDT, F. A. R.
"Analytical Radiation Shielding Calculations for Concrete. Formulas and Parameters," *Nucl. Eng. Design* (August 1969).
- SCHMIDT, F. A. R., E. A. STRAKER, and V. R. CAIN
"Applications of Adjoint Flux Calculations to Monte Carlo Biasing," ORNL-TM-2454 (Dec. 26, 1968).
- SILVER, E. G.
"A Pulsed-Neutron Investigation of the Effect of Temperature on the Decay of a Thermal-Neutron Population in H₂O Ice," *Nucl. Sci. Eng.* **34**, 275–84 (1968).
- SOLOMITO, M., and H. C. CLAIBORNE
"A Simple Method for Determining a Combined Lead-Steel Shield for Shipping Casks That Is Equivalent to a Lead Shield," ORNL-TM-2591 (May 29, 1969).
- SOLOMITO, M., J. J. RITTS, and H. C. CLAIBORNE
"AVKER: A Program for Determining Neutron Kerma Factors for Use in Energy Deposition Calculations," ORNL-TM-2558 (Apr. 15, 1969).
- STRAKER, E. A.
"Sensitivity of Neutron Transport in Oxygen to Various Cross-Section Sets," Technical Note, *Nucl. Sci. Eng.* **34**, 332 (1968).
"Experimental Evaluation of Minima in the Total Neutron Cross Sections of Several Shielding Materials," *Nucl. Sci. Eng.* **34**, 114–21 (1968).
"Fast-Neutron Collimator Studies and the Design of the TSF-SNAP Core Mapping Collimator," *Nucl. Appl.* **6** (February 1969); ORNL-TM-2299 (Aug. 26, 1968).
"Measurements of the Absolute Power and Fission Distribution in the TSF-SNAP Reactor and Comparison with Monte Carlo and Discrete Ordinates Calculations," ORNL-TM-2265 (Sept. 3, 1968).
- STRAKER, E. A., W. W. ENGLE, and P. N. STEVENS
"Some Calculated Milestone Solutions to Time-Dependent Radiation Transport Problems," ORNL-TM-2499 (Apr. 22, 1969).
- STRAKER, E. A., and F. J. Muckenthaler
"Measured and Calculated Absolute Power and Fission Distribution in the TSF-SNAP Reactor," *Nucl. App.*, **6** (April 1969).
- TRUBEY, D. K.
"Use of ICRU Defined Quantities and Units in Shielding," ORNL-RSIC-16 (October 1968).

TRUBEY, D. K., and J. GURNEY

"Bibliography, Subject Index, and Author Index of the Literature Examined by the Radiation Shielding Information Center (Research and Weapons Radiation Shielding)," ORNL-RSIC-5 (Vol. II) (1969).

VERBINSKI, V. V., and W. R. BURRUS

"Direct and Compound-Nucleus Neutrons from 14~18 MeV Protons on ^9Be , ^{14}N , ^{27}Al , ^{56}Fe , ^{115}In , ^{181}Ta , and ^{208}Pb and from 33-MeV Bremsstrahlung on ^{27}Al , ^{206}Pb , ^{208}Pb , and ^{209}Bi ," *Phys. Rev.* **177**, 1671 (January 1969).

VERBINSKI, V. V., W. R. BURRUS, T. A. LOVE, W. ZOBEL, and N. W. HILL

"Calibration of an Organic Scintillator for Neutron Spectrometry," *Nucl. Instr. Methods* **65**, 8-25 (1968).

VERBINSKI, V. V., FRANCIS G. PEREY, J. KIRK DICKENS, and WALTER R. BURRUS

"Neutrons from $^9\text{Be}(\alpha, n)$ Reaction for E_α Between 6 and 10 MeV," *Phys. Rev.* **170**, 916-23 (1968).

WACHTER, J. W., W. A. GIBSON, and W. R. BURRUS

"Neutron and Proton Spectra from Targets Bombarded by 450-MeV Protons," ORNL-TM-2253 (Nov. 18, 1968).

WEBSTER, J. W.

"05R Monte Carlo Calculations of Low-Enriched Uranium Thermal Critical Assemblies, and Evidence of Errors in ^{238}U Cross Sections," ORNL-TM-2187 (November 1968).

WESTON, L. W., R. GWIN, G. de SAUSSURE, R. W. INGLE, J. H. TODD, C. W. CRAVEN, R. W. HOCKENBURY, and R. C. BLOCK

"Neutron Fission and Capture Cross-Section Measurements for ^{233}U in the Energy Region 0.02 to 1 eV," ORNL-TM-2353 (Feb. 1, 1969).

WESTON, L. W., R. GWIN, G. de SAUSSURE, R. R. FULLWOOD, and R. W. HOCKENBURY

"Measurement of the Neutron Fission and Capture Cross Sections for ^{233}U in the Energy Region 0.4 to 2000 eV," *Nucl. Sci. Eng.* **34**, 1-12 (1968).

YAMAKOSHI, H.

"An Examination of Several Computational Models for Use in Computing Gamma-Ray Penetration of Structures," ORNL-TM-2520 (Mar. 7, 1969).

YOST, K. J., and S. M. KREMER

"The Application of a Gamma-Ray Cascade Model to the Calculation of Neutron Energy-Dependent Capture Gamma-Ray Production Cross Sections," *Nucl. Sci. Eng.* **36**, 220 (May 1969); ORNL-TM-2404 (Nov. 6, 1968).

YOST, K. J., P. H. PITKANEN, and C. Y. FU

"A Unified Nuclear Model for the Generation of Nuclear Data," *Nucl. Sci. Eng.* **36**, 189 (May 1969).

"Compilation of Data on Experimental Shielding Facilities and Tests of Shields of Operating Reactors," ORNL-RSIC-24 (November 1968).

"Abstracts of the Literature Examined by the Radiation Shielding Information Center (Reactor and Weapons Shielding)," ORNL-RSIC-6 (Vol. II) (January 1969).

PAPERS

American Nuclear Society Meeting, November 10–15, 1968, Washington, D.C.; Trans. Am. Nucl. Soc., vol. 11, No. 2 (November 1968).

MAERKER, R. E., and F. J. MUCKENTHALER, "Gamma-Ray Spectra Arising from Thermal-Neutron Capture in Iron, Aluminum, and Copper."

WEBSTER, J. W., "Monte Carlo Studies of the Use of Borosilicate-Glass Raschig Rings as a Fixed Neutron Absorber in Solutions of Fissile Material."

YOST, K. J., "A Computational Method for Obtaining Neutron Energy-Dependent Capture Gamma-Ray Yields for Production Cross Sections."

YOST, K. J., and S. M. KREMER, "A Comparison of Measured and Calculated Neutron Capture Gamma-Ray Spectra."

American Physical Society Winter Meeting, December 18–20, 1968, San Diego, California; Bull. Am. Phys. Soc., Ser. 2, vol. 13, No. 12 (December 1968).

BERTRAND, F. E., R. W. PEELLE, and J. K. DICKENS, "High Resolution Study of Charged Particle Reactions Induced by 30–60 MeV Protons."

American Nuclear Society National Topical Meeting, January 28–30, 1969, Albuquerque, New Mexico (Fast Burst Reactors Meeting).

HOLLAND, L. B., "Operational Experience with Fast Burst Reactors."

American Physical Society Meeting, February 3–6, 1969, New York; Bull. Am. Phys. Soc., vol. 14, No. 1 (January 1969).

GABRIEL, T. A., and R. G. ALSMILLER, Jr., "Nucleon and Pion Emission Spectra for High-Energy (<350 MeV) Photon-Nucleus Collisions."

Conference on Computer Systems in Experimental Physics, March 3–6, 1969, Skytop, Pennsylvania.

BETZ, N. A., J. W. REYNOLDS, and G. G. SLAUGHTER, "Rapid Data Acquisition into More than 10^5 Channels at ORELA."

American Physical Society Meeting, April 28–May 1, 1969, Washington, D.C.; Bull. Am. Phys. Soc., Ser. II, vol. 14, No. 4 (April 1969).

BERTINI, H. W., "Absorption, Charge Exchange, and Double-Charge Exchange Reactions of π -Mesons with Complex Nuclei."

American Nuclear Society Meeting, June 15–19, 1969, Seattle, Washington; Trans. Am. Nucl. Soc., vol. 12, No. 1 (1969).

ARMSTRONG, T. W., and R. G. ALSMILLER, Jr., "Calculation of the Residual Photon Dose Rate Around High-Energy Proton Accelerators."

CLAIBORNE, H. C., and D. K. TRUBEY, "Gamma-Ray Dose Rates in a Slab Phantom."

DENNING, R. S., and R. B. PEREZ, "The Dispersion Law of a Neutron Die-Away Experiment."

De SAUSSURE, G., R. B. PEREZ, and M. N. MOORE, "Statistical Tests for the Detection of Intermediate Structures in the Fission Cross Sections of ^{235}U and ^{239}Pu ."

FRENCH, R. L., and J. M. NEWELL, "Analysis of Initial Radiation Protection Aboard Ship."

GWIN, R., L. W. WESTON, G. de SAUSSURE, R. W. INGLE, J. H. TODD, F. E. GILLESPIE, R. W. HOCKENBURY, and R. C. BLOCK, "Measurement of Neutron Fission and Absorption Cross Sections of ^{239}Pu ."

LEWIN, JOSEPH, "Ten Years of Contacts with the Soviet Nuclear Community – Is the Study of Russian Necessary?"

- MAERKER, R. E., and F. J. MUCKENTHALER, "Gamma-Ray Spectra Arising from Thermal-Neutron Capture in Silicon, Calcium, Potassium, Sodium, and Barium."
- PEELLE, R. W., W. ZOBEL, and F. C. MAIENSCHIN, "Spectrum of Prompt Gamma Rays from Thermal Fission of ^{235}U ."
- PENNY, S. K., K. J. YOST, and J. WHITE, "Calculation of Neutron Capture Gamma-Ray Yields for Tungsten and Neutron Inelastic Scattering Cross Sections for Iron."
- STRAKER, E. A., "The Effect of the Ground on the Transport of Neutrons and Secondary Gamma Rays in the Atmosphere."
- WESTON, L. W., R. GWIN, G. de SAUSSURE, R. W. INGLE, J. H. TODD, C. W. CRAVEN, R. W. HOCKENBURY, and R. C. BLOCK, "Neutron Fission and Capture Cross-Section Measurements for ^{233}U Below 1 eV."
- YOST, K. J., P. H. PITKANEN, and C. Y. FU, "A Nuclear Model for Data Generation and Analysis in Light Nuclei."

INTERNAL DISTRIBUTION

1. L. S. Abbott
2. F. S. Alsmiller
3. R. G. Alsmiller, Jr.
4. T. W. Armstrong
5. J. Ashe
6. J. Barish (K-25)
7. H. W. Bertini
8. F. E. Bertrand
9. N. A. Betz
10. J. A. Biggerstaff
11. A. L. Boch
12. T. V. Blosser
13. R. S. Booth
14. R. T. Boughner
15. C. E. Burgart
16. V. R. Cain
17. G. T. Chapman
18. R. O. Chester
19. H. C. Claiborne
20. F. H. S. Clark
21. C. E. Clifford
22. W. C. Colwell
23. R. G. Couch
24. R. R. Coveyou
25. S. N. Cramer (K-25)
26. C. W. Craven
27. J. T. DeLorenzo
28. G. de Saussure
29. J. K. Dickens
30. L. Dresner
31. E. Eichler
32. M. B. Emmett
33. W. W. Engle, Jr. (K-25)
34. W. E. Ford III (K-25)
35. J. L. Fowler
36. K. D. Franz (K-25)
37. R. M. Freestone, Jr.
38. C. Y. Fu
39. T. A. Gabriel
40. F. E. Gillespie
41. L. W. Gilley
42. J. H. Gillette
43. N. M. Greene (K-25)
44. M. L. Gritzner (K-25)
45. Jane Gurney
46. M. P. Guthrie
47. R. Gwin
48. J. A. Harvey
49. K. M. Henry, Jr.
50. R. F. Hibbs
51. N. W. Hill
52. L. B. Holland
53. J. L. Hull
54. R. W. Ingle
55. D. C. Irving
56. W. H. Jordan
57. D. T. King
58. W. E. Kinney
59. K. Kumar
60. R. Kuebbing
61. J. Lewin
62. E. C. Long (K-25)
63. T. A. Lewis
64. T. A. Love
65. H. G. MacPherson
66. E. Madden
67. R. E. Maerker
- 68-117. F. C. Maienschein
118. J. J. Manning
119. B. F. Maskewitz
120. J. W. McConnell
121. C. O. McNew
122. J. K. Millard
123. H. S. Moran
124. F. J. Muckenthaler
125. F. R. Mynatt (K-25)
126. D. O. Nellis
127. C. E. Newlon (K-25)
- 128-129. R. B. Parker
130. J. W. Paul
131. R. W. Peelle
132. S. K. Penny
133. C. M. Perey
134. F. G. Perey
135. R. Perez
136. P. H. Pitkanen
137. H. P. Raaen
138. S. Ramon
139. J. W. Reynolds
140. J. J. Ritts
141. R. J. Rodgers (K-25)
142. B. W. Rust (K-25)
143. R. D. Sabin
144. R. T. Santoro

- | | |
|---------------------------|--|
| 145. G. R. Satchler | 167. A. M. Weinberg |
| 146. W. W. Scott | 168. L. W. Weston |
| 147. Y. Shima | 169. J. D. White |
| 148. R. J. Silva | 170. L. R. Williams (K-25) |
| 149. E. G. Silver | 171. D. R. Winkler |
| 150. M. J. Skinner | 172. H. Q. Wright |
| 151. G. G. Slaughter | 173. R. Q. Wright |
| 152. E. Solomito | 174. K. Yamada |
| 153. P. H. Stelson | 175. G. Young |
| 154. P. N. Stevens | 176. K. J. Yost |
| 155. J. R. Stockton | 177. W. Zobel |
| 156. E. A. Straker | 178. E. R. Cohen (consultant) |
| 157. D. A. Sundberg | 179. B. C. Diven (consultant) |
| 158. R. Textor (K-25) | 180. H. Feshbach (consultant) |
| 159. C. L. Thompson | 181. H. Goldstein (consultant) |
| 160. H. A. Todd | 182. RSIC Library |
| 161. J. H. Todd | 183. Biology Library |
| 162. D. K. Trubey | 184-186. Central Research Library |
| 163. J. W. Wachter | 187-188. ORNL - Y-12 Technical Library
Document Reference Section |
| 164. D. H. Wallace (K-25) | 189-238. Laboratory Records Department |
| 165. D. R. Ward | 239. Laboratory Records, ORNL R.C. |
| 166. J. W. Webster | |

EXTERNAL DISTRIBUTION

- 240-694. Given external distribution
695. P. B. Hemmig, Division of Reactor Development, U.S. Atomic Energy Commission, Washington, D.C.
696. W. H. Hannum, Reactor Physics Branch, U.S. Atomic Energy Commission, Washington, D.C.
697. W. W. Grigorieff, Assistant to the Executive Director, Oak Ridge Associated Universities, Oak Ridge, Tennessee
698. K. O. Laughon, AEC Site Representative, ORNL
699. J. A. Swartout, Union Carbide Corporation, New York, N.Y.
700. Laboratory and University Division, AEC, ORO
- 701-960. Given distribution as shown in TID-4500 under Physics category (25 copies - CFSTI)